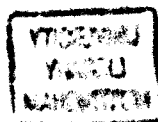

**Low Frequency Impedance and Structural properties of
High Temperature Superconducting
YBa₂Cu₃O_x Thin Films**

by Bryan Gerrard Murray, BSc(Hons) MSc

University of Nottingham
Department of Electrical and Electronic Engineering

Thesis submitted to the University of Nottingham for the degree of Doctor of
Philosophy, January, 1994.



Acknowledgements

I would like to thank Dr. M. S. Raven for his support and ideas. I also would like to thank Eyo Inameti and Yuk Wan for the thin films and results that I used in the course of my work. My thanks to Maurice Brown for performing the X-ray analysis and for teaching me how to use the scanning electron microscope. My thanks to Davina Martin for her help. My thanks also to the Science and Engineering Research Council for their financial support. Finally, I would like to thank anyone else who helped in one way or another. Thanks.

Abstract

R.F. sputtering was used to deposit thin films of YBCO onto a variety of substrates. The films were found to be superconducting with critical temperatures in excess of 77 Kelvin. Using x-ray diffraction the orientation of the YBCO thin films on MgO(100) was found to be c-axis. The films deposited on SrTiO₃(100) were found to be a and c axis orientated, where as on SrTiO₃(110) the thin films were (110/013) orientated. Using scanning electron microscopy the films were found to be granular in nature. The films deposited on MgO(100) had circular grains. The films deposited on SrTiO₃(110) had elongated sausage like grains. The shape of the grains is due to spiral and ridge type growth respectively. Electrical measurements were taken using a 4 probe contact technique. The rf experiments were used to calculate the paraconductivity. The coherence length and superconducting sheet thickness were calculated for c-axis YBCO thin films using the Lawrence-Doniach theory. The coherence length was found to be 4 Å, the sheet thickness was 11 Å for T=0 Kelvin. Examination of the transition region revealed a flux flow region in films deposited on MgO(100). The temperature dependence of the flux flow region was found to be in agreement with that predicted by Kosterlitz-Thouless and independently by Berezinskii. This implies that the films were 2 dimensional in nature. Some films deposited on SrTiO₃(110) do not appear to have a flux flow region. Films deposited on SrTiO₃(110) may be 3 dimensional. Examination of the magnetic properties were in agreement with existing theory, namely that the resistance was directly proportional to the applied magnetic field. In order to perform critical current measurements the films were wet etched into strips. The temperature dependence of the critical current of the granular thin films was found to be in agreement with Ambegaokar-Baratoff theory for a 2 dimensional film of Josephson junctions. An ac electrical technique was used to investigate the reactive properties of YBCO thin films. Results show that the normal inductance was very anisotropic. The inductance for temperature below T_c was used to calculate the penetration depth. The penetration depth, for T=0K, was found to be between 2.24-10.58µm. Penetration depths of this magnitude are predicted by Ambegaokar-Baratoff for certain cases. The temperature dependence of the penetration depth was investigated in terms of the London theory and good agreement was found. Anomalous behaviour was found to occur in certain thin films. The anomaly was present as a change in the temperature dependence of the kinetic inductance. The anomaly may be due to 2D-3D crossover, known to occur in YBCO thin films. An anomalous resonance effect was observed in very thin film at 48 Kelvin. The behaviour of the anomaly is very similar to a dielectric but may be due to substrate effect.

	Page
Chapter 1: Introduction - This Thesis	1
1.1: Introduction to Superconductivity	3
1.1.1: Kamerlingh Onnes, Meissner and Oschenfeld	4
1.2: Development of Superconductor Theory	5
1.2.1: Two Fluid Theory	5
1.2.2: Ginzburg and Landau	6
1.2.3: Abrikosov Theory	6
1.2.4: Bardeen, Cooper and Schrieffer	8
1.2.5: Josephson Effect	9
1.3: The Discovery by Bednorz and Muller	9
1.3.1: Perovskite Superconductivity	10
1.3.2: High T_C Superconductors	11
1.4: Yttrium Barium Copper Oxide	13
1.4.1: Mechanisms for High T_C Superconductors	14
1.5: References	16
Chapter 2: Review of YBCO Thin Films	
2.1: Introduction	19
2.2: Production of Thin Films	20
2.2.1: Introduction	20
2.2.2: Substrate Materials	20
2.2.3: Deposition Techniques	22
2.2.4: R.F. Sputter Deposition	22
2.2.4.1: Gas pressure and Back Sputtering	23
2.2.4.2: Substrate Temperature During Deposition	24

2.2.4.2.1: High Temperature Deposition	24
2.2.4.3: Substrate Temperature and Thin Film Orientation	25
2.2.4.4: Off Axis Sputter Deposition	27
2.2.4.5: Growth Mechanisms	28
2.3: Film Characterization	
2.3.1: Introduction	29
2.3.2: Resistance Temperature Measurements	29
2.3.3: Non Ohmic Resistance Region	30
2.3.4: Penetration depth	33
2.3.5: Anisotropy	36
2.3.5.1: Superconducting Anisotropy	36
2.3.5.2: Normal Behaviour and carrier type	37
2.4: Summary	38
2.5: References	40
 Chapter 3: Theory	
3.1: Introduction	45
3.1.1: Experimental Theory Intro.	46
3.2: Theory	48
3.2.1: Meissner Effect	48
3.2.2: Gorter-Casimir Theory	49
3.2.3: London Theory	51
3.2.4: Ginzburg Landau Theory	53
3.2.5: BCS Theory	56
3.2.6: Ginzburg Landau Parameter	59
3.2.7: Abrikosov Theory	60

3.2.8: Type II Superconductors	61
3.2.8.1 YBCO and Type II Superconductivity	61
3.2.9: Paraconductivity	61
3.3: Flux Dissipation in YBCO	63
3.3.1: Anderson's Flux Flow Theory	63
3.3.2: Kosterlitz Thouless Berezinskii Transition	66
3.3.2.1: Current Induced Vortex Unbinding	67
3.3.3: Normal Transport Equations	71
3.3.4: Josephson Junctions and Critical Current	73
3.3.5: 2 Dimensional to 3 Dimensional Crossover	74
3.4: Low Frequency Impedance of YBCO Thin Films	76
3.4.1: Revised Current Density Equations	76
3.5: Structure and X-ray Diffraction	80
3.6: Summary	82
3.7: References	84

Chapter 4: R.F.Sputtering

4.1: Introduction - The Radio Frequency Sputtering System	86
4.1.1: The Vacuum System	86
4.1.2: Substrate Heater	86
4.1.3: The Target	88
4.2: Thin Film Production	90
4.2.1: Substrates and Substrate Preparation	90
4.2.2: Loading the Substrate and System Preparation	90
4.2.3: Deposition Procedure	91
4.2.4: Evaporation of Silver Contact Pads	92

4.3: References	94
4.4: Figure Captions	95
Chapter 5: Experimental Procedure	
5.1: Introduction	100
5.2: Cooling Unit	100
5.2.1 : Device Under Test	101
5.3: Radio Frequency Experiments	102
5.3.1 : Impedance Analyser	102
5.3.2 : Calibration by Shorting Method	103
5.3.3 : Hewlett - Packard Self Calibration	104
5.3.4 : Frequency Response Experiments	105
5.4 : DC Resistance Experiments	106
5.5 : Critical Current Experiments	107
5.5.1 : Photomask Production	108
5.5.2 : Film Etching	109
5.6 : Experiments in an Applied Magnetic Field	110
5.7 : X-ray Diffraction	111
5.8 : Substrate Reclamation	112
5.9 : References	113
5.10: Figure Captions	114
Chapter 6 : Film Deposition, Results and Discussion	
6.1 : Introduction	120
6.2 : Film Deposition	120
6.3 : Ex-situ Deposition	120
6.4 : In-situ Deposition on SrTiO ₃ (110)	122

6.4.1 : Sputtering Gas Pressure	122
6.4.2 : Post Annealing	123
6.4.3 : Substrate Position	124
6.4.4 : Substrate Temperature	124
6.5 : In-situ Deposition on MgO(100)	125
6.5.1 : Sputtering Gas Pressure	125
6.5.2 : Substrate Position	125
6.5.3 : Substrate Temperature	126
6.6 : In-situ Deposition on SrTiO ₃ (100)	127
6.6.1 : Substrate Position	127
6.7 : Films Deposited on SrTiO ₃ (100) and SrTiO ₃ (110)	128
6.8 : Films Deposited on SrTiO ₃ (100) and MgO(100)	128
6.9 : X-ray Diffraction	129
6.9.1 : YBCO Films Deposited on SrTiO ₃ (110)	130
6.9.2 : YBCO Films Deposited on MgO(100)	131
6.9.3 : YBCO Films Deposited on SrTiO ₃ (100)	132
6.10 : Summary	134
6.11 : References	136
6.12 : Figure Captions	137

Chapter 7 : Transport Measurements, Results and Discussion

7.1 Introduction	154
7.2 Transport Measurements	154
7.2.1 Film Anisotropy	155
7.3 : Resistivity and Anderson's Resonating Valence Bond Model	156
7.3.1 : C-axis Orientated Thin Films	158

7.3.2 : Films Deposited on SrTiO ₃ (110)	159
7.3.3 : Films Deposited on SrTiO ₃ (100)	159
7.4 : Paraconductivity	160
7.4.1 : Interpretation of Paraconductivity Results	160
7.5 : Interpretation of the Intermediate Region in Terms of Kosterlitz Thouless Berezinskii Theory	163
7.6 : Dissipation due to Application of External Magnetic Field	164
7.6.1 : Interpretation using Anderson Flux Flow Model	165
7.7 : Summary	167
7.8 : References	169
7.9 : Figure Captions	170
Chapter 8 : Reactance and Other Measurements	
8.1 : Inductance Measurements	186
8.1.1 : Substrate Effects	186
8.1.2 : Stray Inductance	186
8.2 : Normal Inductance Measurements	188
8.3 : Superconducting Inductance Measurements	188
8.3.1 : Kinetic Inductance and London Theory	189
8.4 : Anomalous Behaviour in YBCO Thin Films	191
8.4.1 : Anomalous Thin Films	192
8.5 : Film with Resonance at 50 Kelvin	193
8.6 : Investigation of Etched Thin Films	194
8.6.1 : Normal Region	195
8.6.2 : Temperature Dependence of Etched Thin Films	195
8.6.3 : Superconducting Region	196
8.6.4 : Critical Current Measurements	197
8.6.4.1 : Interpretation of Results	197
8.7 : New Equivalent Model for YBCO Thin Films	198

8.7.1 : Equivalent Model	198
8.7.2 : For $T < T_{KTB}$	199
8.7.3 : For $T_{KTB} < T < T_C$	200
8.7.4 : AC Dissipation in a Magnetic Field	201
8.7.5 : Simulated Results using the Model	202
8.8 : Summary	204
8.9 : References	206
8.10: Figure Captions	207
Chapter 9 : Summary and Future Work	229
9.1 : Summary	
9.2 : Future Work	234
9.3 : References	238
Appendix	241
RLFREQ	
RLTEMP	
DCTEMP	
Tables for Silicon Diode	

CHAPTER 1: INTRODUCTION

1: Introduction - This Thesis

This thesis is separated into nine chapters. The first chapter is a short review of the history of superconductivity since its discovery in 1911. This chapter will introduce the more important theoretical models that have appeared over the years. The end of this chapter reviews the discovery of Yttrium Barium Copper Oxide (YBCO) and its impact since 1987.

The second chapter takes a more in depth look at YBCO thin films. This chapter will include the methods available for the production of thin films. It will centre mainly on RF sputtering and how it has developed over the last few years to become a very successful method of deposition. The review will also take a look at the electrical properties of the thin films around the transition region. This work will include the various theories used today to explain the resistive properties of YBCO. Experiments to calculate values of penetration depth, coherence length, sheet thickness and various other parameters will be reviewed, accompanied by the results of this work.

Chapter three is the theoretical section of this thesis. Due to the complexity of both the RF sputtering and electrical properties of YBCO, it quickly became apparent that to review or investigate both aspects of YBCO in the detail necessary for clear understanding would be overwhelming. It was necessary therefore to concentrate on one aspect only. In this thesis I have chosen to review the electrical theories of YBCO and superconductivity rather than sputtering theory. For this reason chapter three will consist of the theories presently used to explain the electrical behaviour of YBCO thin films. This chapter will review much of the early work, since this is often used by researchers to describe the YBCO thin films. This will include London and Ginzburg-Landau theories and Andersons' flux flow model. This chapter also contains more modern ideas

such as the Kosterlitz-Thouless and Berezinskii theories of two dimensional superconductivity and Anderson's Resonating Valence Bond Theory. Theories relating to paraconductivity will also be reviewed since some believe that the mechanism responsible for superconductivity may be magnetically orientated. These theories will be used to obtain theoretical results that will be compared with the results from experiments. The close of this chapter is a review of the present theory relating to the experimental technique used in this thesis. This will enable us to see how the results obtained from the ac experiments can be used to calculate the parameters derived from theory.

In Chapter four a review of the apparatus used to produce the thin films is described. The method of production used here is RF sputtering. The extra equipment required for successful sputtering of YBCO, such as a substrate heater and target material will be reviewed in this section. The experimental technique of RF sputtering will also be reviewed in this chapter.

Chapter five describes the equipment and experimental techniques used to determine the electrical properties of YBCO thin films. This chapter will include details of mask production and etching techniques. The low temperature experiments will be reviewed in detail in this chapter.

Chapter six contains the results and discussion. This chapter will review the results obtained from the experiments described in chapter five. The first section of this chapter will review the production of thin films. This will include the effect of the growth parameters on the quality of the YBCO thin films. The structural properties of the YBCO thin films investigated using x-ray diffraction will be covered in this chapter.

Chapter seven is concerned with the electrical results obtained from the thin films that exhibited superconductivity. This will include the steps required and used to

calculate parameters such as coherence length and sheet thickness from the experimental data. The various transport theories mentioned in chapter three will be examined here and the results from the experiments will be given in terms of these theories.

Chapter eight covers the investigation into the reactive properties of YBCO thin films. The inductive properties of YBCO at 13 MHz will be used to determine the penetration depth of the YBCO thin films. This chapter will also include the anomalous results that have occurred. A resonance effect observed in a very thin film will be reported along with a model used to simulate the films peculiar transport properties. This chapter will also include the results obtained from etching YBCO thin films. Critical current measurements will be reported here. The final section of this chapter will include a simple model to explain some of the properties observed in experiment. The model is based on an equivalent circuit and is not meant to be a theoretical model of superconductivity. It is designed to explain the properties observed in the experiments performed and presented here in terms of a simple electrical circuit, consisting of inductors, resistors and capacitors. This is therefore an attempt to simplify, qualitatively, the electrical behaviour of YBCO thin films.

The final chapter will be a review of this thesis as a whole. The value of the research performed and presented here, will be given. It shall therefore be a review of what has actually been achieved. Suggestions for future work will also be reviewed.

1.1: Introduction to Superconductivity

The story of superconductivity started with its discovery in 1911⁽¹⁾. For decades theoretical physicists and experimentalists strived to obtain a thorough understanding of this remarkable property, and following the publication of a quantum mechanical model in 1956⁽²⁾ it was generally assumed that this had been achieved. Thirty years later it was

realised however that this was not so. The discovery in 1987 of high temperature superconductivity raised questions that cannot be fully explained or understood using existing theory. This fact, coupled with the high temperature at which the materials become superconducting, resulted in a massive amount of work in recent years on this subject. The work given here represents one small area of this research.

1.1.1: Kamerlingh Onnes, Meissner and Oschenfeld

The initial discovery of superconductivity was made by Kamerlingh Onnes⁽¹⁾. His experiments were designed to investigate the electrical properties of metals to verify the Drude - Lorentz theory of metallic resistance. He discovered that instead of the temperature dependence predicted by the existing theory, the resistance of the mercury sample fell sharply to zero at around 4 Kelvin. This behaviour became known as superconductivity, since the material appears to have zero resistance. (Experiments to determine the resistivity of a superconducting sample have shown that for lead the resistivity is less than 10^{-23} ohms-meter⁽⁴⁵⁾). Theories to explain this phenomenon began almost immediately though physicists soon realised that the property of infinite conductivity was rather difficult to explain. Thus it was not until 1933 with a discovery by Meissner and Oschenfeld⁽³⁾ that acceptable theoretical arguments began to appear.

Meissner and Oschenfelds' experiments demonstrating the exclusion of the magnetic field from the bulk of a superconductor by screening currents revolutionised thinking. The importance of their work was that it solved the problem of perfect conductivity that existed until that point. The experiment proved that below the critical temperature of the sample, namely the temperature at which the sample becomes superconducting, any small magnetic field would be expelled from the sample irrespective of the sample's previous history. In other words it does not matter whether

the sample is first cooled and the field is then applied or the field is applied first and then the sample is cooled, the effect is still the same. The Meissner effect, as the phenomena is known, proved that the "superconducting state" was a reversible equilibrium state, a stable thermodynamic one.

1.2: Development of superconductor theory

1.2.1: Two Fluid Theory, Gorter-Casimir, the Londons and Pippard

Soon after the discovery of the Meissner effect, phenomenological theories began to appear. Gorter and Casimir developed a two fluid theory⁽⁴⁾. The theory, as the name suggests, considers the superconductor to consist of two independent fluids, a normal fluid and a superconducting fluid. The normal fluid is simply the normal electrons. The second fluid known as the superfluid or superconducting fluid consists of electrons having no resistance. The superconducting electrons can travel through the material without dissipation. Gorter-Casimir theory described various properties of superconductivity including the temperature dependence of the superelectrons.

Pursuing the two fluid theory the London brothers were able to develop a theory from Maxwell's equations to explain the Meissner effect⁽⁵⁾. Their work led to the definition of a new parameter, now known as the penetration depth. The value of penetration depth is linked directly to the number of superconducting electrons. Combining Gorter and Casimir's results with their own, the Londons were thus able to establish the change in penetration depth with temperature. The London equations fitted experiment remarkably well.

Work by Pippard⁽⁶⁾ led him to realise that for certain pure superconductors the London equations were no longer valid and that they should be replaced by non local equations. The evidence for this came from Pippard's measurements on the anisotropic

nature of tin. Pippard pointed out that the very fact that the penetration depth is anisotropic in certain materials is sufficient reason to investigate new ideas. Pippard's work resulted in equations to replace the Londons' equations as well as the definition of a new parameter called the coherence length. The coherence length is the length of the boundary of the superconducting phase. Pippard also proposed that the only time that the Londons equations were still valid was when the penetration depth was very much larger than the coherence length. This is an important point, since in the new high temperature superconductors, the penetration depth, although being anisotropic, is very much larger than the coherence length at low temperatures⁽⁷⁾.

1.2.2: Ginzburg and Landau

In 1950, Ginzburg and Landau⁽⁸⁾ proposed an extension to an idea developed by Landau in 1937⁽⁹⁾. The work by Landau was based on the superconductor being represented by an order parameter. This parameter tended to zero at the transition temperature. Ginzburg and Landau realised that the order parameter was a wave function of the system. From Landau's earlier work, they were able to derive a term equivalent to the London penetration depth. They also discovered a second dimensionless parameter κ . It later became clear that this parameter was the ratio of the penetration depth and the coherence length. The importance of this parameter is in its relationship to type I and II superconductors. Abrikosov⁽¹⁰⁾ pointed out that for values of $\kappa < 1/\sqrt{2}$ the superconductors are type I, where as for $\kappa > 1/\sqrt{2}$ the materials are type II superconductors.

1.2.3: Abrikosov Theory

In 1957, Abrikosov put forward a theory he conceived in 1952 to explain the

magnetic properties of type II superconductors⁽¹¹⁾. His theory described a mixed state consisting of vortex lines arranged periodically throughout a type II superconductor. He suggested that vortices, namely the normal regions, would be surrounded by circulating superelectrons that would cause any magnetic flux flowing through the normal region to be quantised. This was a revolutionary idea, though its importance was not fully realised until later. Cribier⁽¹²⁾ used the idea to explain his observations on vortices in niobium and lead bismuth alloys.

The theory by Abrikosov led Anderson⁽¹³⁾ to develop a flux flow model in which the vortices would move from their lattice space and travel throughout the sample, resulting in a measurable dissipation. The model suggested that a current flowing through the superconductor would interact with the flux flowing in the normal region to produce a Lorentz force⁽⁴⁶⁾. He argued that if this force passed a critical value, then the fluxons would actually start to move through the sample, dissipating energy as they went.

Further work by Kosterlitz and Thouless⁽¹⁴⁾ and independently by Berezinskii⁽¹⁵⁾ established that if the system was two dimensional, for example, a strongly anisotropic superconductor; then an external magnetic field would not be necessary to produce quantised vortices. Dislocations in the film could produce a vortex-antivortex pair simultaneously. The pair would then separate because of the Lorentz force acting in opposite directions on the vortices. The theory further suggests that if vortices are produced simultaneously the number free to move would be dependent on the magnitude of the current density. The resulting dissipation, the resistance, would therefore be dependent on the current and not ohmic in nature. It also implies that a two dimensional superconductor could not sustain any current without the production of vortices. In other words the superconductor's critical current, the current required to drive the superconductor into the mixed or normal state from the superconducting state, would be

zero⁽⁴⁷⁾.

1.2.4: Bardeen, Cooper and Schrieffer

When Ginzburg and Landau first proposed their phenomenological theories, the first of the quantum mechanical (QM) models began to appear. The difficulty that had delayed the QM models was understanding the type of interaction responsible for superconductivity. In 1950, Frohlich⁽¹⁶⁾ proposed a mechanism involving a coupling between electrons via the positive ions in the lattice. Frohlich was able to show that the mechanism responsible for superconductivity in the non transition metals was due to the coupling of the electrons to the ionic lattice. Experimental results on isotopes of mercury gave support to this idea. It was from this theory that Bardeen, Cooper and Schrieffer⁽²⁾ were able to put forward a microscopic theory to explain superconductivity in 1956. The theory was the solution to the problem of a gas of electrons in the presence of an attractive interaction. Their theory was able to explain the Meissner Effect, the Isotope effect, the discontinuity in specific heat and was considered by many to be the correct theory of superconductivity.

The BCS theory, due to its importance, was soon followed by several papers offering reformulations of the BCS calculations. In 1959 Gorkov⁽¹⁷⁾ was able to show that the Ginzburg-Landau equations could be derived from the microscopic theory, thus adding strength to the validity of the phenomenological theories. Eliashberg⁽¹⁸⁾ then used Gorkov's method to derive an electron-phonon interaction that became the starting point for a theory on strong coupling superconductors. Carbotte⁽¹⁹⁾ later pointed out that this was applicable to situations where gap anisotropy is important, namely, high temperature superconductors.

1.2.5: Josephson Effect

Besides the theories described above, all of whose validity are somewhat in question, there is one theory that is likely to remain unaffected by the discovery of the high temperature superconductors. The theory was the work of Josephson⁽²⁰⁾.

Several years after the BCS and Abrikosov theories, Josephson, while considering certain quantum mechanical properties of the superconductors discovered that tunnelling of electron pairs could take place between a junction made from two superconductors. The problem he was considering was the behaviour of two superconductors separated by a very thin insulating or oxide layer. He demonstrated, that under certain conditions, tunnelling of superconducting Cooper pairs between the two superconductors could take place.

An experiment to investigate this theory was undertaken and found that the tunnelling did take place. A junction of this type is now called the Josephson Junction. By placing two of these junctions in parallel it was found that a very sensitive magneto interferometer could be produced. These devices are known as Superconducting *QU*antum *I*nterference *D*evices, SQUIDS. These are extremely useful for measuring very small magnetic signals, for example brain waves, and have already been in use for over a decade. SQUIDS made from the new HTS materials would have the advantage of requiring less refrigeration and would be far cheaper to run than conventional superconductors. More importantly to this work, is that YBCO films may be made up of many such junctions. This, along with the other theories, will be investigated more in chapter six.

1.3: The Discovery by Bednorz and Muller

The profound impact that high or room temperature superconductors would have

on society has led many groups to investigate materials that may become superconducting at high temperatures. Researchers over the years continued to search for these high T_c materials, although progress had become very slow. Experiments had shown that binary systems, systems consisting of two elements, existed with critical temperature greater than those of single elements⁽²¹⁾. This led to the idea that it may be possible to produce tertiary materials with even higher critical temperatures. The drawback to this philosophy is that there are thousands, possibly millions, of tertiary materials that could be produced. Work based on this idea, however, did pay dividends, with the peculiar discovery of the perovskite superconductors.

1.3.1: Perovskite Superconductivity

The mineral perovskite, CaTiO_3 , was first named in 1925 and large amounts of research were undertaken into this material after the discovery of ferro-electricity in 1943. The ferro-electric behaviour resulted from the off-centre atomic displacements in the material. These materials regularly occur in tetragonal, orthorhombic, rhombohedral and monoclinic structures. Only a few compounds of this nature are metallic. The discovery in 1973 by Lango and Raccah⁽²²⁾ of superconducting La_2CuO_4 was therefore very surprising. This was followed by Sleight⁽²³⁾ in 1975 with the $\text{BaPb}_{1-x}\text{Bi}_x\text{O}_3$ compound. $\text{BaPb}_{(1-x)}\text{Bi}_x\text{O}_3$ also exhibited superconductivity. (For $x > 0.35$ these alloys are semiconducting and have a bronze colour whereas for $x < 0.35$ the compound is black and metallic and superconducting at low temperatures). The critical temperatures of the barium, lead bismate and the lanthanum cuprate were lower than other materials in existence. The fact that materials of this type could become superconducting however, inspired research into these compounds. Throughout the Seventies and Eighties groups regularly replaced the alkaline metals for rare earths in the Lanthanum cuprate

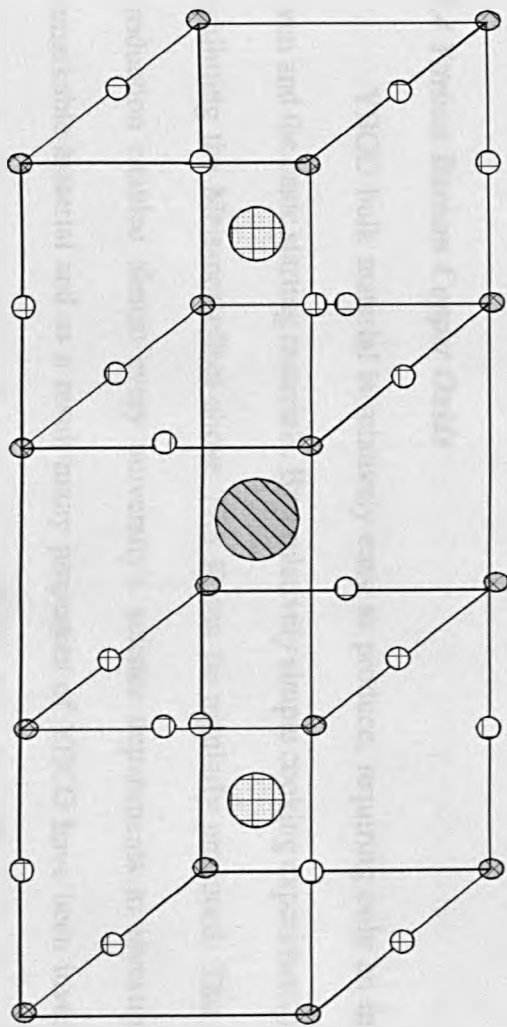
compound and it was as a result of these investigations that in 1986 Bednorz and Muller⁽²⁴⁾ discovered $\text{La}_{2-x}\text{Ba}_x\text{CuO}_4$ (LBCO). This material, described as a pseudo-ternary, was found to become superconducting at 30 Kelvin, better than previous materials by over 7 Kelvin. The results were to become arguably the most important in physics in the 1980's.

1.3.2: High T_c Superconductors

The discovery of LBCO renewed interest in superconductivity and groups immediately started to investigate the possibility of similar substances with even higher critical temperatures. Wu et al⁽⁴⁴⁾ realised that higher T_c materials may be produced by altering the internal pressure generated by a large A-B size difference in an ABCuO compound. In January 1987 they announced the discovery of a new perovskite like material consisting of Yttrium, Barium, Copper and Oxygen.

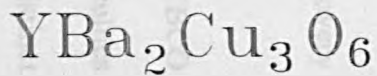
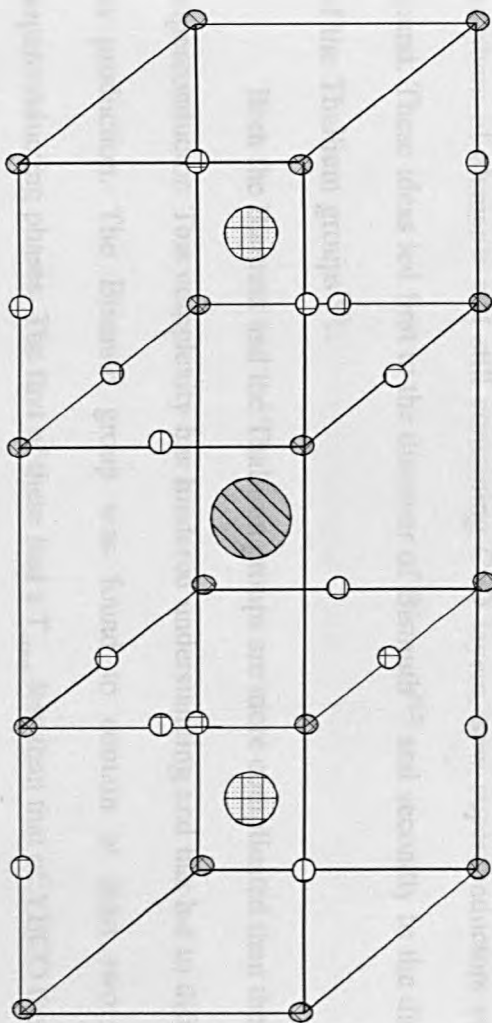
$\text{YBa}_2\text{Cu}_3\text{O}_x$, as the compound is now known, is an open, layered structure, with some similarity to a perovskite in the sense that the Cu ions in the lattice can be octahedrally co-ordinated, see figure 1.1. The material is the first true quaternary metallic structure and appears ceramic in nature. The metallic behaviour is a surprising discovery. More surprising however, is that when cooled to temperatures below 93 Kelvin, YBCO becomes superconducting. This discovery has resulted in massive amounts of work being published by groups around the world. Thousands of papers are now published every year on subjects relating to high T_c superconductivity.

With the discovery of YBCO, it became apparent that a new series of superconductors had been discovered. The world record for a critical temperature had risen by over 70 kelvin from what it had been only one year before. This led to the hope that materials with even higher T_c 's may exist. Theory had shown that the CuO layers



$\text{YBa}_2\text{Cu}_3\text{O}_7$
Orthorhombic

- ⊗ Copper
- ⊘ Yttrium
- ⊕ Barium
- Oxygen



Tetragonal

Figure 1.1

were probably responsible for the superconducting behaviour. This is not fully understood, however. Suggestions were made that by obtaining materials with greater numbers of elements and still containing CuO layers, new superconductors could be found. These ideas led first to the discover of Bismuth⁽⁴²⁾ and secondly to the discovery of the Thallium groups⁽⁴³⁾.

Both the Bismuth and the Thallium groups are more complicated than the YBCO superconductor. This complexity has hindered understanding and has led to difficulties in production. The Bismuth group was found to contain at least two distinct superconducting phases. The first of these had a T_{czero} less than that of YBCO the second having a T_{czero} of 110 Kelvin. The problem of producing the higher T_c phase however has slowed the progress of the research on this group.

Thallium also has production problems, not only is it difficult to produce the superconducting phase, but thallium is very toxic. Special care must be taken when handling this material. The toxic nature has reduced the amount of research that has been performed on this group. This is unfortunate since there exists a thallium group with a T_c of 128 Kelvin, the highest ever recovered.

1.4 Yttrium Barium Copper Oxide

YBCO bulk material is relatively easy to produce, requiring only an industrial oven and the basic starting materials. By a relatively simple cooking experiment, material exhibiting the Meissner effect above 77.3 K can be regularly produced. This ease in production enabled almost every university's science departments to investigate this remarkable material and as a result many properties of YBCO have been investigated. Papers on the production of bulk materials⁽²⁵⁾, thin films⁽²⁶⁾, critical currents⁽²⁷⁾, anisotropy⁽²⁸⁾, flux creep⁽²⁹⁾ and flux flow⁽³⁰⁾, as well as penetration depth⁽³¹⁾, surface

resistance⁽³²⁾, hall effect⁽³³⁾, susceptibility⁽³⁴⁾ and critical magnetic fields⁽³⁵⁾ have all been reported. It is these results that will help to validate the new theories of high temperature superconductivity.

1.4.1: Mechanisms for High Tc Superconductors

The results obtained from the experiments on of the high temperature superconductors has placed doubt on the validity of existing theories. Explaining the isotope effect in high temperature superconductors, which is far smaller than expected, as well as the type of interaction responsible for superconductivity, are just two of the problems theoreticians now face. For high temperature superconductors the question is what type of mechanism is responsible?

In conventional superconductors pairs of electrons with opposite spin and momentum, form a bound state that leads to a coherent and highly correlated many body superconducting state. This may still be true of course, since it must be realised that a full examination of BCS theory has not yet been accomplished. This will be a very difficult task. Anisotropic properties need to be included, anti-ferromagnetic ordering is also present and the possibility of the spin-triplet pairing being responsible for the observed behaviour must be investigated before this theory is discounted. This has not however stopped theoreticians proposing entirely new mechanisms for high temperature superconductors.

An important new theory is the Resonating Valence Bond model proposed by Anderson⁽³⁶⁾. In this theory the mechanism responsible for superconductivity is magnetic in origin and not BCS-like. The starting point is a two dimensional Hubbard model and this is important since the superconductivity results from the formation of a condensed state made up of holons. Bose-Einstein condensation cannot exist in a two dimensional

system, however, and this implies that the interplanar coupling is important within this model. Rice and Wang⁽³⁷⁾ have proposed a model in which a phonon interaction is responsible for the attraction between bosons. Alternatively Schrieffer et al⁽³⁸⁾ put forward a spin bag mechanism. The pairing mechanism here is a result of an attractive interaction between two holes that are able to overcome the coulomb interaction. These are not the only mechanisms proposed thus far. Models based on plasmons⁽³⁹⁾, excitons⁽⁴⁰⁾, and a strong coupling mechanism between oxygen holes and copper sites, have also been investigated⁽⁴¹⁾. The correct solution or solutions are at this point still unknown. With new theories being proposed regularly it is likely to take years to distinguish the good theories from the bad. It is because of this ambiguity in theoretical mechanisms that of the new theories only the RVB theory will be investigated or used to interpret the results in this thesis. The well established theories will be employed, making it possible for us to see the gaps in these theories.

1.5 References

- 1 Kamerlingh Onnes, H. Leiden Comm, *112b*, 124c, (1911)
- 2 Bardeen J., Copper L.N., Schrieffer J.R., Phys Rev *108*,1175, (1957)
- 3 Meissner W., Oschenfeld R., Naturwissen, *21*, 787, (1933)
- 4 Gorter C.J., Casimir H.B.G., Physica, *1*, 306, (1934)
- 5 London F., London H., Proc Roy Soc *A149*, 71, (1935)
Physica, *2*, 341, (1935)
- 6 Pippard A.B., Proc Roy Soc *A216*, 547, (1950)
- 7 Horie Y., Kuroumaru S., Zhao B., Qiu X., Zhang Y., Zhao Y., Xu P., Li L.,
Okubo H., Mase S., Physica *C170* (1990) 513
- 8 Ginzburg V.L., Landau L.D., Zh Eksperim, i Teor, Fiz *20*, 1064, (1950)
- 9 Landau L.D., Phys Z Sowjet U *11*, 545, (1937)
- 10 Abrikosov A.A., Dokl Akad Navk SSSR *86*, 489, (1952)
- 11 Abrikosov A.A., Zh Eksperim, i Teor, Fiz *32*, 1442, (1957)
(English Trans : Soviet Phys JEPT, *5*, 1174, (1957))
- 12 Cribier D., Jacrot B., Rao L.M., Farnoux B., Phys Lett *9* (1964) 106
- 13 Anderson P.W., Phys Rev Lett *9*, 309, (1962)
- 14 Kosterlitz J.M., Thouless D.J., J Phys C: Solid State Phys *6*, 1181, (1973)
- 15 Berezinskii V.L., Sov. Phys. JETP *34* (1972) 610
- 16 Frohlich J.C., Phys Rev *79*, 845, (1950)
- 17 Gorkov L.P., Zh Eksperim, i Teor, Fiz *36*, 1918 and *37*, 833 and 1407, (1959)
English Trans : Soviet Phys JETP *9*, 1364, (1959) and *10*, 593 and 998, (1960)
- 18 Eliashberg G.M., Zh Eksp Teor Fiz *38*, 966, 1960 (English Trans : Soviet
Physics JETP *11*, 969, 1960)
- 19 Carbotte J.C., 1977 Anisotropy Effects in Superconductors (H.W.Weber, New

- York, Plenum)
- 20 Josephson B.D., *Phys Lett.* **1** (1962) 251
 - 21 Tilley D.R., Tilley J. *Superfluid and Superconductivity* 3 ed. pp 13,23
(Adam Hilger 1990)
 - 22 Longo J.M., Raccach P.M., *J. Solid State Chem* **6**, 526, (1973)
 - 23 Sleight A.W., Gillson J.L., Bierstedt P.E., *Solid State Comms* **17**, 299, (1975)
 - 24 Bednorz J.G., Muller K.A., *Z Phys* **B64**, 189, (1986)
 - 25 McN Alford N., Button T.W., Birchall J.D., *Supercond. Sci. Technol.* **3** (1990) 1
 - 26 Takano S., Hayashi N., Okuda S., Hitotsuyanagi H.,
Physica C **162-164** (1989) 1535
 - 27 Ohlsen H., Stolt L., Hudner J., Ostling M., *Physica C* **153-155** (1988) 772
 - 28 Cava R.J., Batlogg A.B., *Nature* **332** (1988) 814
 - 29 Zhao B., Kuroumaru S., Horie Y., Yanada E., Aomine T., Qiu X., Zhang Y.,
Zhao Y., Xu P., Li L., Ohkubo H., Mase S., *Physica C* **176** (1991) 409
 - 30 Artemenko S.N., Gorlova I.G., Latyshev Y.I., *Phys Lett A* **138** (1989) 428
 - 31 Flueckiger P., Gavilano J.L., Leemann C., Martinoli P., Dam B.,
Stollman G.M., Srivastava P.K., Debely P., Hintermann H.E.,
Physica C **162-164** (1989) 1563
 - 32 Cooke D.W., Gray E.R., Houlton R.J., Javadi H.H.S., Maez M.A.,
Bennett B.L., Rusnak B., Meyer E.A., Arendt P.N., Beery J.G., Brown D.R.,
Garzon F.H., Raistrick I.D., Rollett A.D., Bolmaro B., Elliott N.E., Klein N.,
Muller G., Orbach S., Piel H., Josefowicz J.Y., Rensch D.B., Drabeck L.,
Gruner G., *Physica C* **162-164** (1989) 1537
 - 33 Hagen S.J., Lobb C.J., Greene R.L., Forrester M.G., Kang J.H.,

- Phys Rev B *41* (1990) 11630
- 34 Muller K.H., Physica C *168* (1990) 585
- 35 Tewksebury S.K., Hornak L.A., Hatamain M., Solid State Elec. *32* (1989) 947
- 36 Anderson P.W., Mater. Res. Bull. *8* (1973) 153, Science *235* (1987) 1196
- 37 Rice M.J., Wang Y.R., Phys Rev B *37* (1988) 5893
- 38 Schrieffer J.R., Wen X.G., Zhang S.C., Phys Rev Lett *60* (1988) 944
- 39 Varma C.M., Schmitt-Rink S., Abrahams E., Solid State Comm *62* (1987) 681
- 40 Rivalds J., Phys Rev B *36* (1987) 8869
- 41 Emergy V., Phys Rev Lett *58* (1987) 2794
- 42 Chu C.W., Bechtold J., Gao L., Hor P.H., Huang Z.J., Meng R.L., Sun Y.Y.,
Wang Y.Q., Xue Y.Y., Phys Rev Lett *60* (1988) 941
- 43 Sheng Z.Z., Herman A.M., El Ali A., Almasan C., Estrada J., Datta T.,
Maitson R.J., Phys Rev Lett *60* (1988) 937
- 44 Wu M.K., Ashburn J.R., Torng C.J., Hor P.H., Meng R.L., Gao L.,
Huang Z.J., Wang Y.Q., Chu C.W., Phys Rev Lett *58*, 908, (1987)
- 45 Quinn D.J., Ittner W.B., J. Appl. Phys. *33* (1962) 748
- 46 Gorter C.J., Phys. Letters, *1* (1962) 69
- 47 Kadin A.M., Epstein K., Goldman A.M., Phys Rev B *27* (1983) 6691

Chapter 2: REVIEW OF YBCO THIN FILMS

2.1: Introduction

Due to the large amount of papers that have been published over the seven years since the first discovery of YBCO, the task of carrying out a thorough analysis of the literature is onerous. In this chapter I have attempted to include as many papers as possible that have relevance to this thesis. This chapter is divided into two sections. The first section is concerned with the production of the thin films, and the second reviews the relevant electrical aspects of the thin films.

The first section reviews the deposition of thin films. This is a very important part of high temperature superconducting (HTS) research. Film quality and structural properties, for example, must be well understood if there is to be a cost effective method of producing devices from the new HTS materials. The reproducible deposition of YBCO thin films onto a variety of substrates will decide the extent that YBCO will be viable for use. Due to the importance of deposition and because of the complexities surrounding the techniques it is necessary to investigate the difficulties and successes encountered by other groups if high quality YBCO thin films are to be produced. The most important parameters are the temperature of the substrate during deposition, the gas pressure and content, and the composition of the target material. Further, the position of the substrate in the growth chamber and the substrate material are also important in film production. Each of these aspects will be reviewed below.

The possibility of superconducting devices operating at liquid nitrogen temperatures has inspired thousands of papers on parameters important to device fabrication. The second section reviews some of the more relevant (to this thesis) areas of this research. The behaviour of the transport properties will help in the understanding of high T_c materials.

2.2: Production of Thin Films

2.2.1: Introduction

Both thin films and bulk samples of YBCO prepared by different techniques are found to give similar superconducting transition temperatures^(1,2). The critical current densities of the films and bulk however vary by orders of magnitude^(1,3). The differences in the J_c are explained by differences in microstructure, in particular grain boundaries, defect density and crystallographic structure. A typical critical current, at 77 Kelvin, of bulk YBCO is 10^3 A cm^{-2} , compared with $4 \times 10^6 \text{ A cm}^{-2}$ for a thin film. It is this large difference in current carrying capabilities that prompted the view that devices dependent on the ability to carry large current densities would have to be based on thin films. The production of high quality superconducting thin films emerged therefore, as one of the most active areas of research into YBCO.

2.2.2: Substrate Materials

The production of thin films raised several questions that required attention before any success could be achieved. The choice of substrate material was one such question. The substrates were required to have large surface areas, be single crystal in nature and have a lattice constant very similar to that of YBCO. Single crystals were preferred since they offer the possibility of producing epitaxial thin films.

Results have proved that the superconducting phase of YBCO is orthorhombic. The room temperature lattice constants of this phase being $a=3.825 \text{ \AA}$, $b=3.887 \text{ \AA}$ and $c=11.68 \text{ \AA}$ ⁽⁴⁾. It was thus necessary to find single crystals with lattice constants similar to these values. It was due to these restrictions that the first substrate to be used was SrTiO_3 . Besides being available in highly polished single crystals with typical dimensions of $10 \times 10 \times 1 \text{ mm}$ this substrate also has an a-axis lattice value of 3.905 \AA . Comparing this

with YBCO it becomes clear that the two materials have a lattice mismatch in the a-axis of about 2 %. If the c-axis value of YBCO is compared with the a-axis value of SrTiO₃ it becomes clear that $3a_{\text{SrTiO}_3} = c_{\text{YBCO}}$ as a lattice mismatch of around 1/2 %. This is significant in so far as epitaxial films can only be deposited when the lattice mismatch is less than 1 %. This is therefore a prime candidate for epitaxial thin film deposition, and has been used many times for this purpose. SrTiO₃ does have one drawback however, and this is the large permittivity values, especially around 77 Kelvin. The permittivity of SrTiO₃ at 77 K is around 1000⁽⁵⁾. This is not a concern in the d.c. measurements. The microwave experiments however incur substantial losses because of the substrate effect and this will be particularly important when designing devices. To overcome this problem other substrates have been investigated. The most prominent being MgO. MgO has a lattice constant of 4.212 Å, this results in a 10 % mismatch in the a and b axis of YBCO, but only a 8 % mismatch with the c-axis. Thus while the mismatch between axis' is larger than hoped the permittivity of only 9.72 at 77 K (using a 4 GHz signal) makes this a useful substrate for device application⁽⁶⁾.

Recent attempts to deposit YBCO onto other substrates with device possibilities have given some very encouraging results. It is highly probable that one of the first uses of HTS materials will be in millimetre and microwave devices. It is therefore essential to use substrates with low permittivity. MgO does fit this criterion, although the lattice mismatch with YBCO is poor. Alternatively LaGaO₃, NdGaO₃ and LaAlO₃ offer good lattice matches of 0.1, 0.27⁽⁷⁾ and 0.92⁽⁵⁾ % respectively. The substrates also have low permittivities, namely LaAlO₃ = 27 at 1kHz⁽⁵⁾, 293 K, LaGaO₃ = 23.1 at 4 GHz, 77 K⁽⁶⁾, NdGaO₃ = 26 at 1kHz⁽⁷⁾. It is likely that future work will be performed using these substrates^(6,7).

2.2.3: Deposition Techniques

The methods used to produce the thin films of YBCO vary widely. They include thermal⁽⁶⁾ and electron beam evaporation⁽⁹⁾, laser ablation⁽¹⁰⁾, RF⁽¹¹⁾ and DC sputtering⁽¹²⁾, metal oxide chemical vapour deposition⁽¹³⁾, plasma spraying⁽¹⁴⁾ and MBE⁽¹⁵⁾. Publications have shown that each of these methods has been successful in producing high T_c superconducting thin films.

Each of these methods involves very complicated growth mechanisms. The complexity of the growth procedure originally made it very difficult to reproduce high quality thin films. Results quoted by a group as reproducible were often not producing thin films of equal quality when deposited in a different system using the same deposition conditions. This problem was particularly true in sputtering methods. Many groups report on the deposition of thin films by conventional on axis sputtering^(16,17). Experiments carried out in this work, like several others^(18,19), found that back sputtering was so severe that it was not possible to produce quality thin films using on axis sputtering.

2.2.4: R.F. Sputter Deposition

R.F. sputter deposition is an excellent method for thin film production, offering large area deposition and reproducibility. Its reproducible nature makes it particularly attractive for large scale production. This method like all those mentioned was not without problems. Growth parameters capable of producing reproducible high quality thin films have been difficult to determine. Changes in gas pressures⁽¹⁷⁾, substrate temperatures⁽²⁰⁾ and gas content⁽¹⁸⁾ have all been shown to influence deposition rates and quality of the thin films. Back sputtering has caused many problems⁽²¹⁾. Deposition temperature has also been shown to influence the orientation of the deposited YBCO⁽²⁰⁾.

Each of these factors need to be addressed and understood if devices are going to be manufactured on a large scale basis.

2.2.4.1: Gas pressure and Back Sputtering

From the work carried out on the deposition of thin films it has become clear that the gas pressure is very important in the deposition of high quality thin films. When using low pressure deposition severe back sputtering often occurs. This effect is probably due to the high energy O^- particles sputtering the lighter elements from the newly deposited thin film. Back sputtering can cause composition changes in the films⁽²¹⁾. The result is a poor superconductor and poor reproducibility, and is often accompanied by a rapid deterioration of the final film due to moisture⁽²²⁾. Various methods have been employed in an attempt to overcome this problem. Non-stoichiometric targets have been used to overcome the selective back sputtering effect^(23,24). Others have used high pressure deposition techniques to overcome this problem⁽²⁵⁾. The theory being, that at high pressures the oxygen ions undergo frequent collisions that result in a reduction in the energy of the O^- particles. A reduction in the energy of the particles leads to a reduction in the back sputtering. This approach has a second advantage in that high oxygen pressures can be used. High oxygen pressures are now thought to be essential for in situ growth.

In experiments using a 50:50 ratio of argon to oxygen have been reported for pressures varying from 4 - 120 Pascals⁽¹⁷⁾. The target material was stoichiometric YBCO and, to ensure no other factors could be responsible for the observations, both the substrate and the deposition temperature were held constant. The results showed that the films deposited at the lower pressures had large c-axis lattice constants (11.93 Å). This was thought to be due to crystal dilation. The films were found to have poor

superconducting qualities. Those films deposited at 120 Pascals were found to have a c - axis lattice parameter of 11.70 Å. This is almost equal to the bulk value of 11.68 Å. The films had good superconducting qualities, thus suggesting that a higher sputtering pressure is desirable. These results agree with work carried out by others using RF sputtering^(84,85).

2.2.4.2: Substrate Temperature During Deposition

Low temperature depositions have been used successfully to produce superconducting thin films. It was soon realised however, that the high temperature anneal required to convert the film from amorphous to a poly-crystalline or epitaxial state often led to film/substrate interactions that sometimes damaged the thin films. This method also had the disadvantage of requiring an oven complete with its own oxygen supply. To overcome this problem and to produce in situ thin films, work on high temperature deposition began. Results of this research soon showed that the use of the high temperature during deposition produced films that following a low temperature anneal were often superconducting.

The use of high temperature deposition is not limited to the R.F. sputtered films. For example, films deposited by chemical vapour deposition⁽²⁶⁾, co-evaporation⁽⁸⁾, Laser Ablation⁽⁷⁾ have all used high substrate temperatures during deposition to improve the quality of the thin films.

2.2.4.2.1: High Temperature Deposition

The high temperature deposition (680 - 780 °C) ensures that the tetragonal YBCO phase forms during the growth⁽⁴⁾. The low temperature anneal allows the oxygen to take up the correct occupancy of the high T_c orthorhombic phase. The ability to produce thin

films without the need for the high temperature anneal is desirable, particularly in multi layer devices. Furthermore by using a heated substrate it is possible to produce the finished thin films within the chamber⁽²⁸⁾.

2.2.4.3: Substrate Temperature and Thin Film Orientation

During the investigation of the heated substrate deposition, it became clear that the temperature at which the YBCO was deposited affected the final orientation. Several groups^(20,29) report that on (100) SrTiO₃ substrates low deposition temperatures, namely those below 730 °C, result in the deposition of a-axis YBCO. Films deposited above 750°C however have a c-axis orientation with the CuO planes parallel to the substrate. Further investigation of this phenomenon has shown that films deposited between 730 - 750 °C are a mixed phase of a and c - axis orientation. The degree of mixed orientation is dependent on the temperature. The films deposited near, but slightly below, 750°C generally contain more c- axis than a axis. For films deposited at temperatures just above 730°C the films are mostly a-axis. This phenomenon is not limited to films deposited on (100) SrTiO₃. Films deposited on SrTiO₃ (110) are also temperature dependent. Films deposited at lower temperatures tend to be (110) orientated, whereas, films deposited at temperatures greater than 800°C are generally (013) orientated⁽³³⁾.

The most likely reason for the change from a to c - axis of the YBCO films with temperature is the change in lattice constants with temperature, as mentioned above. At 700°C YBCO is tetragonal in orientation. The a axis lattice value of YBCO at 700°C is 3.896 Å rising linearly to 3.905 Å at 900 °C. The c axis value at 700 °C is 11.88 Å, rising almost linearly to 11.94 Å at 818 °C⁽²⁷⁾. Using these values it is possible to calculate the lattice values of the a and c axis at 760 °C. YBCO deposited at 760 °C on SrTiO₃ (100) is reported to be c-axis, whereas YBCO deposited at 700 °C on a similar

substrate is a axis oriented. Thus using the above values to calculate a and c at 760 °C gives $a=3.899 \text{ \AA}$ and $c=11.91 \text{ \AA}$. It is immediately clear that the changes in the values of a and c with temperature are very small. It is these small changes however, coupled with the equally small change in the a axis value of the SrTiO_3 that results in the shift from one orientation to the other. This can be explained using the following simplified example. Using the temperature dependence of YBCO given above it is possible to calculate a range of values for a and c axis for temperatures in the region 700-800 °C. If SrTiO_3 also under goes a similar linear expansion it is again possible to calculate a range of values for the specified temperature region. These values can then be used to calculate the lattice mismatch of YBCO with SrTiO_3 . Clearly, at lower temperatures the c-axis has a closer match than the a-axis. This results in YBCO growing with the c-axis normal to the substrate and the a-axis perpendicular to the substrate. At higher temperatures, however, the situation is reversed, resulting in c-axis growth perpendicular to the substrate as observed in experiment. In the mid range of the temperature region the lattice mismatch is similar for both orientations and there is therefore an equal opportunity for both to be deposited, resulting in the mixed phase. For the MgO (100) substrates the lattice mismatch between the YBCO and the MgO substrate is around 10%. This ensures that although the substrate lattice value will change with temperature the c - axis phase of the YBCO perpendicular to the substrate is the most prevalent orientation.

The most important point is that it is possible to choose, prior to deposition, the orientation of the YBCO thin films. This is particularly interesting to those studying the anisotropic nature of YBCO.

2.2.4.4: Off Axis Sputter Deposition

Even with the high temperatures during deposition and the high deposition pressure, problems with uniformity and film quality⁽²¹⁾ continued to arise. To overcome this, groups mounted the substrates at 90° to the target. The change from planar to off axis sputtering resulted in high quality, reproducible thin films being produced and this has been reported on several occasions^(30,31). Films produced this way are very similar to those produced by a successful post annealing method. As a rule thin films deposited in situ are superior to post annealed films in terms of epitaxy, surface smoothness and the reduction of substrate inter diffusion. A comprehensive study has shown that not only T_{co} is dependent on the growth conditions, but other parameters such as normal resistance, superconducting surface resistance are also growth dependent⁽²¹⁾.

Using this off axis arrangement Inameti et al⁽²⁷⁾ studied the effect of substrate position with respect to the target. The target was stoichiometric in nature, since it was argued that this would be the most commonly available composition. It is also the easiest to produce. Thin films were deposited without altering any of the growth parameters, except substrate position. The results showed that although all the films were grown at 90 degrees to the target, films deposited on substrates inside the plasma were of a poor quality and often had a low T_{co} . It was initially expected that the quality was due to damage caused by ion bombardment. Post anneal treatment did not, however, correct the damage, as it does in low temperature deposited films. It was assumed therefore that the film was not pure YBCO but contained other compounds, which acted as impurities. On increasing the distance of the substrate from the target film quality improved, though growth rate decreased. Results showed that films deposited on the edge of the plasma produced the higher quality superconducting thin films. These films required a low temperature anneal at 400°C in pure oxygen to produce the superconducting phase. The

position of the substrate is therefore very important. This method was used to successfully produce many high quality thin films.

2.2.4.5: Growth Mechanisms

It has been shown that by depositing at substrate temperatures between 700 - 800°C the tetragonal phase YBCO is produced. By cooling films produced by this method in an oxygen atmosphere, however, the films were found to be the orthorhombic superconducting phase⁽⁴⁾. Thus, by cooling the thin films in oxygen and annealing at around 400°C it was possible for the YBCO thin film to absorb oxygen. This does not however give us clues as to the deposition mechanism. The films were investigated using Scanning Transmission Microscopy in order to determine possible mechanisms. Some results have revealed that YBCO sputtered on MgO (100) and SrTiO₃(100) show an orientated surface with spiral growth on each grain⁽³²⁾. The effect of this growth method is not fully understood. Growth of this nature may result in many defects. The defects may cause flux pinning⁽³²⁾, hence the increase in current carrying capabilities of the thin films over single crystals. The growth mechanism is reported to be not one but three different processes. Measurements taken using STM of YBCO sputtered on MgO (100) and SrTiO₃(100) show that the clusters grow as spirals around screw dislocations⁽¹¹⁾. The films grown on SrTiO₃(110) substrates have an entirely different surface morphology thought to be a result not of spiral growth but ridge growth⁽²¹⁾.

The results suggest that the growth mechanism of the two orientations are different. Nucleation and island growth occurs on the MgO (100) and SrTiO₃(100) substrates and lateral epitaxial growth on the SrTiO₃(110) substrates, even though the films were deposited under the same conditions. In the experiments reported the MgO (100) and the SrTiO₃(110) substrates experienced the same growth conditions. Therefore,

the only variables concerned are substrate material and orientation. Furthermore, since "spiral growth" has been reported on both SrTiO₃(100) and MgO (100) but not on SrTiO₃(110) then it suggests that the growth mechanism is most certainly dependent on substrate orientation.

2.3: Film Characterisation

2.3.1: Introduction

Measurements on the electrical properties of the new high T_c superconductors are of physical and technical interest. Kinetic inductance measurements of superconducting thin films, for example, are used to give details of the superelectron concentration and the dissipation associated with vortex motion^(34,35). Experiments on critical current^(36,37), critical magnetic fields⁽³⁸⁾, Q factor^(39,40) and anisotropic behaviour^(41,42) are of technical interest since it will be these parameters that decide device limitations. On the other hand, temperature dependence of the superconductors can give clues to the transport mechanism responsible. Current-Voltage measurements^(43,44,45), B field^(46,47), specific heat capacity⁽⁴⁸⁾, muon spin⁽⁴⁹⁾, d.c. resistivity^(50,51), a.c. susceptibility^(52,53,54), Hall effect^(55,56), paraconductivity^(57,58), millimetre⁽⁵⁹⁾ and microwave^(60,61,62) measurements and isotope experiments⁽⁶³⁾ have all been performed so as to understand and categorise the physical properties of the new high temperature superconducting compounds.

2.3.2: Resistance Temperature Measurements

The most common experiment is likely to be that of temperature dependence of the resistance. The critical temperature and film resistivity are the parameters of most interest. The simple experiment requires only a constant current source and a volt-meter as well as the cooling unit. Results from these experiments can be used to give a fairly

accurate assessment of the quality of material. With closer analysis they also yield information concerning the coherence length and sheet thickness of the samples. This experiment was first carried out on YBCO based compounds in 1987 by Wu et al⁽⁶⁴⁾. They discovered that around 93 Kelvin the resistance of the sample fell sharply to zero. They were the first group in the world to produce a superconductor with a critical temperature greater than that of liquid nitrogen. This result was soon verified by other groups including Dubson et al⁽⁴³⁾ who realised that during the transition to superconductivity the bulk material passed through a region that was almost but not quite superconducting. Closer inspection of the transition region showed that the film actually became superconducting via an intermediate non ohmic region.

2.3.3: Non Ohmic Resistance Region

When bulk or thin films of YBCO are cooled through the transition temperature it becomes clear that the superconducting state is sometimes reached after passing through an intermediate state. The intermediate state was defined by Dubson et al⁽⁴³⁾ as the region between the zero dissipation temperature T_{cz} , namely the temperature at which the film is superconducting, and an upper temperature described as the zero resistance temperature T_{c1} . The zero resistance temperature is the temperature below which the electrical resistance appears to be zero. Closer inspection of this region just below T_{c1} reveals that the film is not superconducting since it does not have a critical current. The application of a current results in dissipation. The behaviour is non ohmic and can be summarised by $V = kI^\alpha$, where α is temperature dependent, becoming very large as the temperature reaches T_{c2} , and k is a constant. Below T_{c2} the HTS is in the superconducting state possessing a critical current and exhibiting the Meissner effect etc. The nature of the transition in the intermediate region is strongly dependent on weak

external magnetic fields. The discovery of this behaviour is of particular interest in describing the new superconductors.

The transition to the zero dissipation region in zero applied magnetic field takes place via an intermediate stage. It is thought that the intermediate stage may be due to vortices that flow throughout the sample. This implies that, since there is no magnetic field present, the mechanism responsible must be different to that normally expected for type II superconductors. Existing theory favours work developed by Kosterlitz and Thouless⁽⁶⁵⁾ and separately by Berezinskii⁽⁶⁶⁾ in which they examined excitations in thin film superconductors, Josephson-coupled superconducting arrays and superfluid helium films. When applied to HTS materials their work predicts the ability for vortex anti-vortex pairs to form at lattice defect points throughout the sample. The theory also predicts that these vortices, once in motion, will cause non-ohmic behaviour to be observed within the transition region. This vortex behaviour is different to that predicted by Anderson⁽⁶⁷⁾ in which an external magnetic field is required to produce the vortices. This peculiar current voltage behaviour has been observed on several occasions^(44,45). These results imply that some the YBCO thin films are similar to two dimensional superconductors⁽⁶⁸⁾. If this is the correct interpretation of the results, then the temperature at which dissipation stops, is the Kosterlitz-Thouless, Berezinskii temperature, T_{KTB} . Below this temperature the vortex-antivortex pair are bound within the crystal. Thus, only for temperatures below T_{KTB} will the idea of critical current and critical magnetic field have any real significance.

The behaviour of the electrical transport below T_C is also very interesting. An area of particular relevance to this thesis is the a.c. nature of the YBCO thin films within the superconducting region.

Normal metals are characterised by their surface resistance, which for films

thicker than the skin depth is simply the metal's bulk resistivity divided by the skin depth. In superconductors the resistive losses are much lower because at temperatures well below the transition temperature the vast majority of the electrons are in the paired collisionless state. However, for any non zero temperature, a small fraction of the electron population is not paired. These normal electrons scatter and dissipate energy in the presence of an electric field just as they do in normal metals. The paired electrons, although collisionless, do have inertia and a voltage is required to maintain their oscillating flow. The paired electron motion is out of phase with this voltage and does not dissipate energy, but rather presents a surface inductance⁽⁷⁰⁾.

The surface inductance of YBCO material has been investigated using an induction coil technique^(71,72). Although the perfect diamagnetic behaviour of low temperature superconductors, namely the complete Meissner effect, has been well understood for many years⁽⁷³⁾, the diamagnetic properties of the new materials are not as well understood. The behaviour of the susceptibility and relative permittivity are generally ignored when considering the a.c. aspects of superconductors. However, these properties may be of importance in high T_c superconductors. For example, the vortex has been considered to behave similar to a polarisable material resulting in the superconductor having an effective permittivity^(68,69). Secondly, the poor electrical properties also imply that the displacement current may be detectable⁽⁷⁴⁾. The behaviour of the vortices is most dominant around the critical temperature. Around T_c vortices can move throughout the sample, producing a measurable dissipation. The dissipation not only affects the resistive nature of the sample, but due to the dielectric nature of the vortices, the reactance of the superconductor may also be altered. The reactive nature of superconductors is of particular interest since theory has shown that reactance is normally due only to the kinetic inductance of the superelectrons⁽⁷¹⁾, which is then used

to calculate the penetration depth. Thus, it is quite possible that in YBCO thin films the observed reactance is a combination of kinetic inductance and vortex polarisation. It is worth-while therefore to investigate the penetration depth to determine if it deviates from that predicted by conventional kinetic inductance theory.

2.3.4: Penetration Depth

The penetration depth originally derived by the London s⁽⁷³⁾ is a measure of the super electron concentration. Its temperature dependence is of major interest since it reflects the change in superelectron density as the temperature approaches the critical temperature, T_c . The methods used to calculate the penetration depth vary to include muon spin resonance⁽⁴⁹⁾, microwave⁽⁷⁰⁾ or induction coil techniques⁽⁵¹⁾. The microwave technique uses a cavity injected with microwaves to determine the dissipation due to the surface impedance. The imaginary component of the surface impedance is directly proportional to the penetration depth.

The induction coil technique consists of two coils placed either side of the superconductor⁽⁷²⁾. One coil, the 'primary' coil, carries a current which induces a voltage to occur in the second 'pick up' coil. As the sample passes through the critical temperature region the YBCO film produces a flow of current to compensate for the existence of the magnetic field produced by the primary coil, namely, the Meissner effect. By recording the change in the pick up coil it is possible to obtain information about the nature of the film, such as the penetration depth. The third technique mentioned is that of muon spin resonance. In this experiment, muons are injected into the superconducting sample where they decay. By application of a magnetic field it is possible to calculate a term known as the muon depolarisation rate, which is proportional to the field distribution inside the sample. As the sample becomes superconducting the

partial expulsion of the magnetic field due to the Meissner effect results in an increase in the spin-relaxation rate. This parameter can then be used to calculate the penetration depth λ .

Results show that for $T=0$ K the magnitude of the penetration depth varies depending on the technique used. Early results of measurements on the penetration depth reported that it ranged from 21 \AA to 4500 \AA ⁽⁷⁶⁾. More recent results show that it is possible to distinguish between the penetration depth of the ab plane with that of the c-axis. Due to the anisotropic nature of the materials, these values vary considerably. Values of λ_{ab} range from 950 \AA to 1500 \AA compared with λ_c of 4500 \AA to 8000 \AA ⁽⁷⁶⁾. The variation of penetration depth with temperature has been investigated and compared to existing theory^(34,38,42,51). Both London and BCS theory, which are very successful at describing low temperature superconductors, have been used to describe the temperature dependence. For temperatures not too close to T_c , BCS theory and London theory, with $\lambda(0)=0.15\mu\text{m}$, give a good fit to $\lambda(T)$ in films, ceramics and single crystals with the sharpest transitions⁽⁷⁵⁾. Results appear to show that neither theory is adequate in explaining the behaviour of the new materials near to T_c . A reason for the deviation of the measured penetration depth from that predicted by London and BCS theory may be the two dimensional nature of the films. KTB theory predicts that the penetration depth will tend to infinity with the onset of flux flow, namely the production and movement of vortices within the transition region. This idea is supported by work on YBCO single crystals. The single crystal have very few defects resulting in very few vortices. Single crystals will therefore appear to be similar in behaviour to traditional superconductors, the results of penetration depth experiments tend to agree with conventional pairing theory⁽⁷⁵⁾. Work has shown that for thin films of YBCO with crystal defects, current carrying capabilities are greater than the results obtained from single crystals⁽⁸⁶⁾. In other

words the defects actually help pin the vortices, resulting in a film with increased current carrying capabilities.

Besides the low frequency induction coil, microwave and muon spin techniques, experiments have also been conducted within the radio frequency range, namely between 1-20 MHz^(51,57,76,77). The results from these experiments are particularly interesting since they give values of λ far larger than the values mentioned previously. The magnitude of the penetration depth for these experiments was between 15 and 100 μm , which is approximately 100 times larger than expected. Once again a good fit between experiment and BCS and London theories occurs for these experiments. Why are the values of λ so large? There are suggestions⁽⁷⁸⁾ that the high value is due to the penetration of the ac signal into the crystals of YBCO. The large value of the penetration depth then represents the average of the maximum penetration depth and the maximum crystal size. Thus the large value of λ is a result of the penetration of the RF field into the grains. In this analysis the film is assumed to be an array of two dimensional Josephson junctions and an investigation of this idea demonstrates that in bulk YBCO the observed penetration depth may be far larger than expected⁽⁸³⁾.

The two dimensional behaviour of the high temperature superconductors suggests that there is only weak coupling between the CuO_2 layers. This is because of the very short coherence length, which may be smaller than the distance between the CuO_2 layers. As mentioned, this allows the production of vortex-antivortex pairs to be a favourable energy state for the new high temperature superconductors. These vortices, once excited by thermal fluctuations will travel perpendicular to the current because of the Lorentz force. The reactive nature will appear as capacitive due to the effective dielectric nature the vortices. The KTB theory suggests that this will be observed as a jump in $\lambda^{-2}(T)$ as the temperature rises above T_{KTB} . This will result in a shift from the temperature

dependence predicted by London, BCS, GL etc. Results suggest that this behaviour seems to have occurred⁽³⁴⁾. The theory also suggests that it is possible to calculate the thickness of the 2 dimensional superconducting layer, which is expected to be of the order of the CuO₂ spacing, namely 2-5 Å. Results thus far have quoted values of s as sometimes far larger, varying from 6-500 Å^(34,57), the larger value of s , $s=500$ Å being equal to the film thickness.

Gasparov points out that a more successful method of calculating the sheet thickness, the coherence length, and the critical temperature may be found by examining the fluctuation paraconductivity. The paraconductivity is calculated from the four probe d.c. resistivity measurements, similar to those performed by Wu described earlier. The behaviour is predicted more accurately by the Lawrence and Doniach 2D-3D form of paraconductivity rather than the Aslamazov and Larkin's (AL) theory of two dimensional paraconductivity. The AL theory is based on the measurable paraconductivity that arises from the nucleation and decay of superconducting electron-hole pairs. This theory breaks down with the increase in coherence length around the critical temperature. The LD theory accounts for this increase and results show that values of s , T_c and ξ calculated from experiments using this theory match very closely the values quoted from work performed on YBCO single crystals. Results of these investigations show clearly that the coherence length is very small compared with penetration depth, suggesting that the films are strongly type II in nature.

2.3.5: Anisotropy

2.3.5.1: Superconducting Anisotropy

The new high temperature superconductors are all anisotropic. This phenomenon first identified in YBCO by Cava et al⁽⁴¹⁾ is very important for physical and application

studies. The very strong anisotropy of the penetration depth for example, is very important to models derived to explain high T_c superconductivity. The anisotropic behaviour is evident in other characteristics of YBCO besides penetration depth. The critical current density, for example, is orientation dependent. Results suggest that critical current flow within the ab plane exceeds that in the c-axis. The anisotropy can be observed in both the normal and superconducting phases. In the superconducting phase we have seen that it not only causes differences in critical current values but also influences the penetration depth⁽⁷⁶⁾. The anisotropy may also explain the very small coherence lengths between the CuO planes. It is thought that it may be because of these short coherence lengths that the two dimensional behaviour occurs within these samples. The anisotropy is observed in the normal phase by measuring the resistivity for the various crystal orientations. Anderson argues that it may be here that the clues to the current transport mechanism can be found.

2.3.5.2: Normal Behaviour and Carrier Type

In experiments carried out on single crystals of YBCO, the ratio of resistivity, between current transport in the c-axis and that in the ab plane was 30 at room temperature, rising to 80 around 100 K⁽⁸⁰⁾. Values larger than these have been quoted by Hagen et al who estimates the anisotropy ratio to be between 30 and 300⁽⁸¹⁾. In the BSCCO superconductors the anisotropic ratio is even higher, in the order of thousands⁽⁸²⁾.

Anderson points out that from the resonating valence bond theory terms representing the 'normal' electrical behaviour of YBCO thin films are very simple and results show that the predictions are confirmed for many films⁽⁷⁹⁾.

2.4: Summary

Many groups have reported different methods of thin film production. Thus it has become clear from this work that, although the exact growth mechanism is not fully understood, the reproduction of high quality thin films is possible. Using rf sputtering it is possible to deposit thin films on a regular, reproducible basis. Deposition in the off axis mode, with heated substrates and high sputtering gas pressures, has proved to be a most reliable method of producing the tetragonal phase of YBCO. This is then converted to the superconducting phase by a low temperature anneal in oxygen. The orientation of the YBCO thin films is dependent not only on the substrate material but also on substrate orientation and the temperature at which deposition takes place. The orientation of the films is important because of the anisotropic nature of YBCO.

The anisotropic nature of YBCO is apparent from the resistivity measurements and the penetration depth results. However precise values of the penetration depths for the various orientations are still unresolved. The anisotropy may explain the apparent two dimensional behaviour of YBCO thin films although other theories based on different mechanisms have been used to explain this behaviour.

On the theoretical side, the BCS and London theories appear to explain some of the behaviour of this new class of materials, and therefore may still be valid, requiring only modification. Anderson, among others, has proposed a new transport mechanism based on a resonating valence bond to explain the behaviour of the superconductors. Results again appear to agree to a certain extent with his predictions.

It is worth pointing out however, that others have speculated that the transition and all the behaviour observed and described above is due to a percolation transition, an entirely different mechanism to those mentioned. Using this theory, it is possible to predict the behaviour described above, namely the non ohmic behaviour in terms of

grains connected by Josephson junctions. The question of who is right or wrong, will not be made here, though it is worth bearing in mind that other theories do exist.

Within this thesis, I have attempted to investigate some points raised here, the behaviour of the penetration depth, the flux flow region, paraconductivity, 2D/3D crossover, film anisotropy, the T_{KTB} transition etc. To do this it is necessary to investigate more thoroughly the theoretical behaviour of these remarkable materials. This will take place in the next chapter.

2.5 References

- 1 McN Alford N., Button T.W., Birchall J.D., *Supercond. Sci. Technol.* **3** (1990) 1
- 2 Takano S., Hayashi N., Okuda S., Hitotsuyanagi H., *Physica C* **162-164** (1989) 1535
- 3 Matsuno S., Uchikawa F., Yoshizaki K., *J.J.A.P.* **29** (1990) L947
- 4 Jorgensen J.D., Beno M.A., Hinks D.G., Soderholm L., Volin K.J., Hitterman R.L., Grace J.D., Schuller I.K., Serge C.U., Zhang K., Kleefisch M.S., *Phys Rev B* **36** (1987) 3608
- 5 Yang W.H., Hou D.S., Li C.Z., Fan H., Zhang H., *Solid State Comm.* **75** (1990) 421
- 6 Turner C.W., HTS Workshop on Thin Films, Kings College London 1992
- 7 Mukaida M., Miyazawa S., Sasaura M., Kuroda K., *J.J.A.P.* **29** (1990) L936
- 8 Edlinger J., Fischer H., Koprio J.A., Peter G., Ramm J., *Physica C* **153-155** (1988) 778
- 9 Cooke D.W., Gray E.R., Houlton R.J., Javadi H.H.S., Maez M.A., Bennett B.L., Rusnak B., Meyer E.A., Arendt P.N., Beery J.G., Brown D.R., Garzon F.H., Raistrick I.D., Rollett A.D., Bolmaro B., Elliott N.E., Klein N., Muller G., Orbach S., Piel H., Josefowicz J.Y., Rensch D.B., Drabeck L., Gruner G., *Physica C* **162-164** (1989) 1537
- 10 Warner J.D., Bhasin K.B., Miranda F.A., *Supercond. Sci. Technol.* **3** (1990) 437
- 11 Reydet P.L., Brunel M., Marcus J., Escribe-Filippini C., Bruyere J.C., *Physica C* **153-155** (1988) 806
- 12 Poppe U., Schubert J., Evers W., *Physica C* **153-155** (1988) 776
- 13 Suhr H., Oehr C., Holzschuh H., Schmaderer F., Wahl G., Kruck T., Kinnen A., *Physica C* **153-155** (1988) 784
- 14 Chu W.F., Rohr F.J., *Physica C* **153-155** (1988) 802
- 15 Kwo J., Hong M., Trevor D.J., Fleming R.M., White A.E., Farrow R.C., Kortan A.R., Short K.T., *Appl Phys Lett* **53** (1988) 234
- 16 Tsuda K., Muroi M., Matsui T., Koinuma Y., Nagano M., Mukae K., *Physica C* **153-155** (1988) 788

- 17 Sakuta K., Iyori M., Katayama Y., Kobayashi T., J.J.A.P. **29** (1990) L611
- 18 Xi X.X., Li H.C., Geerk J., Linker G., Meyer O., Obst B., Ratzel F.,
Smithey R., Weschenfelder F., Physica C **153-155** (1988) 794
- 19 Guilloux-Viry M., Karkut M.G., Perrin A., Pena O., Padiou J., Sergent M.,
Physica C **166** (1990) 105
- 20 Chan S.W. et al, Appl Phys Lett
- 21 Eom C.B., Sun J.Z., Lairson B.M., Streiffer S.K., Marshall A.F.,
Yamamoto K., Anlage S.M., Bravman J.C., Geballe T.H., Laderman S.S.,
Taber R.C., Jacowitz R.D., Physica C **171** (1990) 354
- 22 Ono A., Takenouchis A., Ishizawa Y., JJAP **30** No. 3B L464 (1991)
- 23 Adachi H., Hirochi K., Setsune K., Kitabatake M., Wasa K.,
Appl Phys Lett **51** (1989) 3148
- 24 Kawasaki M., Nagata S., Sato Y., Funabashi M., Hasegawa T., Kishio K.,
Kitazawa K., Fueki K., Koinuma H., Jpn J. Appl Phys **26** (1987) L736
- 25 Tanabe K., Lathrop D.K., Russek S.E., Buhrman R.A.,
Jnl Appl Phys **66** (1989) 3148
- 26 Ushida T., Higashiyama K., Hirabayashi I., Tanaka S., J.J.A.P. **30** (1991) L35
- 27 See ref 4
- 28 Murray B.G., Raven M.S., Inameti E.E., Wan Y.M., Vacuum **43** (1992) 134
- 29 Linker G., Xi X.X., Meyer O., Li Q., Geerk J., Solid State
Comms **69** (1989) 249
- 30 Xiong G.C, Wang S.Z., Appl Phys Lett **55** (1989) 902
- 31 Teranda N., Ihara H., Jo M., Hirabayashi M., Kimura Y., Matsutani K., Hirata
K., Ohns E., Sugise R., Kawashima F., Jpn J. Appl Phys **27** (1988) L639
- 32 Hawley M., Raistrick I.D., Beery J.G., Houlton R.J., Science **251** (1991) 1587
- 33 Linker G., Xi X.X., Meyer O., Li Q., Geerk J., Solid State Comms **69** (1989) 249
- 34 Fiory A.T., Hebard A.F., Mankiewich P.M., Howard R.E.,
Phys Rev Lett **61**, 1419 (1988)
- 35 Artemenko S.N., Gorlova I.G., Latyshev Y.I., Phys Lett A **138** (1989) 428
- 36 Gallop J.C., Radcliffe W.J., Langham C.D., Sobolewski R., Kula W.,
Gierlowski P., Physica C **162-164** (1989) 1545
- 37 Chen D.X., Sanchez A., Puig T., Martinez L.M., Munoz J.S.,
Physica C **168** (1990) 652

- 38 Gammel P.L., Hebard A.F., Rice C.E., Levi A.F.J.,
Physica C **162-164** (1989) 1565
- 39 Dilorio M.S., Anderson A.C., Tsaur B.Y., *Phys Rev B* **38** (1988) 7019
- 40 Smith P.A., McN Alford N., Button T.W., *Elect. Lett.* **26** (1990) 1486
- 41 Cava R.J., Batlogg B., van Dover R.B., Murphy D.W., Sunshine S., Siegrist
T., Remeita J.P., Rietmann E.A., Zahurak S., Espinosa G.P.,
Phys Rev Lett **58** (1987) 1676
- 42 Carini J.P., Awasthi A.M., Beyermann W., Gruner G., Hylton T., Char K.,
Beasley M.R., Kapitulnik A., *Phys Rev B* **37** (1988) 9726
- 43 Dubson M.A., Herbert S.T., Calabrese J.J., Harris D.C., Patton B.R.,
Garland J.C., *Phys Rev Lett* **60** (1988) 1061
- 44 Horie Y., Kuroumaru S., Zhao B., Qiu X., Zhang Y., Zhao Y., Xu P., Li L.,
Okubo H., Mase S., *Physica C* **170** (1990) 513
- 45 Bungre S.S., Cassidy S.M., Caplin A.D., McN Alford N., Button T.W.,
Supercond. Sci. Technol. **4** (1991) S250
- 46 Karim R., How H., Seed R., Widom A., Vittoria C., Balestrino G., Paroli P.,
Solid State Comms. **71** (1989) 983
- 47 Zhao B., Kuroumaru S., Horie Y., Yanada E., Aomine T., Qiu X., Zhang Y.,
Zhao Y., Xu P., Li L., Ohkubo H., Mase S., *Physica C* **176** (1991) 409
- 48 Wang Y.R., Rice M.J., *Phys Rev B* **38** (1988) 7163
- 49 Harshman D.R., Aeppli G., Ansaldo E.J., Batlogg B., Brewer J.H.,
Carolan J.F., Cava R.J., Celio M., Chaklader A.C.D., Hardy W.N.,
Kreitzman S.R., Luke G.M., Noakes D.R., Senba M.,
Phys Rev B **36** (1987) 2386
- 50 Drabek L., Gruner G., Chang J.J., Inam A., Wu. X.D., Nazar L.,
Venkatesan T., Scalapino D.J., *Phys Rev B* **40** (1989) 7350
- 51 Gasparov V.A., Oganesyanyan A.P., *Physica C* **178** (1991) 445
- 52 Muller K.H., Collocott S.J., Driver R., Savvides N., *Supercond. Sci.*
Technol. **4** (1991) S325
- 53 Muller K.H., *Physica C* **168** (1990) 585
- 54 Doyle R.A., McLachlan D.S., *Supercon. Sci. Technol.* **4** (1991) S274
- 55 Thier N., Winzer K., *IEEE Trans. Magnetics* **25** (1989) 2293
- 56 Hagen S.J., Lobb C.J., Greene R.L., Forrester M.G., Kang J.H.,

- Phys Rev B *41* (1990) 11630
- 57 Gasparov V.A., Physica C *178* (1991) 449
- 58 Wordenweber R., Abd El Hamed M.O., Schneider J.,
Physica C *171* (1990) 1
- 59 Klein N., Muller G., Orbach S., Piel H., Chaloupka H., Roas B., Schultz L.,
Klein U., Peiniger M., Physica C *162-164* (1989) 1549
- 60 Portis A.M., Cooke D.W., Piel H., Physica C *162-164* (1989) 1547
- 61 Ganne J.P., Kormann R., Labeyrie M., Laine F., Lloret B.,
Physica C *162-164* (1989) 1541
- 62 Withers R.S., Anderson A.C., Oates D.E., Solid State Tech. Aug 1990 83
- 63 Leary K.J., zur-Loye H.C., Faltens T.A., Ham W.K., Michaels J.N., Stacy A.M.,
Phys Rev Lett *59* 1236 (1987)
- 64 Wu M.K., Ashburn J.R., Torng C.J., Meng P.H., Gao L., Huang Z.J., Wang Y.Q.,
Chu C.W., Phys Rev Lett *58* (1987) 908
- 65 Kosterlitz J.M., Thouless D.J., J. Phys *C6* (1973) 1181
- 66 Berezinskii V.L., Sov Phys JETP *34* (1972) 610
- 67 Anderson P.W., Phys Rev Lett *9* (1962) 309
- 68 Fiory A.T., Hebard A.F., Glaberson W.I., Phys Rev B *28* (1983) 5075
- 69 Kadin A.M., Epstein K., Goldman A.M., Phys Rev B *27* (1983) 6691
- 70 Gergis I.S., Kobrin P.H., Cheung J.T., Sovero E.A., Lastufka C.L.,
Deakin D.S., Lopez J., Physica C *175* (1991) 603
- 71 Flueckiger P., Gavilano J.L., Leemann C., Martinoli P., Dam B.,
Stollman G.M., Srivastava P.K., Debely P., Hintermann H.E.,
Physica C *162-164* (1989) 1563
- 72 Fiory A.T., Hebard A.F., Mankiewich P.M., Howard R.E.,
Appl Phys Lett *52* (1988) 2165
- 73 London F., London H., Proc Roy Soc *A149* (1935) 71
- 74 Raven M.S., Inameti E.E., Murray B.G., Wan Y.M., Supercond. Sci.
Technol *4* (1991) 225
- 75 Krusus Elbaum L., Greene R.L., Holtzberg F., Malozemoff A.P., Yesurun Y.,
Phys Rev Lett *62* (1989) 217
- 76 Gasparov V.A., Huguenin R., Pavuna D., van der Maas J., Solid State
Comms vol *69*, 12, pp.1147, 1989

- 77 Nag A., Joarder R., Ghosh B., Deb S.K., Phys Stat Sol **163** (1991) 211
- 78 Sridhar S., Schiffman C.A., Hamdeh H., Phys Rev B **36** (1987) 2301
- 79 Anderson P.W., Zou Z., Phys Rev Lett **60** (1988) 132
- 80 Tozer S.W. et al Phys Rev Lett **59** (1987) 1768
- 81 Hagen S.J., Jing T.W., Wang Z.Z., Horvath J., Ong N.P.,
Phys Rev B **37** (1988) 7928
- 82 Xing D.Y., Liu M., Ting C.S., Phys Rev B **38** (1989) 11992
- 83 Chen J.R., Physica C **153-155** (1988) 50
- 84 Tanabe K., Lathrop D.K., Russek S.E., Buhrman R.A.,
J. Appl. Phys **66** (1989) 3148
- 85 Shah S.I., Carcia P.F., Appl Phys Lett **51** (1987) 2146
- 86 Murphy D.W., Johnson D.W., Jin S., Howard R.E., Science **241** (1988) 922

Chapter 3: THEORY

3.1: Introduction

From chapter one and two it becomes apparent that the 'old' theories of superconductivity fail to predict some of the behaviour of high temperature superconductors. Results from experiments have revealed some remarkable behaviour. This has led to many new ideas being put forward to explain the new materials. This chapter is a review of some of these theories and ideas. This first section of this chapter reviews the well established theories, namely the theories developed after the discovery of the Meissner effect. The work under review will include the theories of Gorter Casimir⁽³⁾, London⁽⁴⁾ and Ginzburg-Landau⁽⁵⁾. Also, Abrikosov's⁽⁶⁾ work on type II superconductors including the theory and magnitude of quantised magnetic flux. The BCS⁽²⁾ theory will be reviewed particularly its reformulation by Gorkov⁽²⁴⁾. Each of these theories are important for defining parameters such as coherence length, penetration depth, critical temperature and critical current etc.

The second section is on more recent ideas concerning flux flow. This is in turn split into two subsections. The first section is a review of traditional flux flow theory as developed by Anderson⁽⁷⁾. The second of these is the theories relating to the possibility of 2 dimensional behaviour and its implications on flux production and behaviour. This section thus includes the Kosterlitz Thouless⁽⁸⁾ and Berezinskii⁽⁹⁾ (KTB) theories. These will be important in explaining the intermediate region observed in certain thin films. The production of spontaneous vortex and anti-vortex pairs will be reviewed. The dielectric nature predicted by this theory will be reviewed due to its possible effect on the temperature dependence of the penetration depth. The temperature dependence of the resistance within the intermediate region will also be reviewed in terms of the KTB theories.

The possibility of 2D behaviour also leads to several other interesting theories. The first of these is paraconductivity. The theory is of interest since it describes the behaviour of the normal phase of the superconductor, namely temperatures greater than the critical temperature. The work under review, namely the Lawrence-Doniach⁽²⁶⁾ 2 dimensional - 3 dimensional theory and Aslamazov Larkin⁽²⁵⁾ 2 dimensional theory make it possible to determine fundamental parameters such as coherence length and superconducting sheet thickness.

Also included in this section is the new theories of superconductivity namely Anderson's⁽¹⁷⁾ Resonating Valence Bond theory and its predictions for the normal resistive behaviour. These predictions have been investigated using single crystals elsewhere and have been found to give good agreement with theory. There will also be a review of the temperature dependence of the penetration depth from the RVB theory as developed by Rice-Wang's work.

In addition to these theories there will also be work performed by Ambegaokar and Baratoff⁽⁴¹⁾ (AB). This work interprets the superconducting thin films as an array of grains connected by Josephson junctions⁽¹⁰⁾. The derivation of the penetration depth is of particular importance since it predicts very large penetration depths to occur in certain circumstances and large values of penetration depth have been reported in the literature. The temperature dependence of the critical current as predicted by AB is also reviewed. There will also be a short section on 2D-3D behaviour and its possible effects on the resistive and reactive nature of YBCO thin films.

3.1.1: Experimental Background Introduction

The third section of the theoretical section is the interpretation of the results obtain from experiments. Throughout this thesis the electrical properties of YBCO thin

films have been investigated using an electrical contact technique. The transport measurements involve the use of a high frequency (13MHz) a.c. signal. This allows for the investigation of, not only the resistive properties of the thin film, but also the reactive properties. This is of particular interest since it is well known that when any ac field is applied to a superconductor, the material supports a potential difference. The potential difference that occurs is due to the inertia of the superelectrons. In 2D superconductors (or 3D films in a magnetic field), at temperatures near to the transition temperature, any electric field that occurs will be complicated by the flux flow phenomenon. Furthermore the insulating/semiconductor nature of electrons travelling perpendicular to the c-axis may cause a large displaced electric field. Although the displaced electric field is normally so small that it can be neglected, it may be large enough to have a measurable effect in the transition region⁽²⁰⁾. It is necessary therefore to analyze possible theoretical models that consider the properties mentioned.

The theory of a current travelling from a normal conductor into a superconducting thin film and then back into a normal conductor was first investigated by London⁽⁴⁴⁾. In the analysis given below this model is extended to include a displacement term that can be used to represent the anisotropic nature of the films. The analysis given below has been applied to a system operating with frequencies ranging from 0.1 - 13 MHz, a range that has not been investigated by electrical contact methods. It may be of interest to the reader to compare the results obtained from these experiments with those obtained from the non-contact techniques, which are usually favoured when carrying out this type of investigation. To do this it is necessary to review the current theory of ac effects within the GHz regions. In these experiments the surface resistance and inductance are measured using a resonant cavity technique and do not involve an electrical contact⁽²¹⁾. It is hoped that the results obtained here will

complement the results obtained by others using the microwave technique mentioned.

The final section in the theoretical chapter concerns the structural analysis of YBCO thin films. Using X-ray diffraction and Scanning Electron Microscopy (SEM) it is possible to investigate the structure of YBCO thin films. This information is of importance for several reasons. Firstly the HTS materials are anisotropic. Furthermore, some existing theories are based on the films being granular as opposed to epitaxial etc. It is important therefore to obtain, if possible, thorough structural properties of the thin films.

3.2: Theory

3.2.1: Meissner Effect

Initially, superconductivity was thought to exist because of a material acquiring infinite conductivity⁽¹⁾. Infinite conductivity would allow a material to pass a current without having an E field present. This idea, however, leads to problems with the energy states that the electrons occupy and, before 1933, theoreticians struggled with the idea of infinite conductivity. The theory until this period assumed that from an analysis of Maxwell's theories $\text{dB}/\text{dt} = 0$ and so B would be constant with time. This implies that any magnetic flux present during transition from the normal to the superconducting state would be 'frozen in' to the superconductor material. In other words the final state of the superconductor would be dependent on the initial state of the system.

In 1933 Meissner and Ochsenfeld⁽²²⁾ proved that the magnetic field was not frozen in but was instead expelled from the superconductor, i.e., the final state of the superconductor was independent of its state while normal. This result also showed that the superconductors were not simply perfect conductors but were also similar in nature to a perfect diamagnet. The results obtained by Meissner did not show perfect exclusion

of the magnetic field even for the highest purity materials. This led them to conclude that, without inhomogeneities and impurities, that may be intrinsic to the material, there would exist a pure superconducting state.

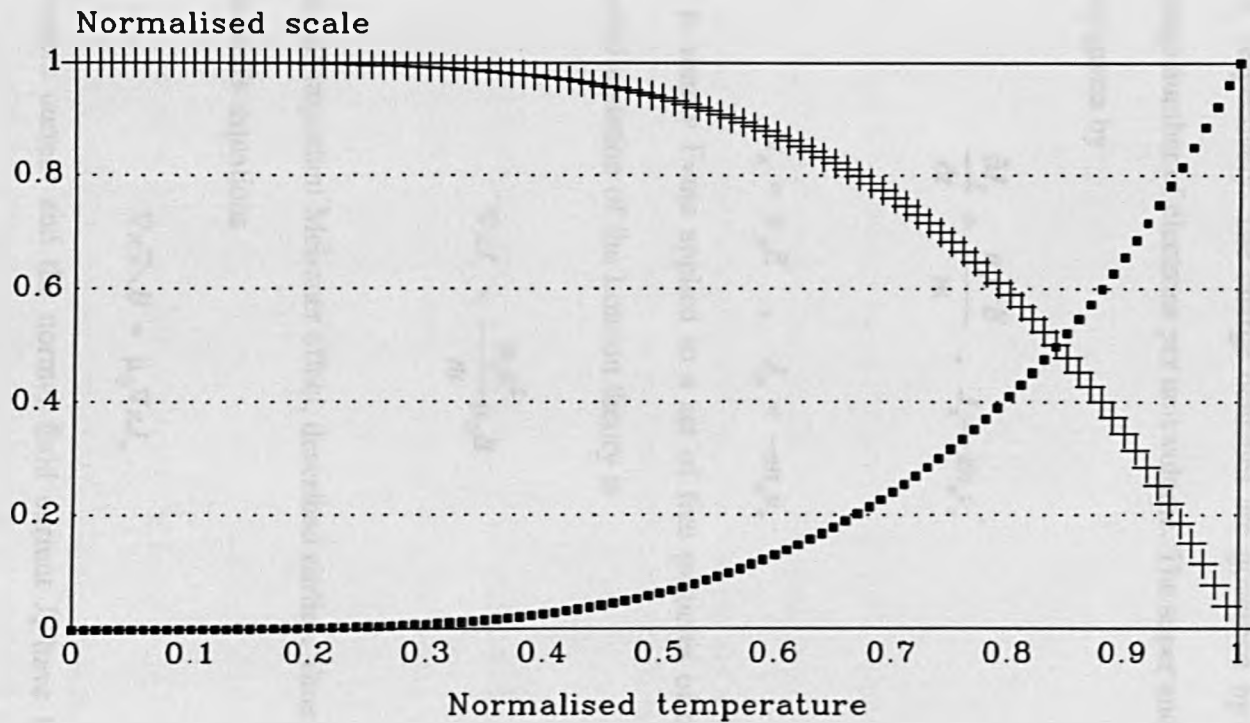
3.2.2: Gorter - Casimir

The work provided by Meissner led Gorter and Casimir⁽³⁾ to put forward the idea that the superconducting material could be considered to consist of two individual phases. A superconducting phase and a normal phase. By using the two fluid approach Gorter and Casimir proposed a phenomenological model based on the thermodynamic properties of a superconducting material. Their ideas proved to be in excellent agreement with practice⁽⁴⁴⁾. In their theory they assumed that besides the electrons in the normal state a proportion α are assumed to condense into a lower energy state. In the lower energy state the electrons are not scattered and are able to flow throughout the material without dissipation. The theory proposed that at $T = 0$ Kelvin, all the electrons in the system would be in the lower energy state and would therefore be superconducting. At the critical temperature, all the electrons would be in the normal state and the system would contain no superelectrons. From the work Gorter and Casimir proposed that the variation of the superelectrons with temperature could be represented by

$$\frac{n_s}{n_T} = 1 - \left(\frac{T}{T_c}\right)^4 \quad 3.1$$

where n_t is the total number of electrons and n_s is the number of electrons in the superconducting phase. The variation of superelectrons with temperature according to this theory can be seen in figure 3.1, note that the normalised temperature = T/T_c .

Theoretical temperature dependence of electrons in Gorter and Casimir model (Normalised)



▪ Normal Electrons + Super Electrons

Figure 3.1

3.2.3: London Theory

London theory, like Gorter and Casimir theory also proposed a phenomenological theory of the electromagnetic behaviour of superconductors. The theory is again based on a two fluid type model, with super fluid and normal fluid densities n_s and n_n , with velocities v_s and v_n respectively. The charge densities are governed by $n_s + n_n = n$, where n is the average number of electrons per unit volume. The super and normal fluid current densities are given by

$$\frac{\partial J_s}{\partial t} = \frac{n_s e^2 E}{m} , \quad J_s = -en_s v_s \quad 3.2$$

and

$$J_n = \sigma_n E , \quad J_n = -en_n v_n \quad 3.3$$

The first of these is simply $F=ma$ applied to a set of free particles of charge $-e$ and density n_s . The second equation of the London theory is

$$\nabla \times J_s = -\frac{n_s e^2}{m} \mu_0 B \quad 3.4$$

and this leads to the all-important Meissner effect, described earlier. Thus by taking the Curl of one of Maxwell's equations

$$\nabla \times \nabla \times B = \mu_0 \nabla \times J_s \quad 3.5$$

where the displacement current and the normal fluid current J_n have been ignored, namely the static Meissner effect. Combining equations 3.4 and 3.5 gives

$$\nabla^2 B = \frac{1}{\lambda_L^2} B , \quad \lambda_L = \left(\frac{m}{\mu_0 n_s e^2} \right)^{1/2} \quad 3.6$$

where λ_L is the London penetration depth. From the number of superelectrons n_s is

possible to obtain information about the density of states $N(0)$ and the Fermi velocity since,

$$n_s = \frac{2mv_F^2}{3}N(0) \quad 3.7$$

Furthermore the solution of equation 3.6 shows that the magnetic field decreases into the superconductor according to

$$B(x) = B(0)e^{-\frac{x}{\lambda_L}} \quad 3.8$$

This equation implies that as x becomes large, the magnetic field vanishes in the bulk of the material and one obtains perfect diamagnetism as required. It is in equation 3.4 that the London's added the important condition that $B=0$ inside the superconductor, irrespective of its history. For YBCO bulk, B is effectively zero for distances of $2 \mu\text{m}$ or more from the surface.

Note that the magnetic field does not vanish at a distance equal to the London penetration depth. The B field for $x=\lambda$, namely the B field at the penetration depth is

$$B(\lambda)=B(0)e^{-1} \quad 3.9$$

this is obviously non zero. In a thin film this result implies that the magnetic field may penetrate the entire film. This implies that perfect diamagnetism is not achieved⁽³³⁾. Many films used in this thesis are around $.2 \mu\text{m}$ thick, therefore the external magnetic field penetrates the whole film to some extent. Since it is likely that pinning centres are field dependent⁽²⁹⁾, the effect of magnetic field penetration may be observable in the behaviour of the flux flow.

Combining the result from Gorter - Casimir model with London's equation of

penetration depth, i.e.,

$$(1-x) = 1 - \left(\frac{T}{T_c}\right)^4 = \frac{n_s(T)}{n_t} \quad 3.10$$

one finds

$$\lambda(T) = \frac{\lambda(0)}{\left[1 - \left(\frac{T}{T_c}\right)^4\right]^{1/2}} \quad 3.11$$

This is not as good as that result forthcoming from microscopic theory though it is very good. Using this equation, namely by plotting λ against $(1-t^4)^{-1/2}$, where $t=T/T_c$ the gradient will be equal to $\lambda(0)$. Furthermore by extrapolating the graph back to $T=0$ Kelvin the intercept is also $\lambda(0)$. This result will be of particular use later.

3.2.4: Ginzburg Landau Theory

In 1937 Landau developed a theory for second order phase transitions⁽²³⁾. Although the theory was not valid for all transitions of this type, it did prove to be useful in describing superconductors. The theory was based on the idea that any phase transition could be represented by an order parameter. Ginzburg and Landau realised that the order parameter in a superconductor must be related to a macroscopic wave function. This idea lead them to develop an extraordinary theory based on the assumption that the superconducting state is characterised by a complex order parameter. This makes it clear that the system behaves according to quantum mechanics but on a macroscopic scale, which, although widely accepted now, was a very remarkable statement in 1950.

In going from the normal state to the ordered superconducting state, the material undergoes a phase transition, the new state being described by a complex order parameter

$$\Psi(r) = \Psi_0(r)\exp i\psi(r) \quad 3.12$$

which is a function of both position and time. Above T_c the normal state is the lowest in energy and so $\Psi = 0$ everywhere. Below T_c the order parameter gives an estimate of the fraction of superconducting electrons. This fraction varies from 0 at T_c to 1 at $T=0$ Kelvin. From the analysis it can be shown that the current density carried by the superconductor in a magnetic field is given by

$$j = -\frac{ieh}{2\pi m}(\Psi^*\nabla\Psi - \Psi\nabla\Psi^*) - \frac{4e^2}{m}\Psi^*\Psi A \quad 3.13$$

using the value of Ψ given above this then becomes

$$j = \frac{eh}{\pi m}|\Psi_0|^2\nabla\Psi - \frac{4e^2 A}{m}|\Psi_0|^2 \quad 3.14$$

if this is examined for large distances from the phase boundary, namely distances greater than the coherence length, ξ_0 , then

$$\nabla\Psi = 0 \quad 3.15$$

and therefore

$$j = \frac{-4e^2 A}{m}|\Psi_0|^2 = \frac{-4e^2\alpha A}{m\beta} \quad 3.16$$

again using Maxwell's equation linking current and magnetic field, namely, $\nabla\times B = \mu_0 j$, and combining with the equation 3.16 this gives

$$\nabla^2 B = \frac{4e^2\mu_0\alpha}{m\beta}B = \frac{B}{\lambda_{GL}^2} \quad 3.17$$

where λ_{GL} is known as the Ginzburg Landau penetration depth

$$\lambda_{GL} = \left(\frac{m\beta}{4e^2\mu_0\alpha} \right)^{1/2} \quad 3.18$$

This theory goes further to predict that ξ will have the same temperature dependence as the penetration depth but this is not supported by experiment. This is not surprising since the theory is only valid very close to T_c . By comparing this equation with the result obtained by the Londons, it is clear that the term n_s has been replaced by $\beta/4\alpha$. β is a constant and α is represented by

$$\alpha = k \frac{T_c}{T_c - T} \quad 3.19$$

comparing this temperature dependence with that in equation 3.11, it becomes clear that in the limit $T \rightarrow T_c$ they are the same, namely

$$\frac{1}{1 - (T/T_c)^4} \rightarrow \frac{1}{1 - T/T_c} \quad 3.20$$

as $T/T_c \rightarrow 1$. This is most easily demonstrated graphically. It is possible to represent the Ginzburg-Landau penetration depth by

$$\lambda_{GL}^2 = \lambda_{GL}(0)^2 \frac{T_c}{T_c - T} \quad 3.21$$

where $\lambda_{GL}(0)$ would be the zero temperature penetration depth. Taking logarithms of both sides this becomes

$$2 \ln \frac{\lambda_{GL}}{\lambda_{GL}(0)} = - \ln \frac{(T_c - T)}{T_c} \quad 3.22$$

Thus by plotting $2 \ln \lambda_{GL}/\lambda_{GL}(0)$ against $\ln (T_c - T)/T_c$, the normalised temperature, the resulting curve will be a straight line. Performing a similar task on the London penetration depth

$$2\ln \frac{\lambda_L(T)}{\lambda_L(0)} = -\ln \frac{(T_c^4 - T^4)}{T_c^4} = -\ln \frac{(T_c - T)}{T_c} - \ln \frac{(T_c^2 + T^2)(T_c + T)}{T_c^3} \quad 3.23$$

and by again plotting $\ln(\lambda_L(T)/\lambda_L(0))$ against $\ln(T_c - T)/T_c$ it is possible to obtain a very similar curve. Overlaying one curve upon the other, (as shown in Figure 3.2, page 58), it becomes apparent that for values of $(T_c - T)/T_c < 0.1$ the curves are the same. If therefore $T > 0.9T_c$, namely that $T > 81$ Kelvin in a film with $T_c = 90$ K, the curves are the same, except for a small scaling constant. The significance of this becomes apparent when considering Gorkov's⁽²⁴⁾ reformulation of BCS theory using Green's theorem and the experimental results.

3.2.5: Bardeen, Cooper and Schrieffer Theory (BCS theory)

The BCS theory was the first successful microscopic quantum mechanical model of superconductivity. The theory was the solution to the problem of a gas of electrons in the presence of an attractive interaction. In this solution the repulsive Coulomb interaction is overcome by the coupling of the electrons to the ionic lattice, as proposed several years earlier by Frohlich⁽³⁴⁾. The theory was able to explain with accuracy the various properties associated with superconductivity, the Meissner effect, isotope effect, etc. Due to its importance and success, it was soon followed by many papers offering reformulations etc. One of the most applicable to this thesis was the work of Gorkov⁽²⁴⁾.

Gorkov realised that, with the use of Green's theorem, it was possible to redefine the Ginzburg Landau equations from the BCS theory. He discovered that for a 'dirty' superconductor, namely a superconductor with a coherence length far greater than the mean free path, the terms α and β , defined above by Ginzburg and Landau, could be represented by

$$\alpha = 1.36 \frac{\hbar^2}{2m} \frac{1}{\xi_0 l} \frac{T - T_c}{T_c} \quad 3.24$$

$$\beta = 0.2 \frac{1}{N(0)} \left(\frac{\hbar^2}{2m} \frac{1}{\xi_0 l} \right)^2 \frac{1}{(k_B T_0)^2} \quad 3.25$$

where ξ_0 is the coherence length and $N(0)$ is the density of state. Substituting these equations into the GL penetration depth gives

$$\lambda_{GL}^2 = \frac{1.838 \cdot 10^{-2} \hbar^2}{e^2 \mu_0 N(0) \xi_0 l k_B^2 T_c^2} \frac{T_c}{|T - T_c|} \quad 3.26$$

Gorkov also pointed out that

$$\lambda_{GL}^2 = .378 \lambda_L(0)^2 \frac{\xi_0}{l} \frac{T_c}{|T_c - T|} \quad 3.27$$

It is immediately obvious therefore that

$$\lambda_L(0)^2 = \frac{4.862 \cdot 10^{-2} \hbar^2}{e^2 \mu_0 N(0) \xi_0^2 k_B^2 T_c^2} \quad 3.28$$

Comparing this with the London penetration depth given by equations 3.6 and 3.7

$$\frac{4.862 \cdot 10^{-2} \hbar^2}{e^2 \mu_0 N(0) \xi_0^2 k_B^2 T_c^2} = \frac{3}{\mu_0 e^2 2 v_F^2 N(0)} \quad 3.29$$

with a little rearranging this becomes

$$\xi_0 = 0.18 \frac{\hbar v_F}{k_B T_c} \quad 3.30$$

the coherence length, where v_f is the Fermi velocity. Thus given $\lambda_L(0)$ it is possible to calculate $N(0)\xi_0^2$. If the value of the coherence length can be determined it is possible to calculate the density of states of the YBCO thin film and the Fermi velocity. The coherence length can be determined from the theories of paraconductivity.

Theoretical temperature dependence
of London and G-L penetration depth (Normalised)

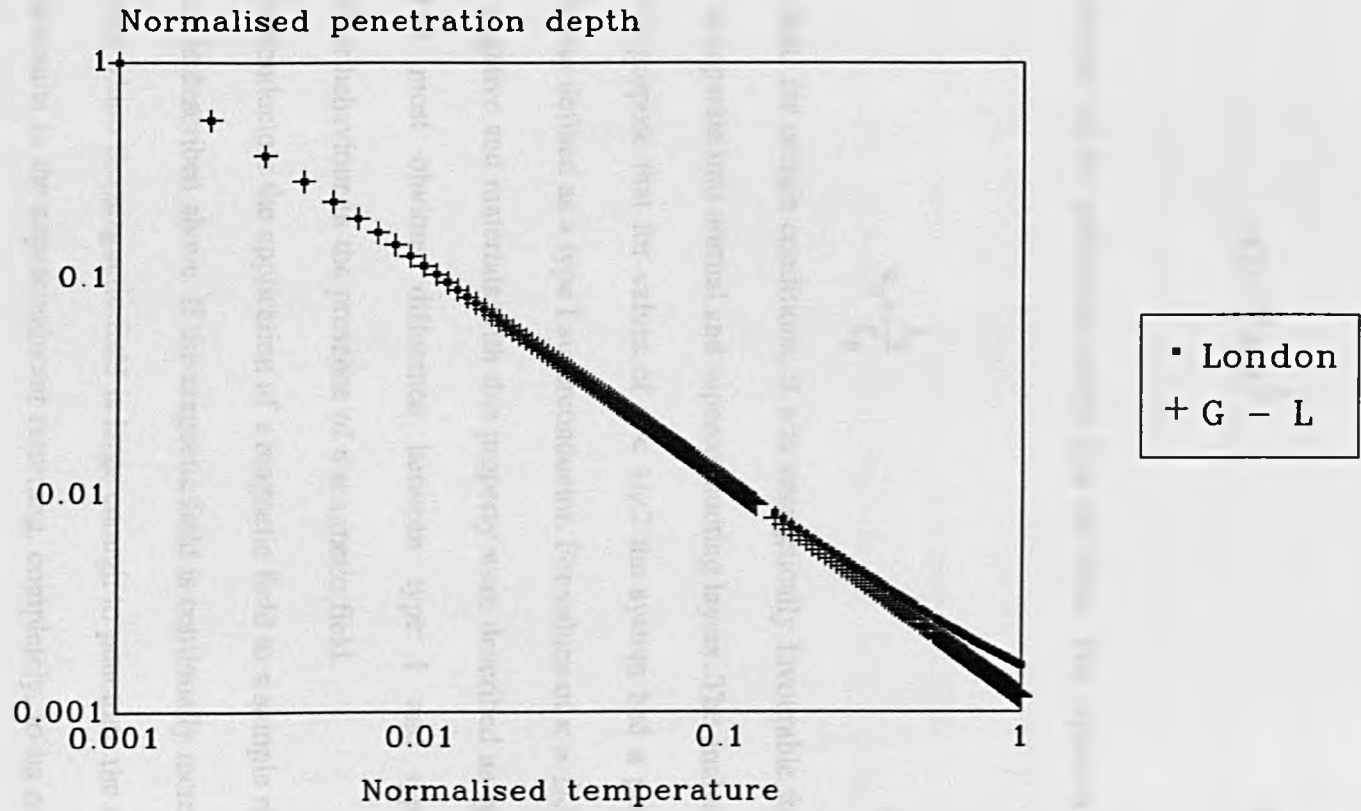


Figure 3.2

3.2.6: The Ginzburg - Landau parameter, H_{C1} and H_{C2}

In the original paper by G - L, they defined a dimensionless parameter κ by the expression

$$\kappa(T) = \frac{m}{2} eh\beta^{\frac{1}{2}} \quad 3.31$$

since they were unaware of the coherence length ξ_0 at the time. The equation later became

$$\kappa_0 = \frac{\lambda_0}{\xi_0} \quad 3.32$$

London had shown that, for certain conditions, it was energetically favourable for the bulk of the material to separate into normal and superconducting layers. The analysis by G - L went further to propose that for values of $\kappa < 1/\sqrt{2}$ the system had a positive surface energy and it was defined as a type I superconductor. For values of $\kappa > 1/\sqrt{2}$ the surface energy was negative and materials with this property were described as type II superconductors. The most obvious difference between type I and type II superconductors is their behaviour in the presence of a magnetic field.

In type I superconductors the application of a magnetic field to a sample results in the Meissner effect as described above. If the magnetic field is continually increased, there will come a point where the magnetic field is large enough to penetrate the entire superconductor. This results in the superconductor returning, completely, to its normal state. The magnetic field required to achieve this transition is called the critical field and is often referred to as H_C or H_{C1} . The behaviour of type II superconductors in magnetic fields is slightly more complicated. If a small magnetic field is applied the Meissner effect occurs, as expected. When the magnetic field is increased passed H_C however,

rather than the superconductor returning to the normal phase, it first enters an intermediate or mixed phase. The mixed phase allows the partial penetration of the magnetic field, while still retaining superconducting properties. A further increase in the applied magnetic field results eventually in the normal properties being restored. The magnetic field required to induce the mixed state is known as H_{C1} , where as the magnetic field required to drive the type II superconductor into the normal state is H_{C2} .

3.2.7 Abrikosov Theory

Following the work of Ginzburg and Landau, Abrikosov published a theory explaining the peculiar magnetic properties of type II superconductors. The theory was based on a 2 dimensional periodic array of vortices. The core of each filament contained a magnetic flux and was to be surrounded by a vortex of superconducting electrons. In 1950 London had suggested that a flux trapped by a superconducting ring would be quantized. London had foreseen a situation in which a superconducting ring would trap a quantized amount of flux, given by

$$\Phi = \frac{h}{2e} \tag{3.33}$$

and in type I superconductors this could only be achieved by using a superconductor with the geometry of a ring. In type II material the situation is different. Abrikosov proposed that flux quantisation could occur in any geometry because the mixed state consists of superconducting regions circling normal regions. The normal regions allow flux to penetrate them. The flux flowing through the normal region must be quantised. Results showed that flux quantisation in type II superconductors did occur. Experimental results also showed that even at values close to H_{C2} each filament carries only one flux

quantum. The idea of single fluxons is particularly important when considering results in which large amounts of flux are observed, since it implies that flux bundles, namely a batch of individual flux grouped together, most occur.

3.2.8 Type II Superconductors

Since it is possible for the coherence length to be shorter than the penetration depth, even in a pure superconductor, it is more likely to be the case in superconductors with high critical temperatures since

$$\xi_0 = 0.18 \frac{h\nu_0}{2\pi k_B T_c} \quad 3.34$$

Such substances are known as intrinsic type II superconductors.

3.2.8.1 YBCO and Type II Superconductivity

For YBCO, $\kappa \gg 1/\sqrt{2}$ and YBCO is therefore a type II material. It is energetically more favourable for YBCO superconductors to exist in a mixed state of normal/superconductor material under certain conditions. Measurements show that there does not appear to be a H_{c1} value for bulk YBCO⁽¹²⁾. In other words there is no lower limit below which the material behaves as if it were type I. On becoming superconducting the YBCO material exists in a mixed state of fluxons and superconductor. The reasons and the consequences of this behaviour will be discussed below.

3.2.9 Paraconductivity

In a magnetic system, the magnetic susceptibility can be represented by the Curie Weiss Law

$$\chi = \chi_0 \frac{T_c}{T - T_c} \quad 3.35$$

as the temperature tends towards the critical temperature T_c , the susceptibility increases and becomes very large. The result of this is that the spin system becomes spontaneously arranged at the phase change. It was realised that in superconductors a similar effect may be at work, namely that as $T \rightarrow T_c$ the conductivity diverges. Aslamazov and Larkin⁽²⁵⁾ investigated this idea and realised that the conductivity of a thin film could be represented by

$$\sigma_{AL}^{-1} = \frac{8sh}{\pi e^2} \frac{T - T_c}{T_c} \quad 3.36$$

where s is the thickness of the superconducting sheet. This is an important parameter since it represents the thickness of the superconducting sheet which is not necessarily equal to the thickness of the thin film. This is particularly true in 2 dimensional systems, where s will be very small. Gasparov⁽¹⁹⁾ point out however that due to the peculiar nature of these HTS materials it is more appropriate to replace equation 3.36 with the Lawrence Doniach⁽²⁶⁾ 2D-3D form of paraconductivity

$$\sigma_{LD}^{-1} = \frac{8sh}{\pi e^2} \left[1 + \left(\frac{2\xi_0}{s} \right)^2 \frac{T_c}{T - T_c} \right]^{1/2} \frac{T - T_c}{T_c} \quad 3.37$$

The conductivity can be calculated from experiment using

$$\sigma_{LD}^{-1} = [\rho_N(T)^{-1} - \rho(T)^{-1}]^{-1} \quad 3.38$$

where ρ_N and ρ represent the normal resistivity and the resistivity of the sample respectively. By examining the region close to T_c it becomes clear that if

$$\left(\frac{2\xi_0}{s} \right)^2 \frac{T_c}{T - T_c} \gg 1 \quad 3.39$$

then the above expression for σ_{LD}^{-1} simplifies to

$$\sigma_{LD}^{-1} \sim \frac{16h\xi_{L0}}{\pi e^2} \left(\frac{T-T_c}{T_c}\right)^{1/2} \quad 3.40$$

By plotting σ_{LD}^{-1} against $[(T-T_c)/T_c]^{1/2}$ the gradient would be

$$\frac{16h\xi_{L0}}{\pi e^2} \quad 3.41$$

and hence, the coherence length. The coherence length value can then be substituted to calculate the sheet thickness, s . The values of coherence length and sheet thickness may prove to be very important to the understanding of the YBCO thin films.

3.3 Flux Dissipation in YBCO

3.3.1 Anderson's Flux Flow Theory

The application of a magnetic field to a type II superconductor that exceeds the H_{C1} value, results in the penetration of magnetic flux into the sample. The flux lines are quantised with a flux quantum given by

$$\Phi_0 = \frac{h}{2e} \quad 3.42$$

In 1962 Gorter⁽²⁷⁾ put forward the theory that these flux quanta would experience a Lorentz force if a transport current were to flow through the sample. The magnitude of this force being

$$F_L = J \times \Phi \quad 3.43$$

perpendicular to the direction of flow. Anderson⁽⁷⁾ then went further to suggest that if this force exceeded the restraining force due to the pinning potential then the flux could actually move throughout the sample. The movement of flux would result in a measurable dissipation and this dissipation was first observed in 1965 by Giaever⁽²⁸⁾. The

fluxons are held in place by pinning centres/sites. The pinning sites are potential wells that have an energy U_0 . This energy must be overcome if flux are to flow. The sites thus prevent the movement of flux until the transport current is large enough to produce a Lorentz force capable of displacing a flux from the pinning site. The movement of flux can be viewed as the end of superconductivity. The current required to produce flux motion can therefore be called the critical current. In YBCO thin films the critical currents are often very large, in the order of 10^6A/cm^2 thus implying that effective pinning takes place. The pinning sites are thought to be because of defects in the thin film. It is possible to test this idea using single crystals of YBCO. Single crystals have far fewer defects than thin films and therefore also have fewer pinning centres. If the defects are pinning centres then the movement of flux would be most easily achieved in the system with fewest defect. This would result in the single crystals having a lower critical current than that of a thin film. It is found that this is indeed the case⁽⁴³⁾.

The Lorentz force is also helped by the thermal energy in the system. The thermal energy can enable the flux lines to escape from the pinning centre. Once free the flux lines are driven by the Lorentz force. The thermally activated behaviour can be summarised by the equation

$$R_{net} = v_0 \exp\left(-\frac{U_0}{k_B T}\right) \quad 3.44$$

where v_0 is the attempt to escape rate or attempt frequency and R_{net} is the number of fluxons free to move under the direction of the Lorentz force. The work done due to the Lorentz force is given by

$$\Delta W = JBV^*d \quad 3.45$$

where V^* is the volume of magnetic flux moving with the de-pinned flux line and d the

distance over which that volume moves. By realising that U_0 is altered by ΔW , namely

$$U_F = U_0 - \Delta W, \quad U_B = U_0 + \Delta W \quad 3.46$$

where U_F is the preferred hopping direction and U_B is the backward hopping direction.

It is thus possible to recalculate R_{net} using this result, this then becomes

$$R_{net} = 2v_0 \exp\left(-\frac{U_0 - \Delta W}{k_B T}\right) \quad 3.47$$

Considering the case when $\Delta W = U_0$, the transport current used to produce ΔW would represent the critical current, therefore

$$J_c = \frac{U_0}{BV^*d} \quad 3.48$$

R_{net} then becomes

$$R_{net} = 2v_0 \exp\left(-\left(1 - \frac{J}{J_c}\right) \frac{U_0}{k_B T}\right) \quad 3.49$$

This translates into a resistivity ρ (using $E = vB$, $v = R_{net} a_0$ and $\rho = E/J$) given as

$$\rho = \frac{2v_0 a_0 B}{J} \exp\left(-\left(1 - \frac{J}{J_c}\right) \frac{U_0}{k_B T}\right) \quad 3.50$$

From work on YBCO single crystals, even for temperatures approaching T_c , U_0/k_B is approx 10^5 K in a 0.1 T field⁽²⁹⁾. The resulting flux flow is, according to this theory, very small. This result implies that for small fields and currents the resistance will be negligible. Extrapolating the graph of resistance against B field back to a point where $B=0$, namely a point where the applied field is below H_{c1} , this theory predicts that the resistance will be zero. Results show however that in thin films of YBCO there is a substantial zero B field resistivity. The magnitude is larger than that expect from the above theory. To account for this behaviour it is necessary to examine theory put forward by Kosterlitz and Thouless⁽⁸⁾ and separately by Berezinskii⁽⁹⁾. This work is based

on a two dimensional systems.

3.3.2 *Kosterlitz-Thouless, Berezinskii Flux Flow*

The model of flux flow described by Anderson and outlined above was found to be consistent with magnetic field results. As mentioned, however, when the applied magnetic field was zero the flux flow was not zero as proposed in Anderson's model. To explain this behaviour, theoreticians turned to an alternative theory. The theory favoured by most is that proposed by Kosterlitz and Thouless and by Berezinskii. The original theory is based on the two dimensional ordering of a helium system. It was realised however that this system could be equally valid in describing a two dimensional superconducting system. Work on low temperature superconductors confirmed that this was indeed the case. The theory depends on the system under investigation being two dimensional in nature. From the literature it became clear that some researches believe that the superconducting sheet thickness of YBCO may be as small as $6.4 \text{ \AA}^{(19)}$, thus implying that the film is very thin indeed. The KT theory predicts, among other things, a transition to occur in 2 D systems. One key feature of this transition is that its occurrence takes place through the unbinding of pairs of topological defects, whose interaction energy exhibits a logarithmic dependence on separation. In a two dimensional superconductor, the topological defects are vortices that interact with a logarithmic potential. The interaction occurs for distances less than the transverse penetration depth λ_c . It has been shown that the low temperature electrical properties are dominated by logarithmically bound vortex pairs. This behaviour will be summarised below. Before this, however, it is interesting to consider exactly what happens to the coherence length as the temperature approaches T_c . Due to the temperature dependence of ξ , there will come a point where ξ exceeds s . Once the sheet thickness is smaller than the coherence

length it is no longer possible to consider the film as two dimensional. This is important, since the KTB theory would no longer be valid. This may then explain why it has been difficult to observe the singularity in λ^{-2} predicted to occur by KT theory. Furthermore, it is interesting that the cross over from 2 D to 3 D paraconductivity above T_c appears to be accompanied by a change in the carrier type, as observed in the Hall effect measurements^(16,35,36). No attempt to explain this phenomenon will be made here.

3.3.2.1 Current Induced Vortex Unbinding

Measurements of the d.c. voltage characteristics of YBCO thin films have been demonstrated on several occasions. The log-log plots tend to fit a straight line over a large range of currents and voltages. The gradient of the curves is not however equal to one. The results imply that the voltage varies as a power of the current, namely

$$V \sim I^{a(T)} \quad 3.51$$

From the idea of the KT transition, below the mean field transition temperature T_{co} , there exists a local order parameter, but long range order is destroyed by the presence of vortex excitations of both polarities (even if $B=0$). The current density causes a force on the vortex (Lorentz Force) that is perpendicular to the direction of current, i.e.

$$F_L = J_s \Phi_0 \quad , \quad J_s = n_s e v_s \quad , \quad \Phi_0 = \frac{h}{2e} \quad 3.52$$

If there is no flux pinning then this would produce a steady state flow of vortices resulting in dissipation. The vortex-antivortex (antivortex- one with opposite polarity) pairs tend to attract each other and below a certain temperature T_{KTB} they are effectively bound together as a pair. The current exerts a force on these vortices. The net force must be zero if the vortices are stationary, when this occurs there will be no resistance.

Because the applied currents exert opposite force on the members of a pair, some

will break apart and undergo dissipating interactions, until they re-combine. It can be shown (see below) that for an arbitrary small current there will be some vortices free to move around, in other words the critical current of a two dimensional system is zero. The number of free vortices does, however, become so small as to be immeasurable for low T_c . As the current increases a larger amount of vortices will become unbound resulting in a larger resistive term. The resistance will therefore, be dependent on current.

The vortex/antivortex pair energy for zero applied current, can be written in the form

$$U_0(r) = 2E_c + q^2 \ln \frac{r}{\xi} \quad 3.53$$

where E_c is the core energy, r is distance between vortices and ξ is the vortex core dimension. By analogy with 2D coulomb gas

$$q = \sqrt{\frac{n_s \hbar^2}{8\pi m}} \quad 3.54$$

where $n_s = n_s^{3D} d$, where d is the film thickness. In the presence of an applied supercurrent, this energy is modified by the Lorentz force to give

$$U(r) = U_0(r) - F_L r \quad 3.55$$

$$U(r) = 2E_c + q^2 \left(\ln \frac{r}{\xi} - \frac{4m v_s r \pi}{\hbar} \right) \quad 3.56$$

This energy will have a saddle point orientated so that the vector connecting them is perpendicular to the direction of the current. The distance corresponds to a maximum in the potential in that direction, given by

$$r_c = \frac{h}{4\pi m v_s} = \frac{h n_s e}{4\pi m J_s} \quad 3.57$$

with an energy at the saddle of

$$U(r_c) = 2E_c + q^2 \left(\ln \frac{r_c}{\xi} - 1 \right) \quad 3.58$$

By rearranging in this way it becomes clear that the logarithmic term is larger than 1 since $r_c \gg \xi$. This implies therefore, that the modification of the saddle energy due to the Lorentz force is very small and can be neglected, therefore

$$U(r_c) \sim U_0(r_c) \quad r_c \gg \xi \quad 3.59$$

$$U(r_c) = 2E_c - q^2 \ln \frac{J_s}{J_0} \quad J_s < J_0 \quad 3.60$$

where

$$J_0 = \frac{h n_s e}{4\pi m \xi} \sim G-L \text{ critical current} \quad 3.61$$

Now, by assuming a thermal assisted escape over the pinning point, the rate of production of free vortices is given by

$$\Gamma_c \sim \exp - \frac{U(r)}{k_B T} \quad 3.62$$

Clearly this is similar to equation 3.44 shown above, as expected. The difference is of course the nature of the pinning potential. In this analysis the magnitude of $U(r)$ is dominated by the logarithmic term, namely that

$$q^2 \ln \frac{r_c}{\xi} > 2E_c \quad 3.63$$

substituting this into the above gives

$$\Gamma_e \sim \left(\frac{r_c}{\xi}\right)^{-q^2/k_B T} \quad 3.64$$

using the term for J_{GL0} given above, this then becomes

$$\Gamma_e = \left(\frac{J_s}{J_0}\right)^{q^2/k_B T} \quad 3.65$$

Further analysis shows that the resistance is then given by

$$R = 2\pi\xi^2 R_n \Gamma_e^{1/2} \quad 3.66$$

using $V=IR$, this becomes

$$V = I_s 2\pi\xi^2 R_n \left(\frac{I_s}{I_0}\right)^{\frac{q^2}{2k_B T}} = k I_s^\alpha \quad 3.67$$

where

$$k = \frac{2\pi\xi^2 R_n}{I_0^{q^2/2k_B T}}, \quad \alpha = 1 + \frac{q^2}{2k_B T}$$

The temperature dependence of the resistance can be summarised by⁽¹⁹⁾

$$R \sim R_N \exp\left[-2b \frac{(T_c - T_{KTB})}{(T - T_{KTB})}\right]^{\frac{1}{2}} \quad 3.68$$

This can be simplified by taking logarithms, thus becoming

$$\left(\ln \frac{R}{R_N}\right)^2 = -4b \frac{(T_c - T_{KTB})}{(T - T_{KTB})} \quad 3.69$$

This temperature dependence will be examined in chapter 6.

One further important point from this work is the screening of the

vortex/antivortex interaction, due to vortex pairs situated between the test vortices. As $T \rightarrow T_c$ and the number of vortices increases, screening will become important. This phenomenon can be represented by dielectric. The screening effect causes the effective vortex charge to alter so that

$$q^2 = \frac{q_0^2}{\epsilon} = \frac{n_s h}{4m\epsilon} \quad 3.70$$

where ϵ is the value of the permittivity. Thus

$$a = 1 + \frac{q^2}{2k_B T} = 1 + \frac{q_0^2}{2k_B T \epsilon} \quad 3.71$$

At T_{KT} the value of a , according to Kosterlitz and Thouless, is 3. Therefore at this temperature

$$\frac{q_0^2}{2k_B T_c \epsilon_c} = 2 \quad 3.72$$

rearranging this, and using the value of q_0 given above

$$\epsilon_c = \frac{\Phi^2 d}{\lambda^2 k_B T_c} \quad 3.73$$

Thus it is possible to calculate the permittivity at T_{KT} .

3.3.3 Normal Transport Equations

The most promising of the new theories of superconductivity is likely to be that of Anderson's resonating valence bond model. In this model Anderson argues that the pairing mechanism responsible for high T_c superconductivity is due to a magnetic property and not BCS type. The theory is based on a two dimensional Hubbard model

at half filling with strong in site Coulomb repulsion U and an attractive intersite hopping energy t . Superconductivity arises from the condensate made up of holon pairs. The theory predicts that the normal resistivity in both the ab or c planes can be fitted by

$$\rho = AT + \frac{B}{T} \quad 3.74$$

this can be approximated to

$$\rho_c = AT, \quad \rho_{ab} = \frac{B}{T} \quad 3.75$$

This result can easily be investigated from the normal behaviour of the thin films.

A more relevant result to this thesis is the penetration depth derived by Rice and Wang⁽³⁷⁾. Using the RVB model they are able to show that the London penetration depth of a holon superconductor is

$$\lambda(T)^2 = \lambda(0)^2 \left(1 - \frac{\zeta_n(T)}{\zeta}\right)^{-1} \quad 3.76$$

where

$$\lambda(0)^2 = \frac{md}{\mu_0 \zeta e^2} \quad 3.77$$

and

$$\zeta = N/A, \quad \zeta_n(T) = -A^{-1} \sum_k \epsilon_k \frac{\partial n_k}{\partial E_k} \quad 3.78$$

ζ is the mean number of holons per unit area and ζ_n is the number of 'normal' holons per unit area at temperature T . ζ is a constant. The term n_k is the quasi-particle occupation number given by $n_k = [\exp(E_k/k_B T) - 1]^{-1}$, also $\epsilon_k = \hbar^2 k^2 / 2m$, namely the kinetic

energy of a free holon, with mass m and momentum hk . E_x is the excitation energy of the holon and d is the lattice constant along the c direction. As T tends to T_c , $\zeta_n(T)/\zeta$ tends to T/T_c , namely,

$$\lambda(T) = \lambda(0)[1-T/T_c]^{-1/2} \quad 3.79$$

given penetration depth therefore, it is thus possible to calculate the mean number of holons from $\lambda(0)$, and therefore the variation of normal holons with temperature.

It is interesting to note that this theory is dependent on the superconductor being clean, namely that the holon mean free path l is greater than the coherence length. Earlier, however, the results obtained by the Gorkov formulation of BCS were for a dirty superconductor. The reason for this is that there is insufficient information, at this time, as to the true nature of YBCO, namely dirty or clean, since there have been claims for both dirty⁽³⁸⁾ and clean^(30,37). The effect of changing from dirty to clean in the Gorkov formulation results in the penetration depth given by

$$\lambda_{pure}(T) = \frac{1}{\sqrt{2}} \lambda_L(0) \left[\frac{T_c}{T_c - T} \right]^{1/2} \quad 3.80$$

If the superconductor is clean it will be necessary to replace this for equation 3.26 given above.

3.3.4 Josephson junctions and critical current

It was soon realised that many of the superconducting thin films were granular in nature. This led to the idea that at the grain boundaries, namely, where one grain touches another, there may be a Josephson junction. Ambegaokar and Baratoff⁽⁴¹⁾ amongst others have already investigated this idea namely, a superconductor being a 2 dimensional array of Josephson junctions. This theory considers the effect of intragranular and intergranular interactions. Work has shown that in the case of YBCO

bulk the intergranular penetration depth can exceed the intragranular penetration depth. A bulk YBCO sample, with a critical current J_0 of 10^4 A/cm^2 and an average grain size of $1 \mu\text{m}$, will have an effective penetration depth of $3 \mu\text{m}^{(38)}$, almost 20 times larger than the London penetration depth. Several workers using RF induction coil experiments have reported measurements of penetration depth far larger than expected^(39,40). This analysis makes it possible to determine not only the penetration depth but also the temperature dependence of the critical current. The penetration depth is given by

$$\lambda(T)^{-2} = \frac{\Delta(T)\pi}{\mu_0 R_n d \hbar} \tanh \frac{\Delta(T)}{2k_B T} \propto [1 - T/T_c] \quad 3.81$$

which is proportional to $[1 - T/T_c]^{1/2}$ as T tends to T_c . The critical current on the other hand is proportional to $[1 - T/T_c]^{3/2}$. If the thin films are simply an array of two dimensional Josephson junctions this behaviour will be observed.

3.3.5 Two Dimensional to Three Dimensional Crossover

Thus far in the theoretical section several theories have been reviewed. This resulted in several derivations of penetration depth as well as a number of theories explaining flux flow. The first of these was the Anderson flux flow model and the second was the Kosterlitz Thouless Berezinskii model. Furthermore work performed on paraconductivity as well as work on the RVB model and Josephson junctions was presented.

In the section on paraconductivity it was shown that two theories exist namely, the Aslamazov-Larkin 2 dimensional theory or the Lawrence-Doniach 2D/3D theory. The question as to which theory is right is very significant to the understanding of YBCO thin films. If the AL theory is correct and the films are 2 dimensional they will be explained in terms of the KTB theories. The Anderson flux flow model will not

therefore, be needed. Furthermore the equations for penetration depth, given above, will also be invalid. This is because one property of a KTB transition is a discontinuous jump in penetration depth at T_{KTB} . If however, the LD theory is correct and the film becomes 3 dimensional in nature when $\xi(T) > s/\sqrt{2}$, where s is the sheet thickness, then the reverse is true. In this case the KTB theories are no longer valid and the traditional theories of London, Ginzburg Landau, Anderson etc. are applicable.

Since the two groups of theories are different and have different predictions as to the electrical behaviour, it raises the question as to what will be observed, if anything, at the cross over point? This in turn leads to the question of what happens if the cross over temperature is below or above the T_{KTB} temperature?

If the cross over were to take place below the transition temperature then the film would behave similar, if not identical, to a traditional superconductor. In other words there would be no flux flow without an applied magnetic field in excess of H_{C1} , the changes in penetration depth would be those predicted by London etc.

If, however, the cross over takes place at temperatures above the critical temperature, namely the zero dissipation temperature⁽¹²⁾ then there will be the spontaneous production and movement of vortices according to Kosterlitz Thouless Berezinskii theory, resulting in dissipation. The characteristics of the dissipation will of course be those described in the section on KTB given above. If the film then becomes 3 dimensional, what happens to the vortices? After all, in 3 dimensional superconductors the vortices cannot exist without the application of a magnetic field. According to theory the vortices will be stable. Lawrence and Doniach predict that the vortices will be forced to align themselves from sheet to sheet, one on top of the other. This change may be visible as a change in the temperature dependence of the penetration depth. If the film is 2 dimensional then according to KTB theory the penetration depth will tend to infinity

more sharply than that predicted by 3 dimensional theory. If the film becomes 3 dimensional before the penetration depth reaches infinity then the remaining superelectrons should dissociate according to the temperature dependence of London, Ginzburg Landau, BCS theories etc. Thus it may be possible to observe the change from 2 dimensional to 3 dimensional behaviour as a deviation in the temperature dependence of the penetration depth.

3.4 Low frequency impedance of superconducting YBCO thin films.

In order to investigate the behaviour of the electrical properties of YBCO, it was decided to use an alternating electric signal technique. It is therefore necessary to analyse the theory behind the experimental arrangement used.

In this thesis I have chosen to use a contact technique to investigate the electrical behaviour of the YBCO thin films. By choosing this method one immediately has the problem of contact resistance and inductance and complications due to wiring. These problems can be overcome. The advantage of this method is that it is possible to investigate small areas of the sample, this improves the sensitivity of the results. It is also possible to carry out other experiments, such as critical current, B field or dc experiments without having to alter the experimental arrangement. This is advantageous, since an entire range of experiments can be performed in a short time.

In the experiments conducted here, it is possible to use the London analysis given above to analyse the thin films grown by this group. The above analysis is altered however to include a new term due to the displacement current. This term is normally very small in normal superconducting materials, though it may be of significance in these materials especially around the critical temperature.

3.4.1 The revised current density equations.

The revised current density is obtained by summing the normal current and supercurrent and solving the two dimensional wave equations as described by Raven⁽³²⁾. In this type of analysis the displacement current is normally ignored. In the High T_c oxide materials however there is a suggestion that the capacitive displacement current may be significant, at least near the transition temperature. Furthermore the vortices produced spontaneously in the transition region of the HTS materials also contribute to the electrical measurements. It is therefore necessary to include these new terms with the normal conductive term and a modified inductive term. The revised total current density is now given by

$$J = (\sigma_e + j\omega\epsilon - \frac{j}{\omega L_e})E \quad 3.82$$

σ_e is an equivalent normal conductivity, $\epsilon = \epsilon_0\epsilon_r$ where ϵ_r is the permittivity of the film material. L_e is the equivalent inductive term that includes the normal inductance and the inductance due to the supercurrent. The modification by the normal inductance is discussed below. Equation 3.82 becomes

$$J = \frac{\gamma^2 E}{j\omega\mu} \quad 3.83$$

$$\text{where } \gamma^2 = \lambda_e^{-2} + j\omega\mu\sigma_e \quad , \quad \lambda_e^{-2} = \frac{\mu}{L_e} - \omega^2\epsilon\mu \quad . \quad 3.84$$

Therefore the stationary state theory will apply providing there is no charge build up. It is well known that due to the inertia of the superconducting electron pairs, the E field is only zero when the frequency of the signal is zero. A potential difference will appear

between the inner contact probes when an a.c. signal is applied. The solution for the current density is still similar to that given by London and follows the same analysis. According to the above analysis the reciprocal penetration depth β is replaced by the propagation constant γ . The film is assumed to be infinite in the x- direction and has a thickness of $2a$ in the y direction. The current enters at $-b$ and leaves at $+b$. Experimentally the thin film impedance is determined by the four terminal method and in this analysis the potential terminals are at points $z=A$ and $z=B$. By solving the Maxwell's equations using the same arguments as above, this gives

$$j_z = J\gamma a \frac{\cosh\gamma y}{\sinh\gamma a} \quad 3.85$$

as expected. This result is easily verified by finding the total current I by integrating over the film section area $ds=xdy$. In this analysis the limits of integration are $\pm a$. The film is assumed to be infinite in the x direction and the resulting current given in units of amps/meter width of x. The final result is equal to the current that enters the contact, namely $I=J(2ax)$.

The potential difference due to the frequency that can be measured by the inner probes is determined by integrating the electric fields in equation 3.83 between the limits A and B at distance d . This gives

$$V_{ab} = \frac{j\omega\mu}{\gamma} J_{ad} \frac{\cosh\gamma y}{\sinh\gamma a} \quad 3.86$$

The impedance is then calculated from the ration $Z=V_{ab}/I$ and by putting $y=a$ in 3.86 giving

$$Z_{ab} = \frac{j\omega\mu d}{\gamma 2X} \coth\gamma a \quad . \quad 3.87$$

This can be expanded using the power series

$$\theta \coth\theta = 1 + \sum_{n=1}^{\infty} (-1)^{n-1} 2^{2n} B_n \frac{\theta^{2n}}{(2n)!} = 1 + \frac{\theta^2}{3} - \frac{\theta^4}{45} + \dots \quad 3.88$$

where $\theta=\gamma a$, n is an integer and B_n is the Bernoulli number. Using the first two terms only from this expression the impedance becomes

$$Z_{ab} = \frac{j\omega\mu}{\gamma} \left(\frac{1}{\gamma a} + \frac{\gamma a}{3} \right) \frac{d}{2X} \quad . \quad 3.89$$

The impedance should decrease with γa according to equation 3.89. Furthermore by substituting for γ from equation 3.84

$$Z_{ab} = \left(\frac{\rho_e}{1 + \frac{1}{4} \left(\frac{\delta}{\lambda_e} \right)^4} + j\omega \left[\frac{\mu \lambda_e^2}{1 + 4 \left(\frac{\lambda_e}{\delta} \right)^4} + \frac{\mu a^2}{3} \right] \right) \frac{d}{A} + j\omega L_w \quad . \quad 3.90$$

Where A is the film cross sectional area $2aX$, ρ_e is the equivalent normal resistivity and L_w is the inductance due to the contact.

The first point to note is that the last term, $\mu a^2/3$, is due to the film dimensions and represents the geometric inductance. The first term represents the real part, namely resistivity and the second term is the inductance, which for low temperatures is simply the kinetic inductance due to the superelectrons. Analysis of this theory combined with an equivalent circuit has been carried out elsewhere⁽³²⁾. In the analysis the capacitive term is due to the displacement current generated by the normal transport mechanism. Furthermore the resistivity term is due to the normal electrons flowing within the thin film. It is clear that by reducing the frequency of the a.c. signal to zero, the impedance will in turn tend to zero. This model breaks down at T_{∞} unless an alternating signal is

used. Results show that above T_{∞} vortex flow can occur without the need for an external alternating current. This model does not include a flux flow term at present. It should be possible to include vortex motion in the above analysis, and by following a similar process to that described above it should be possible to redefine the transport equations. This will be discussed later in chapter 6.

3.5 Structure and X-ray Diffraction

The compound of YBCO as several phases, the only difference between them is the amount of oxygen they possess. Experiments have shown that the superconducting phase has 7 oxygen atoms whereas the semiconducting phase contains 6.5 or less. This variation in oxygen results in a slight difference in physical structure. The superconducting phase of YBCO is orthorhombic, whereas the semiconducting phase is tetragonal. YBCO is also anisotropic and it is advantageous therefore to know the orientation of the sample under test. Using X-ray diffraction to analyse a sample it is possible to determine not only the orientation but in some cases also which compound has been deposited. This is particularly useful for determining growth parameters.

The condition for diffraction is given by Bragg's equation

$$2d \sin\theta = n\lambda \quad . \quad 3.91$$

This equation gives the angle θ at which a set of planes, of spacing d , co-operatively reflect X-rays of wavelength λ in the n th order. Assuming d and λ are constant and since θ cannot exceed 90° ($\sin 90=1$) there exists a limited series of solutions corresponding to all values of n for which $\theta < 90$. This condition places a limit on the number of reflections that can emanate from a crystal. These are described as first, second, third order reflections etc., for $n=1,2,3 \dots$ Alternatively, it is possible to set $n=1$ and to calculate the change in d with $\sin \theta$. This second method of analysing diffraction

patterns is particularly useful in analysing YBCO.

Of the 14 Bravais lattices (ie the 14 distinct space lattices that can be used to represent any crystal) the YBCO tends, as mentioned, to be either orthorhombic or tetragonal. The orthorhombic phase being the superconducting phase, the tetragonal the semiconductor phase, see figure 1.1, page 12.

An orthorhombic structure is one in which all the lattice constants are different, but the angle between them is 90°. In the case of the tetragonal however, the a and b lattice constants are equal but different to the c axis. Again, the angle between them is 90°. It can be shown that for the orthorhombic structure, d the lattice spacing, described above, is given by

$$\frac{1}{d^2} = \frac{h^2}{a^2} + \frac{k^2}{b^2} + \frac{l^2}{c^2} \quad 3.92$$

where as for a tetragonal structure

$$\frac{1}{d^2} = \frac{h^2+k^2}{a^2} + \frac{l^2}{c^2} \quad 3.93$$

where a,b and c are the lattice constants and h,k and l are the Miller indices. The Miller indices define the orientation of the crystal, for example, in a (110) orientated crystal, h=1, k=1 and l=0, where as in an (013) orientated crystal h=0, k=1 and l=3. Therefore given a,b and c it is possible to calculate d and hence θ for every orientation of a given crystal. Comparing the calculated values of θ with those obtained from experiment it is possible to identify the orientation of the crystal. Alternatively, if the orientation is known it may be possible to calculate the value of the lattice parameters. This is of particular use in YBCO thin films deposited on MgO(100) and SrTiO₃(100). Research has shown that these films are c-axis orientated, (00l), the changes in the values of d with θ correspond to changes in l, namely l=1,2,3,4... etc. This is because h=k=0, and

therefore equations 3.92 and 3.93 simplify to

$$\frac{1}{d} = \frac{l}{c} \quad 3.94$$

by plotting $1/d$ against l , the gradient gives $1/c$, where c is the c -axis lattice constant. Knowledge of the orientation is of particular interest in this work because of the anisotropic nature of YBCO.

Finally, it is important to realise that X-ray diffraction describes only those parts of the sample which contain coherently scattering lattice planes. Regions of the samples which are less well ordered may contribute only a small background to measured diffraction spectra. These regions, however, may represent a substantial volume of the samples. These areas may be inhomogeneously oxidised and only partially ordered with respect to metallic layering. With 3 metallic components and such a complex deposition mechanism there is no reason to expect perfect ordering. The level of residual disorder is unknown at the present time. Some experiments which are not based on diffraction suggest substantial disorder. It has been argued⁽⁴²⁾ that even grains of YBCO with the best transitions may only consist of thin superconducting shells surrounding normal and probably semiconducting cores.

3.6 Summary

In this chapter several aspects of superconductivity have been reviewed. London's, Ginzburg-Landau, BCS, Rice-Wang and Ambegaokar-Baratoff theories have been used to derive the penetration depth. The penetration depth seems to have approximately the same temperature dependence close to the critical temperature, irrespective of the initial theory. Depending on which theory is correct however, will determine whether the results represent super electron density, super holon density etc.

Furthermore Abrikosov's theory, to explain type II behaviour based on a mixed state, was examined by Gorter and later by Anderson in which they realised that a Lorentz force would result in the film if a transport current were present. Using this model it has been shown that flux flow can exist. The magnitude of the flux flow from this model appears to be too small to account for that observed in YBCO thin films⁽²⁹⁾. To explain the excess flux flow, Kosterlitz-Thouless and Berezinskii theories were employed. From these theories it is possible to explain the non linear behaviour observed in YBCO. Using models explaining the paraconductive nature of thin films it may be possible to calculate the thickness of the 2 dimensional superconducting sheets. It is also possible to calculate the coherence length. Using this information it will then be possible to calculate the density of states and the Fermi velocity using Gorkov's formalisation. It is also possible to observe a cross over from two dimensional to three dimensional behaviour from the penetration depth measurements.

Using an ac contact process it is possible to obtain information not only about the resistive nature of YBCO, but also information about the inductance behaviour of the thin films. From these results it should be possible to determine the parameters defined in the theoretical section above, namely, sheet thickness, coherence length, penetration depth, density of states as well as observing the flux flow phenomena.

In the final section the technique of X-ray diffraction was described and examined with respect to its use in analysing the structure of YBCO thin films. It is possible to determine lattice parameters and film orientations from analysis of the x-ray results.

3.7 References

- 1 Kamerlingh Onnes, H. Leiden Comm, *I22b*, 124c, (1911)
- 2 Bardeen J., Copper L.N., Schrieffer J.R., Phys Rev *108*, 1175, (1957)
- 3 Gorter C.J., Casimir H.B.G., Physica, *1*, 306, (1934)
- 4 London F., London H., Proc Roy Soc *A149*, 71, (1935)
Physica, *2*, 341, (1935)
- 5 Ginzburg V.L., Landau L.D., Zh Eksperim, i Teor, Fiz *20*, 1064, (1950)
- 6 Abrikosov A.A., Dokl Akad Navk SSSR *86*, 489, (1952), Zh Eksperim, i
Teor, Fiz *32*, 1442, (1957) (English Trans : Soviet Phys JEPT, *5*, 1174,
(1957))
- 7 Anderson P.W., Phys Rev Lett *9*, 309, (1962)
- 8 Kosterlitz J.M., Thouless D.J., J Phys C: Solid State Phys *6*, 1181, (1973)
- 9 Berezinskii V.L., Sov. Phys. JETP *34* (1972) 610
- 10 Josephson B.D., Phys Lett. *1* (1962) 251
- 11 Koelle D., Kober F., Gross R., Huebener R.P., Gupta A., Mannhart J.,
Roas B., Supercond. Sci. Technol. *4* (1991) S115
- 12 Dubson M.A., Herbert S.T., Calabrese J.J., Harris D.C., Patton B.R.,
Garland J.C., Phys Rev Lett *60* (1988) 1061
- 13 Gergis I.S., Kobrin P.H., Cheung J.T., Sovero E.A., Lastufka C.L.,
Deakin D.S., Lopez J., Physica C *175* (1991) 603
- 14 Flueckiger P., Gavilano J.L., Leemann C., Martinoli P., Dam B.,
Stollman G.M., Srivastava P.K., Debely P., Hintermann H.E.,
Physica C *162-164* (1989) 1563
- 15 Zhao B., Kuroumaru S., Horie Y., Yanada E., Aomine T., Qiu X., Zhang Y.,
Zhao Y., Xu P., Li L., Ohkubo H., Mase S., Physica C *176* (1991) 409
- 16 Hagen S.J., Lobb C.J., Greene R.L., Forrester M.G., Kang J.H.,
Phys Rev B *41* (1990) 11630
- 17 Anderson P.W., Mater Res Bull *8*, (1973), 153, Science *235* (1987) 1196
- 18 Wordenweber R., Abd El Hamed M.O., Schneider J.,
Physica C *171* (1990) 1
- 19 Gasparov V.A., Physica C *178* (1991) 449
- 20 Raven M.S., Inameti E.E., Murray B.G., Wan Y.M, Supercond. Sci.
Technol *4* (1991) 225

- 21 Cooke D.W., Gray E.R., Houlton R.J., Javadi H.H.S., Maez M.A., Bennett B.L., Rusnak B., Meyer E.A., Arendt P.N., Beery J.G., Brown D.R., Garzon F.H., Raistrick I.D., Rollett A.D., Bolmaro B., Elliott N.E., Klein N., Muller G., Orbach S., Piel H., Josefowicz J.Y., Rensch D.B., Drabeck L., Gruner G., *Physica C* **162-164** (1989) 1537
- 22 Meissner W., Oschenfeld R., *Naturwissen*, **21**, 787, (1933)
- 23 Landau L.D., *Phys Z Sowjet U* **11**, 545, (1937)
- 24 Gorkov L.P., *Zh Eksperim, i Teor, Fiz* **36**, 1918 and **37**, 833 and 1407, (1959)
English Trans : *Soviet Phys JETP* **9**, 1364, (1959) and **10**, 593 and 998, (1960)
- 25 Aslamazov L.G., Larkin A.I., *Sov Phys Solid State* **10** (1968) 875
- 26 Lawrence W.E., Doniach S., Proc of the LT12 Conference Kyoto (1970)
ed Kanda (Keigaku, Tokio, 1971) p361
- 27 Gorter C.J., *Phys Lett* **16** (1962) 242
- 28 Giaever P.W., *Phys Rev Lett* **15** (1965) 825
- 29 Tewksbury S.K., Hornak L.A., Hatmain M., *Solid State Elec.* **32** (1989) 947
- 30 Fiory A.T., Hebard A.F., Mankiewich P.M., Howard R.E.,
Appl Phys Lett **52** (1988) 2165
- 31 Dilorio M.S., Anderson A.C., Tsaur B.Y., *Phys Rev B* **38** (1988) 7019
- 32 Raven M.S., Inameti E.E., Murray B.G., Wan Y.M.,
Physica C **178** (1991) 275
- 33 Neumann Ch., Ziemann P., Geerk J., Xi X.X., *Physica C* **162-164** (1989) 321
- 34 Frohlich J.C., *Phys Rev* **79** (1950) 845
- 35 Thier N., Winzer K., *IEEE Trans on Magn* **25** (1989) 2293
- 36 Zhang Q., Xia J., Fang M., He Z., Wang S., Chen Z.,
Physica C **162-164** (1989) 999
- 37 Wang Y.R., Rice M.J., *Phys Rev B* **38** (1988) 7163
- 38 Clem J.R., *Physica C* **153-155** (1988) 50
- 39 Gasparov V.A., Huguenin R., Pavuna D., van der Maas J.,
Solid State Comm. **69** (1989) 1147
- 40 Sridhar S., Shiffman C.A., Hamdeh H., *Phys Rev B* **36** (1987) 2301
- 41 Ambegaokar V., Baratoff A., *Phys Rev Lett* **10** (1963) 486
- 42 Ginley et al, *Phys Rev B* **36** (1987) 829
- 43 Murphy D.W., Johnson D.W., Jin S., Howard R.E., *Science* **241** (1988) 922
- 44 London F., *Superfluids Vol.1*, (Dover, New York, 1961).

Chapter 4: R.F. Sputtering

4.1: Introduction - The Radio Frequency Sputtering System

The sputtering system used throughout these experiments is shown in schematically in Figure 4.1. A radio frequency generator was used to produce a 13.56 MHz voltage across the terminals, namely the target and the substrate holder. The R.F. voltage of the system could be altered using a variable transformer voltage divider. The sputtering current was measured with an ammeter in the primary winding of the divider⁽¹⁾. Throughout these experiments the current was used as a guide to the rate of deposition. In general, low current values resulted in lower deposition rates. The lower the deposition rate the better quality the thin films appear to be⁽²⁾.

4.1.1 The Vacuum System

High vacuums were achieved using an Edwards high vacuum system model 303 with an oil based diffusion pump. In the sputtering system there was also a liquid nitrogen cooled cold trap between the water cooled baffle and the vacuum chamber. This reduces back streaming of oil vapour and decomposition products. The vacuum chamber also contained a liquid filled coil which further trapped water vapour inside the chamber, see Figure 4.1. With this arrangement it was possible to obtain base pressures of less than 10^{-6} Torr.

4.1.2: Substrate Heater

To produce high quality thin films substrate temperatures (T_{sub}) >650 °C are necessary⁽³⁾. The heater also had to operate in oxygen needed for post deposition oxygenation to convert the semiconducting tetragonal phase into the superconducting orthorhombic phase⁽⁴⁾. To reach the high temperatures a heater capable of heating

consistently for long periods of time within an oxidising environment was therefore required. Several heaters are available though each has its limitations, e.g., filament bulbs. Filament bulbs have a limited life span and can cause serious damage to both the target and the chamber if they explode. Ceramic heaters are also available but could not easily be fitted to the system used. Because of these problems a heater was designed capable of producing the temperatures required for deposition. The heater described below was designed by my co-worker Dr. E.E.Inameti and has been used to produce many good superconducting films, see Figures 4.1 and 4.2.

The heating element is a Thermocoax heating element produced by Thermocoax (Philips). It consists of a coaxial element made of Ni/Cr wire. Around the wire is compacted MgO, which isolates the wire from the rest of the heater. The outer part of the heater is made of zirconium copper alloy. The element wire is wound into a rectangular spiral, Figure 4.2. The bends have to be made with care to ensure that they are not acute enough to damage the insulation and cause a short circuit between the wire and the alloy. The coaxial connectors are brazed onto the holder and then the exposed Ni/Cr wire using a high temperature brazing material. The other parts of the element including nuts, bolts and sandwich material, are all made from stainless steel. The element is held between two flat stainless steel plates. The dimensions of the plates are 65 x 50 x 1.2 mm. On the upper plate a rectangular slot 45 x 10.5 x 0.4 mm deep was milled out. The slot made it easier to mount the substrates. The substrates were held firmly in place by the 2 pieces of metal that could be tightened to hold the substrates at the top and bottom. Later, silver paint was used to attach the substrates and the 2 pieces of metal became obsolete. The second advantage of the slot is that the heat transfer between the element and the substrates is improved, since this is the thinnest area on the upper plate. To reduce the heat loss further, the two stainless steel plates that make up

the sandwich are encased in two radiation shields, one on either side. The inner shield has 90° flaps at the ends to enclose the plates. The assembly of the plates uses four screws, which helped to guarantee that the element is in contact with both plates along the entire length of the plates. Both shields over the top plate have openings that allow sputtering to take place. The support for the connectors of the element are attached to the inner lower shield into which the leads from the power supply can then be screwed. The heater is attached to the chamber by two screws. The screws make it easy to move the heater from position to position. Furthermore, due to their small size they helped to reduce heat loss due to conduction. It was possible to mount the heater vertically or horizontally without the need for further alteration. To measure the temperature of the slot a type K thermocouple was spot welded onto the slot where the substrates were to be held, see Figure 4.1.

The heater was tested and found to have an almost uniform temperature along the growth channel, namely the position where the substrates were held. The variation of the temperature being less than 5°C from one end of the slot to the other, while operating at 730°C. The heater can operate at this temperature for long periods of time in an oxygen atmosphere. This is particularly important since there is activated oxygen in the chamber, which readily oxidises bare surfaces.

4.1.3: The Target

Throughout the experiments performed and mentioned here two types of target were used. The first was stoichiometric superconducting YBCO powder. The powder was spread uniformly on the target using a spatular. Alternatively, the second target was a stoichiometric YBCO disk produced by pressing YBCO powder at a pressure of 50 tons per square inch. The targets were produced using a die consisting of 3 metal

plates designed by Dr. Inameti as shown in Figure 4.3. The disk has a radius of 30 mm and is 3 mm thick. Although targets of this size were available commercially, their cost was prohibitive for this project. Besides the large disks used for sputtering smaller disks were produced using a small press. By immersing these in liquid nitrogen and placing a small magnet on top of the disc superconductivity was indicated by the levitation of the magnet due to the Meissner effect.

The $\text{YBa}_2\text{Cu}_3\text{O}_x$ powders were prepared by solid state reaction using high purity barium carbonate, BaCO_3 , copper oxide, CuO and yttrium oxide, Y_2O_3 . The starting materials were better than 99.99% pure. High purity is essential in the production of high quality bulk YBCO. The starting powders were mixed in the ratio of 1:3.5:2.12, $\text{Y}_2\text{O}_3:\text{BaCO}_3:\text{CuO}$. The mixture was ground together using a mortar and pestle for approximately 30 minutes. The powder was then heated to 940°C and held at this temperature for 12 hours in air. The sample was then cooled to 700°C over a 2 hour period, then to 600°C over a 2 hour period, then to 400°C over a 3 hour period. Finally the sample was allowed to cool to room temperature in its own time. The resulting powder could then be pressed as described above to produce disk targets. The powder or disk then required a second heat treatment. The sample was heated to 950°C and held at this temperature for 12 hours. The sample was then allowed to cool in flowing oxygen. This process resulted in high quality superconducting bulk $\text{YBa}_2\text{Cu}_3\text{O}_x$.

The target was bonded directly onto a water cooled copper block, using silver paint see Figure 4.1. The paint ensured good thermal and electrical contact. The target was surrounded by an earthed stainless steel sheath to ensure that the copper block onto which the YBCO was mounted was not sputtered. Targets produced by the method described above were used throughout the growth experiments to produce the thin films examined in this thesis. The targets were found to be very reliable and could be used for

over 100 hours of sputtering.

4.2: Thin Film production

4.2.1: Substrates and substrate preparation

The MgO and SrTiO₃ substrates were supplied by Furuchi Chemical Corporation (Japan) and Superconductive Components inc (USA). These substrates had dimensions of 10x10x1 mm, the large dimension cut to +/- 1% of the <110> or <100> axis. Substrate cleaning was performed using organic solvents and de-ionised water. The substrates were immersed first in trichloroethylene, followed by acetone and then methanol. Finally the substrates were immersed in de-ionised water to remove the organic residues. Any water that remained on the surface was blown off with air or removed by gently touching the substrate with filter paper. Following the cleaning process it was advantageous to mount the substrates quickly to avoid dust or any other contamination settling on the surface.

4.2.2: Loading the substrate and system preparation

The substrates were loaded onto a substrate heater which could be mounted at 90 degrees to the target. The earliest substrate were held in place by two rails and thermal contact was ensured by using silver foil. In later depositions the substrates were first painted on one side with silver paint. The substrates were then held against the substrate heater slot for approximately 15 seconds. This allowed time for an adhesive bond to occur. This was repeated for each substrate. Once all the substrates were mounted the paint was allowed to dry for about 30-60 minutes. When the paint had dried the chamber was lowered into position and the system evacuated.

4.2.3: Deposition Procedure

Before deposition started the baffle valve was turned to the glow discharge setting. This had the effect of reducing the efficiency of the pumping system and allowed for greater control of the pressure inside the chamber. The gas inlets were then opened.

The Ar and O₂ had separate inlets that allowed for the easy control of the gas mixture. A typical Ar:O₂ mixture was 4:1. While the gas was leaking into the system, the substrates were brought up to the deposition temperature. The deposition temperature was normally between 690 and 750° C. There was a visual difference between the colour of the heater slot and the colour of the substrate surface. However, once silver paint was employed the colour of the substrate was almost identical to the colour of the slot and it is thought that the temperature difference between the heater plate and the substrate surface was less than 10 Kelvin.

The gas pressure was set to that required for deposition, typically around 280 mTorr. Once the required temperature and pressure had been reached the target was pre-sputtered. With the target shutter in place, an r.f. signal was produced and a discharge occurred. At this point liquid nitrogen was poured into both traps to remove water vapour from the system. This period enabled the target and the system to reach equilibrium before deposition. Any alterations to gas pressure, substrate temperature etc were made during this period. After one hour of presputtering the shutter was opened and deposition started.

Deposition normally lasted for around 5-8 hours during which time the deposition temperature and pressure were held constant. Films grown for 5-8 hours normally had a film thickness of .1 to .5 microns. Following deposition the shutter was closed, the oxygen pressure was increased and the argon flow was stopped completely. This allowed the system to fill with pure oxygen. The pressure was raised to atmospheric as quickly

as possible while maintaining the same substrate temperature. The film was then allowed to cool in flowing oxygen until it reached a temperature of around 400-470°C. The cooling process took approximately 5 minutes, though this could be extended if required by adjusting the electrical supply to the heater. When the YBCO/substrates had reached the required temperature, the substrate temperature was held constant for 1 hour. The annealing process was performed in flowing oxygen or in a closed system; the results appeared to be the same. The low temperature anneal allowed the film to absorb the oxygen needed to ensure a good superconducting film⁽⁴⁾. Following the one hour anneal the unit was closed down and the substrate allowed to cool to room temperature.

By depositing thin films of YBCO by this method it has been possible to produce films with $T_c > 80$ K on a reproducible basis. Throughout the experiments, various pressures, gas combinations and substrate temperatures were used in an attempt to optimise the growth conditions. The deposition process was however, basically the same, namely, cleaning the substrates, mounting the substrates, evacuating the system, presputtering while reaching equilibrium, sputtering and post anneal. Due to the similarity in the various growths, the results given in chapter 6 will only outline the conditions in the system. Gas ratio, gas pressure, substrate temperature and post anneal temperature will be given and unless stated otherwise, the reader can assume that the experiment is the same as that described above.

4.2.4: Evaporation of Silver Contact Pads

Before the evaporation of silver contact pads, the sample along with the appropriate mask were cleaned in acetone to remove dirt and grease. The acetone appears to have no detrimental effect on the thin films. The 99.998% pure silver was also cleaned by this method and then placed into an evaporation basket that was in turn

placed in the evaporation system. The films were placed directly above the basket, approximately 15 cm from the silver, see Figure 4.4. A shutter was placed between the silver and the sample and this could be controlled from outside the chamber. The vacuum chamber was evacuated to a pressure greater than 10^{-5} torr before evaporation. The silver was evaporated from the tungsten filament which was heated from an external current source.

4.3 References

- 1 Belmekki B. PhD Thesis (1983) University of Nottingham
- 2 Inameti E.E., Raven M.S., Wan Y.M., Murray B.G., *Vacuum* **43** (1992) 61
- 3 Eom C.B., Sun J.Z., Lairson B.M., Streiffer S.K., Marshall A.F., Yamamoto K., Anlage S.M., Bravman J.C., Geballe T.H., Laderman S.S., Taber R.C., Jacowitz R.D., *Physica C* **171** (1990) 354
- 4 Jorgensen J.D., Beno M.A., Hinks D.G., Soderholm L., Volin K.J., Hitterman R.L., Grace J.D., Schuller I.K., Serge C.U., Zhang K., Kleefisch M.S., *Phys Rev B* **36** (1987) 3608

4.4 Figure Captions

Figure 4.1 : Schematic diagram of R.F. sputtering system. The system was used to produce the thin films examined in this thesis.

Figure 4.2 : The heater unit. High temperature deposition (700-750°C) was achieved using this unit.

Figure 4.3 : Schematic diagram of the 3 piece die used to produce the YBCO disks/targets.

Figure 4.4 : The schematic diagram of the evaporation unit used to deposit silver contacts onto YBCO thin films.

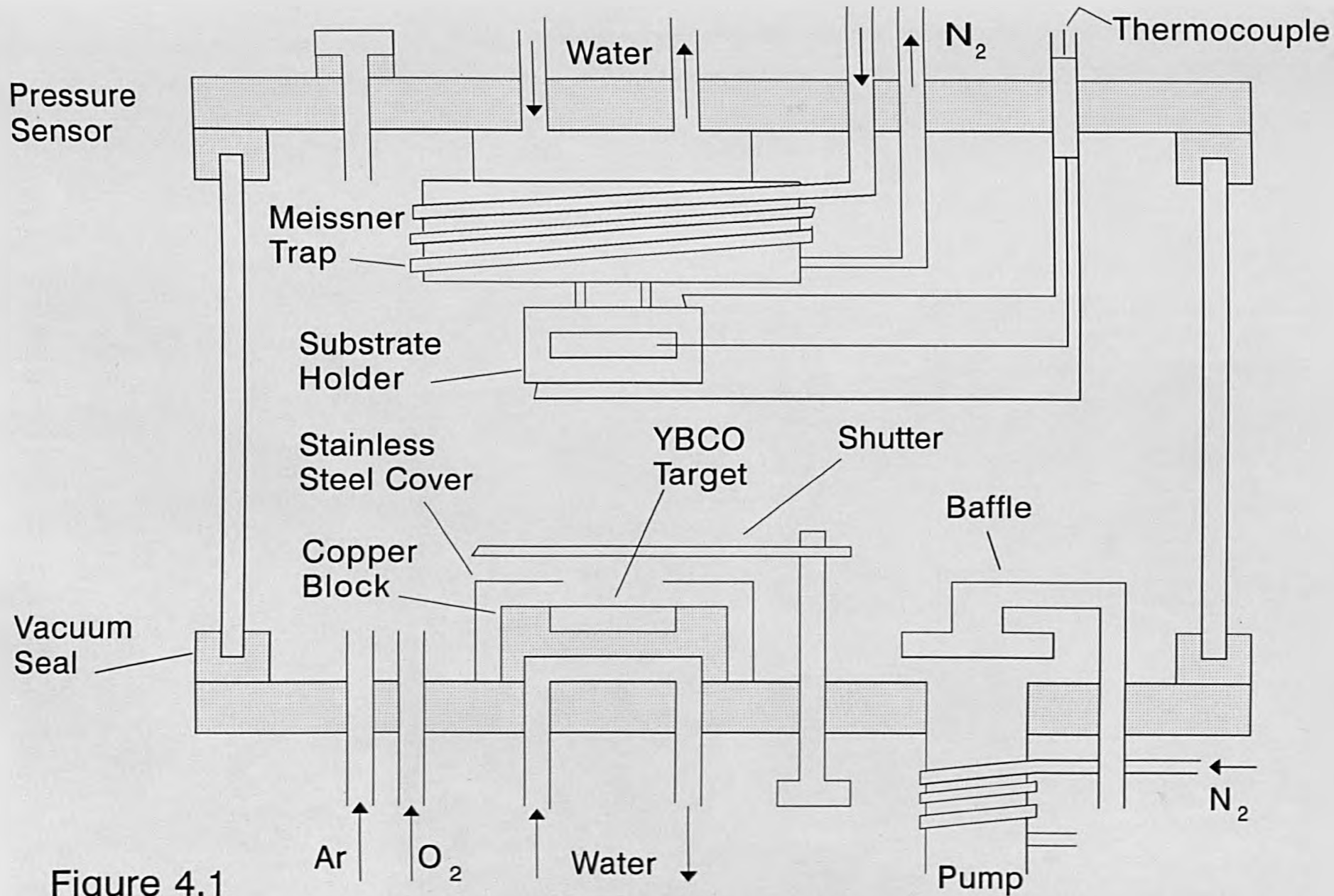


Figure 4.1

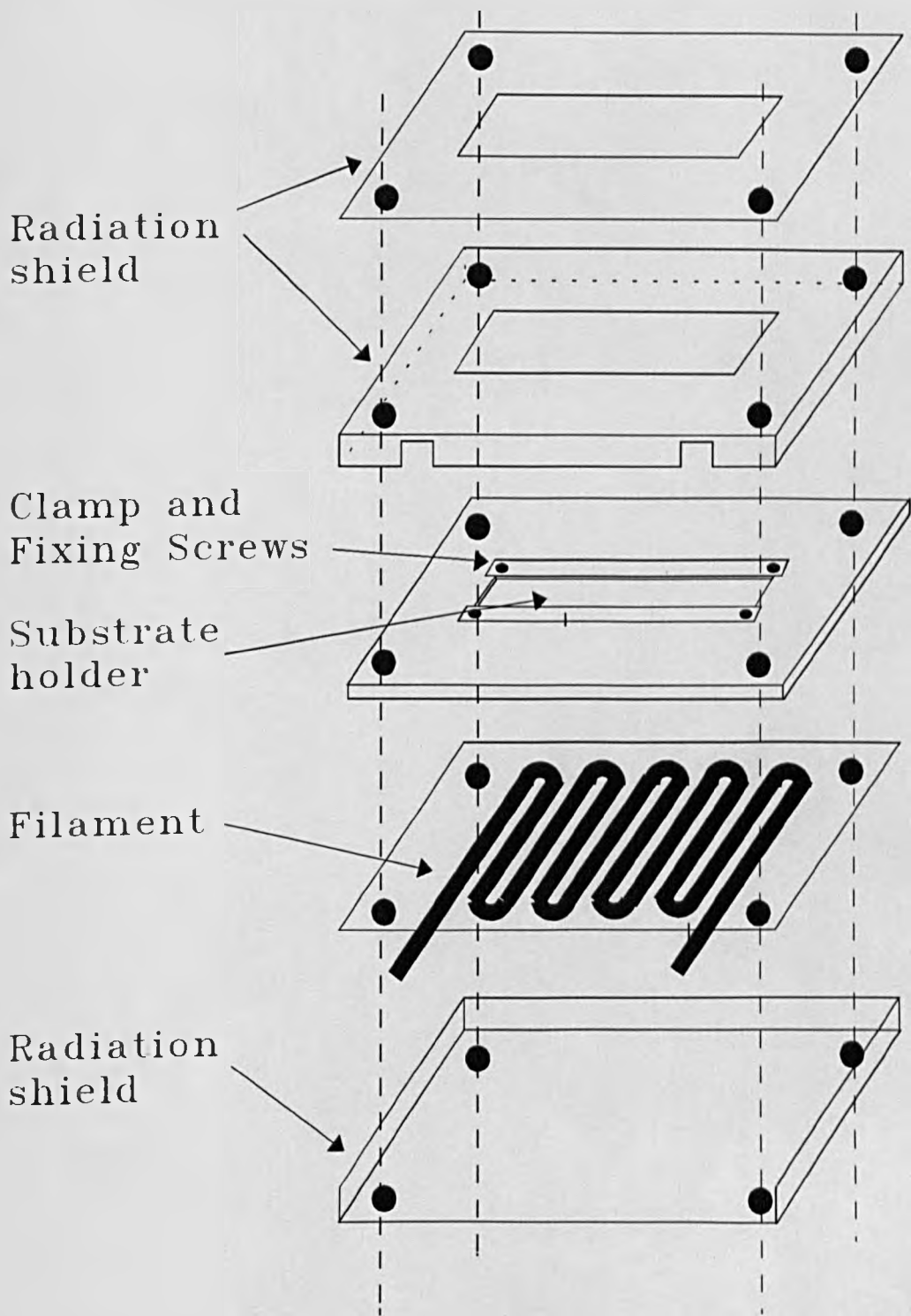


Figure 4.2

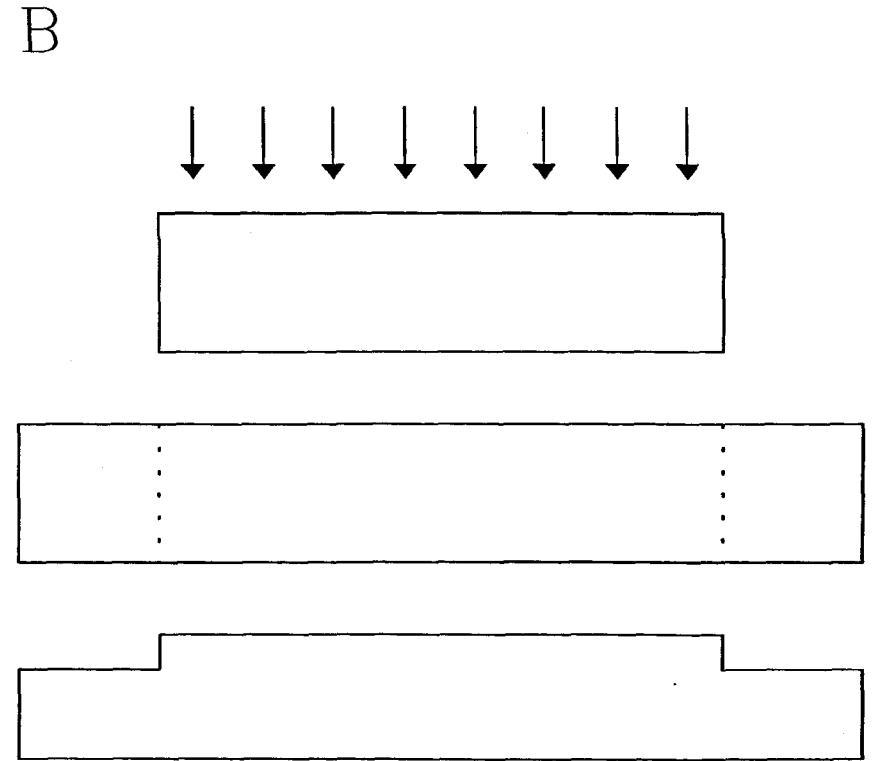
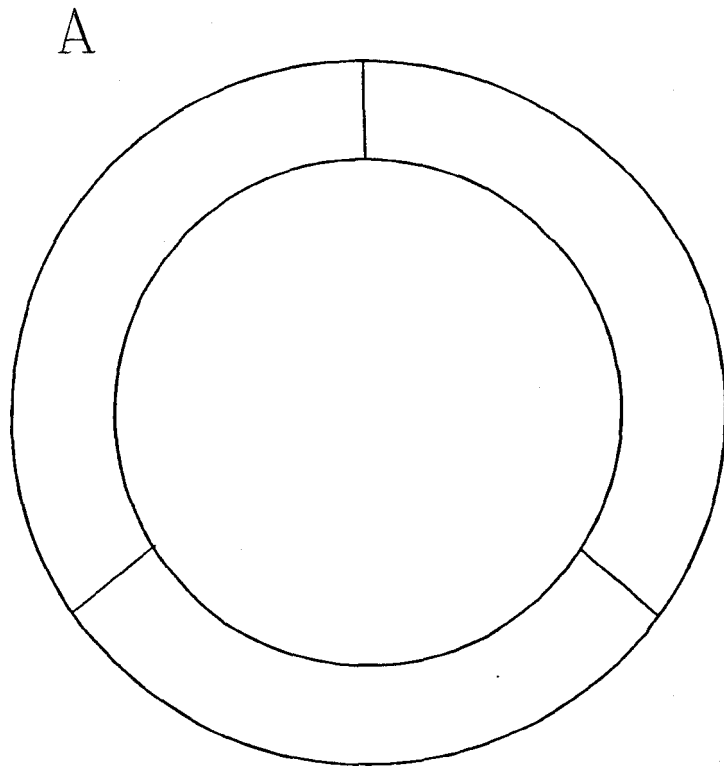


Figure 4.3 : YBCO targets are pressed using a 3 piece die cast (A). The die is placed onto the base plate and then filled with YBCO powder. A stainless steel piece is then placed on top of the die and pressure is applied evenly to the surface (B).

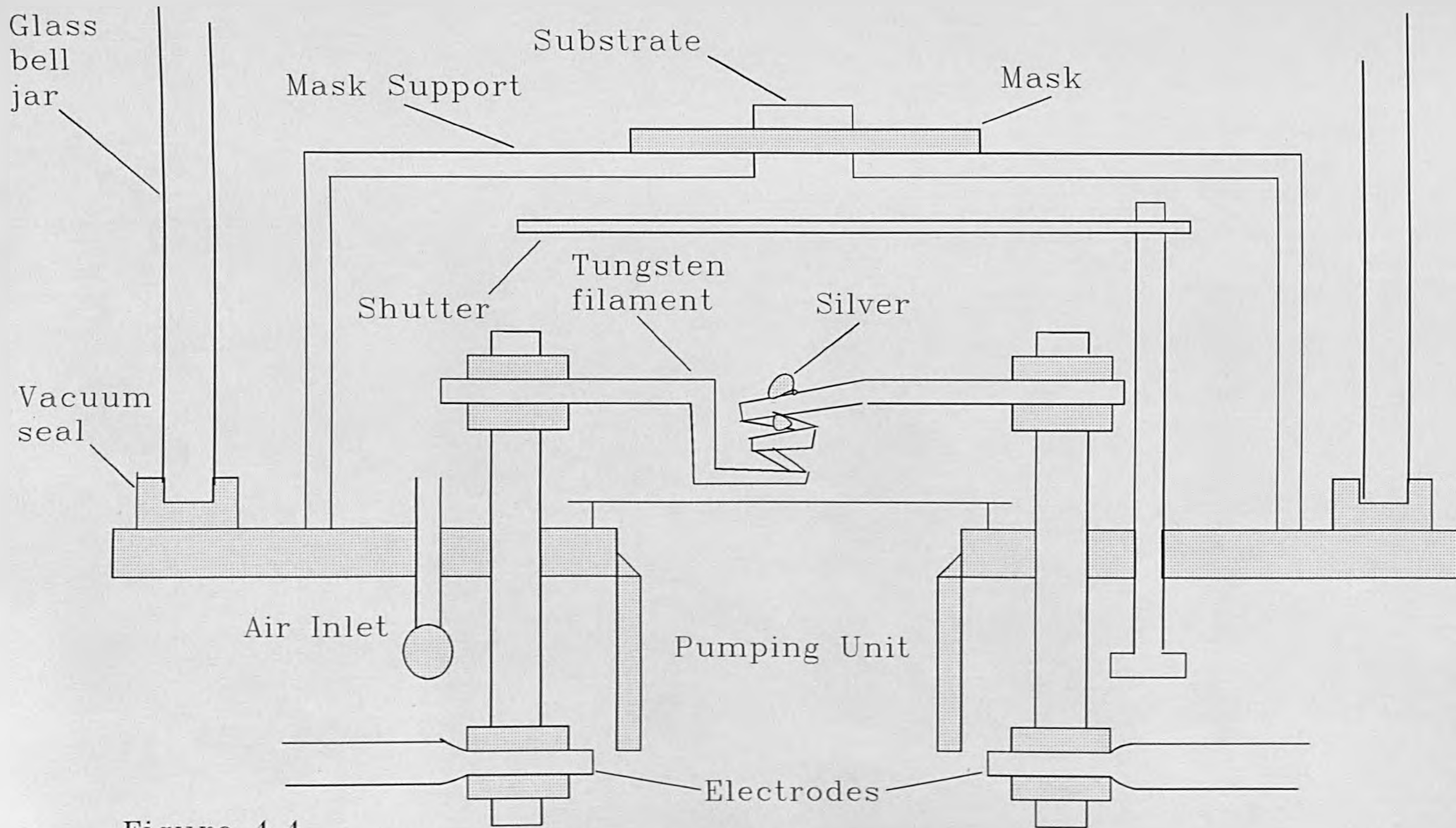


Figure 4.4

Chapter 5: EXPERIMENTAL PROCEDURE

5.1: Introduction

This chapter covers the electrical and structural measurements carried out on YBCO thin films. The electrical experiments include AC and DC resistance measurements, critical current and magnetic field experiments.

5.2: Cooling Unit

The films to be tested were mounted onto a cold head inside a closed cycle helium cryostat. The cold head consisted of a two stage cold head cylinder and drive unit displacer assembly. Together they produce closed cycle refrigeration at temperatures that ranged from 60-120 Kelvin for the first stage cold station and from 10-20 Kelvin for the second stage cold station, depending on the operating conditions. During operation, high pressure helium from the compressor enters the cold head at the helium supply connector. This then flows through the displacer regenerator assembly, crank case and motor housing before exiting through the helium gas return connector and returning to the compressor. Helium expansion in the displacer-regenerator assembly provides cooling at the first and second stage cold stations. When cold head operation reaches a steady state condition, further pressure regulation is unnecessary.

The cryostat is shown in Figure 5.1 and schematically in Figure 5.2. The unit contains two temperature sensors situated either side of the sample position. The first temperature sensor was a silicon diode type DT470, see (D) in Figure 5.2. By passing a 10 μ A current through the diode a voltage appears across the device. The magnitude of the diode voltage is inversely proportional to the diode temperature and is used to measure the temperature of the sample (see appendix for conversion tables). The voltage was measured using a digital voltmeter (Keithley 617DMM) on-line to a computer. The silicon diode was already fitted and calibrated when the system was purchased. Further

calibration was carried out at 293 K and 77.4 K and the results agreed with those of the manufacturer. The diode measured temperatures down to 1 Kelvin. The silicon diode is approximately 1 cm from the sample. Since a small temperature difference may result between the sample and the silicon diode a second temperature sensor was added (E). This is a platinum resistor temperature sensor linked directly to a Oxford Instruments model 3120 temperature controller. The sensor material was calibrated at 293 K, 273 K and 77.4 K. The platinum resistor has the drawback of becoming very inaccurate for temperatures below 65 Kelvin.

On top of the cold head was placed a large lid (B) that sits on top of a rubber ring (A) that ensured that the unit was sealed. The chamber was evacuated by closing valve (J) and opening (I). Evacuation was necessary to avoid heating due to conduction. A vacuum of $5 \cdot 10^{-2}$ Torr was adequate. Upon cooling the unit, the refrigerator cryopumps the residual gasses in the chamber and an insulating vacuum of between 10^{-4} and 10^{-5} Torr is achieved.

5.2.1 Device Under Test

The film under investigation (F) was attached to the cold head by either silver paint or double sided tape. Silver paint proved to be the best adhesive. It was not always possible to use silver paint as problems with earthing between the film and the cold head sometimes occurred. If there was a problem with earthing then double sided tape, which insulated the film from the cold head, was used. To test that the film was not earthed, each contact was tested individually. Once the film was mounted, wires (G) were bounded to the silver islands on the film surface. The wires were bonded in place using the same silver paint (Electrolube) that was used to bond the film to the cold head. These wires made up the four probes. The wires were in turn linked via a vacuum sealed

sealed BNC to leads outside the cooling chamber (H). The external leads were altered depending on the experiment being performed. For example, while performing an experiment using d.c. sources short coax cables were used to carry the current. The cables were then attached to either a constant current source, device ZN5245 or a high impedance voltmeter, Keithley 196DMM. In the RF experiments the wires were connected, via the BNC's, to 4 x 1 metre calibrated coax cables which link the Hewlett Packard 4192A impedance analyzer to the film. The impedance analyzer and/or Keithley's were in turn linked to a personal computer via an IEEE 488 interface unit. The interface unit allowed the instruments to be remote controlled. The measurements from the impedance analyzer/ Keithley were then stored directly into permanent hard disk memory by a simple computer program (see appendix for programs).

Below the cold head and wrapped around the column making up the cold head is a filament heater (K). By cooling the sample, while allowing a current to pass through the filament, it was possible to hold the temperature at the cold head stable long enough to complete a set of readings at a constant temperature (temperature +/- 0.1 K).

5.3: Radio Frequency Experiments

5.3.1: Impedance Analyzer

The a.c. measurements were obtained using an impedance analyzer (Hewlett Packard 4192A). The impedance analyzer is calibrated for use with one metre cables. For the low impedance measurements and variable frequency measurements it was necessary to re-calibrate the analyzer to determine the impedance due to the extra wires from the end of the coax cable to the film, the silver contact pads and the silver paint used to bond the wires to the silver contact pads. It is assumed that the YBCO sample once installed in the bio rad and wired to the impedance analyzer can be represented by

the equivalent circuit given in figure 5.6. The region of interest is that between the dotted lines, namely the part of the circuit encountered by the voltmeter, figure 5.6b. The signal received by the voltmeter is distorted, the difference between C and D is given by

$$Z_{CD} = Z_{sample} + 2Z_w$$

the distortion due to the extra wiring is $2Z_w$, assuming the wires have the same impedance. The stray impedance should therefore, appear as a linear offset. By shorting together the voltage contacts the circuit becomes that given in figure 5.3C, the impedance measured being due to the extra wiring, silver paint etc. This impedance can then be subtracted from the measured results to leave the impedance due to the sample alone. Two separate methods of calibration were used.

5.3.2: Calibration by shorting method

To perform the re-calibration, the wires used to provide the electrical contacts from the coax cables to the substrate were short circuited. The short circuit was achieved by placing a copper block into the system and bonding the four wires to it as if the copper block were a film. The copper block was bonded to the cold head using double sided tape to avoid earthing. The copper block had previously been filed and washed in acetone to produce a clean surface onto which the wires could be bonded. The Bio Rad was sealed and the system was evacuated. The HP 4192A impedance analyzer was set to measure the equivalent series inductance and resistance of the sample namely, the wires, silver paint and copper block. The frequency response of this arrangement was taken for values between 0.1 and 13 MHz (in 50 kHz steps). The results obtained were assumed to be due to the wires and the bonding silver. It was assumed that the copper block had a negligible effect on the inductance and resistance due to its excellent current

carrying characteristics.. Note that the copper was not a perfect conductor and there was a residual resistance. This is not a problem if the stray impedance is in the form of a linear offset.

The results of this experiment demonstrated that the effect of the wires and silver paint was to offset the inductance by approximately 8 nH at .1 MHz, rising to 9.5 nH at 13 MHz. The resistance was offset by 0.003 Ohms at 0.1 MHz rising to .022 Ohms at 13 MHz. Providing that the calibration results are in series with the inductance and resistance due to the thin film it is possible to subtract the calibration results directly from those results obtained from thin film measurements to give the reactance and resistance of the sample alone, as described in 5.3.1.

5.3.3: Hewlett - Packard Self Calibration

The HP 4192A analyzer used throughout these experiments was designed to be self calibrating when required. This entails calibrating the analyzer for a set frequency. The analyzer then alters the measured results and displays the calibrated equivalence values of the film for all the frequencies⁽²⁾.

To calibrate the analyzer was first set to short circuit. The short circuit was achieved using a copper block as described above. The analyzer was set for the series mode. The impedance analyzer calibrated itself for this arrangement, at frequency chosen by the user, usually 13 MHz. The impedance and resistance were set automatically to zero. The film under test was then loaded into the system. The four wires were placed onto the silver pads in the same arrangement as they were on the copper block. The film was then cooled and tested.

The effect of the calibration by this method can be seen in Figure 5.4. Here, the impedance analyzer was calibrated using the self calibration technique mentioned. The

resistance and inductance were recorded as a function of temperature. The second set of readings are for the same device without the self calibration. The experiments were carried out within minutes of each other in exactly the same way. It is safe to assume therefore that any difference in the results is due to the stray impedance. The stray impedance results in a linear offset in the inductance and the resistance of the sample. This is in agreement with section 5.3.1 and figure 5.6. The magnitude of the offset is similar to that determined in section 5.3.2.

Since the stray impedance appears as a linear offset it can be shown, (see section 8.1.2), that provided the geometric inductance and the kinetic inductance are very small, in comparison to the stray inductance, it is possible to calculate the value by extrapolation. It is not necessary therefore to perform the calibration experiments, described here, for each film. These calibration experiments prove that parts of the analysis used in section 8.1.2, concerning the stray impedance, are valid.

5.3.4: Frequency Response Experiments

Frequency response measurements were taken between the frequencies of 0.1 and 13 MHz in 50 kHz steps using the RLFREQ program, see appendix A program 2. Experiments were typically carried out at 293, 100 and 70 Kelvin. Readings taken at 100 and 70 Kelvin required the cold head to be held at constant temperature. This was achieved by heating the column of the cold head onto which the sample was fixed while engaging the compressor. This allowed the temperature to be held constant (± 0.1 K) for 3-5 minutes, giving time to complete the readings. Data was stored directly from the impedance analyzer onto disk to speed up the process. These results made it possible to observe the difference in inductance and resistance response between the normal and superconducting phase.

The second type of experiment was to measure the impedance with respect to temperature at constant frequency. The results obtained by this method were the equivalent series resistance and inductance of the YBCO thin films. Analysis of the inductance was expected to yield information about the critical temperature, flux flow, penetration depth and displacement current, an element that is normally ignored in superconductor research.

During cooling, a signal of 13 MHz was passed through the sample and the

resistance and inductance of the film were measured with respect to the temperature. Due to the position of the temperature sensors there was a slight temperature difference between the temperature sensors. The difference arises because of the distance of the sensor from the cold head. This only occurs during the cooling process. Due to the slight discrepancy that does occur, results taken during cooling were only used as a rough guide to the quality of the thin films. More accurate results were taken during the warming process. When the films were warming, the rate of warming was slower than that of cooling. The temperature discrepancy between the two temperature sensors was less than 0.1 K.

This process was repeated to record results with the application of a magnetic field. The magnetic field produced by the solenoid was used to ensure the mixed state within YBCO. The effect of applying a magnetic field to a sample can be seen within the results section. Note that with this arrangement the applied magnetic field was perpendicular to the sample.

During the experiments in which a magnetic field was used, the film was first cooled through the transition temperature. While the sample was allowed to warm the frequency/temperature response was measure again. This was then repeated for fields of different magnitude. Readings were taken every 0.1 Kelvin whilst the sample was warming. This allowed the change in resistance and inductance to be followed very closely. By cooling and repeating this process for different magnetic fields a series of results was obtained.

5.4: DC Resistance Experiments

Resistance-temperature measurements were performed in the cooling unit described above. The film to be investigated was mounted onto the cold head of the

cryostat as described above. Four wires were bonded to the silver strips previously evaporated onto the surface of the thin film with silver paint. The 4 probe method uses the outer contacts to supply a constant current. The constant current source used here was a model ZN5245. The inner two contacts were wired to a high impedance voltmeter and measured the potential drop across the film, as demonstrated in Figure 5.2. The voltmeter in these experiments was a Keithley 196DMM. The Keithley was IEEE 488 compatible. A simple programme (see appendix, program DCTEMP) was devised to take readings from the temperature sensor and the voltmeter almost simultaneously. By programming the computer, the resistance could be measured every 1 Kelvin or 0.1 Kelvin. The temperature sensors were used along with the Keithley voltmeter to record the change in resistance with temperature.

5.5: Critical Current Experiments

Critical current measurements were carried out using a 4-probe arrangement and an etched film. To achieve this four silver strips, 1 cm x 1.25 mm, were evaporated onto the thin film. The high current strip and the high potential strip were separated by 0.5 mm. The high potential and low potential strips were separated by 2 mm and the low potential and low current strips were separated by 0.5 mm. The films were etched using a photolithographic technique described below. Following etching, the silver strip was reduced in size to 1 mm x 1.25 mm and were separated as described above, see figure 5.4a. The etched film was mounted onto the cold head of the Bio Rad unit using silver paint as the bonding agent. Wires were bonded to the silver contacts using silver contact paint as the bonding agent. This allowed the formation of good ohmic contacts needed. The contacts were deliberately made large to accommodate the currents that would be necessary to drive the film into the normal state .

The cryostat was cooled to around 10 Kelvin and the current applied to the sample was increased. Due to the nature of the arrangement an offset voltage occurred and this was zeroed before increasing the current. By applying a large enough current it was possible to produce a voltage across the sample. The current needed to produce a voltage of 1 microvolt was defined as the critical current. The nature of the dissipation will be discussed elsewhere. The critical current was measured using this process at several different temperatures. Theory predicts that the response of critical current will be dependent on the structural properties of the thin films. The temperature dependence of the critical current may give some information about the structure of the thin film deposited. The magnitude of the current carrying capabilities of a thin film is determined.

5.5.1: Photomask Production

The photomask used for the photolithography was designed to allow for critical current measurements and to improve the sensitivity of the inductance measurements, see Figure 5.4b. The design consisted of five strips varying from 140 μm to 1 mm as shown in Figure 5.4b. The thinnest strip was to be used for critical current or magnetic field measurements. The mask was produced using a computer aided design package, PADS. The mask design, which was 256 times larger than the final product was plotted onto mylar paper using a standard HP plotter with a 0.5 mm pen filled with black india ink. To reduce the number of pin holes the mylar sheets were touched up by hand before reduction. Reduction consisted of a two-stage process. First the design was reduced to 1/16 of its original size and converted to a negative using a standard reduction technique. The negative was reduced further by photographing the negative using a camera placed directly above the negative. The distance between the camera and the negative was varied until the entire mask image was less than 1 cm^2 as required. Once the image was

in correct focus the camera was loaded with film. Since the final pattern would need to be on a rigid base that could protect it from damage and allow for easy use, the second reduction used Kodak High Resolution plates type 1A as the film. The glass plates were mounted into a camera placed above the negative. The plate was exposed to the negative using green light for 15 minutes. The exposed plate was then immersed for 5 minutes in Kodak HRP developer. The developer was diluted with water in the ratio of 1:4 respectively. After developing, the design was washed in water for 2 minutes. The plate was then fixed by a further 2 minutes in Kodak 3000:water fixer solution. The ratio of fixer to water was 1:1. The pattern was then washed for 10-15 minutes to guarantee all chemicals had been removed. This process reduced the negative by a further 16 times.

5.5.2: Film Etching

The films were etched using photolithographic technique. A positive photoresist, Microposit AZ1350, was applied to the film surface which was then spun at 3000 rpm for 30 seconds to produce a uniform film of resist. After drying for 10 minutes at 100°C, the resist was exposed to ultraviolet light for 20 seconds through a photographic mask of the required thin film pattern.

The photoresist was developed in Microposit HPR developer. The substrate was placed in the developer for 45 seconds. Once developed the film with photoresist was washed in water to remove any developer that was left. The excess water was then spun off. The substrate was then reheated to 100 °C and held at this temperature for 10 minutes. This ensured that the photoresist would remain bonded to the thin film, thus protecting the area where the thin film coating was to remain on the substrate.

The etchant used was Ferric (III) Nitrate. The ferric nitrate solution was prepared using equal masses of etchant and water. Once the films were exposed to the Ferric Nitrate, etching took place at a reported $1.5 \mu\text{m}/\text{sec}^{(3)}$. Since most of the films were less than $1 \mu\text{m}$ thick, simply dipping the substrate in the solution and then straight into water was normally enough to etch the film. Since the thin film with photoresist was well protected it was possible to use the etchant for longer periods, say 2-3 seconds to remove the more stubborn areas (those areas with silver deposited on them). If the films were exposed for more than 1 second however, the ferric nitrate had the opportunity to etch into the thin film underneath the edges of the protective photoresist. This was not a serious problem in this work and it is thought that the amount of undercutting is, in the worst case, only about 25% of the width of the thin film⁽⁴⁾. The etchant does not react with the substrate and the advantage of this as we shall see later was that it made recycling of old substrates possible. Once the etching had taken place the remaining photoresist was removed by simply brushing the surface of the thin film with acetone.

5.6: Experiments in an Applied Magnetic Field

In type II superconductors the application of a magnetic field can result in the familiar mixed state, in which normal and superconducting states exist in unison. The production of the mixed state usually requires the application of a magnetic field greater than some critical field H_{c1} , see chapter 3 for more details. Although the value of H_{c1} is not known for YBCO, experiments have shown that it is very small⁽¹⁾. Values lower than 100 Gauss have been found to produce the mixed state⁽⁵⁾. To achieve a magnetic field of the size, namely 100 Gauss or more, which could be used with the cooling system a solenoid was designed. The diameter of the cooling unit was approximately 105 mm. This meant that to produce the field required the solenoid would have to be physically

large. The inner diameter of the solenoid was 110 mm, were as the outer diameter was 300 mm. The solenoid was 85 mm wide. The copper wire used in the solenoid was capable of carrying 25 amps. With 1500 turnings the solenoid designed could produce a field of 0.075 T. During experiments the current used was no larger than 12 Amps, producing a field of 360 Gauss. The solenoid was calibrated using a hall probe and the results are displayed in Figure 5.5. The solenoid was used to ensure the YBCO thin film was in the mixed phase during testing.

5.7: X-ray Diffraction

X-ray diffraction was used to investigate the crystal structure of YBCO thin films. The X-rays used throughout this work were produced by a copper target with a nickel filter. The X-rays generated had a wavelength of 1.5418 Å. Since the substrates used were single crystal there was a high intensity of X-rays at the corresponding 2θ values, for example, in SrTiO₃(100) there was a large intensity of X-rays at $2\theta = 22.78$, 41.71 and 104.14. Below is a summary of the X-ray diffraction parameters of the substrates used throughout this thesis.

Substrate	Orientation	$K_{\alpha} / 2\theta^{\circ}$	$K_{\beta} / 2\theta^{\circ}$
MgO	100	21.07	19.00
MgO	200	42.91	38.53
MgO	400	93.99	82.57
SrTiO ₃	110	32.42	29.18
SrTiO ₃	220	67.8	60.43
SrTiO ₃	100	22.78	20.53
SrTiO ₃	200	46.48	41.71
SrTiO ₃	300	72.54	64.52
SrTiO ₃	400	104.14	90.75

5.8: Substrate Reclamation

Because of the cost of the substrate materials it was necessary to reclaim substrates. YBCO films on SrTiO₃ were removed using Ferric III Nitrate. For films deposited on MgO(100) examination of the surface often shows that it had sustained damage. It is not the ferric nitrate that caused the scratches, although it may have reacted with the scratches causing further damage. The origin of the scratches was not fully understood but it was probably due to a substrate/film interaction caused by the high temperatures during growth. The substrates were repolished by mounting onto a circular weight using dental wax as the adhesive. Once attached the substrates are moved from side to side by an arm. This side to side movement coupled with the rotating pad and a fluid consisting of particles 0.05µm in diameter, PP503 polishing compound enables the surface scratches to be removed. The length of time needed to remove the damage depended on the severity of the scratches, although a typical substrate generally took between 2-4 hours. Once polished, the substrates were cleaned using TAM and de-ionised water. Recycled substrates have been used successfully to produce high quality superconducting thin films of YBCO.

5.9 References

- 1 Fiory A.T., Hebard A.F., Mankiewich P.M., Howard R.E., *Phys Rev Lett* **61** (1988) 1419
- 2 Hewlett Packard 4192A user manual
- 3 Shih I., Qui C.X., *Appl Phys Lett* **51** (1988) 1523
- 4 Wan Y.M., Raven R.S., Inameti E.E., Murray B.G., *Vacuum* **43** (1992) 67
- 5 Clem J.R., *Physica C* **153-155** (1988) 50

5.10 Figure Captions

Figure 5.1 : The bio-rad cooling unit used to investigate the low temperature electrical properties of YBCO thin films.

Figure 5.2 : Schematic diagram of the bio-rad unit shown from the side and from above.

Figure 5.3 : The results of the calibration experiment. The results show that the wires and the silver contacts produce a linear offset in the inductance measurements.

Figure 5.4 : Diagram of a YBCO thin film before (5.4a) and after (5.4b) etching.

Figure 5.5 : The magnetic field/ current characteristics of the solenoid.



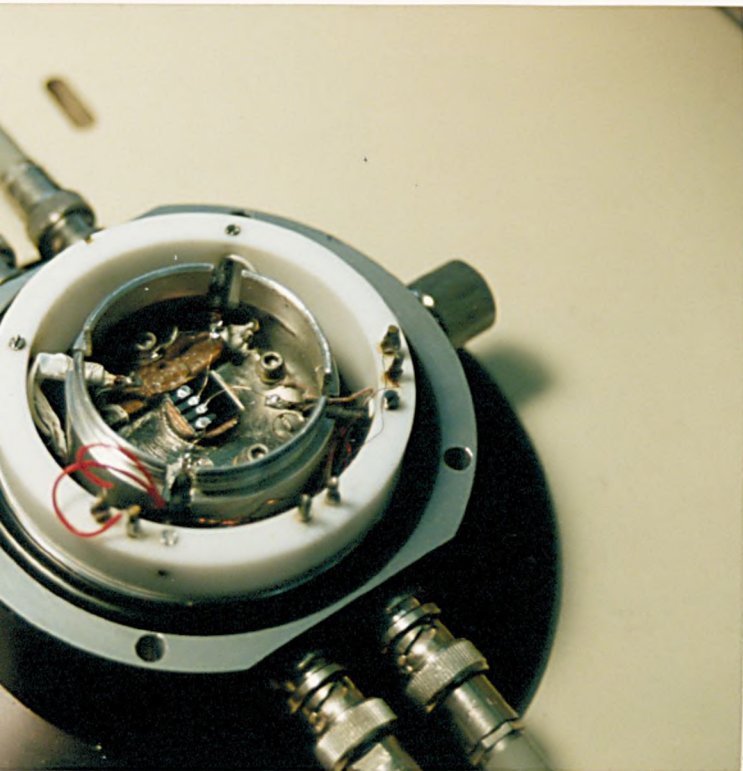


Figure 5.1

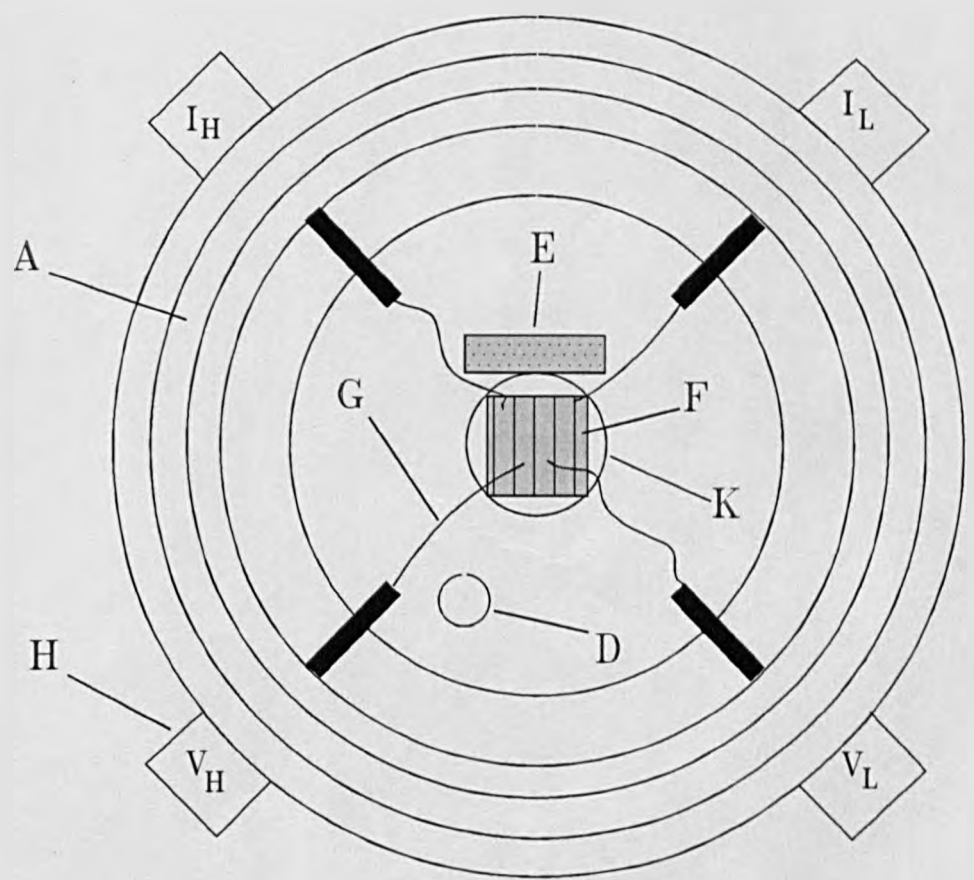
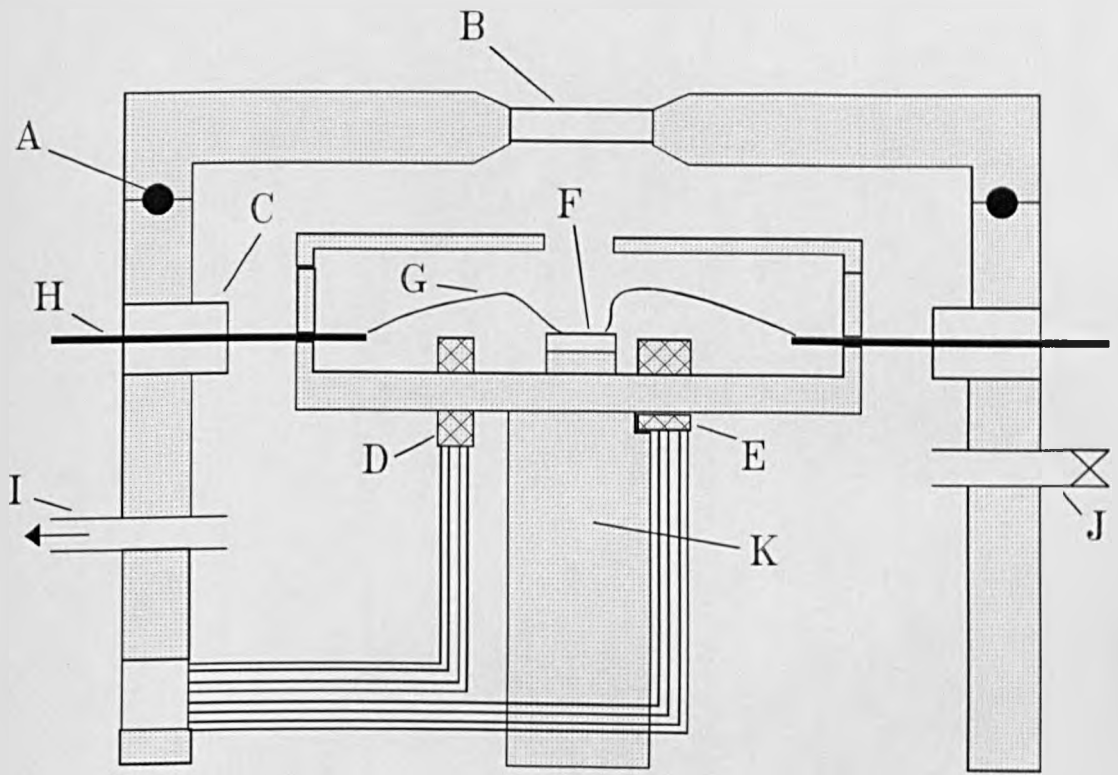


Figure 5.2

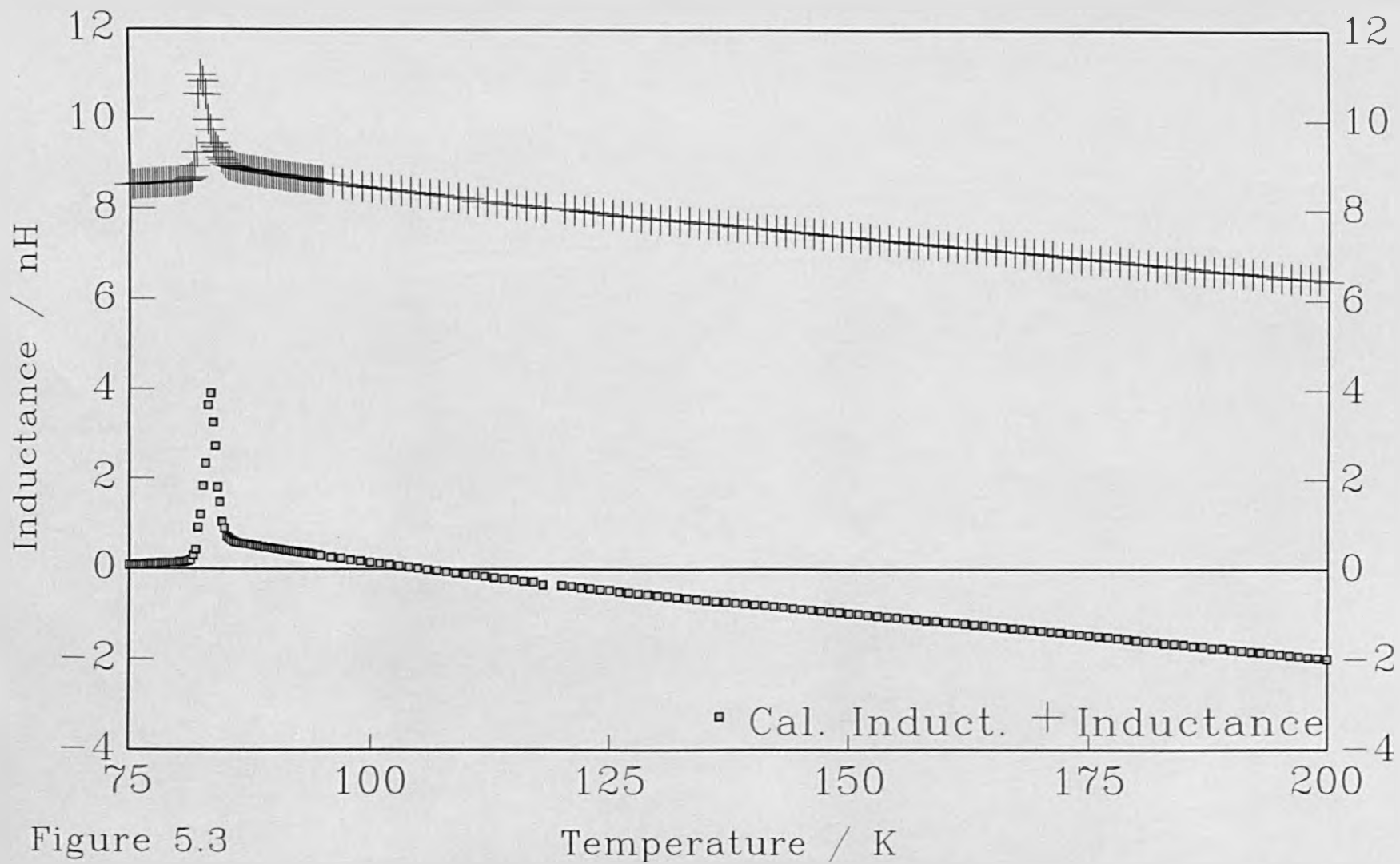


Figure 5.3

Temperature / K

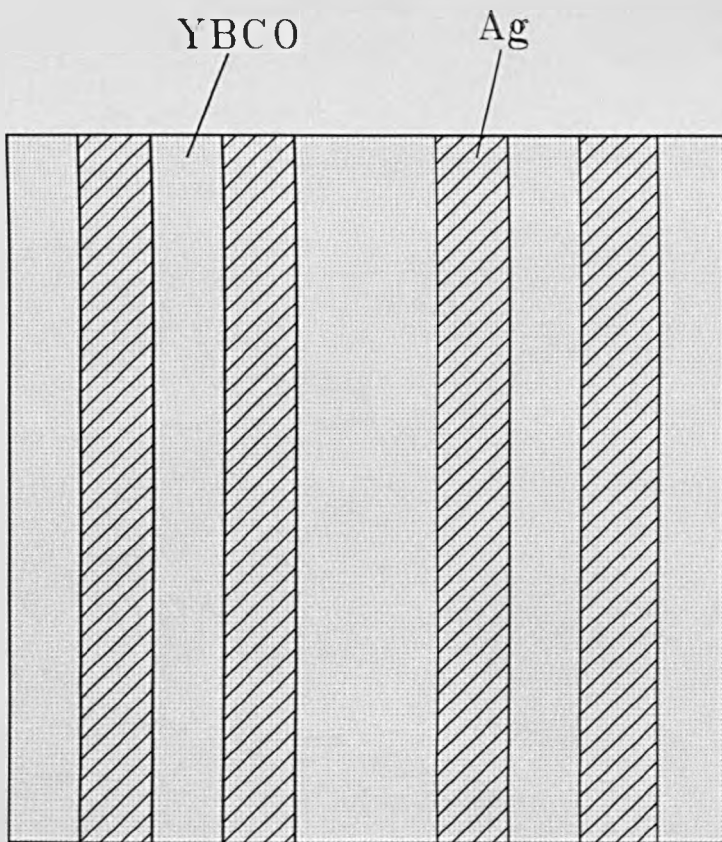


Figure 5.4a

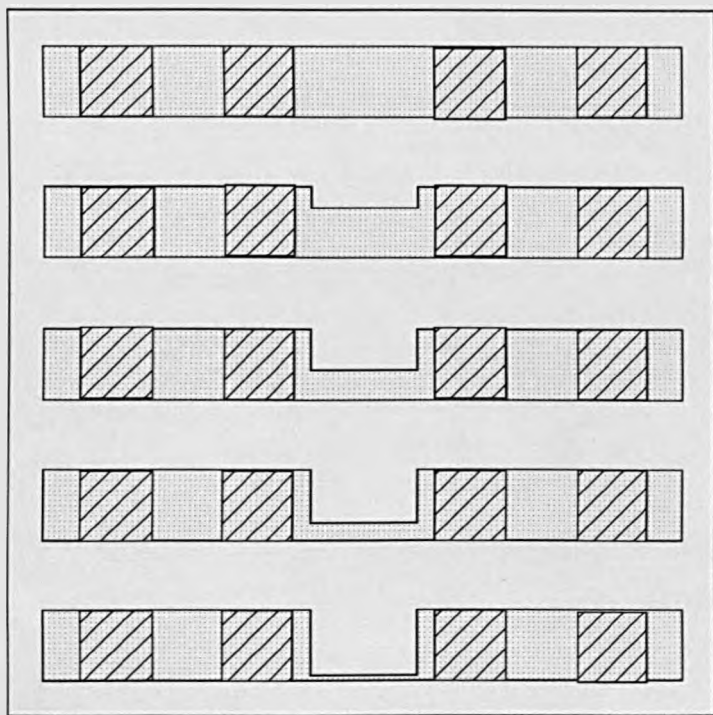


Figure 5.4b

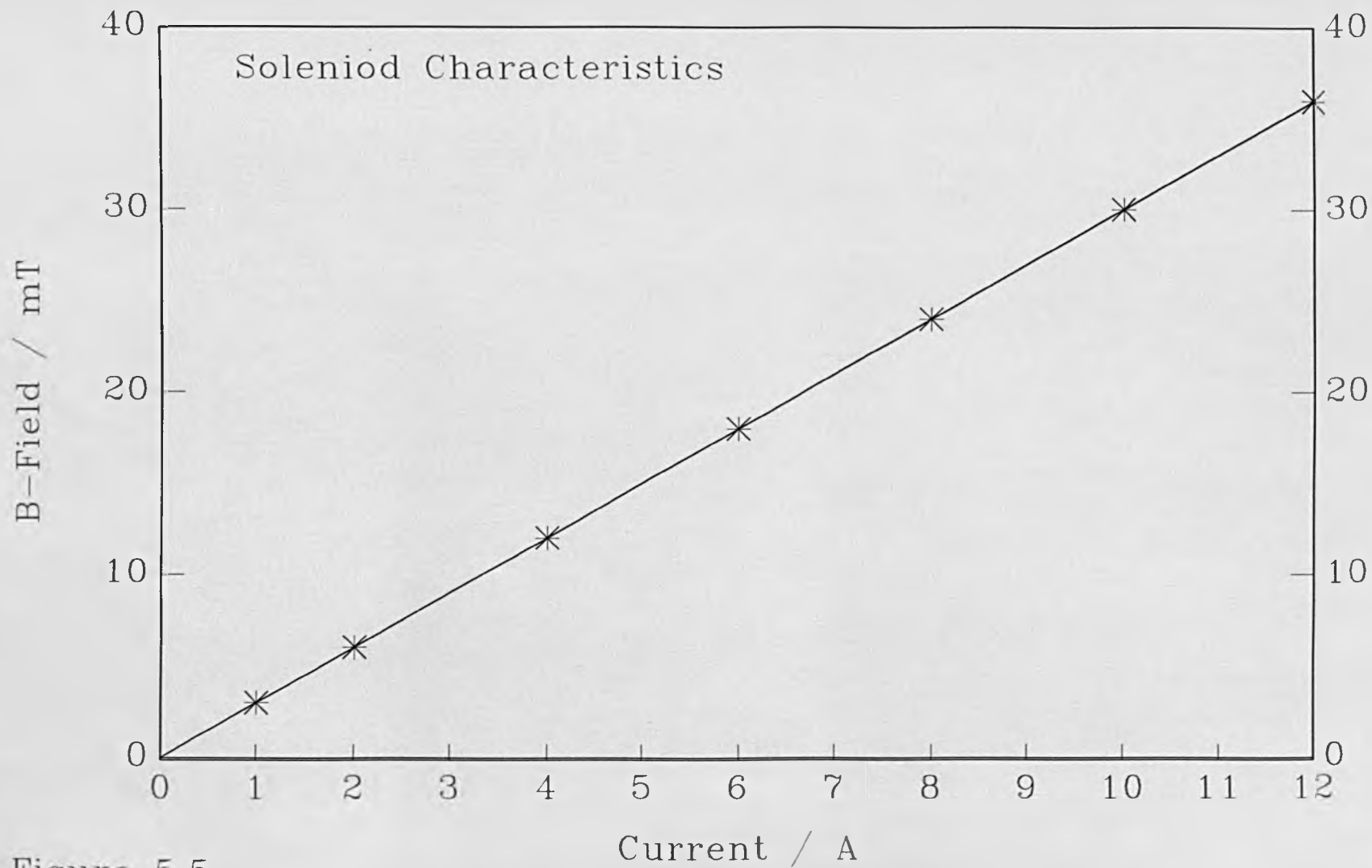


Figure 5.5

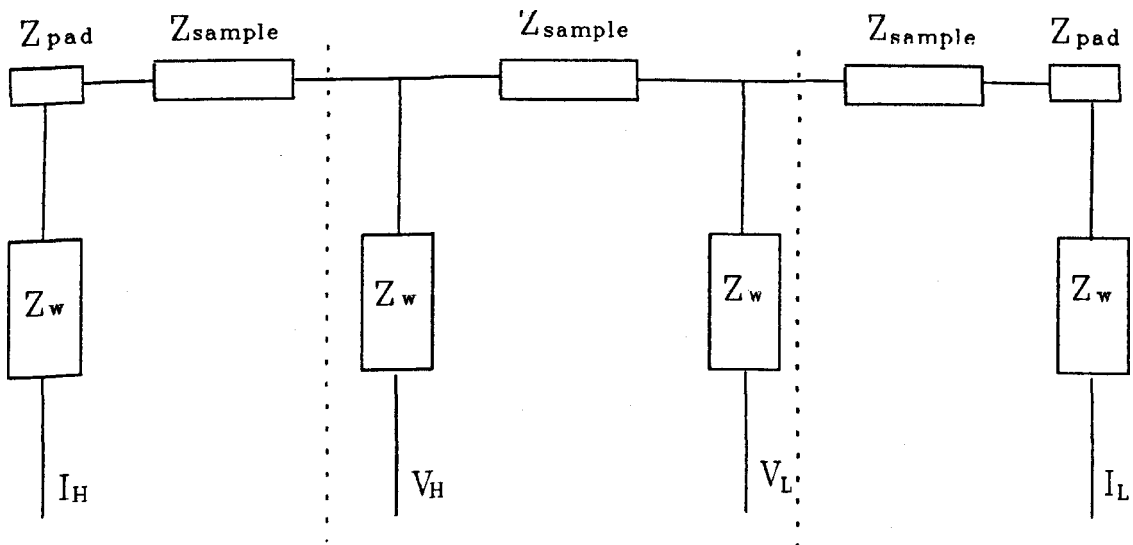


Figure 5.6a

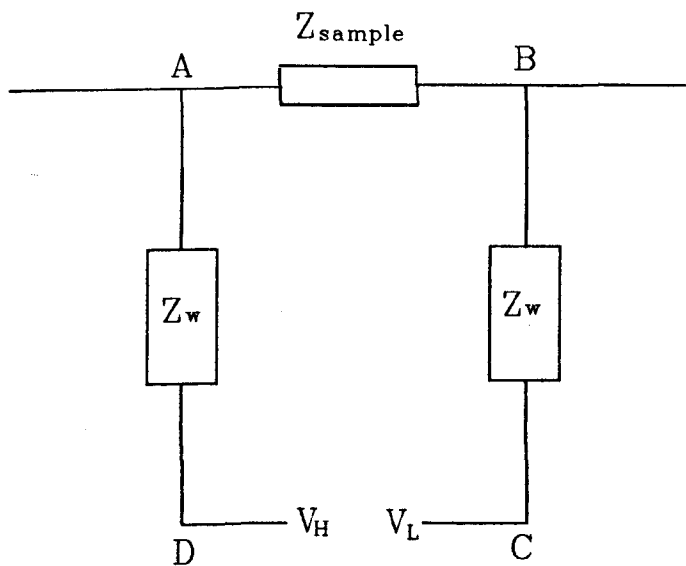


Figure 5.6b

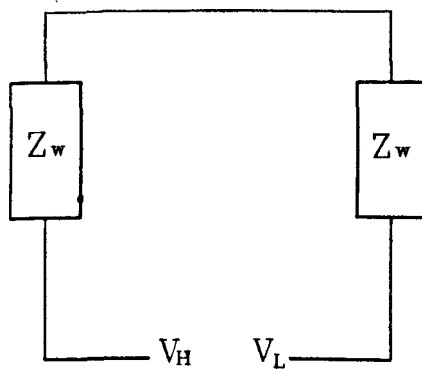


Figure 5.6c

CHAPTER 6: FILM DEPOSITION, RESULTS AND DISCUSSION

6.1 Introduction

This chapter describes the results of experiments performed on YBCO thin films. The first sections concern the deposition and structural analysis of YBCO thin films where the conditions used to produce YBCO thin films on a reproducible basis are described. This involved varying the substrate temperature, sputtering gas composition and pressure, position of the substrates, i.e. off-axis or on-axis sputtering. This is followed by X-ray diffraction results used to determine the orientation and lattice constants of the YBCO thin films.

6.2 Film Deposition

A summary of the growth conditions is given in Table 6.1. This includes the substrate material, gas pressure and content during deposition. The substrate temperature, R.F. sputtering current and deposition length are also given, as well as the critical temperature and film thickness. Each of the parameters given above was investigated in order to determine the effect on the quality of the thin films. This enabled the most favourable conditions for film deposition to be determined. The following section is an investigation into each of the parameters.

6.3 Ex-situ deposition

Deposition at low substrate temperature of about 100°C - 450°C followed by post anneal treatment can give superconducting thin films and this is of considerable interest^(1,2). By performing similar experiments with T_{sub} approximately 100 °C on-axis sputtering with a stoichiometric target, thin films of YBCO were deposited. A typical film is featured in Figure 6.1. The film featured in Figure 6.1 was deposited on axis, at

a substrate temperature of 420°C. The gas ratio was 4:1, Ar:O₂, the chamber pressure 200 mTorr, deposition length was 10 hours. Following deposition the thin film was heated in an oven to a temperature of 850°C. The film was held at this temperature for 3 minutes in flowing oxygen. The film was then allowed to cool in O₂ to room temperature.

In order to achieve superconducting thin films a series of experiments was performed. The gas content of the chamber was varied from 1:1 to 1:10, Ar:O₂ and the substrate was placed in the on-axis and off-axis arrangements. The pressure during deposition was also altered, from 150 mTorr to 280 mTorr. Although each of the deposition parameters namely, the gas content, pressure, substrate position and post deposition treatment were varied, 'cold' deposition proved to be an unsuccessful method of producing good quality superconducting thin films. From analysis of the bulk target and sputtered thin films using EDAX it became clear that on several occasions the bulk and the thin films were very similar in composition, namely that the barium, copper and yttrium content were similar for both film and bulk. It was not possible however to detect the oxygen content. The superconducting properties are of course dependent on the oxygen content, lower oxygen content resulting in semiconducting properties⁽³⁾. It is possible therefore that although YBCO may have been deposited, the poor oxygen content of the material resulted in the formation of the tetragonal semiconducting phase. If this is the case then this would imply that the post deposition treatment used was incorrect. The effect of this type of deposition was poor quality films that degenerated visibly with time. X-ray analysis of these films, gave very few if any clear spikes that could be used for identification purposes. This implies that the films were not epitaxial or even oriented and were probably still amorphous in nature. Several attempts were made to deposit superconducting thin films using this method and some were successful,

6.4 In-situ deposition on SrTiO₃(110)

The initial experiments in which the substrates were heated were more successful than the low temperature experiments, in the sense that the films had metallic as opposed to semiconducting electrical characteristics after deposition. The films were of poor quality however and did not become superconducting until very low temperatures. The solution to the problem lay in the overall growth conditions. Gas pressure, composition, substrate position, substrate temperature during deposition as well as post anneal treatment all effected the quality of the thin film deposited. The effect of each of these parameters is investigated here.

The substrates were initially cleaned in Trichloroethylene, Acetone and Methanol followed by a wash in deionised water. The substrates were mounted off axis to the target. Silver foil was placed behind the substrates to improve thermal contact. In later experiments silver paint was used. A presputtering period varying from 30-60 minutes allowed the system to reach equilibrium. The substrate temperature, T_{sub} , during deposition was generally between 700 - 750 °C. The sputter depositions lasted from 4 - 12 hours.

6.4.1 Sputtering Gas Pressure

The gas pressures available for use were limited to a relatively small window. Low pressure discharges, around 50 mTorr were too low to maintain effective sputtering. At higher pressures, greater than 300 mTorr, the system became unstable and it was difficult to maintain equilibrium. Due to these restrictions films were deposited at pressures varying from 200-280 mTorr. Within this small pressure range the effect on the quality of the thin films was still visible. The film deposited on SrTiO₃(110) at a pressure of 280 mTorr (YRF57), with Ar:O₂ of 4:1, was of better quality, $T_C > 71$ Kelvin,

than the film grown under the same conditions but with the pressure at 200 mTorr, $T_c=53$ K, (YRF56). Initially this result was thought to be due to the lower oxygen partial pressure in the 200 mTorr deposition, namely 40 mTorr instead of 56 mTorr. Increasing the amount of oxygen from 20 % to 50 % in the sputtering gas, at a sputtering pressure of 200 mTorr, did not however improve the quality of the thin film deposited on $\text{SrTiO}_3(110)$. The increase in the partial pressure of the oxygen to 100 mTorr resulted in a poorer quality film. The film, deposited with all the other growth parameters kept constant, had a $T_c=32$ K, (YRF59).

Although the oxygen partial pressure did influence the quality of the thin film it was difficult to determine, from the experiments performed, the exact relationship between the oxygen partial pressure and the quality of the thin films deposited. It was clear however that the film deposited at the higher total pressure of 280 mTorr was the better of the films. In all the experiments after YRF61 on $\text{SrTiO}_3(110)$ the sputtering pressure was set to 280 mTorr and the gas ratio to 4:1, Ar: O_2 .

6.4.2 Post Annealing

Although each of the films described above was cooled to room temperature in pure O_2 , there was no post anneal, the films were simply allowed to cool to room temperature. A further experiment using the same technique and deposition parameters as YRF57, which also included a post deposition anneal at 450°C for 1 hour in pure oxygen, YRF62, resulted in a film with a T_c 6 Kelvin higher than the film without the anneal, see Figure 6.2. All subsequent films were post annealed in pure oxygen at temperatures ranging from $400\text{-}450^\circ\text{C}$ for 1 hour.

6.4.3 Substrate Position

In order to improve the films further, the horizontal distance of the substrate from the centre of the target was altered. Using the off axis mode, with the vertical distance from the target held constant, several films were deposited at varying horizontal distances from the centre of the plasma. The growth parameters were the same throughout the various depositions. The growth parameters were Ar:O₂, 4:1 at 280 mTorr, T_{sub}=735 °C, deposition length of 6 hours. Post deposition anneal at 425 °C in pure O₂ for 1 hour.

Results demonstrated that the off axis distance from the centre of the target did have an effect on the quality of the thin films. At a distance $x = 8$ cm from the centre of the target, a film with T_{Co} in excess of 87 K was produced, YRF67. The film was 680 Å thick, an average deposition rate of 1.89 Å/min. Shortening the distance x , lead to a reduction in the T_{Co} of the subsequent films. At $x=63$ mm, the T_{Co} was 71 K, with an onset temperature of 77 K, YRF70. At $x=43$ mm, the T_{Co} was less than 20 K, YRF66. These films were visibly thicker than those deposited at $x=80$ mm. The results were reproducible, see Figure 6.3.

6.4.4 Substrate Temperature

The substrate temperature during the deposition was varied from 700-750 °C. It was not possible to establish any clear link between deposition temperature and film quality within this temperature region, for films deposited on SrTiO₃(110). However, there was a suggestion that the orientation of the YBCO thin film was dependent on the substrate temperature. This will be discussed in the section on X-ray diffraction given below.

6.5 In-situ Deposition on MgO (100)

The MgO(100) substrates were polished and cleaned and mounted in the same way as the SrTiO₃(110) substrates. The deposition parameters were also similar to those described above. The effects on the thin films of altering the various growth parameters appears to be different to those films deposited on SrTiO₃(110). All the films described below were deposited off axis. Each film, except YRF59, was post annealed in pure oxygen for approximately 1 hour in the temperature region 400-450°C.

6.5.1 Sputtering Gas Pressure

The pressure and content of the sputtering gas was less critical for the films deposited on MgO(100). Successful deposition occurred for sputtering pressures of 200 mTorr, YRF59, see Figure 6.4. The gas ratio during deposition was 1:1, Ar:O₂. The critical temperature of the thin film on MgO(100) was 72 K. Increasing the deposition pressure to 280 mTorr and changing the ratio of the sputtering gas to 4:1, Ar:O₂ did not have any detrimental effect on the thin films deposited on MgO(100). This was fortunate since it allowed films to be deposited on SrTiO₃(110) and MgO(100) simultaneously. YRF67, YRF68 and YRF70 are examples of this.

6.5.2 Substrate Position

The off axis position of the MgO(100) was important to the quality of the thin films deposited. Several experiments were performed in which the only parameter to be altered was the off-axis position.

The substrates were cleaned and mounted and thermal contact was improved using silver foil. Presputtering lasted for 55 minutes. The gas pressure during deposition was 280 mTorr, the gas ratio was 4:1, Ar:O₂ and $T_{\text{sub}}=735$ °C. The length of the

deposition was 6 hours. The post anneal took place in flowing pure oxygen. The substrate temperature during the post anneal was 425 °C and the anneal lasted 1 hour.

The results of the experiments demonstrated that the position of the MgO(100) substrate did influence the quality of the thin film, see Figure 6.5. The film deposited closest to the centre of the plasma, $x=43$ mm, was the poorest, $T_c=60$ K (compared with $T_c=50$ K for the film deposited on SrTiO₃(110)). For $x=63$ mm the $T_c=75$ K for the film on MgO, compared with $T_c=80$ K for the film on SrTiO₃(110). The best films were deposited on the edge of the plasma, $x=80$ mm. The resulting critical temperatures of the thin films deposited on MgO(100) and SrTiO₃(110) was 82 and 88 K respectively.

6.5.3 Substrate Temperature

The exact effect of the substrate temperature during the growth is difficult to determine since it was not specifically investigated. Results demonstrate that the effect of the substrate temperature may be important in the thin films deposited on MgO(100). During the course of producing thin films several experiments were repeated to determine the reproducibility of RF sputtering. Many of the films deposited on SrTiO₃(110) were found to be reproductions of the earlier experiments, having a similar T_{Conset} and T_c etc. For the films deposited on MgO(100) however the results were not always reproduced, for example YRF67 and YRF68, see Figure 6.6. Although the change in normal resistance is due to the difference in thickness (see Table 6.1), the reason for the change in T_c is unclear, though the most plausible reason is the thermal contact. If the thermal contact between the substrates and the heater were to deteriorate the effect would be similar to depositing the thin film at a lower temperature. It would also mean that the temperature of the post anneal would be lower than expected. This could have a dramatic effect since it is well known that the low temperature anneal

converts the thin film from the tetragonal to the orthorhombic phase and that the temperature of the anneal is required to be above 400°C. (This idea is supported by thin films deposited when the silver foil, used to ensure thermal contact, was replaced by silver paint. The quality of the films deposited on MgO(100) became more consistent.) If this is the case then it implies that the films deposited on the SrTiO₃(110) substrates are effected less by changes in the deposition and annealing temperatures than those deposited on MgO(100). If this is correct then it raises the question of whether the orientation or the substrate material is responsible for this difference. In order to investigate this idea it is necessary to examine the results from the experiments performed on SrTiO₃(100) substrates.

6.6 In-situ Deposition on SrTiO₃(100)

Deposition of YBCO thin films onto SrTiO₃(100) makes it possible to determine the effect of substrate orientation on the thin film. Furthermore by comparing the results of films deposited on SrTiO₃(100) with those deposited on MgO(100) it is also possible to determine the effect of substrate material on film quality. For all the films deposited on SrTiO₃(100) the sputtering gas pressure was 280 mTorr, 4:1, Ar:O₂. The films were also post annealed in pure oxygen at 400-450°C for 1 hour.

6.6.1 Substrate Position

The effect of the change in the off axis position of the substrates prior to deposition was more evident in films on SrTiO₃(100) than those on SrTiO₃(110). The change in critical temperature was not as great as that observed in films deposited on MgO(100). These results imply that the substrate and the substrate orientation influence the quality of the thin film, see Figure 6.7.

6.7 Films deposited on SrTiO₃(100) and (110)

The first experiments to be performed on SrTiO₃(100), were under conditions that had been used successfully to deposit YBCO thin films on SrTiO₃(110). In order to verify the reproducibility of the rf sputtering method, a SrTiO₃(110) substrate was mounted next to the SrTiO₃(100) substrate. Both substrates were held in place by the rails and thermal contact had been improved with the use of silver foil. The target was presputtered, prior to deposition, for 40 minutes. During deposition the substrate temperature was 735°C and deposition lasted for 6 hours. The resulting films were post annealed in flowing pure oxygen for 1 hour at 405°C. Testing the films with the 4 probe method revealed that the critical temperatures were 77 and 76 K for the films on SrTiO₃(110) and SrTiO₃(100), respectively, Figure 6.8. The onset temperatures of the films were 87 and 82 K respectively, YRF62. The reason for the difference in the onset temperatures was assumed to be due to differences in film orientation and crystal structure. Resistivity measurements on the two films revealed anisotropy, this is investigated below. It is interesting to note that if the ΔT ($\Delta T = T_{\text{Conset}} - T_C$) is taken as a measure of film quality, namely that the smaller the ΔT the better the film then the film deposited on SrTiO₃(100) is in fact the better quality film.

Further experimentation revealed that in every simultaneous deposition on to SrTiO₃(110) and SrTiO₃(100) the films deposited on the (110) substrates had higher critical temperatures, as well as a small ΔT . The difference in critical temperatures of the two films ranged from 1 K in YRF62 to 14 K in YRF86. It is thus evident that under the growth conditions used here that SrTiO₃(110) is the most suitable substrate.

6.8 Films deposited on SrTiO₃(100) and MgO(100)

Films were deposited simultaneously on MgO(100) and SrTiO₃(100). Growths

YRF80 and YRF83 produced thin films on SrTiO₃(100) with $T_{\text{Conset}}=82$ K, $T_{\text{Co}}=70$ K and $T_{\text{Conset}}=80$ K, $T_{\text{Co}}=72$ K respectively, see Figure 6.9 for example. The corresponding films deposited on MgO(100) had $T_{\text{Conset}}=70$ K, $T_{\text{Co}}=65$ K and $T_{\text{Conset}}=59$ K, $T_{\text{Co}}=52$ K respectively. One reason for this difference in critical temperature of the films may be due to the lattice mismatch, which is smaller in SrTiO₃(100) than in MgO(100). However the ΔT was smaller in the films deposited on MgO(100).

6.9 X-ray Diffraction

The X-ray diffraction measurements were carried out using an X-ray diffractometer, the Siemens K-4, in the Materials and Materials Design Engineering Dept at the University of Nottingham. The samples were scanned from 0 - 90 ° using an X-ray source of copper with a characteristic wavelength of 1.54 Å. The angle over which the sample was scanned represented 2θ , where θ is the angle in the Bragg equation

$$n\lambda = 2d\sin\theta \quad 6.1$$

Each 2θ value of each peak on a diffraction pattern was recorded. The data was analysed using a computer program, XANAL.BAS. The program identifies at least two peaks due to the substrate materials using a 'look up' table containing values given in the ASTM files. The peaks given by the film substrate were compared with the ASTM results and the 2θ values of the peaks given by the films were corrected accordingly. The corrected 2θ values are compared with the various orientations of YBCO. The program displays any orientations which lie within 0.1 ° of the peaks obtained from experiment. These results enable the user to identify the most likely orientation(s) of the YBCO thin films. When a series of peaks have been identified they can be used to calculate the lattice parameters of the film using the theory given in chapter 3.

A problem in this work is the substrate materials. The substrates are high quality

single crystals and thus generate some very clear diffraction peaks. This is unavoidable since 90 % of the X-rays penetrate to about 2 μm . Since many of the films are 0.5 μm or less, a large number of X-rays are diffracted by the single crystal substrates. To overcome this problem the sensitivity of the X-ray detector is sometimes reduced. This reduces the clarity of the peaks due to the YBCO thin film. A compromise is thus made that is not always satisfactory.

6.9.1 YBCO films deposited on $\text{SrTiO}_3(110)$

A typical X-ray diffraction pattern of a YBCO thin film on $\text{SrTiO}_3(110)$ is shown in Figure 6.10. The YBCO peak is dwarfed by the $\text{SrTiO}_3(110)$ peak although it is large enough to identify. The 2θ value of the YBCO peak is 68.5° . Comparing this with the ASTM files it becomes clear that either of two orientations could be present, namely (110) or (013) or a combination of (110/013). It is not possible from these results to determine the orientation of the films. This is very unfortunate since the films are anisotropic. It will be shown below that the anisotropic nature of these thin films may help solve the problem of identifying the orientation. Besides the peaks identified as (013/110) there were also several other peaks. These peaks were identified as a-axis and c-axis peaks. The X-ray diffraction patterns of YRF42, YRF67 and YRF82 give evidence of a and/or c-axis orientation. From the peaks it was possible to calculate the lattice constants which are summarised here, in Table 6.2

Sample	YRF42	YRF67	YRF82
a-axis / \AA	3.88	3.86	-----
c-axis / \AA	-----	11.69	11.66
T_{c0} / K	-----	88	-----

Table 6.2

6.9.2 YBCO thin films deposited on MgO(100)

A typical X-ray diffraction pattern of a YBCO thin film deposited on MgO(100) is shown in Figure 6.11. From the ASTM files these are identified as being from the (00l) series. Although this has been reported elsewhere it is worth noting that there is no evidence of any (h00) peaks except for those of the MgO(100). Due to the amount of peaks it is possible to calculate the c-axis lattice values of the thin films. Table 6.3 gives a summary of the samples investigated using X-ray diffraction and the corresponding c-axis lattice constants.

Sample	YRF47	YRF65	YRF68	YRF70	YRF72	YRF78	YRF83	YRF87
c-ax. / Å	11.73	11.85	11.83	11.76	11.81	11.81	11.76	11.71
RF I/mA	140	140	140	120	140	130	120	125
T _{c0} / K	----	49	72	76	----	65	72	73

Table 6.3

From these results it is possible to see that there does appear to be some relationship between the c-axis lattice constant and the critical temperature. The films with the higher T_{c0}'s, except YRF68, tend to have the smaller lattice constant. There also appears to be a link between the c-axis value and the sputtering current. Namely the higher the sputtering current the lower the critical temperature, again with the exception of YRF68. It is worth noting that every film except YRF68 was deposited over a 6 hour period. YRF68 was deposited over a 10 hour period. It may be that the film deposited in the last four hours was of YRF68's deposition was of better quality than that deposited in the first 6 hours.

Since it has been reported in the literature that current transport is easiest in the a-b planes, namely c-axis perpendicular to the substrate surface as is the case for films

deposited on MgO(100) it is expected that the resistivity of the films deposited on MgO should be less than for films deposited on SrTiO₃(110). This is investigated in the following chapter.

6.9.3 YBCO Films deposited on SrTiO₃(100)

The films deposited on SrTiO₃(100) gave some very interesting results featured in Figure 6.12. Films were deposited simultaneously on MgO(100) and SrTiO₃(100). The X-ray diffraction patterns of several films deposited on SrTiO₃(100) were investigated and the results as well as the deposition temperature and critical temperature are given here in table 6.4.

Sample	YRF74	YRF80	YRF81	YRF83	YRF116
a axis / Å	3.89	3.86	3.82	3.83	-----
c-axis / Å	11.68	11.76	11.76	11.67	11.75
T _{SUB} / K	715	735	735	735	705
RF I / mA	130	130	130	120	130
T _{C0} / K	64	65	72	72	81

Table 6.4

The X-ray diffraction results demonstrated clearly that c-axis orientated thin films had been deposited on the SrTiO₃(100). There were also several other peaks which were identified as (100), (200) and (300), namely a-axis orientated YBCO. The a-axis peaks were not present on the films deposited on MgO(100). The reason for the a-axis deposition on SrTiO₃(100) is presumably due to the small lattice mismatch between the substrate and thin film. The YBCO thin films are therefore mixed orientated consisting of (h00) and (00l). The deposition of the mixed phase is temperature dependent. All the films deposited for T_{SUB}=735 K were mostly a-axis orientated, namely that the peaks due

to the a-axis were larger than the c-axis peaks. Further work YRF116 revealed that c-axis films could be deposited by using a lower deposition temperature. There was no evidence of a-axis peaks in the X-ray diffraction pattern of this film.

Comparing the sputtering current with the critical temperatures did not reveal any relationship. The temperature of the substrate during the deposition did not appear to have a significant effect on the critical temperature.

6.10 Summary of Chapter Six

From the results discussed in this chapter the SrTiO₃(110) substrate was found to be the best for deposition of YBCO thin films. The difference in quality between films on SrTiO₃ and MgO is expected simply because of the considerable lattice mismatch between the MgO and YBCO. The difference in quality between YBCO on SrTiO₃(110) and SrTiO₃(100) is however quite surprising. The results imply that the orientation is an important parameter in thin film production. Evidence has shown that the growth mechanism is dependent on orientation. It is thus likely therefore, that the results obtained here demonstrate that the growth mechanism varies between the (110) and (100) orientated SrTiO₃ substrates.

The quality of the thin film is dependent on the growth parameters as expected. What is interesting is that certain conditions exist which produce superconducting thin films on MgO and not on SrTiO₃(110) and vice versa. This can also be interpreted as further evidence for the idea of different growth mechanisms.

The most successful depositions were YRF67 and YRF68 on SrTiO₃(110). The films were deposited off-axis in an Ar:O₂, 4:1, atmosphere at a pressure of 280 mTorr. The substrates were situated 8 cm from the centre of the target and were heated to a temperature of 730 °C during deposition. The films were also post annealed in pure oxygen for 1 hour.

The X-ray diffraction patterns of the YBCO thin films revealed that film orientation was dependent on substrate material, orientation and deposition conditions. Films deposited on MgO(100) were all c-axis orientated, although the magnitude of the c-axis lattice constant did vary, ranging from 11.71 to 11.85 Å. This corresponded to a change in critical temperature of 73 to 49 K respectively. It thus appears that as the c-axis becomes elongated the superconductor phase deteriorates.

The orientation of the films deposited on $\text{SrTiO}_3(100)$ were dependent on growth conditions. Structural analysis revealed that a mixture of the (a00) and (00c) phases had been deposited. The films are however mainly a-axis orientated judging by the magnitude of the X-ray diffraction peaks i.e. the peaks due to the a-axis are greater than those of the c-axis. A later film deposited at a lower temperature (705 °C) was found to be c-axis orientated. It appears that the increase in deposition temperature enhances a-axis deposition in the films deposited on $\text{SrTiO}_3(100)$.

The majority of films deposited on $\text{SrTiO}_3(110)$ were (110/013) orientated as expected. It is not possible to distinguish between the peaks due to the (013) and (110) phases here. Since the films are anisotropic it may be possible to determine the degree of orientation from the resistivity and inductivity measurements. In several films there was also some evidence of a and c-axis orientation. The reason why these orientations have been deposited is unclear. The result is very interesting since the growth mechanism between a and c-axis deposition and (013/110) deposition are different, i.e. spiral growth and ridge growth respectively. It thus seems that in certain films both types of deposition are present.

6.11 References

- 1 Tsuda K., Muroi M., Matsui T., Koinuma Y., Nagano M., Mukae K.,
Physica C **153-155** (1988) 788
- 2 Guilloux-Viry M., Karkut M.G., Perrin A., Pena O., Padiou J., Sergent M.,
Physica C **116** (1990) 105
- 3 Jorgensen J.D., Beno M.A., Hinks D.G., Soderholm L., Volin K.J., Hitterman
R.L., Grace J.D., Schuller I.K., Serge C.U., Zhang K., Kleefisch M.S., *Phys Rev*
B **36** (1987) 3608

6.12 Figure Captions

Figure 6.1 : The variation of series inductance and resistance with temperature for a YBCO thin film deposited onto SrTiO₃(110) on axis at 420°C measured at 13 MHz.

Figure 6.2 : The variation of series resistance for YBCO thin films deposited onto SrTiO₃(110) on axis measured at 13 MHz. The increase in T_c is due to the post anneal.

Figure 6.3 : The effect of substrate position during deposition on the critical temperature of YBCO thin films deposited onto SrTiO₃(110).

Figure 6.4 : The variation of series resistance for YBCO thin films deposited onto MgO(100) on axis measured at 13 MHz.

Figure 6.5 : The effect of off-axis substrate position during deposition on the critical temperature of the YBCO thin films deposited onto MgO(100).

Figure 6.6 : The problems with reproducibility are evident in films deposited on MgO(100). Note that although the films were deposited using the same conditions, the film in (b) was deposited over a 10 hour period.

Figure 6.7 : The effect of off axis substrate position during deposition on the critical temperature of the YBCO thin films deposited on SrTiO₃(100).

Figure 6.8 : The variation of series resistance for YBCO thin films deposited onto SrTiO₃ (100) and (110) on axis simultaneously.

Figure 6.9 : The variation of series resistance for YBCO thin films deposited onto SrTiO₃ (100) and MgO (1)0) on axis simultaneously.

Figure 6.10 : The X-ray diffraction pattern of a YBCO thin film deposited on SrTiO₃(110) showing (013/110) orientation.

Figure 6.11 : The X-ray diffraction pattern of a c-axis orientated YBCO thin film deposited on MgO(100).

Figure 6.12 : The X-ray diffraction pattern of a mixed a and c-axis orientated YBCO thin film deposited on SrTiO₃(100).

	Sub.	P / mTorr	Gas Ratio	Dep. T/ °C	RF I / mA	Dep. / hu	T _{Coast} /K	T _{Co} /K	2a / Å
YRF56	S(110)	200	4:1	735	140	9	86	53	
YRF57	S(110)	280	4:1	735	140	9.5	89	71	
YRF59	M(100) S(110)	200	1:1	735		5	76 76	72 32	
YRF61	M(100)	200	1:1	735	140	5	68	59	
YRF62	S(110) S(100)	280	4:1	735	140	6	87 82	77 76	
YRF63	M(100)	280	4:1	735	140	6	77	67	910
YRF65	M(100) M(100)	280	2:1	730	140	6	60	49	
YRF67	M(100) S(110)	280	4:1	735	140	6	86 93	82 87	680
YRF68	M(100) S(110)	280	4:1	735	140	10	81 93	75 87	
YRF70	M(100) S(110)	280	4:1	735	120	6	83 91	76 85	
YRF71	M(100) S(110)	280	4:1	735	120	12	---- 91	---- 84	4500
YRF73	S(110) S(100)	280	4:1	735	130	7.5	86 86	81 76	
YRF74	S(110) S(100)	280	4:1	715	130	6	86 84	76 64	
YRF75	M(100) M(100)	280	4:1	735	130	6	60	46	
YRF78	M(100)	280	4:1	735	130	6	73	65	2800
YRF79	M(100)	280	4:1	735	130	6	61	49	
YRF80	M(100) S(100)	280	4:1	735	130	6	70 82	65 70	
YRF81	S(100)	280	4:1	735	130	6.3	88	72	2200
YRF82	S(110)	280	4:1	735	120	6	----	----	1200
YRF83	M(100) S(100)	280	4:1	735	120	6	59 80	52 72	
YRF84	M(100) S(110)	280	4:1	735	120	7.75	84 75	79 37	2000
YRF85	M(100)	280	4:1	750	120	8.5	78	68	
YRF86	S(100) S(110)	280	4:1	735	130	6	83 88	68 82	2000
YRF87	M(100)	280	4:1	735	125	6	83	73	
YFR91	S(110)	280	4:1	735	130	4	82	79	1100
YRF95	M(100)	280	4:1	735	140	6	76	72	2000

YRF106	S(110)	280	4:1	750	140	6.75	87	81	2160
YRF107	S(110)	280	4:1						1920
YRF109	M(100) S(110)	280	4:1	750	140	6	81	72	1900
YRF110	S(110) S(110)	280	4:1	740	140	6	89 85	84 80	2000
YRF111	M(100)	280	4:1	750	140	6	83	73	2080
YRF113	M(100)	280	4:1	710	140	6	83	77	1700
YRF114	S(110)	280	4:1	730	130	6	87	83	1500
YRF116	S(100)	280	4:1	705	130	6	88	81	1000
YRF117	S(110)	280	4:1	705	130	4.50			800
YRF118	L(100)	280	4:1	695	130	6	88	84	
YRF119	M(100)	280	4:1	705	130	6	82	79	
YRF120	L(100)	280	4:1	705	130	6	91	88	

Table 6.1

key: S(100) - SrTiO₃(100), S(110) - SrTiO₃(110), M(100) - MgO(100), L(100) - LaAlO₃(100). P / mTorr - system pressure during deposition, Gas Ratio - ratio of Ar to oxygen. Dep. T - Temperature during deposition, RF I/mA - sputtering current during deposition, Dep. / hr - deposition length in hours, 2a / Å - film thickness.

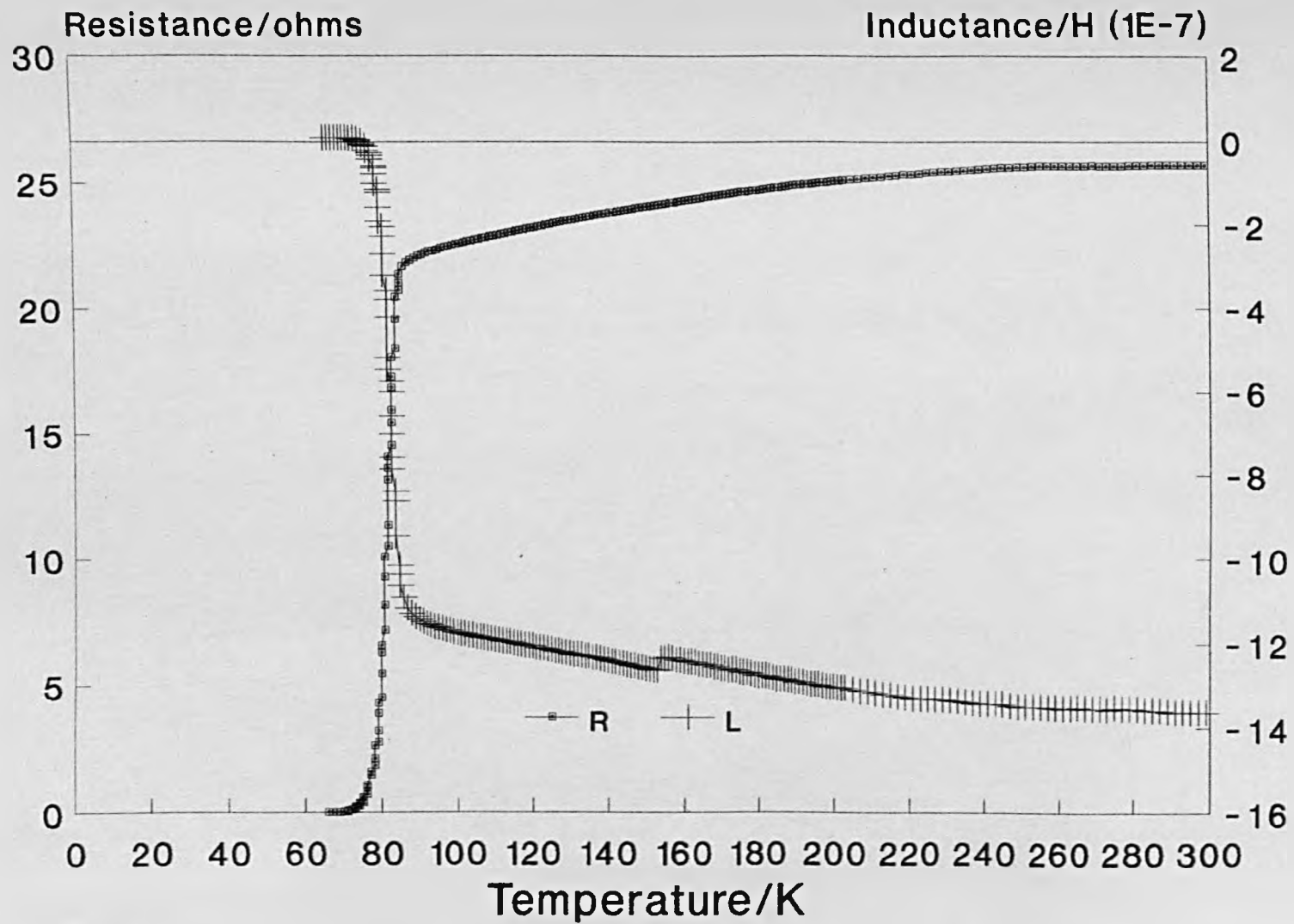


Figure 6.1

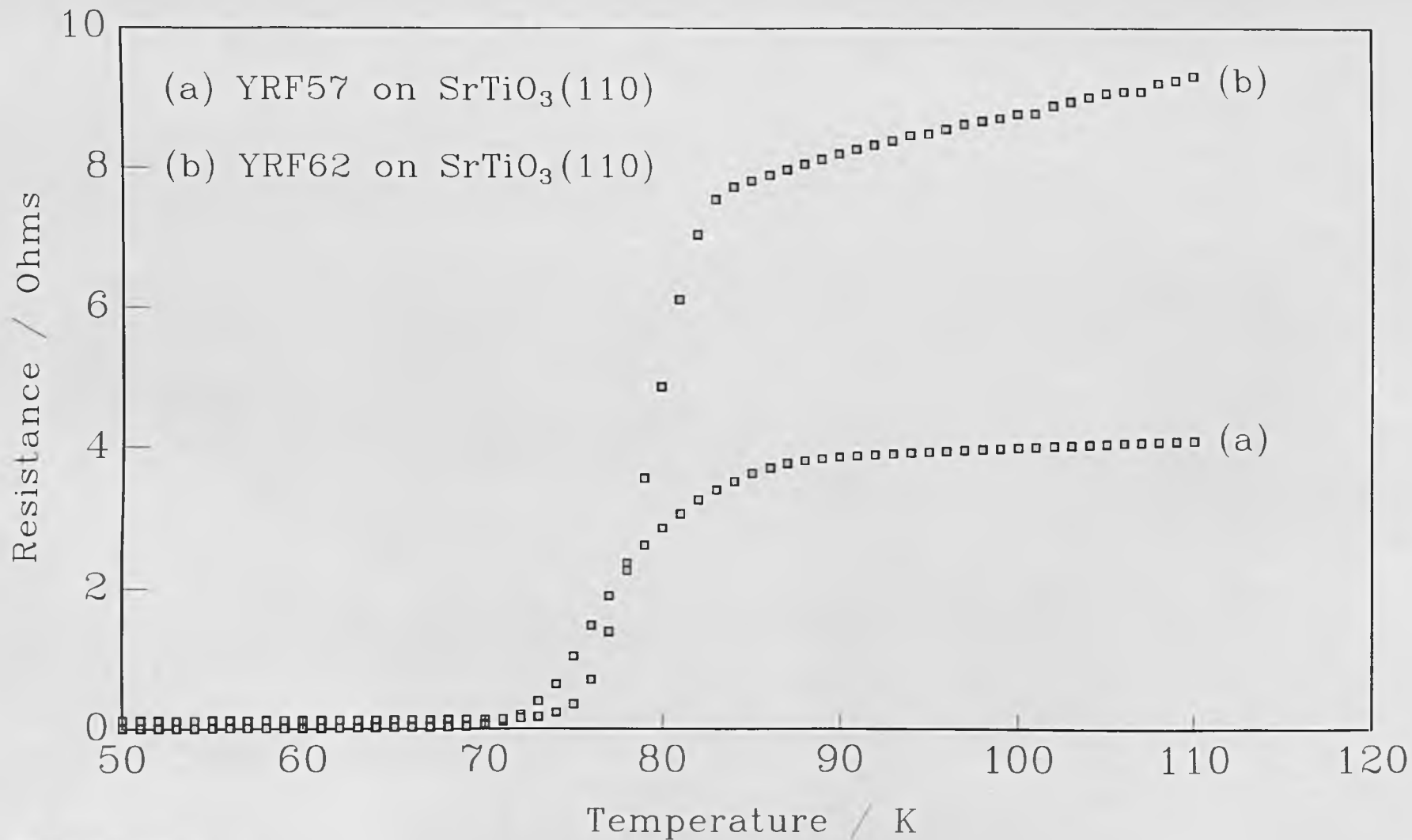


Figure 6.2

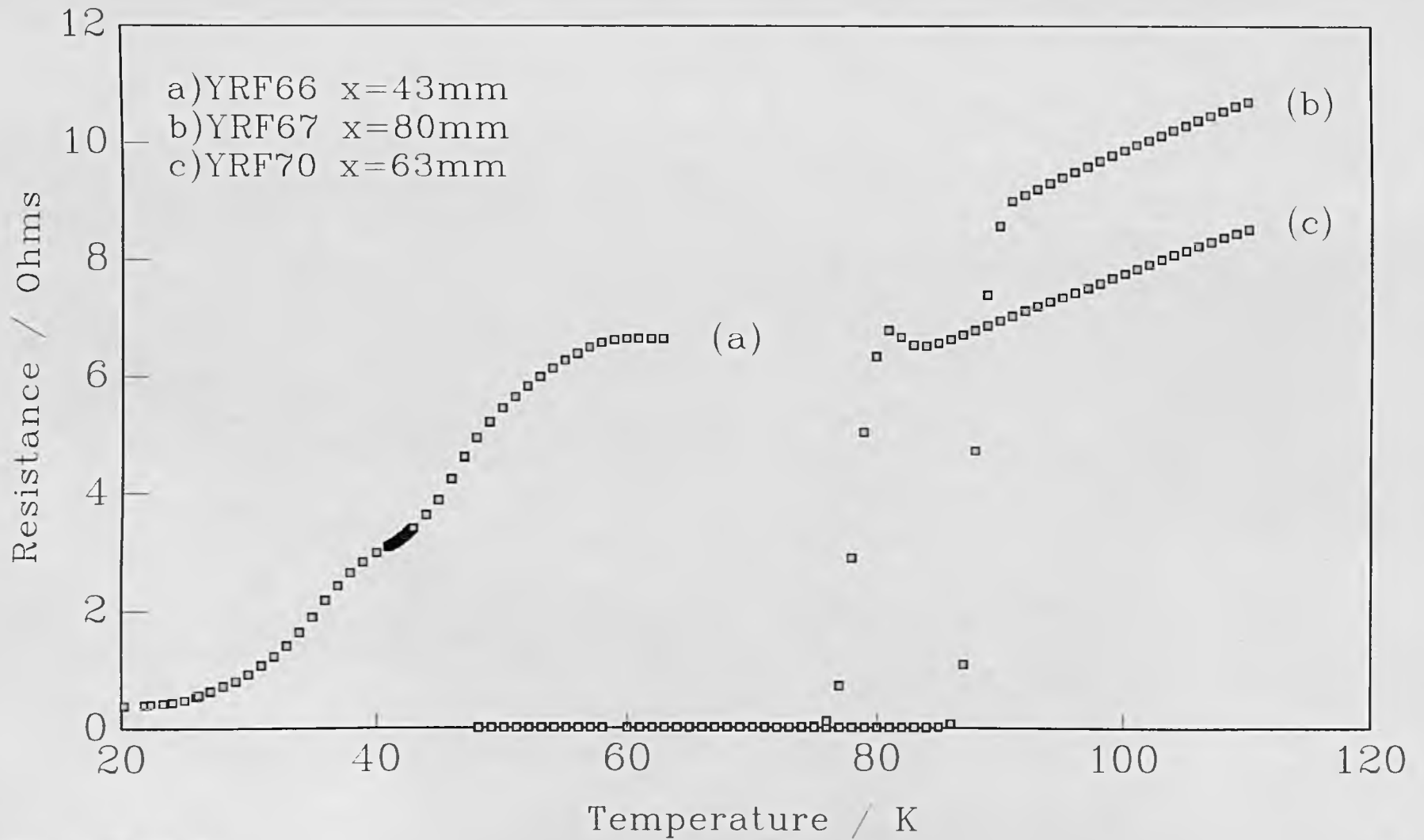


Figure 6.3

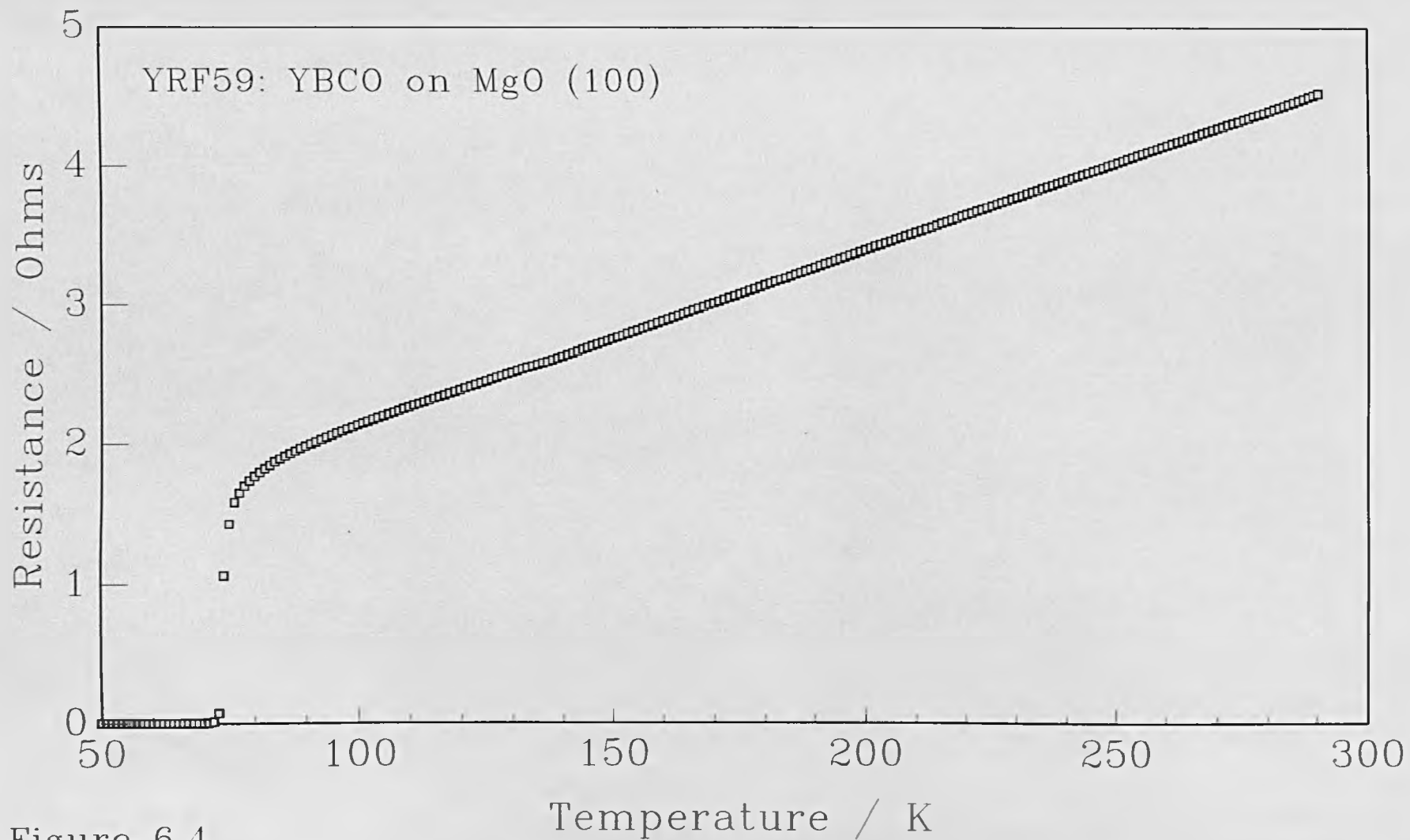


Figure 6.4

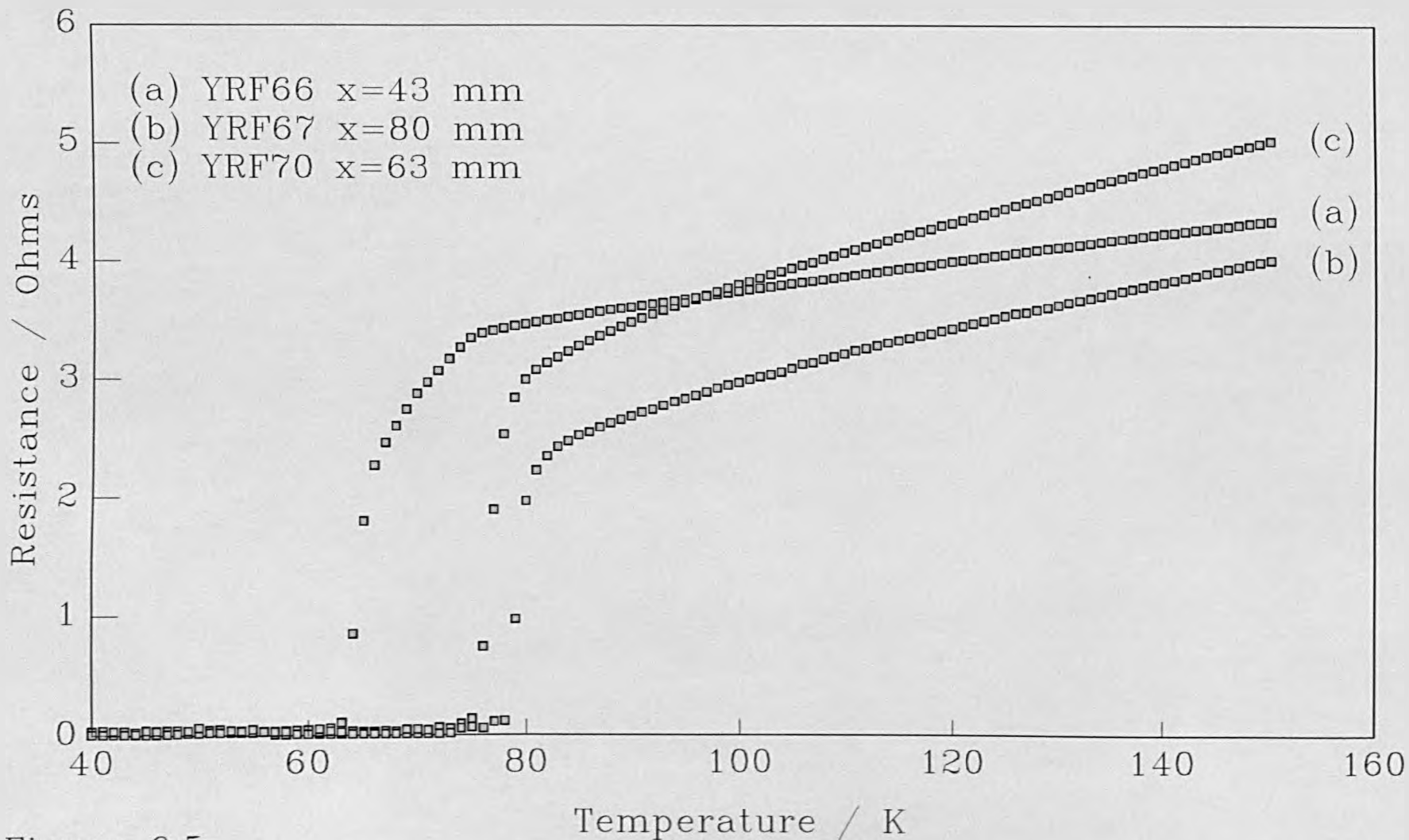


Figure 6.5

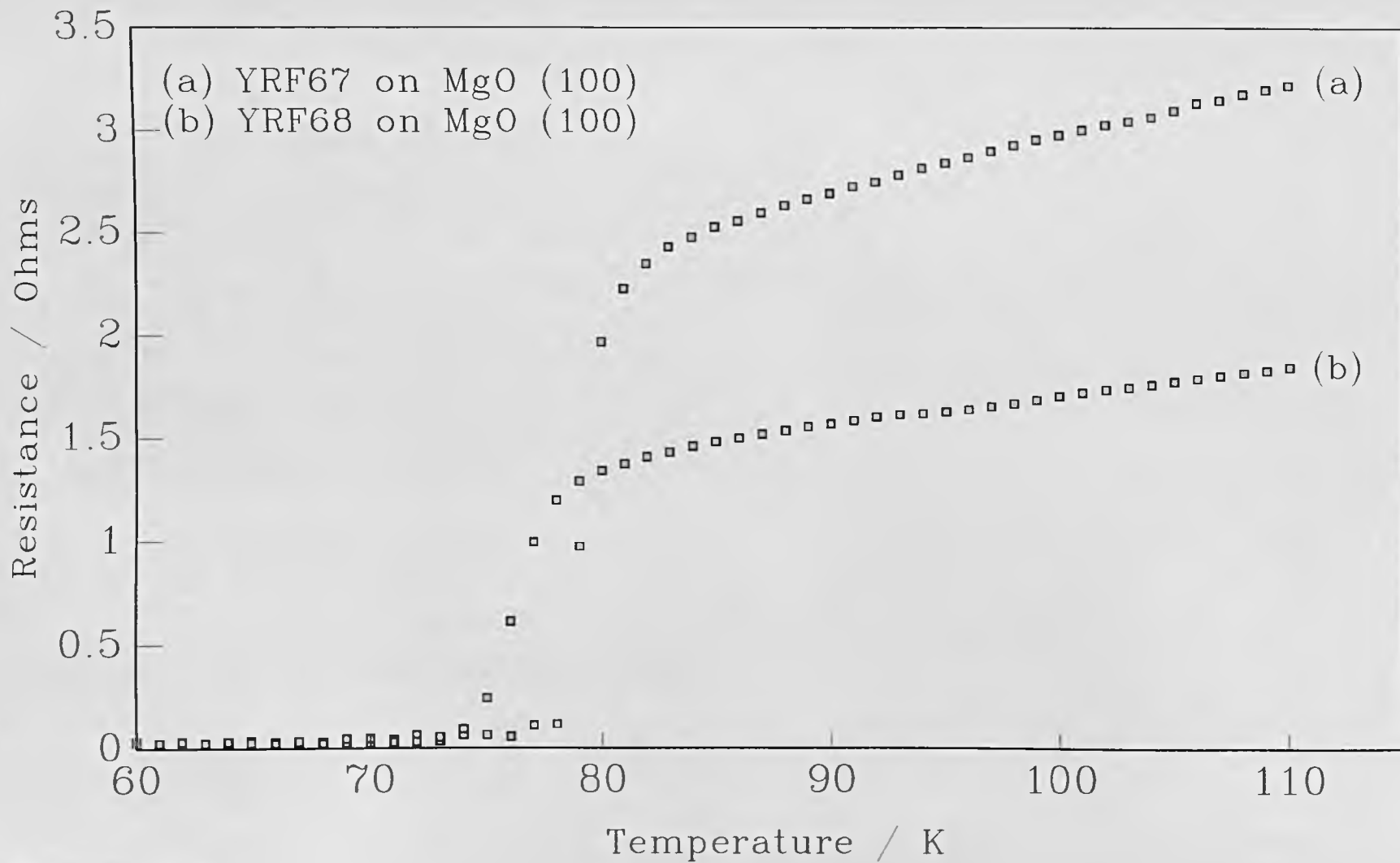


Figure 6.6

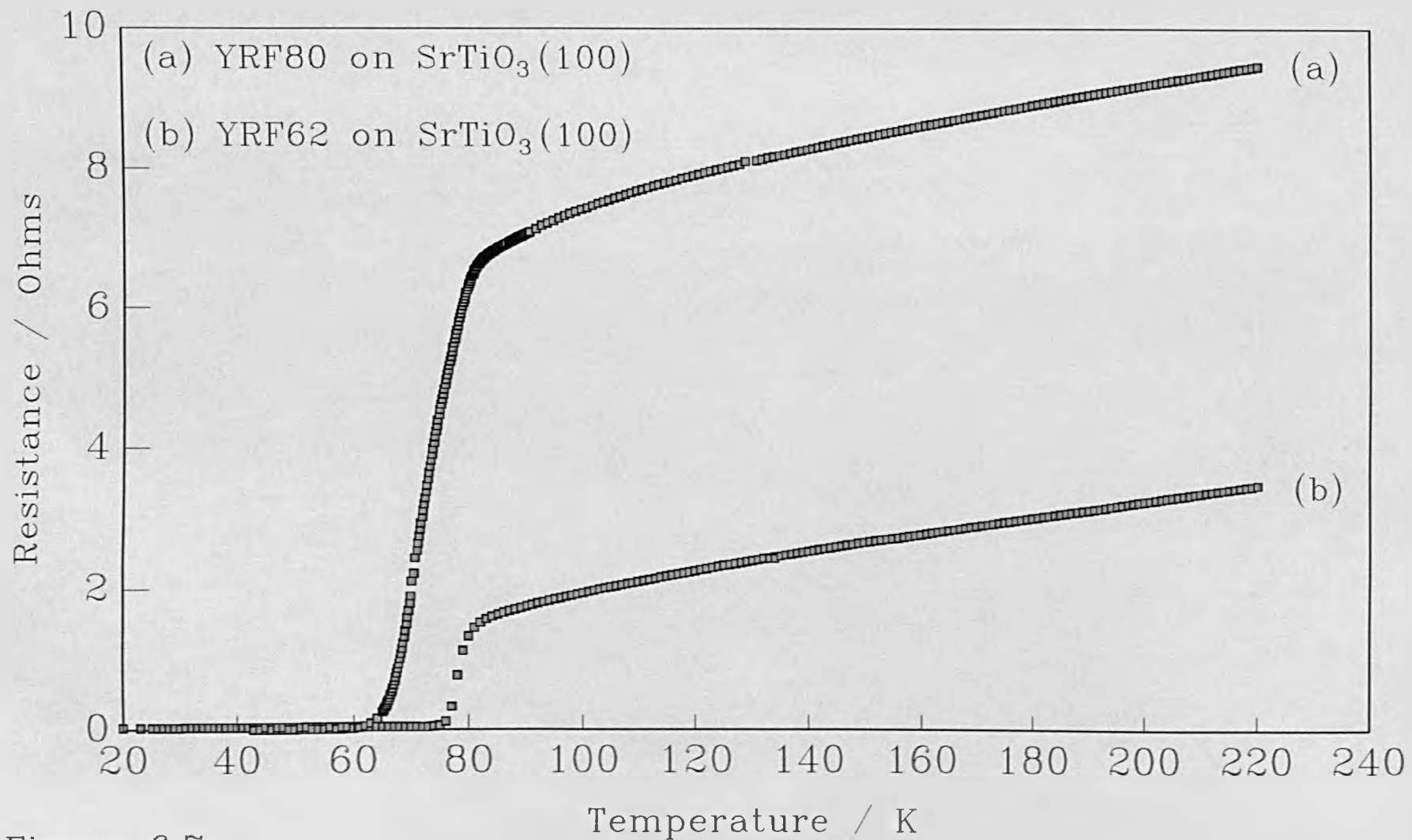


Figure 6.7

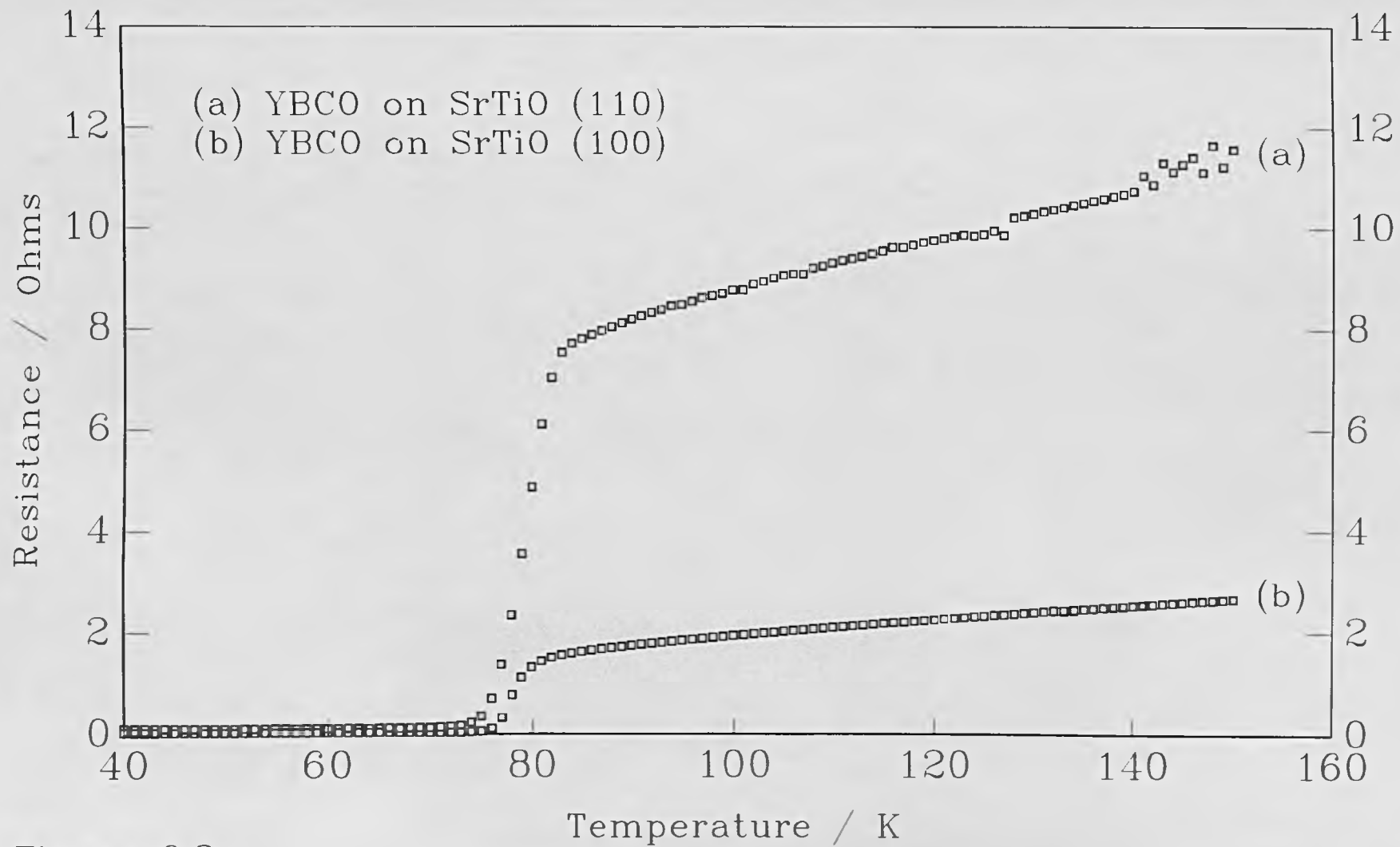


Figure 6.8

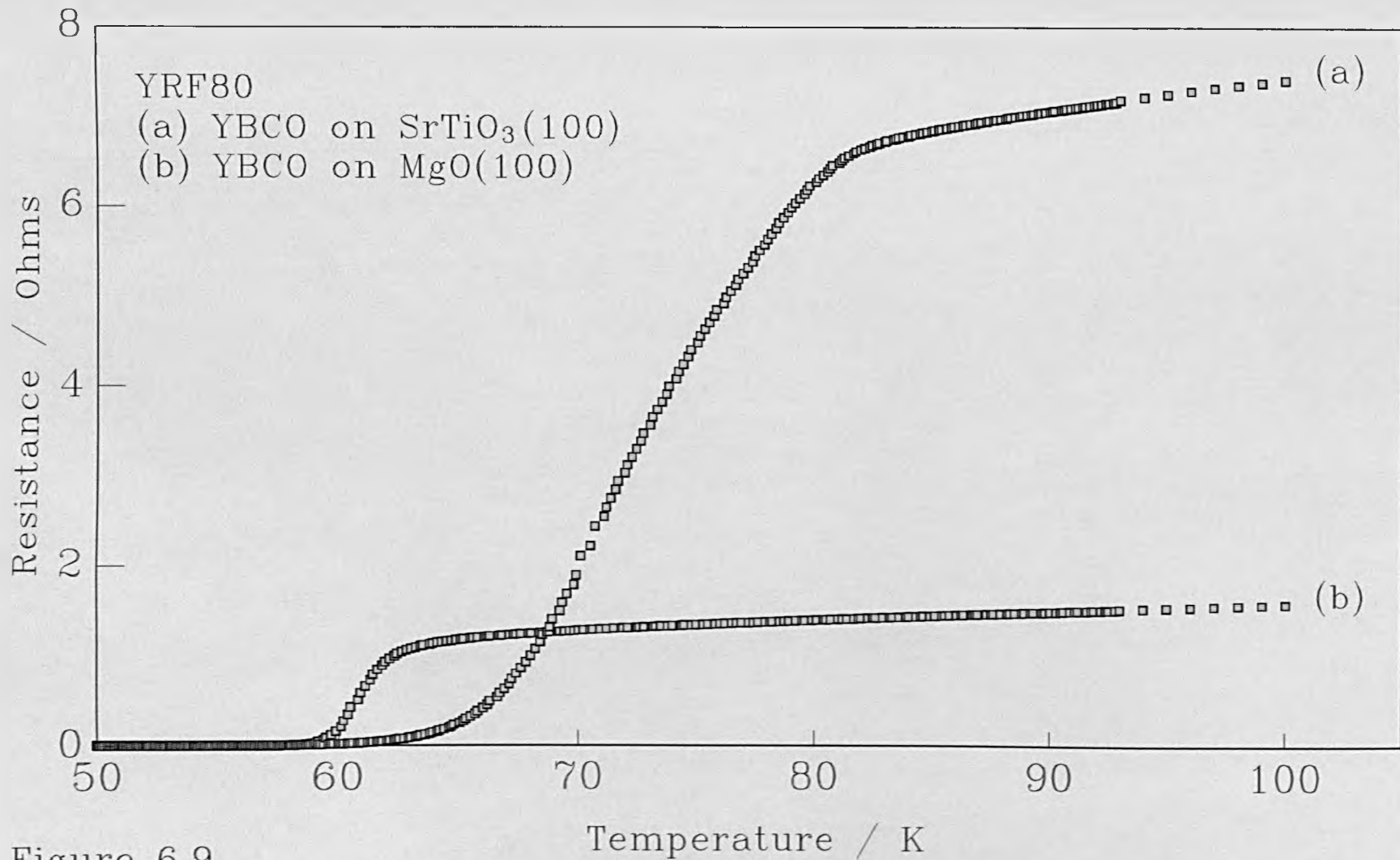


Figure 6.9

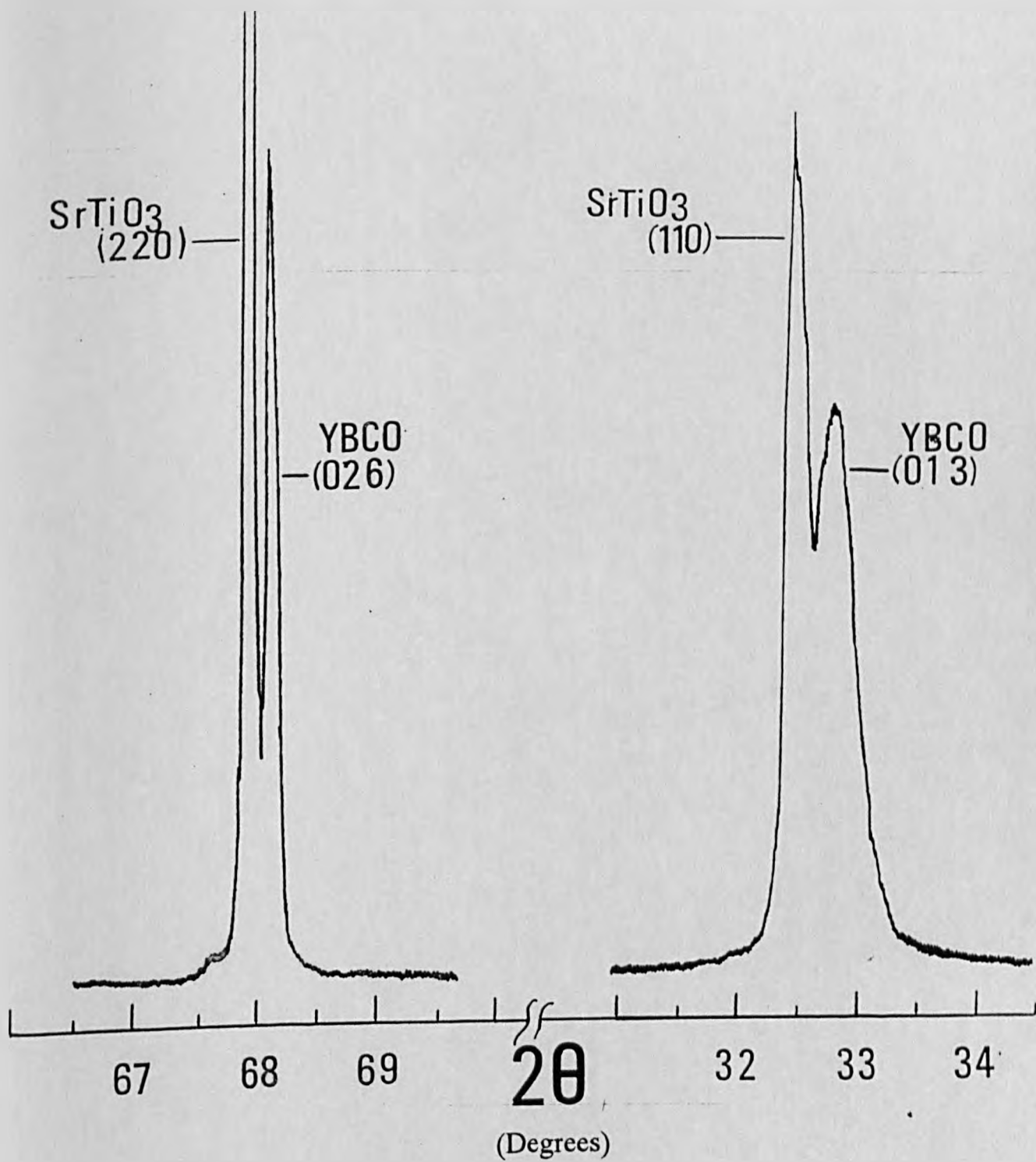


Figure 6.10

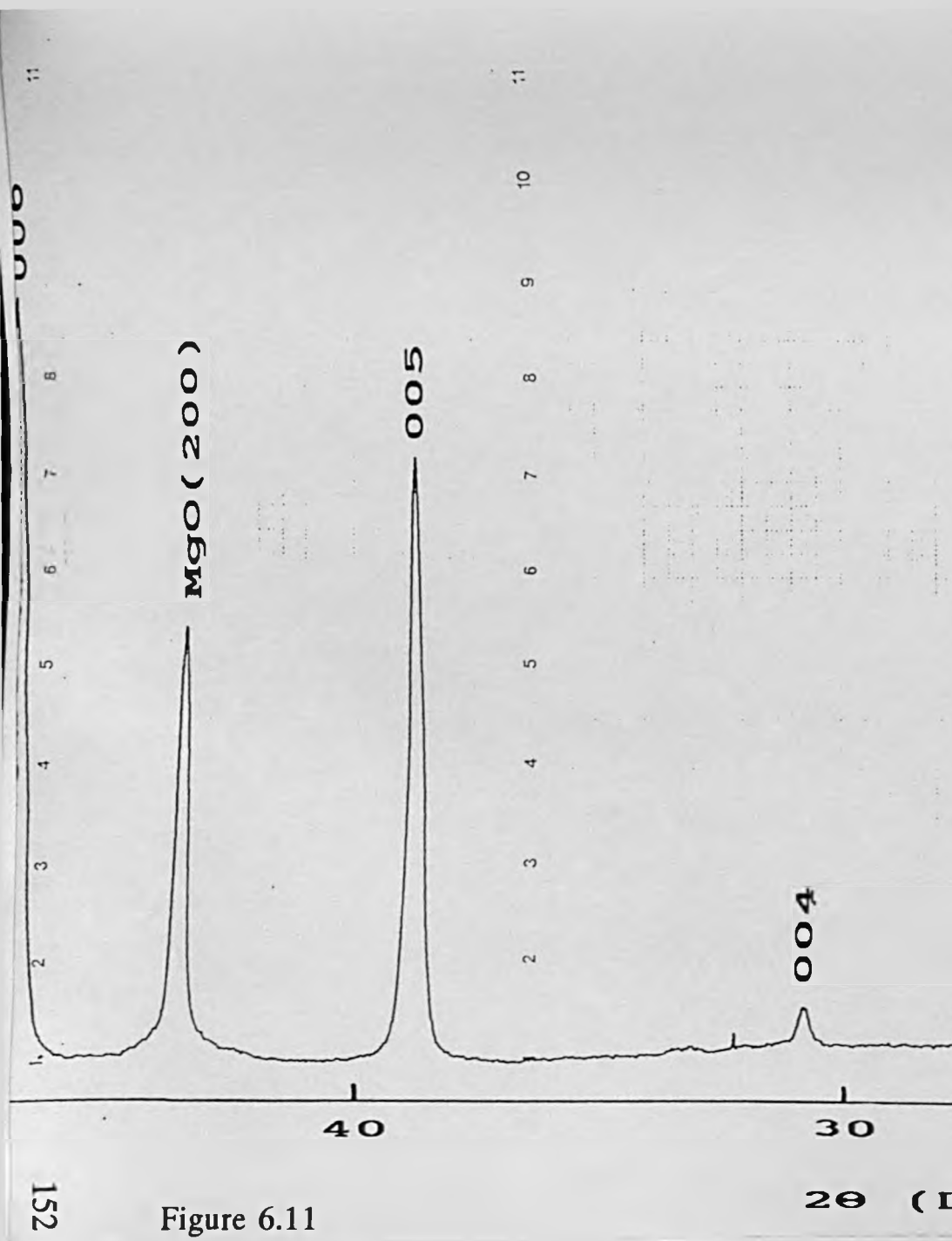
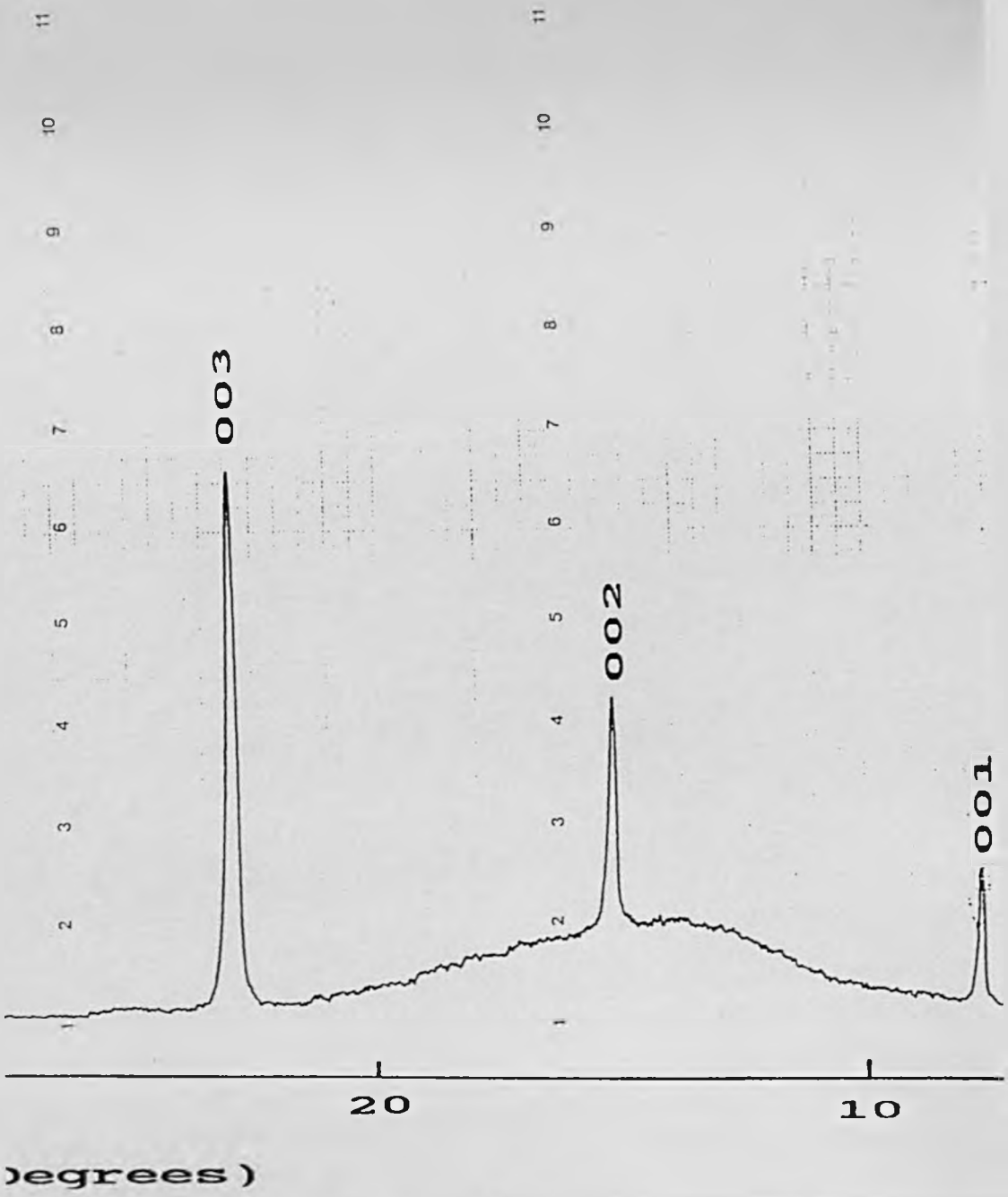
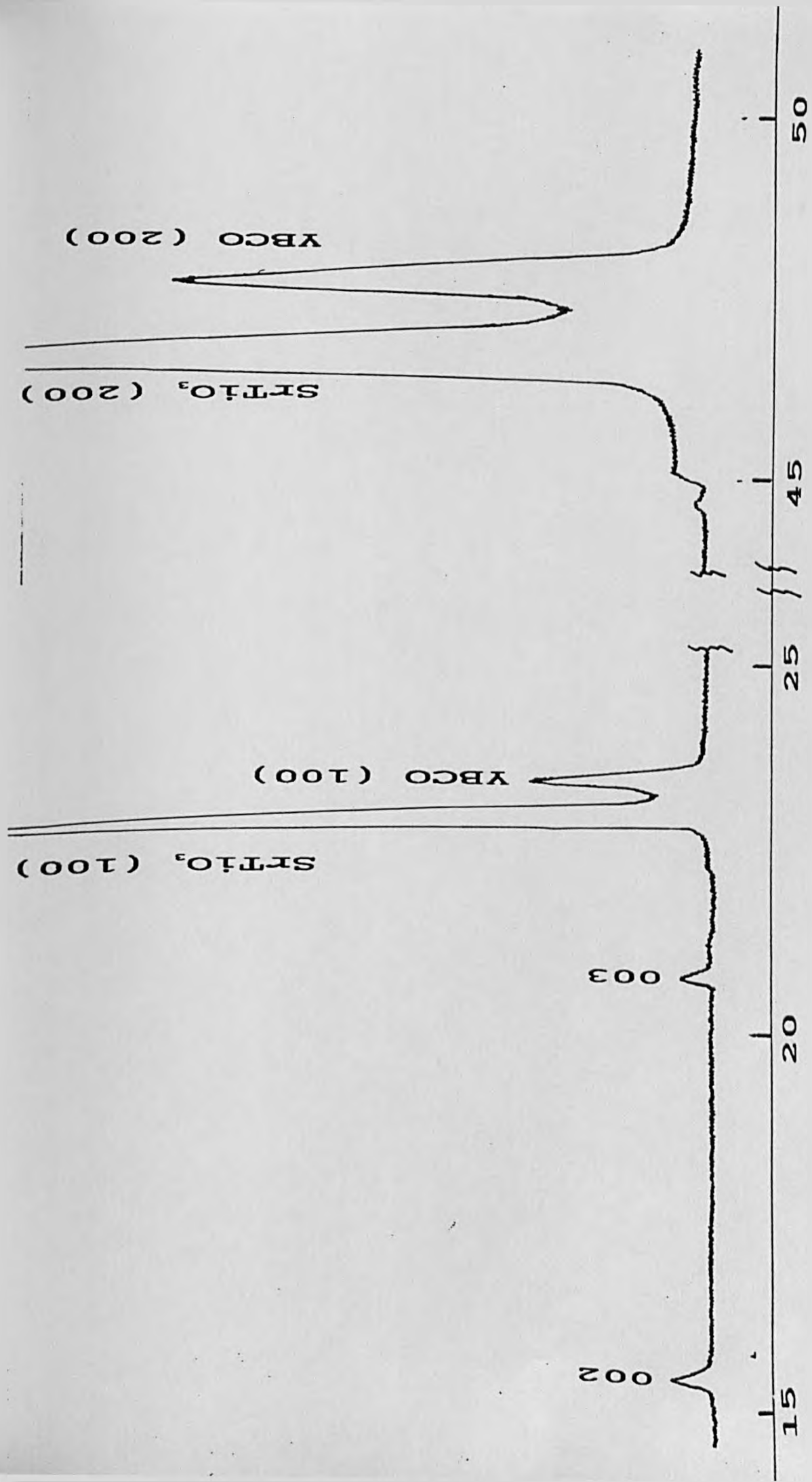


Figure 6.11





2θ (Degrees)

Figure 6.12

CHAPTER 7: TRANSPORT MEASUREMENTS, RESULTS AND DISCUSSION

7.1 Introduction

The following chapter is an investigation of the R.F. transport measurements of YBCO thin films. The results are interpreted using the theories reviewed in chapter 3. This chapter is divided into several sections investigating several aspects of resistivity. From the resistivity results it is possible to investigate the anisotropy of the thin films, the resonating valence bond theory by Anderson⁽¹⁾, the paraconductivity theories of Aslamazov - Larkin⁽²⁾ and Lawrence - Doniach⁽³⁾, as well as the flux flow phenomena of the mixed phase. The paraconductivity measurements will be used to calculate the superconducting sheet thickness and coherence length of the YBCO thin films at 13 MHz. These results will be compared with DC measurements reported here and elsewhere⁽⁴⁾. The flux flow is investigated in terms of the Anderson flux flow theory⁽⁵⁾ and the Kosterlitz-Thouless⁽⁶⁾ and Berezinskii⁽⁷⁾ theories.

7.2 Transport Measurements

The resistivity of the YBCO thin films was calculated from

$$\rho = \frac{RA}{d} \quad 7.1$$

where R is the low frequency measured resistance, A is the cross sectional area and d is the separation between the voltage contacts. A typical resistance temperature curve is shown in Figure 7.1. Resistivity measurements were taken for films deposited on MgO(100), SrTiO₃(110) and SrTiO₃(100). The resistivity was measured at 100 K and 250 K, unless otherwise stated. Table 7.1 is a summary of these results along with the most probable orientation of the corresponding thin films.

Sample	Substrate	$\rho_{250K} /$ $m\Omega cm$	$\rho_{100K} /$ $m\Omega cm$	Film Orientation	T_{Conset} /K	$T_{CO} /$ K
YRF63	M(100)	0.249	0.135	(001)	77	67
YRF67	M(100)	0.334	0.204	(001)	86	82
YRF67	S(110)	1.18	0.672	(110/013)	93	87
YRF71	S(110)		0.865	(110/013)	91	84
YRF86	S(110)	3.022	1.567	(110/013)	91	82
YRF86	S(100)	1.593	0.864	(h00/001)	83	68
YRF91	M(100)	$0.199_{T=150K}$	0.1275	(001)	82	79

M=MgO, S=SrTiO₃

Table 7.1

7.2.1 Film Anisotropy

It is clear from these results that the film resistivities at 13 MHz are anisotropic, as expected. The c-axis films deposited on MgO(100) and SrTiO₃(100) have the smallest resistivities. The film deposited on SrTiO₃(100) which was partially a-axis orientated had a larger resistivity than purely c-axis orientated films. The films deposited on SrTiO₃(110) also demonstrated considerable differences in the resistivity. The ratio of the resistivity of YRF67:YRF86 for the thin films deposited on SrTiO₃(110) was 1:2.33. Note that although the films deposited on MgO(100) substrates are c-axis orientated and have similar T_C 's (YRF67,91), they do have significant variations in resistivity. The reason for this is undoubtedly due to the growth conditions. The cause of this shift is however a little unclear. A possible reason may be crystal twinning within the film, although this phenomena is more commonly observed in films deposited on LaAlO₃. The reason why twinning occurs is due to the similarity in the a and b dimensions of YBCO. This similarity can result in the a and b orientations changing direction during film deposition. This will result in a change in the resistivity of the thin film due to

anisotropy.

7.3 Resistivity and Anderson's Resonating Valence Bond Model

A very common method for the examination of the normal electrical properties is the fitting equation given by

$$\rho = AT + B \quad 7.2$$

namely a straight line graph with a T=0K offset, B. It is thought that B is related to sample quality. This method was employed here to investigate the normal properties of the YBCO thin films. In this analysis the normal resistance R_{NC} is calculated for the temperature range, T = 150 - 200 K using results from experiment and the 'least squares fit' method. The curve obtained from the least squares fit is then extrapolated for lower temperatures, thus

$$R_{NC} = RT + R_0 \quad 7.3$$

R is the resistance value given by the least square fit. R_0 is the zero temperature offset and T is the temperature. Thus by comparison with equation 7.2 above

$$\rho \rightarrow R_{NC} \frac{2ax}{d}, \quad B \rightarrow R_0 \frac{2ax}{d}, \quad A \rightarrow R_T \frac{2ax}{d} \quad 7.4$$

where 2a, x and d are the film dimensions. This calculation was performed on YBCO thin films deposited on MgO(100), SrTiO₃(100) and (110) substrates. The results are summarised in table 7.2. These results will be compared with those given by the Anderson theory below. The theory giving the closest fit will then be used to investigate the Lawrence Doniach and Aslamazov Larkin paraconductivity theories. The accuracy

of the fitting curves are achieved using 'the least squares fit' criterion (Easyplot program).

Sample	Substrate	A / 10 ⁻⁶ Ωcm/K	B / 10 ⁻³ Ωcm	T _{CO} /K	ΣError ² / 10 ⁻⁹
YRF63	M(100)	0.725	0.068	67	5.99
YRF67	M(100)	1.22	0.089	82	12.1
YRF67	S(110)	3.03	0.461	87	60.9
YRF86	S(110)	7.59	1.22	82	101
YRF86	S(100)	4.77	0.414	68	795
YRF91*	M(100)	1.69	0.13	79	43.1
YRF80	S(100)	4.78	1.859	68	372

Table 7.2

(* - etched film, M-MgO, S-SrTiO₃)

From the RVB model of superconductivity the resistivity of the YBCO is given by

$$\rho = AT + \frac{B}{T} \quad 7.5$$

where A and B are constants for a given orientation and T > T_C. Although this equation applies to D.C. it is interesting to see how well it fits for low frequency A.C. By multiplying equation 7.2 by T to give

$$\rho T = AT^2 + B \quad 7.6$$

and by plotting ρT versus T² the gradient will equal A and the intercept will equal B, see Figure 7.2. Note that the parameter B calculated here is different to that given by equation 7.3. The results quoted in table 7.4 and the discussion in sections 7.3.1 - 7.3.3

are concerned with the value of B calculated from equation 7.6, not equation 7.3.

The calculation described by equation 7.6 was performed on films deposited on SrTiO₃(110), SrTiO₃(100) and MgO(100). The best fit was achieved using the least squares fit criterion (Easyplot program). The results are summarised in Table 7.3. While a reasonable fit can be achieved for the temperature range T > 150 K, the curve becomes increasingly inaccurate as the temperature approaches the critical temperature.

By comparing the results obtain from this analysis with those from the linear analysis, over the same temperature range, T = 150 - 200 K, the linear analysis gives the closer fit. It is for this reason that the paraconductivity results given in section 7.4 are calculated using the linear results obtained above.

Sample	YRF63	YRF67	YRF67	YRF80	YRF86	YRF86
Substrate	M(100)	M(100)	S(110)	S(100)	S(100)	S(110)
A / 10 ⁻⁶ Ωcm / K	0.921	1.48	4.35	6.116	5.94	11.12
B / 10 ⁻³ Ωcm K	5.89	7.69	49.5	175	35.5	105.4
T _{CO} / K	67	82	87	68	68	82
ΣError ² /10 ⁻⁹	30.8	48.6	183.1	950	7940	1234

Table 7.3

(M - MgO, S - SrTiO₃)

There is quite a spread of values, it is worthwhile therefore to compare these results with those obtained from D.C. experiments performed on single crystals⁽⁹⁾, as given in Table 7.4.

Orientation	ab	c
A / 10 ⁻⁶	1.4	30
B	0.007	1.35

Table 7.4

7.3.1 C-axis Orientated Thin Films

For c- axis orientated films, namely YRF63 and YRF67 on MgO(100), with current transport in the a-b plane, there is good agreement between the measured A from the thin films and the single crystal. YRF63 had the largest discrepancy with the single crystal and this is reflected in the lower critical temperature. The values of B for the thin films on MgO(100) are also in good agreement with B from the single crystal.

7.3.2 Films Deposited on SrTiO₃(110)

The values of A and B are greater in the films deposited on SrTiO₃(110) than in films deposited on MgO(100). The X-ray diffraction pattern of the films deposited on SrTiO₃(110) revealed that the orientation could be (110), (013) or a mixture of (110/013). Due to the anisotropic nature of YBCO the change in orientation is also accompanied by a change in the value of A and B. It is not possible to determine any information about the film orientation from these results.

7.3.3 Films Deposited on SrTiO₃(100)

The X-ray diffraction patterns revealed that several of the films deposited on SrTiO₃(100) were a mixture of a and c axis orientations. The degree of orientation is evident in the results, namely that the more a-axis orientated the film the larger A and B. The results from YRF80, YRF86 on SrTiO₃(100) and YRF67 on MgO(100) are a good example of this. The YBCO (YRF67) on MgO(100) is entirely c-axis orientated and the values of A and B are 1.48×10^{-6} and 7.69×10^{-3} respectively, compared with 1.4×10^{-6} and 7×10^{-3} for a single crystal. The films deposited in YRF80 and YRF86 are a mixed (h00/001) phase and this is reflected in the increase in the values of A and B. Assuming that the more a-axis phase present the larger the values of A and B it is possible to determine therefore that the thin film deposited on SrTiO₃(100) in YRF80

is more a-axis orientated than the film in YRF86. The effect of a-axis orientation is also evident when comparing the films deposited on SrTiO₃(100) and MgO(100), see Figure 7.3.

7.4 Paraconductivity

The paraconductivity is given by (re. 3.2.9, p61)

$$\sigma_m^{-1} = \frac{\rho_N \rho}{\rho_N - \rho} \quad 7.7$$

and from measurements

$$\sigma_m^{-1} = R_m \frac{2ax}{d} = \left(\frac{R_N R}{R_N - R} \right) \frac{2ax}{d} \quad 7.8$$

R is the resistance, d is the distance between voltage contacts, x is the film width and 2a is film thickness and R_N is the normal resistance calculated using equation 7.3 namely

$$R_N = R_T + R_0 \quad 7.9$$

where R_T is the resistance curve extrapolated from measurements taken between 150 - 200 K and R₀ is the T=0K offset. Equation 7.3 was used to calculate the paraconductivity, since it gave a closer fit to experimental results than equation 7.6, see Figures 7.4, 7.5.

7.4.1 Interpretation of Paraconductivity Results

From Aslamazov Larkin (AL) theory the paraconductivity is given by

$$\sigma^{-1} = \frac{8sh\epsilon}{\pi e^2} \quad , \quad \epsilon = \frac{T}{T_c} - 1 \quad 7.10$$

whereas for Lawrence Doniach (LD) theory the paraconductivity equation is

$$\sigma^{-1} = \frac{8sh\epsilon}{\pi e^2} \left\{ 1 + \left[\frac{2\xi_b(0)}{s} \right] e^{-1} \right\}^{1/2} \quad 7.11$$

where s is the superconducting sheet thickness, h is Planck's constant, e is the charge on an electron and $\xi_b(0)$ is the zero temperature coherence length. The best fit was achieved using the LD theory as opposed to the AL theory. Using the LD equation it was possible to obtain a 'best fit' as described elsewhere⁽³⁾. Briefly, this involves varying the values of coherence length, the sheet thickness and critical temperature in order to obtain the closest fit to the experimental results. The error in the linear measurements used to calculate the paraconductivity does introduce a degree of error in the values of the parameters listed below. The critical temperature does not appear to be effected, although the gradient of the paraconductivity curve is. For this reason the value of the T_C was determined first and the error is small. The sheet thickness and coherence length were determined for the 'best fit', as described above. The results obtained were then compared with the results obtained when using the errors in the linear results. Fortunately the errors were small for each of the films investigated, except for one.

The calculation was performed on films deposited on MgO(100), YRF67, SrTiO₃(110), YRF109, SrTiO₃(100), YRF86, and a 1mm wide strip of YBCO (YRF91, etched). The results are summarised in Table 7.5.

Deposition	Substrate	T_{CO} / K	$\xi(0) / nm$	s / nm
YRF67	M(100)	79.2±0.2	4±0.5	11±1.5
YRF86	S(100)		-----	-----
YRF109	S(110)	84.0±0.2	12±2.0	50±7
YRF91 (etched)	M(100)	82.5±0.2	1.65±0.4	23.4±5.

Table 7.5

From these results the sheet thickness of the film deposited on MgO(100) was

found to be $s=11 \pm 1.5 \text{ \AA}$. The zero temperature coherence length was $4 \pm .5 \text{ \AA}$. The film thickness was 680 \AA indicating that around 60 superconducting layers had been deposited. The film deposited on $\text{SrTiO}_3(110)$ had a sheet thickness $s=50 \text{ \AA}$ with a zero temperature coherence length of 12 \AA . The film thickness was 1900 \AA , namely 38 superconducting layers. It was not possible to obtain a good fit for the film deposited on $\text{SrTiO}_3(100)$ due to noise, which resulted in very large errors.

The coherence length and sheet thickness have anisotropic properties, as expected. It is also clear that the sheet thickness of the YBCO thin films is far smaller than the film thickness. When the coherence length of the YBCO thin film is greater than $s/\sqrt{2}$ the film ceases to behave as 2 dimensional and instead becomes 3 dimensional in nature. Given that s is a constant and that

$$\xi = \frac{\xi_h(0)}{[1 - \frac{T}{T_c}]^{1/2}} \quad 7.12$$

and furthermore, that the cross-over point is defined by

$$\xi > \frac{s}{\sqrt{2}} \quad 7.13$$

it is possible to rearrange the above equations to give

$$T_{2D/3D} = [1 - \frac{2\xi_h(0)^2}{s^2}] T_c \quad 7.14$$

Thus for temperatures above $T_{2D/3D}$ the films will be 3 dimensional. This calculation was performed and the results for three samples are presented in Table 7.6

Deposition	Substrate	T_{CO} / K	$T_{2D/3D} / \text{K}$
YRF67	M(100)	79.2	58.3

YRF91	M(100)	82.5	81.7
YRF109	S(110)	84.0	74.3

Table 7.6

For depositions YRF67 and YRF109 the cross over temperature is some way from the critical temperature and it is likely therefore that no 2 dimensional behaviour will be observable. For YRF91, however, the crossover temperature is less than 1 Kelvin below the critical temperature. The temperature dependence of the resistance below the critical temperature is examined in Figure 7.6. Note that the resistance scale is logarithmic. It is clear that the resistive properties of YRF91 do differ significantly to those of the other films. This behaviour is thought to be due to the flux unbinding and will be examined in more detail below. If it is assumed that the behaviour observed in YRF91 is due to flux flow and the films 2 dimensional behaviour then other films displaying similar behaviour must also be 2 dimensional, namely that they have a significantly smaller coherence length than sheet thickness. Examination of many films revealed that the 2 D behaviour is present in films deposited on MgO(100), SrTiO₃(100) and SrTiO₃(110) see Figures 7.7, 7.8 and 7.9. These results will be investigated below using the Kosterlitz-Thouless and Berezinskii theories.

7.5 Interpretation of the Intermediate Region in terms of the Kosterlitz Thouless Berezinskii Theory

It is clear from the results given above, Figures 7.7-9 that Anderson's flux flow model is not adequate in explaining all of the phenomena observed in the transition region. This is not very surprising in light of the sheet thickness and coherence length measurements that imply that some thin films of YBCO will behave as 2 dimensional films within certain temperature regions. From the KTB theories discussed in chapter

3 the temperature dependence of the resistance was given by

$$R \approx AR_N \exp -2 \left[b \frac{(T_c - T_{KTB})}{(T - T_{KTB})} \right]^{1/2} \quad . \quad 7.15$$

Putting A=1 and taking logarithms of both sides and re-arranging this becomes

$$\left(\ln \frac{R}{R_N} \right)^{-2} = - \frac{T - T_{KTB}}{4b(T_c - T_{KTB})} \quad . \quad 7.16$$

Thus plotting $(\ln (R/R_N))^{-2}$ vs T will enable us to determine the accuracy of this theory with respect to the thin films deposited here. Figures 7.10-13 represents the resistance of films thought to be 2 dimensional in nature. The intermediate region is due to flux flow in the thin films. In Figures 7.10-13 the temperature dependence of the flux flow is calculated using equation 7.16. It is quite clear that for each film the temperature dependence is that predicted by Kosterlitz Thouless and Berezinskii. Using these results it is possible to determine the T_{KTB} temperature and the value of b, a non-universal constant. The results are summarised in Table 7.7.

Deposition	Substrate	T_{CO} / K	T_{KTB} / K	b
YRF57	S(110)	65	40	6.6
YRF65	M(100)	47	23	2.8
YRF81	S(100)	59	43.5	3.99
YRF91*	M(100)	82.5	75.5	2.4

* Etched thin film

Table 7.7

The values of T_{KTB} vary significantly in these results and are often far smaller than the critical temperature. This may help explain some of the anomalies observed and investigated below. The values of b also vary. It is interesting to note that the largest

value of b was for the film deposited on $\text{SrTiO}_3(110)$, were as the smallest value was for the film deposited on $\text{MgO}(100)$. The value of b may be anisotropic, although there are not enough results here for a conclusive interpretation.

7.6 Dissipation due to the application of an external magnetic field

It is possible to examine the magnetic properties of '3D' YBCO thin films using the results obtained from the experiments performed by Y.M. Wan. Using R.F. sputtering a thin film of YBCO was deposited onto MgO. X-ray diffraction showed that the film was c-axis orientated. The zero resistance critical temperature of the film was 79 Kelvin. Using several magnetic fields, the temperature of the sample was allowed to raise through the transition temperature. Using the 4 probe arrangement, with a small dc current source it was possible to obtain a series of curves representing the resistance of the thin film during the superconducting transition for each value of B . Figure 7.14 shows the variation of resistance with B-field at several different temperatures.

7.6.1 Interpretation of the results using Anderson Flux Flow Model

In the flux flow theory, by Anderson, the dissipation due to flux movement within the thin film would increase with the application of a magnetic field. The increased dissipation is given by,

$$\rho = \frac{2v_o a_c B}{J} \exp\left(-\left(1 - \frac{J}{J_c}\right) \frac{U_o}{k_B T}\right) \quad 7.17$$

This equation predicts that the resistivity of the YBCO sample is directly proportional to the applied magnetic field. Results show that a linear relationship exists, namely that R is directly proportional to B , see Figure 7.15. If the resistance is extrapolated back to $B=0$ gauss, however, it does not tend to zero as predicted by equation 7.17. The most

likely reason for this is thermal fluctuations and not KTB flux flow.

The logarithm of the dissipation due to flux flow is inversely proportional to temperature as shown below

$$\ln \rho = \ln \frac{2v_0 a_0 B}{J} - \left(1 - \frac{J}{J_c}\right) \frac{U_0}{k_B T} \quad 7.18$$

For $\log R$ vs $1/T$ for a constant B field, the above equation again predicts linear dependence. Figure 7.16 shows that this is true. It is interesting to note that by extrapolating the linear regions of the $\log(R)$ vs B graphs they all converge at a point, marked by A in Figure 7.16.

7.7 Summary of Chapter 7

The a.c. resistivity results obtained from the YBCO thin films were anisotropic as expected. The a.c. resistivity of the films deposited on MgO(100), namely c-axis orientated films, were the lowest, ranging from 0.177 to 0.271 m Ω cm at 100 K. The a.c. resistivity of the YBCO thin films deposited on SrTiO₃(110) were found to vary from 0.627 to 1.567 m Ω cm at 100 K. The reason for the large range of values is due to the degree of (110)/(013) orientation. The exact relationship between the resistivity and orientation is still to be determined for films deposited on SrTiO₃(110). The resistivities of the films deposited on SrTiO₃(100) also varied. The lowest resistivity occurred in the a/c-axis orientated films deposited on SrTiO₃(100).

The temperature dependence of the normal region was investigated using the Resonating Valence Bond theory. The films deposited on MgO(100), namely the c-axis orientated films were found to be similar in nature to c-axis orientated single crystals. The films deposited on SrTiO₃ gave results implying that mixed orientation had occurred, as expected.

The normal results were also investigated using paraconductivity theory. The results from experiment were found to be in good agreement with the Lawrence Doniach theory of paraconductivity. The theory is based on the film being either 2 or 3 dimensional, depending on the temperature. Using the theory it was possible to calculate the coherence length and the superconducting sheet thickness. These were found to be anisotropic with values of $\xi(0)$ from 1.65 to 12 Å and s from 11 to 50 Å respectively. The theory implies that the films are 2 dimensional except when T is close to T_c , the critical temperature. Results demonstrated that certain films are 2 dimensional to within a few degrees of T_c . Examination of the superconductor region revealed that these films only became superconducting after passing through an intermediate mixed phase region.

The intermediate region is not present in all the films deposited. Many films do not appear to pass through the intermediate stage and these are thought to be 3 dimensional except at low temperatures. The films displaying intermediate behaviour were investigated using 2 dimensional superconductor theories. Results demonstrated that the thin films were in good agreement with theory. A film displaying 3 dimensional behaviour was investigated using an externally applied magnetic field. The results were in agreement with existing 3 dimensional flux flow theory. The films also appear to be both 2 and 3 dimensional, depending on the temperature. The behaviour of the resistivity is in good agreement with existing theories.

7.8 References

- 1 Anderson P.W., Zhou Z., Phys Rev. Lett **60**, 132, (1988)
- 2 Aslamazov L.G., Larkin A.I., Sov. Phys. Solid State **10**, 875, (1968)
- 3 Lawrence W.E., Doniach S., Proc of the LT-12 conference Kyoto (1970) ed Kanda E. (Keigaku, Tokyo, 1971) p.361
- 4 Gasparov V.A., Physica C **178** (1991) 449
- 5 Anderson P.W., Phys Rev Lett **9**, 309, (1962)
- 6 Kosterlitz J.M., Thouless D.J., J Phys C: Solid State Phys **6**, 1181, (1973)
- 7 Berezinskii V.L., Sov Phys JEPT **34**, 610, (1972)

7.9 Captions

Figure 7.1 : A typical resistance-temperature curve of an oxygen deficient YBCO thin film. S, I and N represent the superconducting, intermediate and normal regions respectively.

Figure 7.2 : Resistivity multiplied by temperature versus (temperature)² for a YBCO thin film deposited on MgO(100). Using the curve and equation 7.6 it is possible to determine the values of A and B.

Figure 7.3 : Resistive-temperature curves for films deposited simultaneously onto substrates of MgO(100) and SrTiO₃(100). The anisotropic nature of the YBCO is clear. The film deposited on MgO(100) is entirely c-axis orientated, where-as the film on SrTiO₃(100) shows signs of mixed a and c-axis orientation.

Figure 7.4 : The resistivity and paraconductivity curves of a YBCO thin film deposited on MgO(100). The paraconductivity was calculated using equation 7.8. The extrapolated normal resistivity was calculated using equation 7.9. The theoretical paraconductivity curve is obtained from Lawrence Doniach theory, equation 7.10.

Figure 7.5 : The resistivity and paraconductivity curves of a YBCO thin film deposited on SrTiO₃(110). The paraconductivity was calculated using equation 7.8. The extrapolated normal resistivity was calculated using equation 7.9. The theoretical paraconductivity curve is obtained from Lawrence Doniach theory, equation 7.10.

Figure 7.6 : The logarithmic resistance versus temperature curves of 3 YBCO thin films. It is clear that the transition region of the YBCO thin films varies significantly, namely that although curves (a) and (c) have a different residual resistance, the curves are basically the same. Curve (b) is however, significantly different. The intermediate region of the curve is thought to be due to flux flow as predicted by KTB theory, equation 7.11.

Figure 7.7 : The flux flow region predicted by KTB theory is present in the oxygen deficient YBCO thin film deposited on MgO(100).

Figure 7.8 : The flux flow region predicted by KTB theory is present in the oxygen deficient YBCO thin film deposited on SrTiO₃(100).

Figure 7.9 : The flux flow region predicted by KTB theory is present in the oxygen deficient YBCO thin film deposited on SrTiO₃(110).

Figure 7.10 : The flux flow region of the YBCO thin film deposited on SrTiO₃(110) is investigated using equation 7.16. A good fit is achieved over a large section of the flux flow region.

Figure 7.11 : The flux flow region of the YBCO thin film deposited on MgO(100) is investigated using equation 7.16.

Figure 7.12 : The flux flow region of the YBCO thin film deposited on SrTiO₃(100) is investigated using equation 7.16.

Figure 7.13 : The flux flow region of an etched YBCO thin film deposited on MgO(100) is investigated using equation 7.16.

Figure 7.14 : The transition temperature from normal to superconducting phase is suppressed by the application of an external magnetic field. The effect of the suppression, although small, is visible.

Figure 7.15 : The film was 3 dimensional in nature. The magnetic properties are found to in agreement with existing flux flow theory, namely a linear response to an applied magnetic field, equation 7.17.

Figure 7.16 : The transition region of the 3 dimensional film is inversely proportional to the temperature as predicted in equation 7.18.

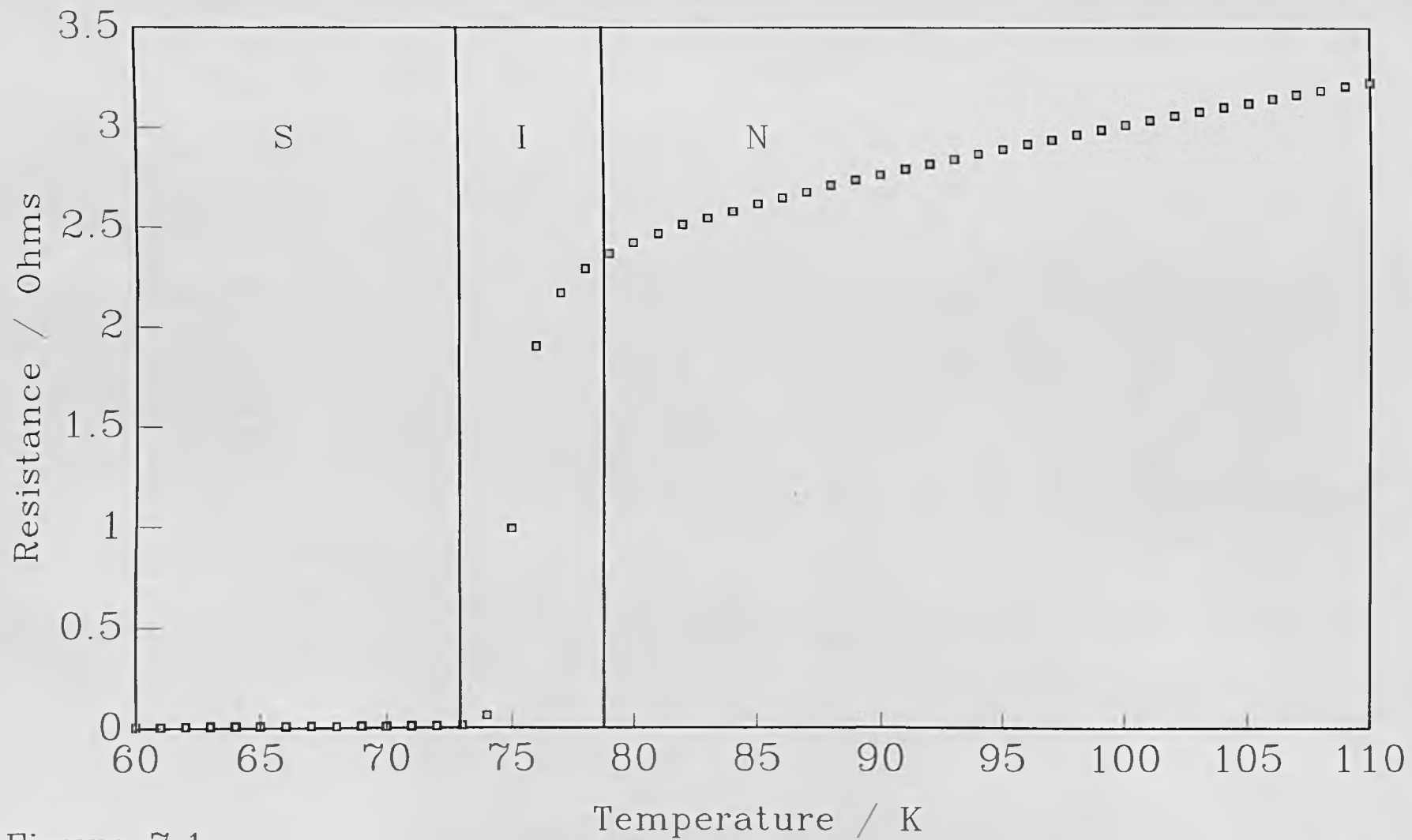


Figure 7.1

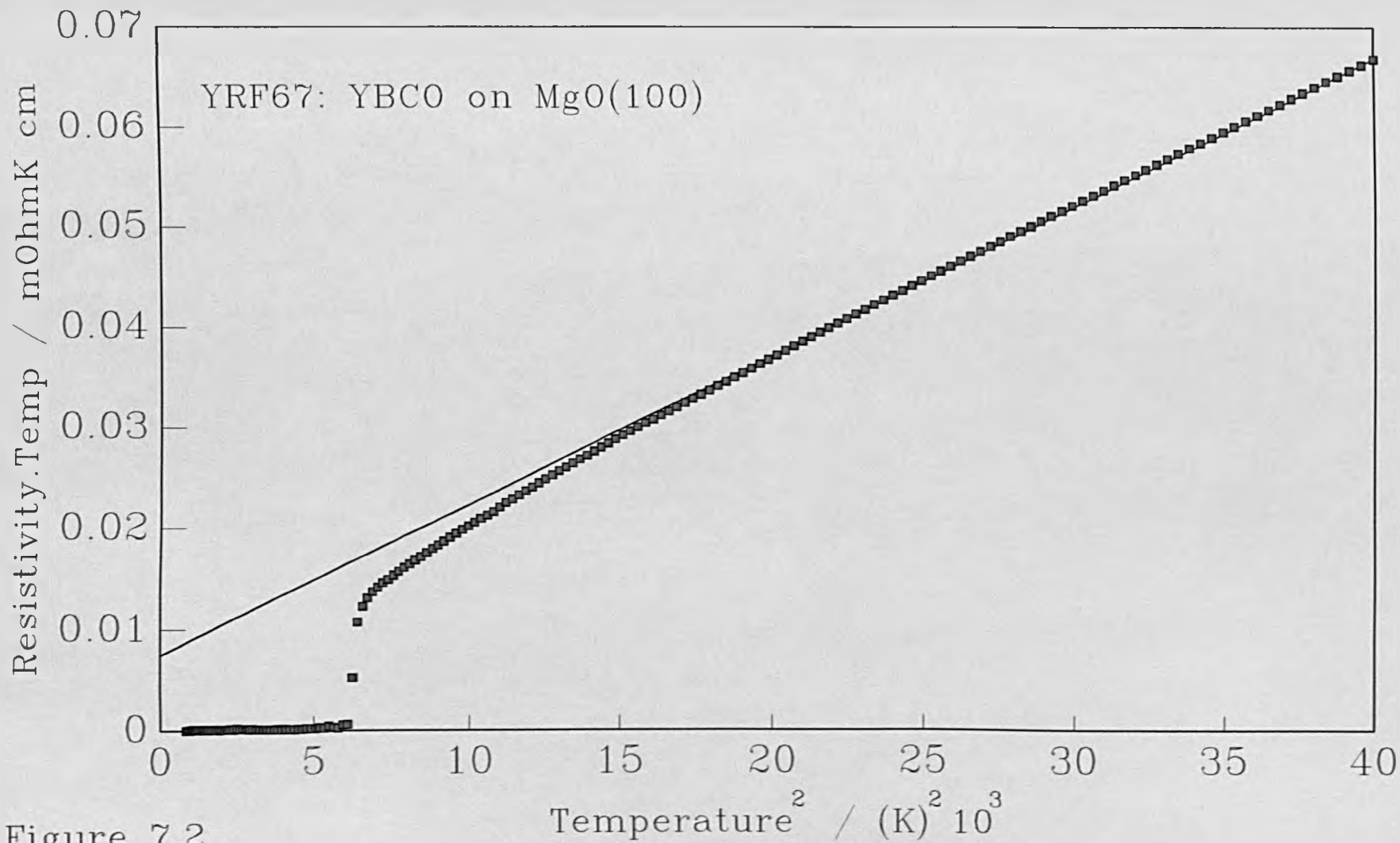


Figure 7.2

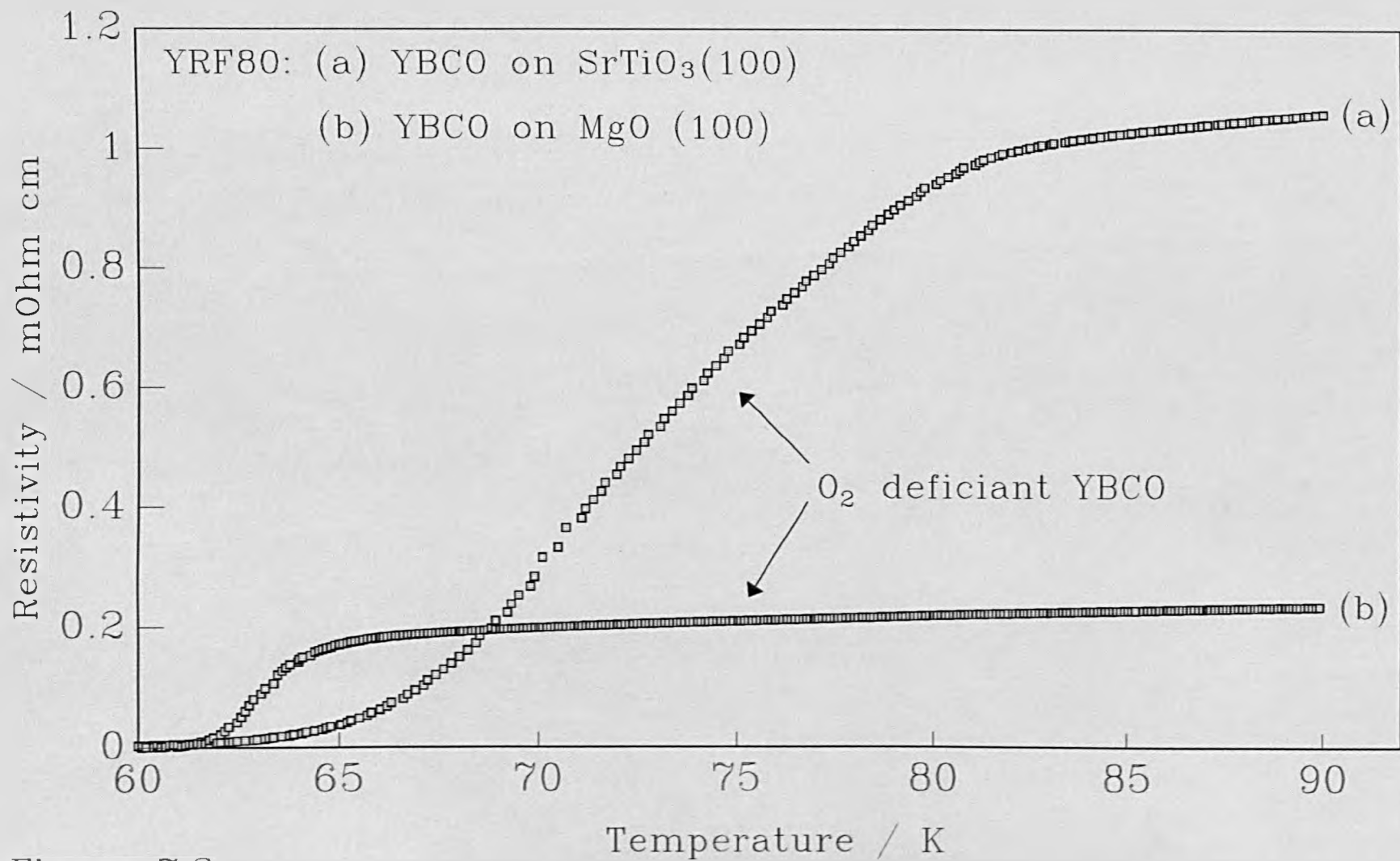
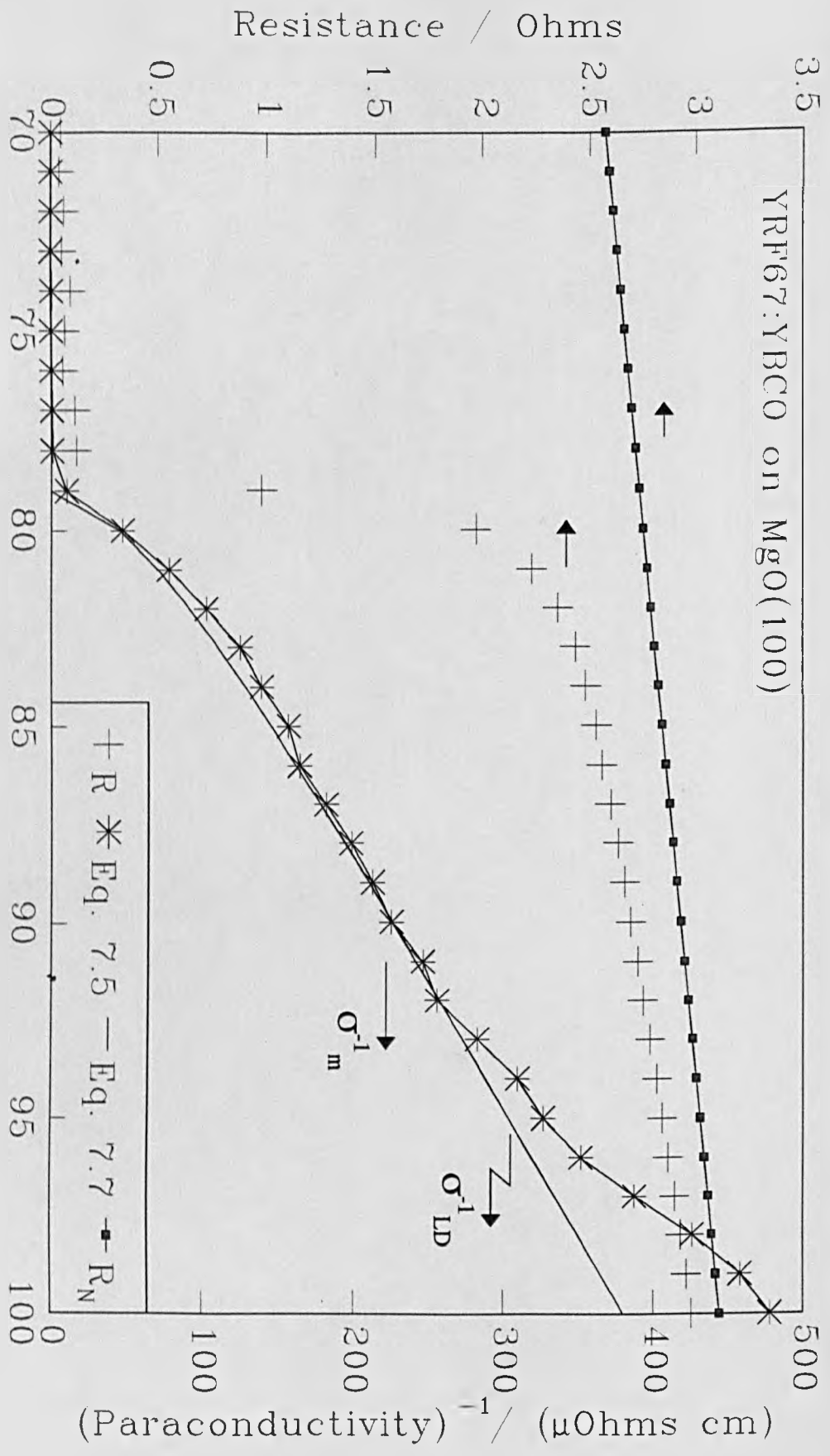


Figure 7.3

Figure 7.1

Temperature / K



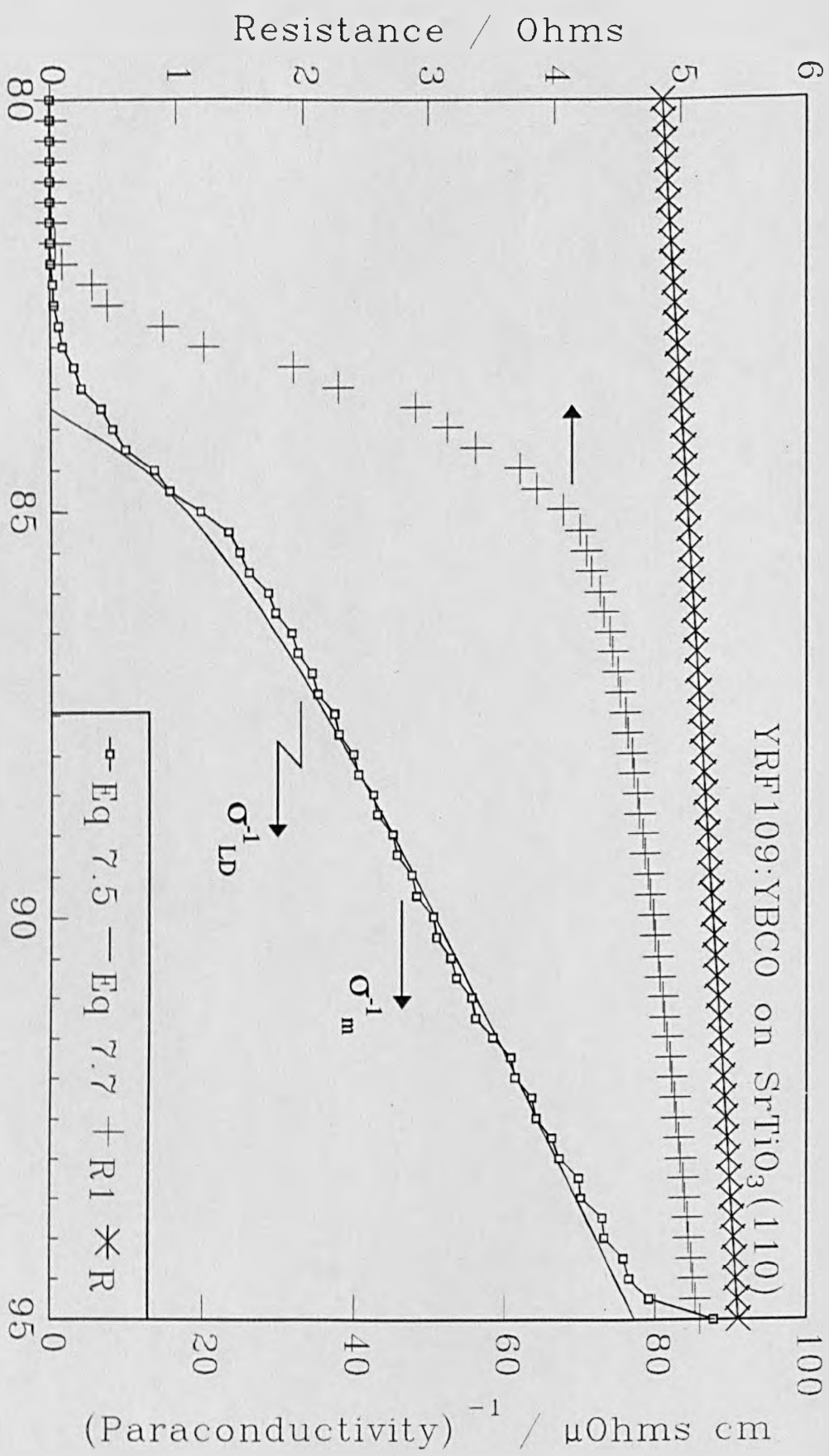


Figure 7.5

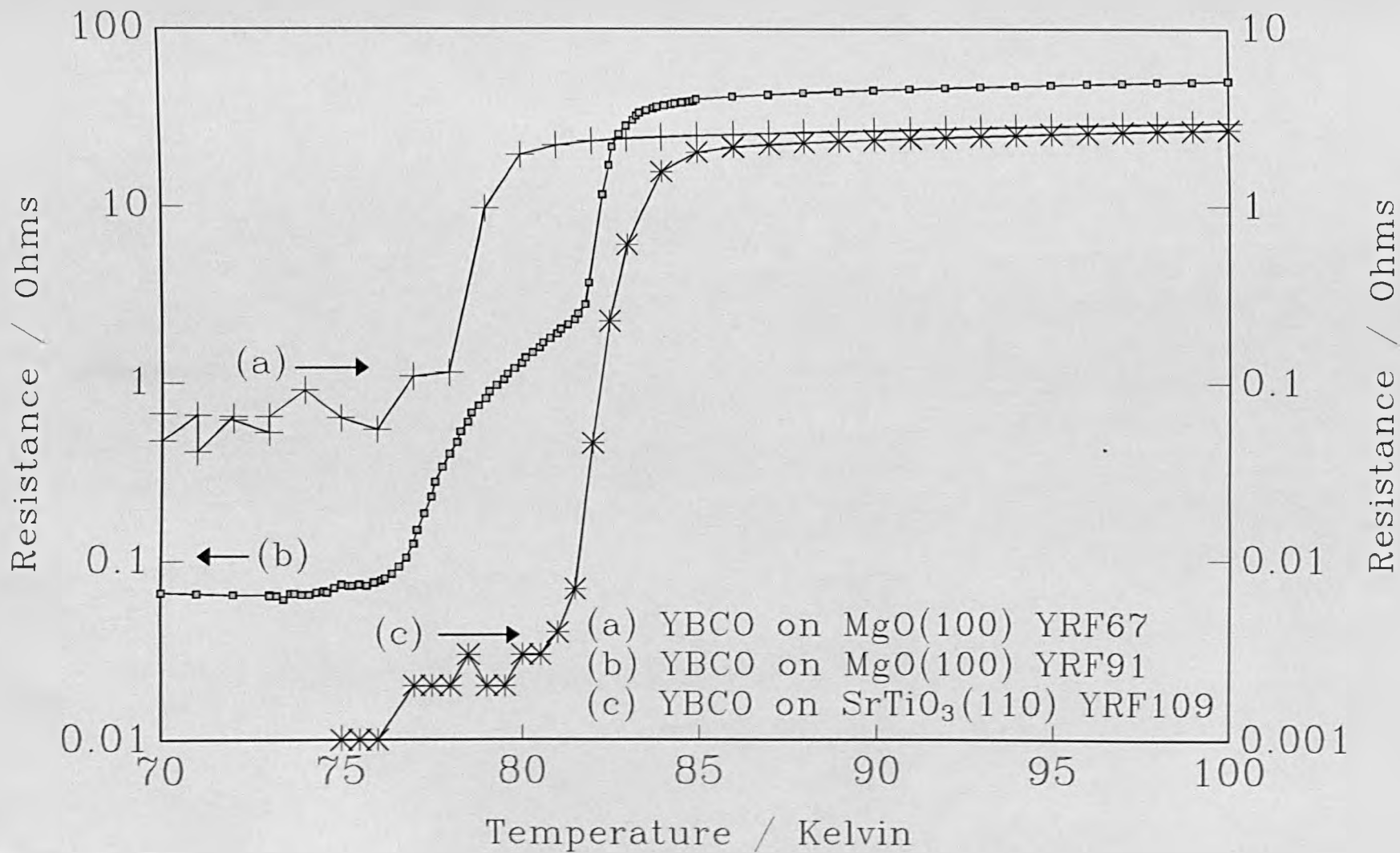


Figure 7.6

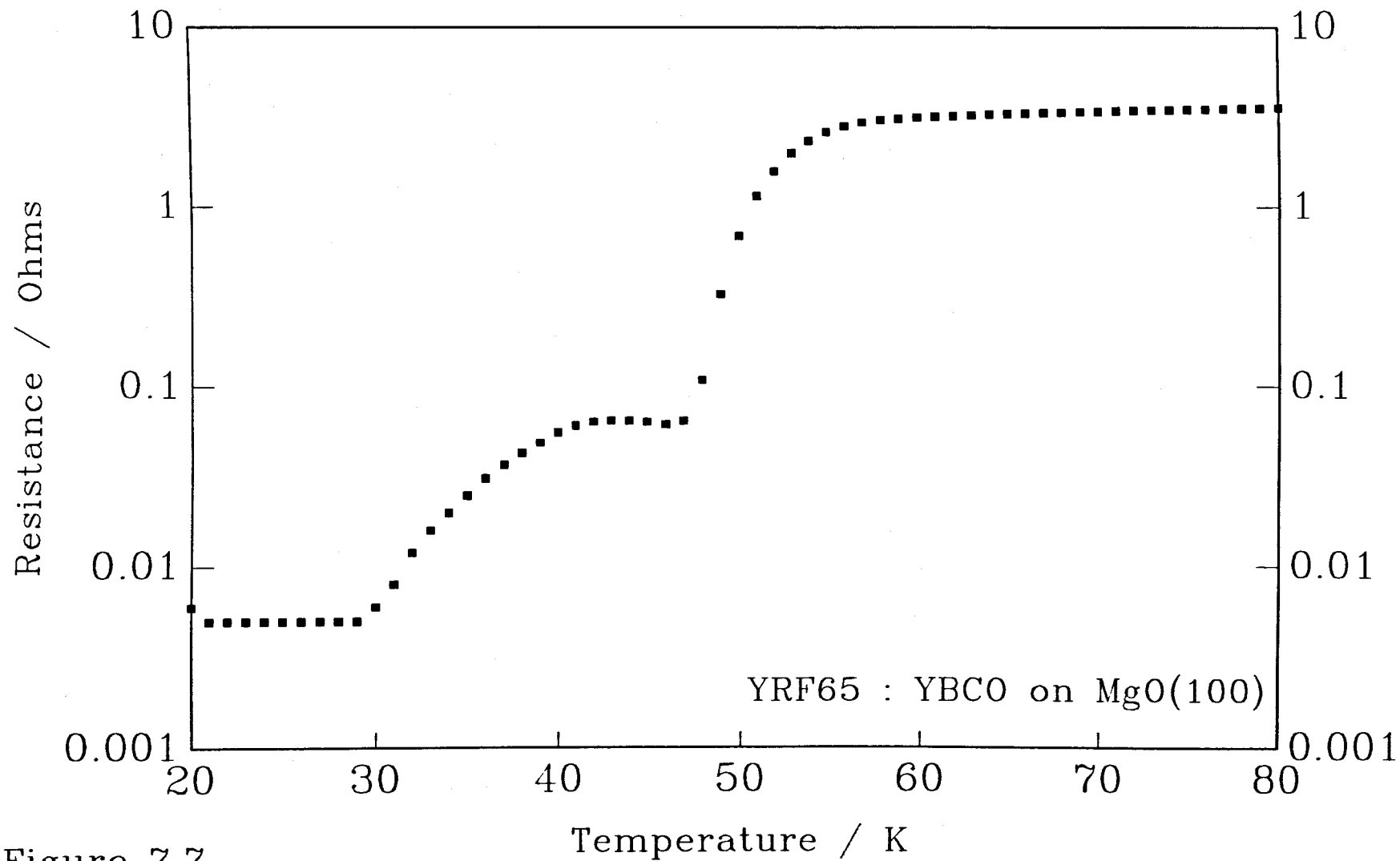


Figure 7.7

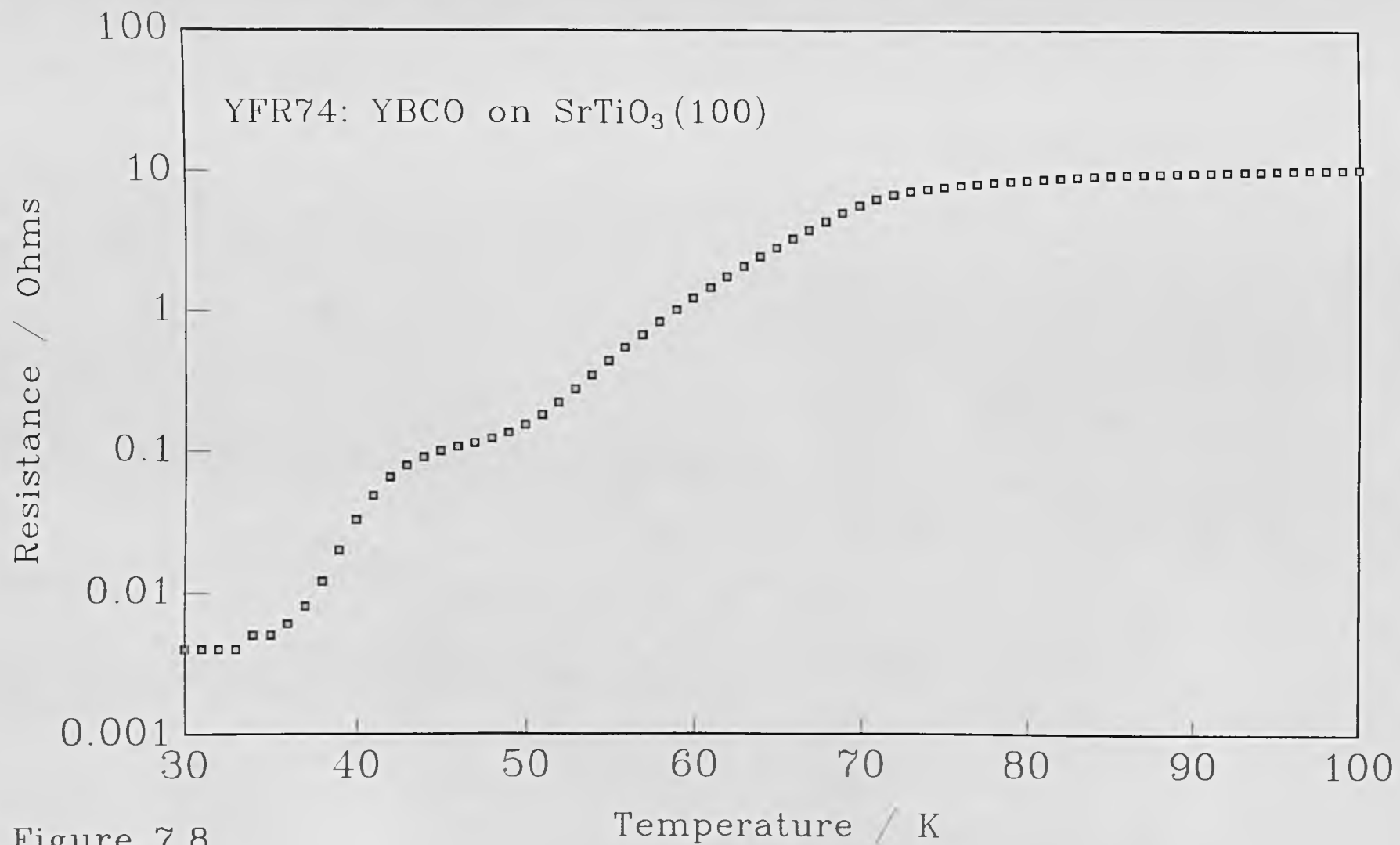


Figure 7.8

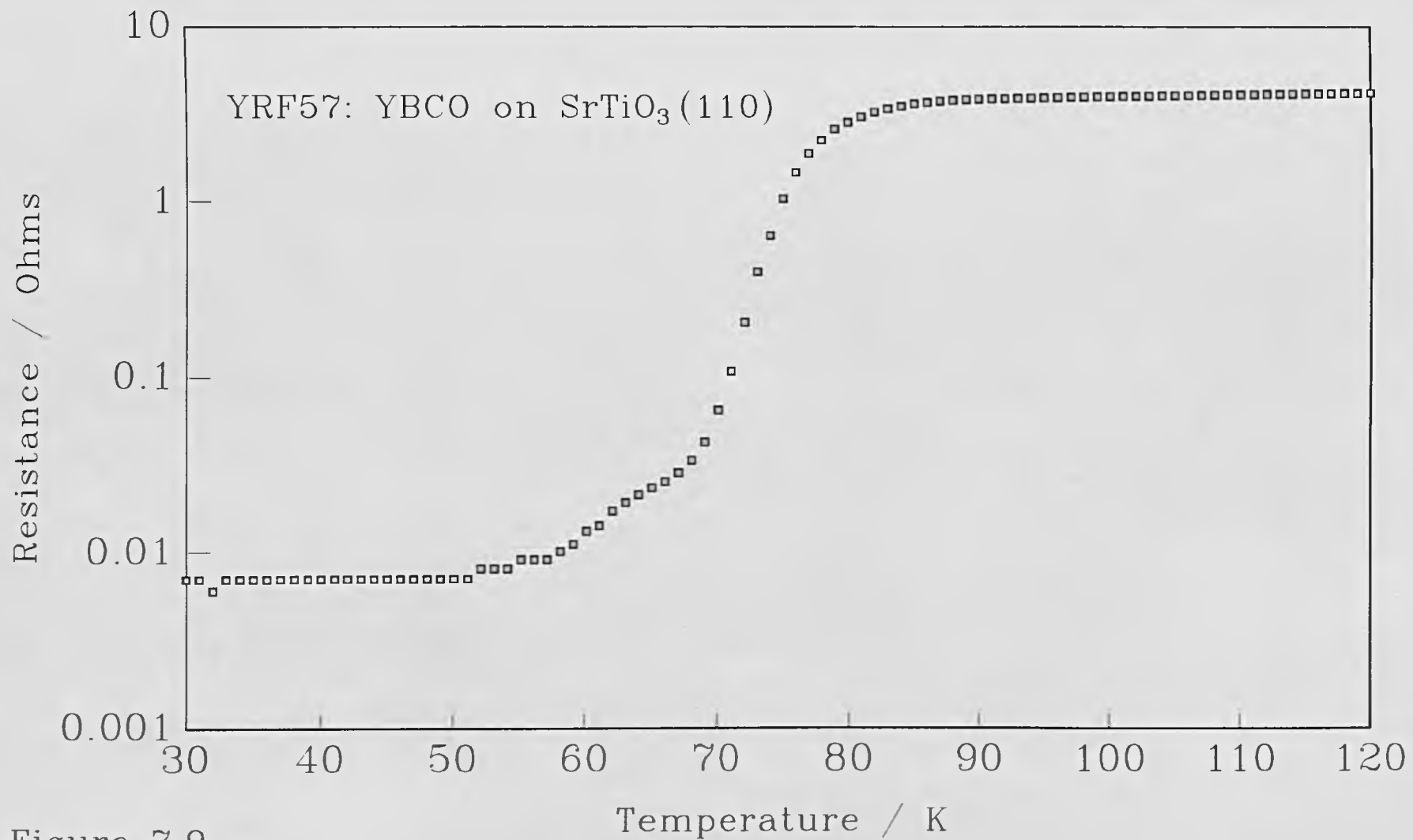


Figure 7.9

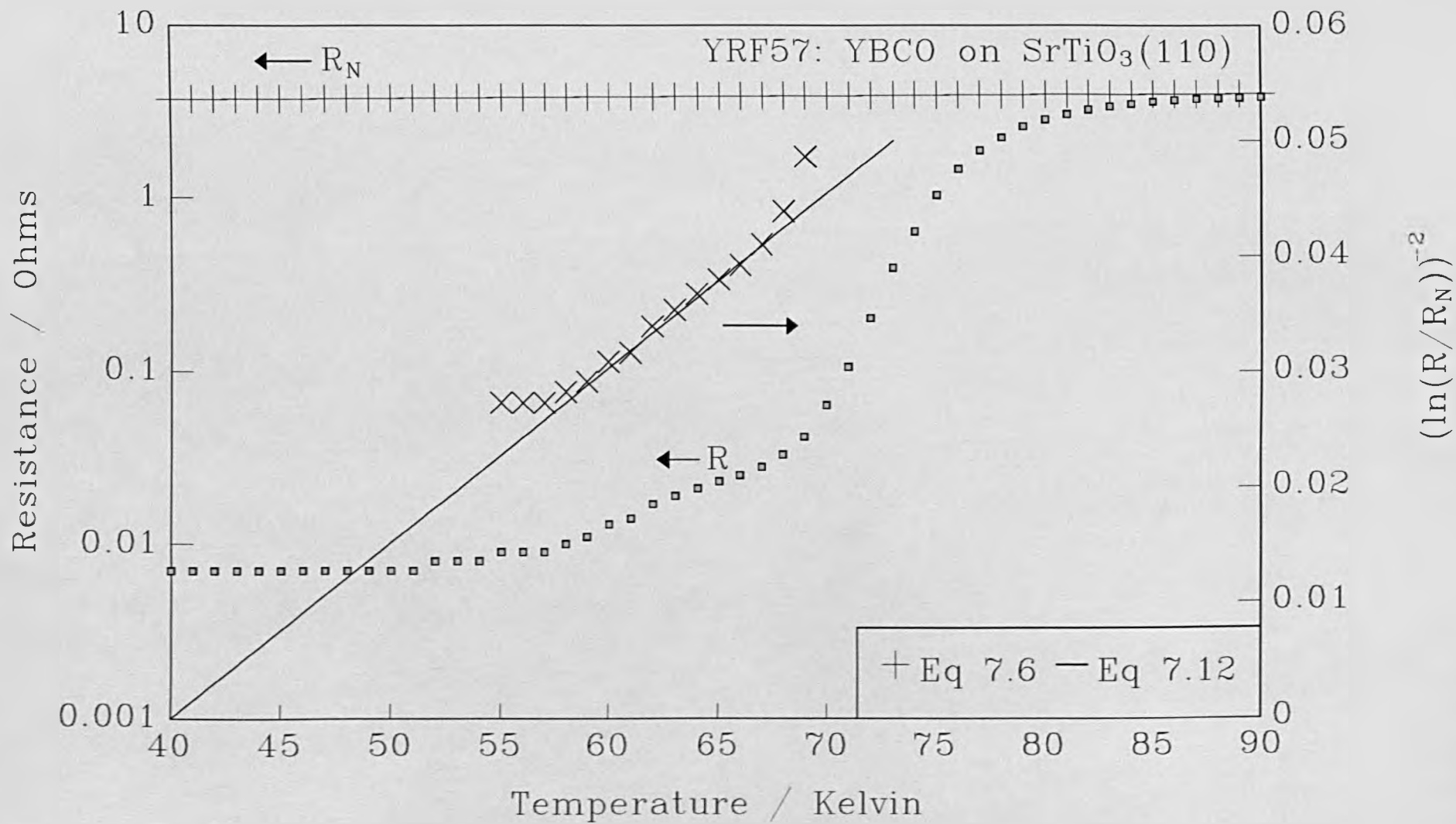


Figure 7.10

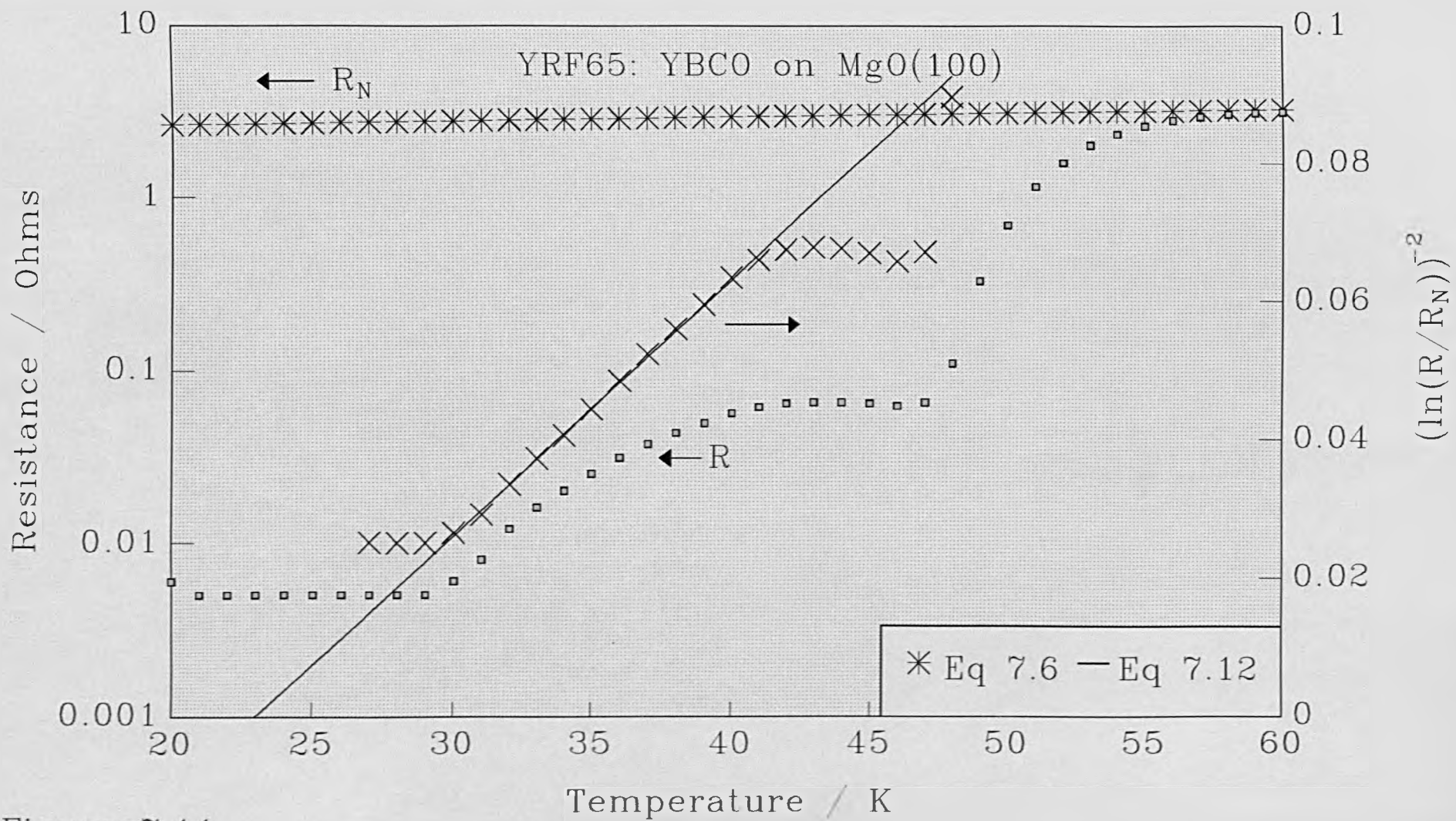


Figure 7.11

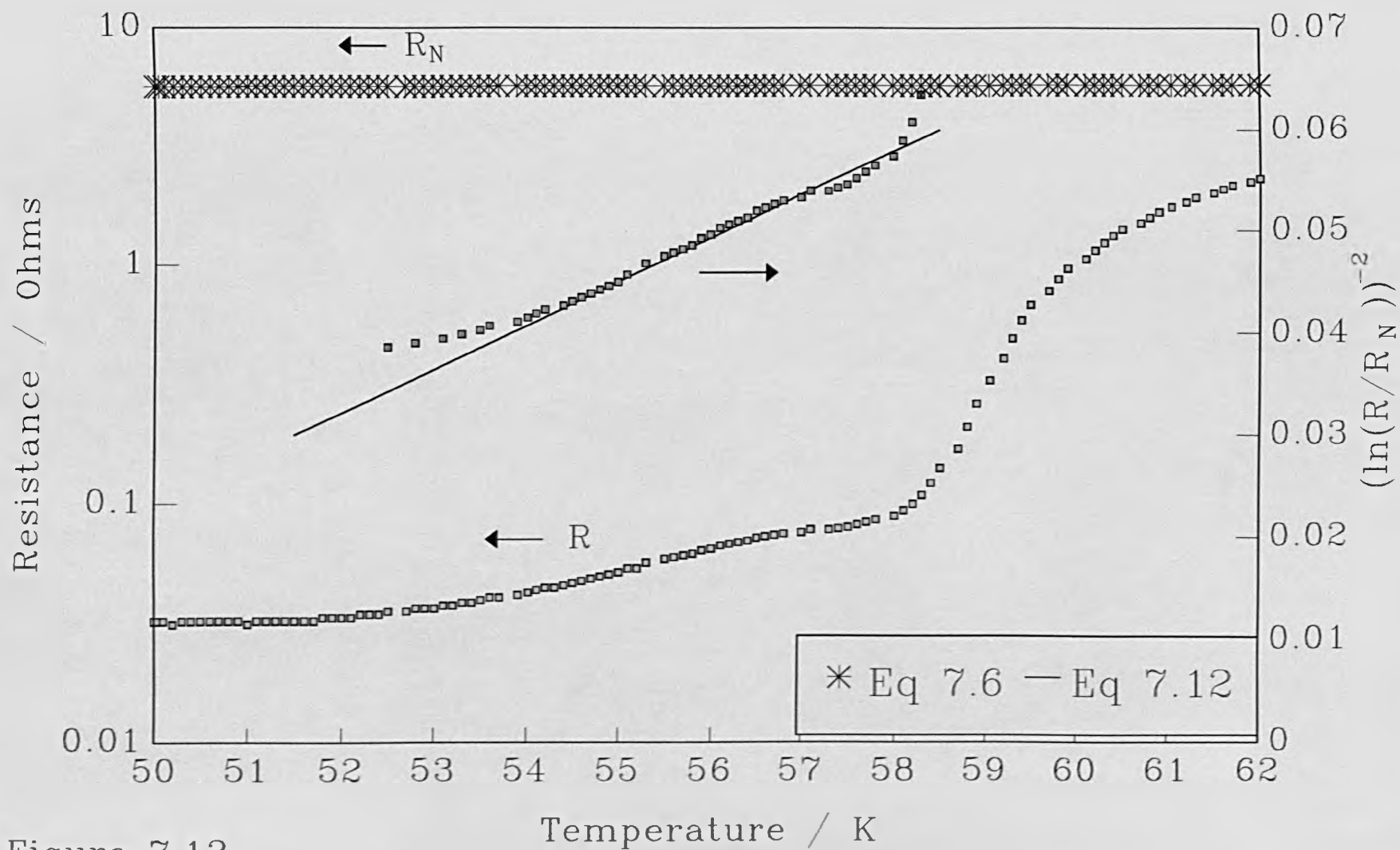


Figure 7.12

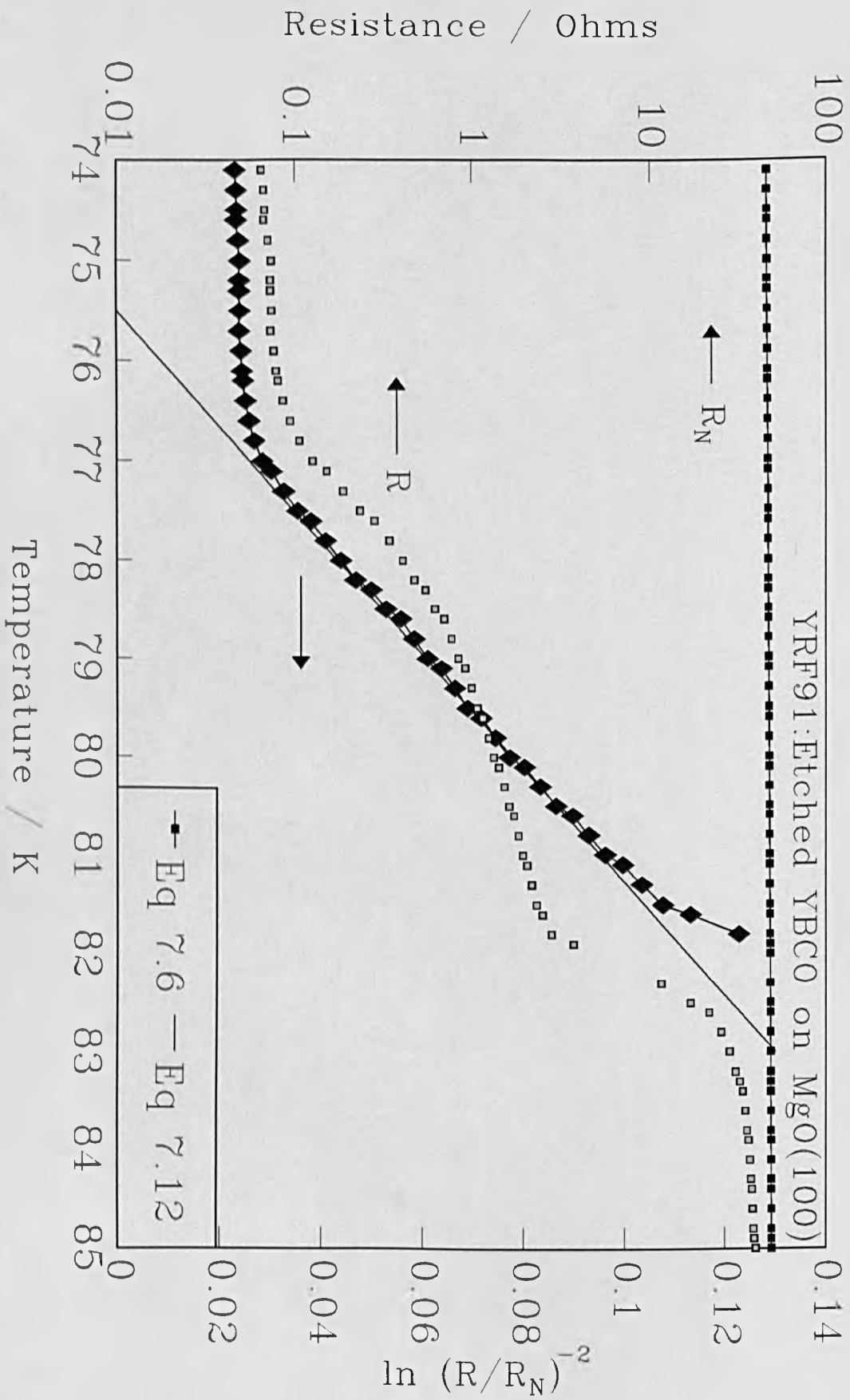


Figure 7.13

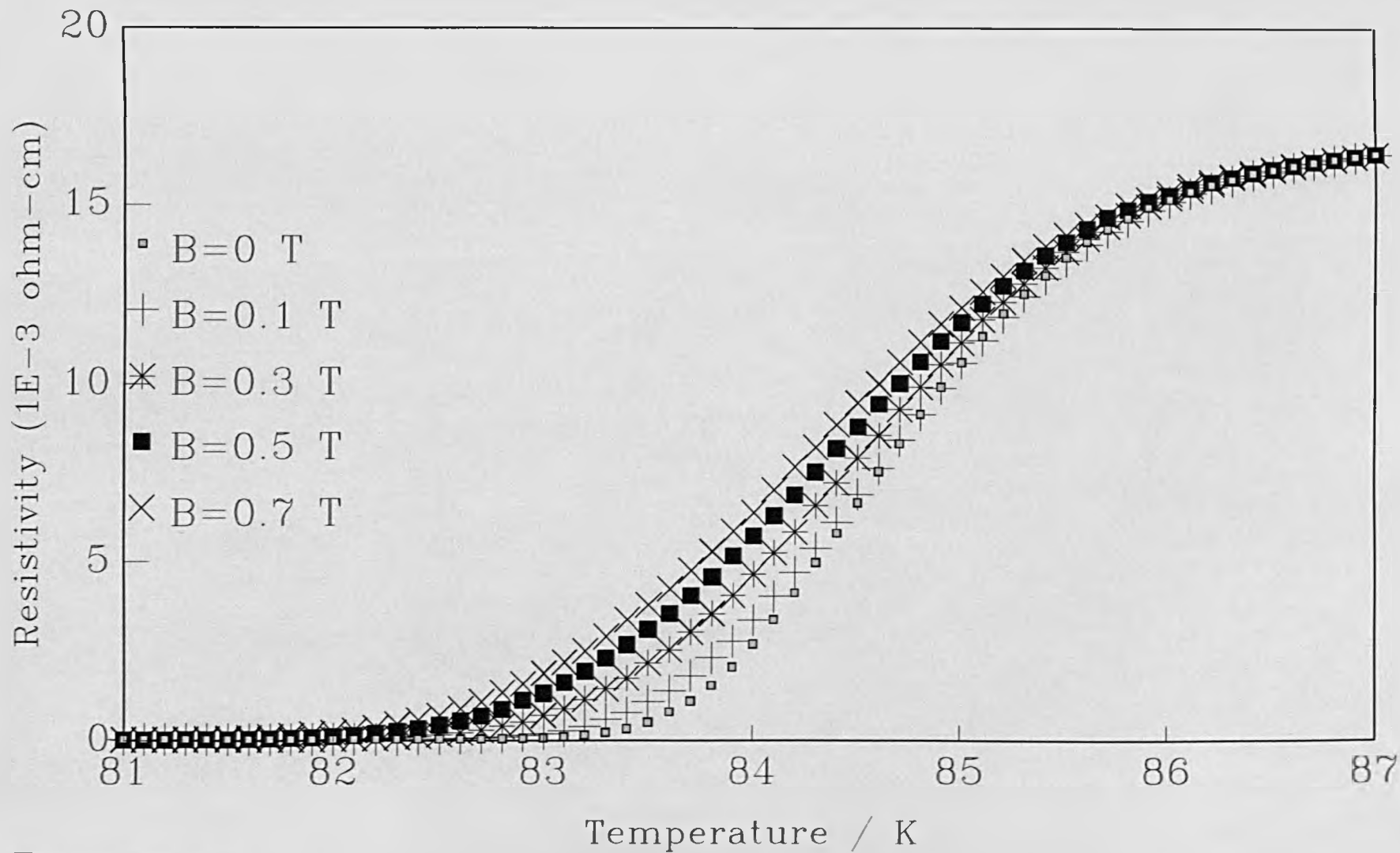


Figure 7.14

Resistance / Ohms

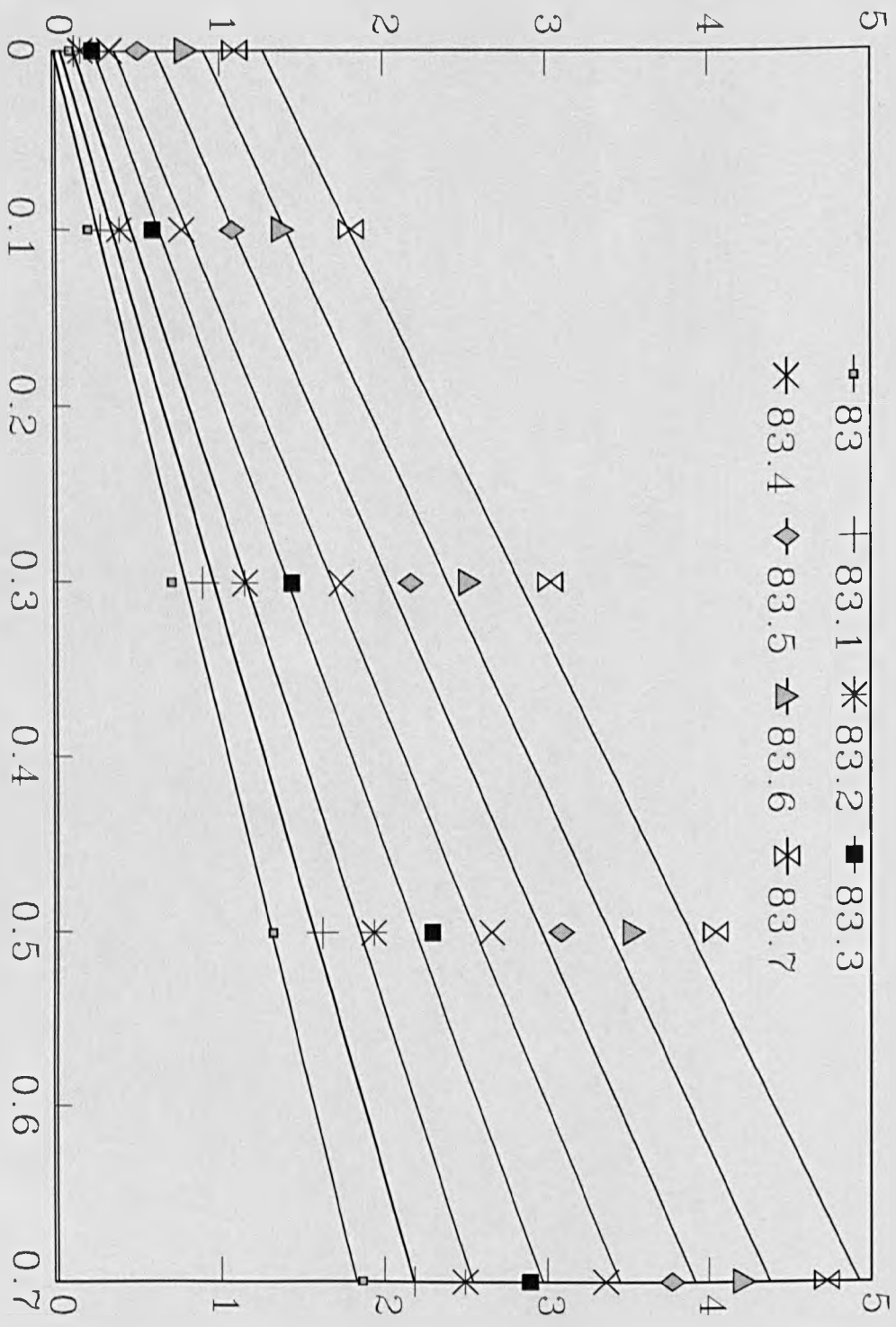


Figure 7.15

Applied B Field / T

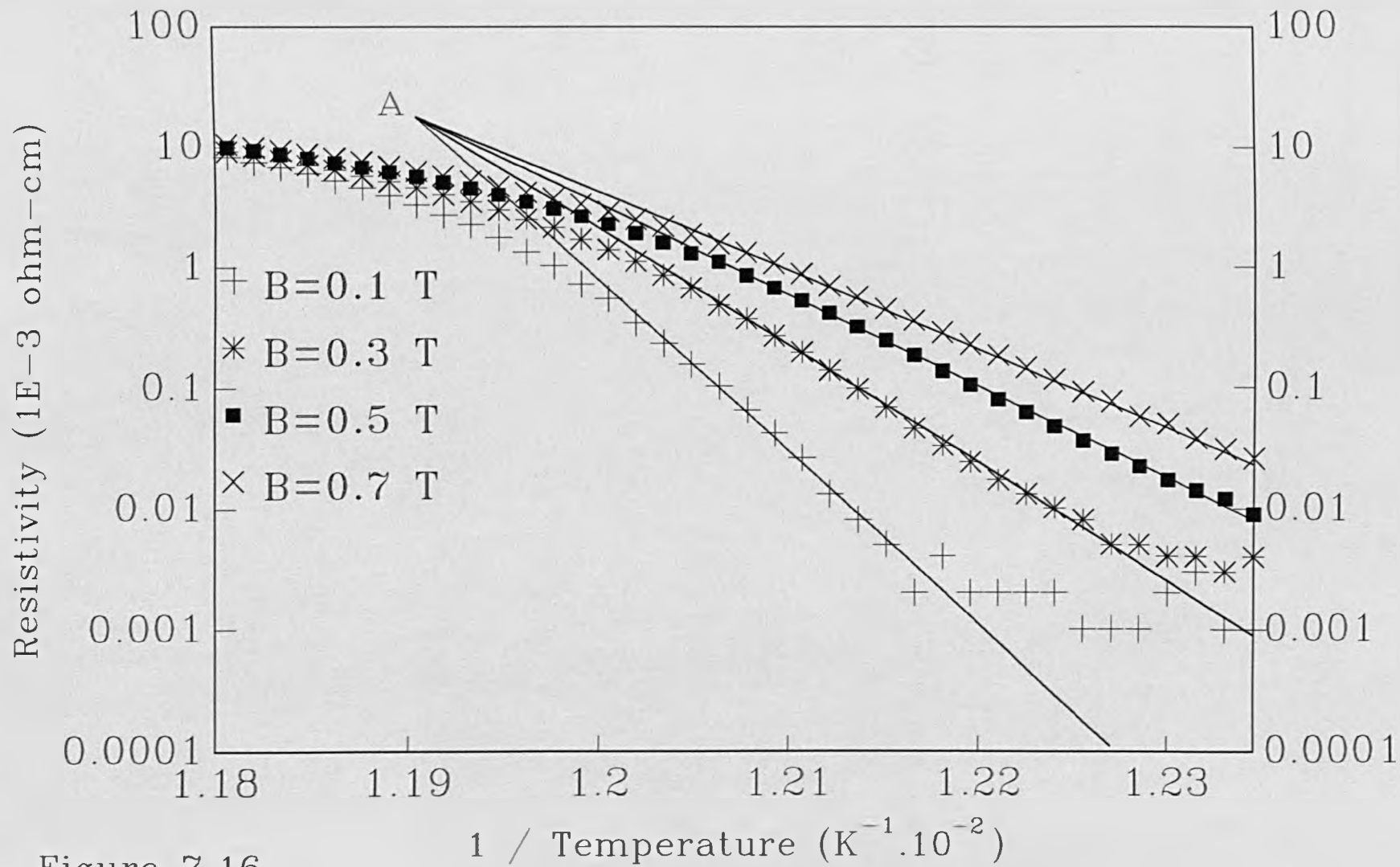


Figure 7.16

CHAPTER 8: IMPEDANCE ANALYSIS

8.1 Inductance Measurements

This chapter concerns the results obtained from the R.F. impedance measurements. The impedance was measured using an impedance analyzer set in the series R-X mode as described earlier. Typical results for films deposited on MgO(100), SrTiO₃(100) and (110) are shown in figures 8.1, 8.2 and 8.3. Note that although the temperature dependence of the reactive term is similar for each film the magnitudes are somewhat different.

8.1.1 Substrate Effects

The variation in the size of the reactance of the samples was initially assumed to be due to the substrate used. Analysis shows that this is not the case. Films deposited on SrTiO₃(100) with c-axis orientation have a similar reactance curve to those films deposited on MgO(100), see figure 8.4. Since the relative permittivities of MgO(100) and SrTiO₃(100) vary by over 70 at 77K it is clear that the substrate cannot be directly responsible for the differences observed in the other films.

The substrate can influence the orientation of the thin film deposited and it is thought that this difference in orientation may cause the changes observed in the reactance.

8.1.2 Stray Inductance

In the graphs given in figs 8.1-8.3 the reactance for $T < T_C$ is positive for each film investigated. This agrees with theory since the only terms influencing the reactance, below T_C are the geometric inductance, the kinetic inductance of the super electrons and the stray inductance due to the external wiring. It is assumed that when using this

technique the kinetic inductance is very small as $T \rightarrow 0\text{K}$. Thus at absolute zero the inductance measured is due to the geometric and stray inductances. From theory the geometric inductance is given by $\mu_0 a^2 d / 6aX$ (from equation 3.90). Thus taking the dimensions of a typical film, namely $2a=10^{-7}\text{m}$, $d=10^{-3}\text{m}$, $X=10^{-2}\text{m}$ and $\mu_0=4 \cdot 10^{-7}$, the stray inductance due to the geometry is of the order of 10^{-14}H . This is 10^{-5} times smaller than the inductance recorded as $T \rightarrow 0\text{K}$. It is thus assumed that the geometric inductance is negligible. The only remaining term is therefore, the stray inductance due to the wiring. The magnitude of the stray inductance is similar in films deposited on the various substrates,. The $T=0\text{K}$ value of the inductance, namely the stray inductance, is subtracted from the measured inductance to leave the inductance due to the film, see section 8.3.1.

From this argument it now appears that each film has a positive reactance for $T < T_C$ and a negative reactance for $T > T_C$. It seems therefore that irrespective of the film orientation and/or substrate the normal reactive properties are negative, i.e. capacitive. The magnitudes do differ however and this is thought to be due to the anisotropic nature of the YBCO. A valid explanation of this phenomena is difficult to find particularly in the films deposited on $\text{MgO}(100)$ which are c-axis orientated. For the films deposited on $\text{SrTiO}_3(110)$ and (100) it may be argued that the capacitance may arise due to the "insulating layers" separating the CuO conducting layers, since the CuO layers are tilted in the $(110/013)$ and (100) orientated films. This would not account for the measured inductance in the films deposited on $\text{MgO}(100)$, although it may account for the small size. It may be that there is a small interlayer capacitance present in the films deposited on $\text{MgO}(100)$, although it seems more likely that the capacitance may arise at the grain boundaries where semi conducting YBCO may exist.

8.2 Normal Impedance Measurements

For the growths YFR67 and YRF62, YBCO was sputtered onto SrTiO₃(110), SrTiO₃(100) and MgO(100). The resistivity and the reactance ratios, measured at 100 K, are shown in Table 8.1.

Sample No.	$\rho_{100K}(110)/\rho_{100K}(100)$	$X_{100K}(110)/X_{100K}(100)$
YRF67	3.32	28.3
YRF62	4.5	31

Table 8.1

Resistivity (ρ) and Reactance (X) ratios for YBCO R.F. Sputtered simultaneously onto MgO(100) and SrTiO₃(110), (YRF67) and SrTiO₃(100) and SrTiO₃(110), (YRF62). ρ and X measured at 100K.

The film on SrTiO₃(100), YRF62 was thought to be almost entirely c-axis orientated. The film deposited on SrTiO₃(100) in YRF80 was a mixed phase and this is reflected in the ratio of the reactance of the films deposited on SrTiO₃(100) and MgO(100) which was 314:1. The reactance of the film on MgO(100) was almost zero. The ratio of the resistance between the films in YRF80 was 4.5:1 respectively.

8.3 Superconducting Inductance Measurements

For temperatures below the critical temperature the inductance change is considered to be due to the inertia of the superelectrons. Figure 8.2 is a typical inductance-temperature curve for temperatures below T_c . Besides curves of this nature there are also several anomalous results that cannot be explained by existing theory and these will be examined below. This first section is an interpretation of the curves using London theory.

8.3.1 Kinetic Inductance and London Theory

The equivalent series inductance L_m is obtained directly from equation 3.90

$$L_m = \frac{\mu_0 \lambda^2}{1 + 4\left(\frac{\lambda}{\delta}\right)^4} \frac{d}{2aX} + \frac{\mu_0 a^2}{3} \frac{d}{2aX} + L_w \quad 8.1$$

where L_m is the measured inductance, $2a$ is the film thickness and X is the film width, λ is the penetration depth and δ is the skin depth. L_w is the inductance due to the stray components, contact wires, silver paint etc., and the second term in the above equation is the inductance due to the geometry of the film. Assuming that the inductance term due to the film geometry is very small compared with the stray impedance then

$$L_m = \frac{\mu_0 \lambda^2}{1 + 4\left(\frac{\lambda}{\delta}\right)^4} \frac{d}{2aX} + L_c, \quad L_c = \frac{\mu_0 a^2}{3} \frac{d}{2aX} + L_w \approx L_w. \quad 8.2$$

Thus at the frequencies concerned, $f = 13\text{MHz}$, $\delta \gg \lambda$, equation 8.2 simplifies to

$$L_m = \mu_0 \lambda^2 \frac{d}{2aX} + L_c. \quad 8.3$$

The penetration depth is given by

$$\lambda^{-2} = \frac{\mu_0}{L_e} - \omega^2 \epsilon \mu_0 \quad 8.4$$

where L_e is the equivalent inductivity of the film (see reference 4 equation 4), $\omega = 2\pi f$, f is frequency of the a.c. signal, $\epsilon = \epsilon_0 \epsilon_r$ is the permittivity and μ_0 is the permeability of free space. For $T < T_c$ the equivalent inductivity is assumed to be dominated by the kinetic inductance, $L_e = \mu_0 \lambda_L^2$. Hence

$$\lambda^2 = \left(\frac{1}{\lambda_L^2} - \omega^2 \epsilon \mu_0 \right)^{-1} = \frac{\lambda_L^2}{1 - \omega^2 \epsilon \mu_0 \lambda_L^2}. \quad 8.5$$

Assuming $\omega^2\epsilon\mu_0\lambda^2 \ll 1$, then $\lambda = \lambda_c$. Substituting the Gorter-Casimir equation for λ , equation 8.3 becomes

$$L_m = \mu_0 \frac{\lambda_0^2}{[1 - (\frac{T}{T_c})^4]} \frac{d}{2aX} + L_c \quad 8.6$$

Taking equation 8.6 for $T=0K$ gives

$$L_{T=0K} = \mu_0 \lambda_0^2 \frac{d}{2aX} + L_c \approx L_c \quad 8.7$$

Equation 8.7 is used to determine L_c . Thus taking $L_{T=0K} = L_c$ gives

$$L_m - L_c = \frac{\mu_0 \lambda_0^2}{1 - (\frac{T}{T_c})^4} \frac{d}{2aX} \quad 8.8$$

as $T \rightarrow T_c$. Defining

$$L_0 = \mu_0 \lambda_0^2 \frac{d}{2aX} \quad 8.9$$

and dividing 8.8 by 8.9 gives

$$\frac{L_m - L_c}{L_0} = \frac{1}{1 - (\frac{T}{T_c})^4} \quad 8.10$$

By plotting $(L_m - L_c)/L_0$ against $1/(1 - (T/T_c)^4)$ the results should give a straight line with gradient of 1. L_0 is chosen to give the curve with the gradient closest to 1. The penetration depth may be calculated from L_0 using eq.8.9. The results are summarised in Table 8.2, see Figures 8.3,4,5.

Deposition	Substrate	L_c / nH	L_0 / pH	T_c / K	$\lambda(0)$ / μm
YRF95	M(100)	16.73	29.67	71	4.86
YRF81	S(100)	11.63	128	57	10.58
YRF67	S(110)	8.35	18.47	86	2.24

Table 8.2

From these results it is clear that $L_0 \ll L_c$, the approximation in equation 8.7 is valid. The measured value of $\lambda(0)$ obtained from the films tested is far larger than expected. The values are not uniquely large however, and several groups have reported penetration depths of similar magnitude^(1,2). It is unfortunate that further work was not performed by others. As a result the reason for such observations is still unclear. The Ambegaokar-Baratoff (AB) theory predicts that the intergranular penetration depth can be far larger than the London penetration depth. The temperature dependence of the AB penetration depth is, in the region $T > 0.9T_c$, almost the same as that of the London penetration depth, hence the good fit of the results. Alternatively, if the superconductor is dirty then from Ginzburg-Landau theory the penetration depth will be given by

$$\lambda_{GL}^2 = 0.378 \lambda_L^2 \frac{\xi_0}{l} \frac{T_c}{T_c - T} .$$

Taking the $T=0$ kelvin London penetration depth $\lambda_L = 0.15 \mu\text{m}$ for a c-axis orientated thin film (YRF95) and assuming the penetration depth value of $3.6 \mu\text{m}$ is the Ginzburg Landau penetration depth, then ξ_0/l is around 1524, i.e. $\xi_0 \gg l$ which is the condition for a dirty superconductor.

8.4 Anomalous behaviour in the YBCO Thin Films

Although the London Theory was found to give good agreement with experiment over certain temperature regions near T_c , marked deviations also occurred. These results

are interpreted in terms of a 2D-3D cross-over as described below.

8.4.1 Anomalous Thin Films

An example of the anomalous behaviour is shown in a film deposited on MgO(100), YRF85, Figure 8.6. The stray inductance has been subtracted using the process described in section 8.1.2. The x-axis is the normalised temperature, given by

$$T_{norm} = \frac{1}{1 - \left(\frac{T}{T_c}\right)^4} \quad 8.11$$

with $T_c=68$ K. For values of the normalised temperature, $T_{norm}>12$, the inductance follows the normalised temperature linearly as T approaches T_c as expected. In the film shown in Figure 8.6 there is an agreement between London's theory and the results for values of $T_{norm}>12$ up to $T_{norm}=250$, corresponding to $T=0.997T_c$, i.e. to within about 0.25 K of T_{c0} . It is for values of $T_{norm}<12$, corresponding to $T=0.9 T_c=61$.K, that the anomalous behaviour occurs. In Figure 8.7, the area of interest has been expanded. The inductance decreases sharply at around $T_{norm}=12$. At the same point there is a corresponding increase in the resistance. The resistance peaks and then decreases as the temperature is lowered. A film deposited on SrTiO₃(110), (YRF70), also showed anomalous properties, as shown in Figure 8.8. Again the region of interest has been displayed. In this film the $T_c=85$ K and the anomaly occurred at $T_{norm}=3$, corresponding to $T=0.66T_c=56.1$ K.

The reason for this anomaly may be the 2D-3D cross-over point as previously discussed. In the section on paraconductivity, the sheet thickness and coherence length of a c-axis YBCO film deposited on MgO(100) were calculated to be $s=11$ Å and $\xi(0)=4$ Å respectively. The cross-over point from 2 D to 3D occurs when the coherence length $\xi>s/\sqrt{2}$. Given that

$$\xi = \frac{\xi_0}{\left(1 - \frac{T}{T_c}\right)^{1/2}} \quad 8.12$$

then for $T=0.9T_c$, $\xi=3.16\xi(0)=12.6 \text{ \AA}$, which is greater than $s/\sqrt{2}=7.8 \text{ \AA}$. This implies that for $T_{\text{nom}}=12$ the film is 3 dimensional. If this is the correct interpretation of the behaviour then the film deposited on $\text{SrTiO}_3(110)$ becomes 3 dimensional when $T_{\text{nom}}>3$, corresponding to $T=56.1 \text{ K}$. This would explain the absence of an intermediate flux flow region observed in films deposited on $\text{SrTiO}_3(110)$, i.e. the films are 3 dimensional and do not have a temperature region where spontaneous flux production takes place.

8.5 Film With a Resonance at 50 K

The film deposited in YRF117 was very thin due to the reduced deposition time. The gas ratio was 4:1, $\text{Ar}:\text{O}_2$, with a pressure of 280 mTorr. The substrate deposition temperature was 700°C . The deposition lasted around 4 hrs 50 min and the resulting film was approximately 800 \AA . The films resistance-temperature curve demonstrated that a superconducting films had been deposited, see Figure 8.9. The resistance and inductance curve was typical of that seen on many other films, namely negative normal reactance becoming positive as the film becomes superconducting with a $T_c>80 \text{ K}$. The normal behaviour of this film was similar to those discussed earlier. Around 70 K the behaviour deviated from that normally expected. Below 70 K the resistance and inductance became negative. For YRF117 the resistance and inductance pass through a resonant point at about 50 K, Figure 8.10. The resonant temperature was found to depend on the frequency of the applied current. The higher the frequency the lower the resonant temperature. The observed resonance can be modelled using the equation

where

$$R_m = \frac{A}{20(1+\chi^2)} , \quad L_m = \left(\frac{\chi A}{1+\chi^2} + 1\right) 7.5 \times 10^{-10} \quad 8.13$$

$$\chi = \beta + \frac{1}{\omega L_\lambda} , \quad 8.14$$

L_λ , β and A are undetermined. From equations 8.13 and 8.14, the theoretical graph shown in Figure 8.11 was produced using

$$A = -\left(1 + \frac{T}{20}\right) , \quad \beta = -\frac{1}{2}(375 + 1.3T) , \quad \frac{1}{\omega L_\lambda} = 24\left(1 - \left(\frac{T}{T_c}\right)^4\right) .$$

By altering the values of the variables in the above equations it is relatively easy to get a very close match to that of experiment. The question is of course what the variables represent. Karim⁽³⁾ carrying out microwave experiments reports anomalous results in this temperature region for single crystals of YBCO. Karim's group report that the absorption of microwaves reaches a maximum between 39.5 and 52 K. They verified that the observed results were due to the YBCO sample alone. They go on to suggest that the anomalous behaviour may be a result of flux lattice melting. According to Nelson⁽⁵⁾ this would take place at 28 K.

8.6 Investigation of Etched Thin Films

According to equation 3.90 the normal and superconducting resistance and inductance are dependent on film dimensions. The theory predicts that by reducing the cross sectional area of the thin film, the resistance and inductance will increase. This increase in resistance or inductance will make observations and changes more pronounced and this will allow for more accurate measurements. To test this theory it was necessary to produce films with varying dimensions. A film was deposited onto an MgO(100) substrate, YRF 91. The film was 1100 Å thick, $T_{\text{Conset}}=84$ K, $T_{c0}=81$ K. The

resistivity was $5.48 \times 10^{-6} \Omega\text{m}$ at 250 K reducing to $2.82 \times 10^{-6} \Omega\text{m}$ at $T=100$ K. A further film was deposited onto an $\text{SrTiO}_3(110)$ substrate, YRF109. The film was 1900 \AA thick, $T_{\text{Conset}}=84$ K and the $T_{\text{Co}}=82.6$ K, the sharp transition implying that a high quality thin film had been deposited. The resistivity of the film at $T=100$ K was $1.942 \times 10^{-6} \Omega\text{m}$. The results of the etched films are shown in Figures 8.12, 8.13 and 8.14 respectively.

8.6.1 Normal region

The effect of etching, on the normal behaviour of the thin films, is quite clear. The low frequency resistance from equation 3.90 is

$$R = \frac{\rho d}{2aX} \quad 8.15$$

Since X represents the film width, any change in X can be observed by plotting $1/R$ against X , Figure 8.15. Repeating this calculation on the inductance

$$L = \mu k_f \frac{d}{2aX} \quad 8.16$$

where $\mu = \mu_0 \mu_r$, μ is the permeability, μ_0 is the permeability of free space, μ_r is the relative permeability and k_f is a numerical constant, a similar result occurs as shown in Figure 8.15. It can be seen from Figure 8.15 that the results are in agreement with equations 8.15 and 8.16.

8.6.2 Temperature dependence of etched thin film

It is possible to use the above results to investigate the effect of etching on the temperature dependence of the normal behaviour. The uniformity of the thin film can be determined from these results. From Figure 8.14 the strips 1 and 2 are of slightly poorer quality than strips 3,4 and 5. Strips 1 and 2 are the thinnest strips. Strips 3-5

have same critical temperature, this implies that a uniform film may exist on at least 60 % of the substrate.

8.6.3 Superconducting region

From the analysis of an alternating electric current in a superconducting thin film⁽⁴⁾ it is possible to derive terms to represent both the resistance and inductance for the low temperature region, namely the region where $T \ll T_c$. These are,

$$R = \frac{\omega^2 \mu_0^2 \lambda^4}{\rho_n} \frac{d}{2aX} \quad 8.17$$

$$L_\lambda = \mu_0 \lambda^2 \frac{d}{2aX} \quad 8.18$$

where λ is penetration depth, $\omega = 2\pi f$, f is frequency of ac signal, ρ_n is the normal state resistivity. Both equations predict a linear relationship with the inverse of X . The results were calculated using the method described in section 8.1.2. The results are shown in Figure 8.16. Fig 8.16 is the inverse of the inductance and resistance of each strip below the critical temperature. The results do not show the predicted linear behaviour. The most likely reason for this is the film inhomogeneity. Examination of the temperature curves reveals that strips 1 and 2 have a different critical temperature. This inhomogeneity will result in each of these strips having a different penetration depth. The magnitude of the penetration depth will not be constant for a given temperature. It seems likely that the film was not linear enough to investigate the equations for superconductivity given above. It is interesting to note that in the normal temperature region, the results fitted the theory well, as described in section 8.6.1.

8.6.4 Critical current measurements

The dc critical current measurements were carried out on YRF91 on MgO(100) and YRF109 on SrTiO₃(100) using the thinnest strip available from the wet etching technique. The strip width was 140 μm for the film deposited on SrTiO₃(110) and 230 μm for the film on MgO(100). Using the criterion that the current required to produce a voltage of 1 μV across the voltage terminals represents the critical current, it was possible to determine the critical current for various temperatures for the film deposited on MgO(100). Figure 8.17 is the critical current measurements versus temperature.

8.6.4.1 Interpretation of the Critical Current Measurements

The temperature observed in Figure 8.17 has been observed on several occasions by different groups and is quite common for YBCO thin films. Using the Ambegaokar-Baratoff theory the critical current behaviour can be represented by

$$I_c^{2/3} = K\left(1 - \frac{T}{T_c}\right) \quad 8.19$$

where $K=0.081$. and T_c is the critical temperature. Performing this calculation on the results shown in Figure 8.18, a relatively close fit occurs. This is a very interesting result since the behaviour described is that expected for Josephson junctions. This implies that the strip is made up from many Josephson junctions. This is supported by the measurements of penetration depth discussed above which also implied that the strip may be many Josephson junctions in the form of a two dimensional array.

For the film deposited on SrTiO₃(110) the current carrying capabilities were far superior to those of the thin film on MgO. At 77 K the critical current of the thin film was $J_c > 3.76 \times 10^4$ A/cm², (note that this was the largest critical current available at the time of the experiment. Later experiments on other films demonstrated that the critical

current was in excess of 3×10^5 A/cm².)

8.7 A New Equivalent Model for YBCO thin films

It has become clear that it is possible to obtain a good fit for London's theory for temperatures not too close to T_c , namely $T < 0.98T_c$. The investigation into the resistive behaviour, predicted by the same theory, clearly demonstrates that for values of $T \ll T_c$ we also obtain a reasonable fit as shown previously. Besides these results there is also anomalous behaviour within the thin films that is contrary to that expected from theory. The most peculiar results occurring in a very thin film, that underwent a resonance effect approximately 30 K below the film's critical temperature. In this next section these results are examined in terms of an equivalent model.

8.7.1 Equivalent Circuit Model

The model developed here is based on the Gorter Casimir (GC) two fluid theory. The present picture of the GC model is of a superconducting phase in parallel with the normal phase. The superconducting phase has no resistance, though it does exhibit an inductance in an alternating electrical or magnetic field. The inductance is due to the inertia of the superelectrons and is directly proportional to the number of superelectrons. This picture is not adequate for describing the present materials since it does not include flux flow phenomena. The model will be further complicated by the broadening of the phase transition, though this will be dealt with elsewhere. Results have shown that above T_{KTB} , but below T_{czero} there can exist a measurable resistance due to flux flow. This resistance is small in magnitude compared with the normal state resistance, i.e. the resistance when $T \gg T_c$. Thus if the resistance due to the fluxons is given by R_f , then an equivalent model is shown in Figure 8.19. The normal component is still in parallel with

the 'super' component. There is now however a flux flow term in series with the kinetic inductance. Analysing this circuit in terms of a series equivalent circuit gives $Z = R + jX$, where

$$R = \frac{R_n R_f (R_n + R_f) + \omega^2 (L_n^2 R_f + L_s^2 R_n)}{(R_n + R_f)^2 + \omega^2 (L_s + L_n)^2} \quad 8.20$$

$$X = \frac{j\omega (L_n R_f^2 + L_s R_n^2 + \omega^2 L_n L_s (L_n + L_s))}{(R_n + R_f)^2 + \omega^2 (L_s + L_n)^2} \quad 8.21$$

8.7.2 Equivalent model for $T < T_{KTb}$

With $T < T_{KTb}$, the dissipation due to the fluxons is zero since $R_f = 0$ due to the flux pinning that takes place at these temperatures. Applying this to the equations 8.20 and 8.21,

$$R = \frac{\omega^2 R_n L_s^2}{R_n^2 + \omega^2 (L_s + L_n)^2} \quad 8.22$$

and

$$X = j\omega L_m = \frac{j\omega (L_s R_n^2 + \omega^2 L_n L_s (L_n + L_s))}{R_n^2 + \omega^2 (L_n + L_s)^2} \quad 8.23$$

assuming that $R_n \gg \omega(L_n + L_s)$ this further simplifies to

$$R = \frac{\omega^2 L_s^2}{R_n} \quad 8.24$$

and

$$L_m = L_s + \frac{\omega^2 L_n L_s (L_n + L_s)}{R_n^2} \approx L_s \quad 8.25$$

which are similar to the results given in Raven's analysis.

8.7.3 Equivalent model with $T_{KTB} < T < T_c$

With the temperature of the thin film in excess of T_{KTB} the flux present in the sample is free to move within the sample. This implies that R_f will no longer be zero. Assuming however that R_f is very small and that $R_n \gg R_f$, $\omega(L_n + L_s)$ namely that the temperature is only slightly greater than T_{KTB} , but still significantly smaller than the critical temperature, then equations 8.20 and 8.21 become

$$R = R_f + \frac{\omega^2 L_s^2}{R_n} \quad 8.26$$

and

$$L_m \approx L_s \quad 8.27$$

Thus the resistive behaviour will be altered by R_f , where-as the inductive term is, to a good approximation, unaltered. This has been born out by the experimental results, namely that in using the London model to describe the results, a better fit exists for the inductive term than for the resistive term. Furthermore by rearranging equation 8.26 and substituting from equation 8.27 we obtain

$$R_f = R - \frac{\omega^2 L_m^2}{R_n} \quad 8.28$$

Since L_m and R are results from measurement and R_n can be calculated from extrapolating the normal resistance, as described in chapter 7, we calculate the resistance

due to the fluxons. As the temperature decreases the dissipation due to the flux flow also decreases and eventually falls to zero, this is the zero dissipation temperature.

8.7.4 AC Dissipation in a Magnetic Field

Using the solenoid described in chapter 5, a magnetic field was applied perpendicular to the thin films. By adjusting the current in the solenoid the magnitude of the applied magnetic field was varied from 0 to 300 gauss. Figure 8.20 shows the behaviour of the inductance for various magnetic fields.

According to the theory the inductance, which is approximately equal to the kinetic inductance does include a term representing the resistance due to the flux, as shown

$$L_m = \frac{L_n R_f^2 + L_s R_n^2 + \omega^2 L_n L_s (L_n + L_s)}{(R_n + R_f)^2 + \omega^2 (L_s + L_n)^2} \approx L_s + \frac{L_n R_f^2}{R_n^2} \quad 8.29$$

where L_n is the normal inductance, R_f is the resistance due to the flux flow, R_n is the normal resistance, L_s is the super inductance and L_m is the measured inductance. The flux term is small and has little effect until the temperature approaches T_c , namely, the point at which the kinetic inductance becomes large. As the temperature increases however and R_f becomes large enough to influence L_m , the inductance should decrease more rapidly as the field increases, since L_n is negative in magnitude. Both predictions are examined in Figure 8.20. The graph shows that at 80 K the magnitude of the inductance increases with an increase in magnetic field. As the temperature rises and the flux begin to flow the inductance decreases as predicted. Since the magnitude of the flux is dependent on magnetic field, the inductance decreases most rapidly for the largest applied magnetic field.

8.7.5 Simulated Results using the Model

A further test of the validity of this model is the simulated resistance and inductance predicted by the above equations. The various parameters were taken to be as close to real results as possible. For example, the normal resistance is linear dependent on temperature and has a small residual value at $T=0$ Kelvin. A similar linear dependency was used to calculate the normal inductance. The super kinetic inductance was calculated using London's equation, namely, the temperature dependency was that given by Gorter and Casimir. The flux flow term was the most difficult to describe, since it is the most complicated and least understood of the four parameters. It is due to the complexity of the flux flow that in this model it has been represented initially as linear dependent. This is an approximation that can be improved on by using the temperature dependence for R_f given by the KTB theories. The immediate point to be made is that this model can be used as a fair representation of the behaviour of the inductance and the resistance.

Using a $T_c=88$ Kelvin, $R_n= 4 + 0.03T$, $L_n= 6e-11T - 1e-8$, $R_f= 0.5 (85-T)$ with $R_f=0$ for $T<85$ K i.e. the film is considered to have zero dissipation due to flux for $T<85$ K, for $T>85$ K the flux increases linearly and $L_f= L_0/(1-t^4)$, where $t=T/T_c$, equations 8.20 and 8.21 give the results shown in Figure 8.21. The sharpness of the transition compared with experiment is due to ignoring the broadening of the transition due to thermal fluctuations. Examining Figure 8.22, which represents the inductance and resistance below T_c , a similar behaviour from that given by experiment occurs. Namely the peak in the inductance and the reduction of the resistance to a very small value. Taking the model a step further by including broadening of the transition and by replacing the linear resistance with that predicted by Kosterlitz Thouless and Berezinskii it will be possible to obtain even better results. From the curves already shown it is

possible to see the similarity between experiment and theory. Thus it seems that this is a reasonable model for representing the YBCO thin films in this type of electrical measurement.

8.8 Summary of Chapter 8

R.F. contact experiments revealed that the reactive nature of the YBCO thin films was anisotropic. The reactance seems to be more sensitive to changes in the orientation than the resistivity. This may prove more useful for determining the orientation, or degree of orientation in the case of the mixed phase, of a thin film.

The inductance measurements were used to calculate the penetration depth. The penetration depth was found to be much larger than expected, having values ranging from 2.24-10.58 μm . The Ambegaokar and Baratoff theory suggests that this is due to the granular nature of the thin films, namely that the films may be similar to a 2 dimensional array of Josephson Junctions. There is some evidence from the critical current, namely a $I^{2/3}$ vs temperature dependency, that this may be the case. It is also possible however that the films measured were dirty superconductors i.e. $\xi \gg \lambda$, this would also explain the large penetration depth.

The inductance measurements also revealed anomalous results in certain YBCO thin films. The anomaly was observed as a sharp deviation from the expected temperature dependence of the inductance. Examination of the resistivity revealed that the anomaly caused a temporary increase in the resistance as demonstrated in Figures 8.7,8.8. The reason for the anomaly is not clear although the 2D-3D crossover may be the reason.

A thin film revealed a resonance effect at 48 K, previously unseen. The effect was easily modelled using dielectric theory equations, although an explanation for the behaviour as yet to be found. This phenomena is particularly interesting since Karim also reports absorption of microwaves around this temperature region.

The resistive behaviour in a magnetic field was investigated for a thin film thought to be 3 dimensional in nature. The results were in good agreement with

Anderson's flux flow theory. The behaviour of the inductance in a magnetic field was found to be in qualitative agreement with theory.

An etching technique using ferric nitrate was successfully used to produce thin strips of YBCO. Examination of the normal region was in agreement with theory. The transition region revealed that after etching 60% of the film was uniform having the same critical temperature. The other region was degraded slightly resulting in a T_c 1 K lower. It was not possible to investigate the superconducting region of the thin strips accurately because of the contact inductance and resistance. The reason for this is not clear although the most likely reason is changes in film structure across the film.

Critical current measurements revealed that some films deposited on MgO(100) did have an $I^{2/3} \propto T$ dependency. This is predicted by the Ambegaokar Baratoff theory and is in agreement with the penetration depth measurements mentioned above. The largest critical current measurements were taken from films deposited on SrTiO₃(110). At 77 K the $J_c > 3 \times 10^5$ A/cm².

8.9 References

- 1 Gasparov V.A., Huguenin R., Pavuna D., van der Maas J., Solid State Comms vol **69**, 12, pp.1147, 1989
- 2 Sridhar S., Shiffman C.A., Hamdeh H., Phys Rev B **36** (1987) 2301
- 3 Karim R., How H., Seed R., Widom A., Vittoria C., Balestrino G., Paroli P., Solid State Comms. **71** (1989) 983
- 4 Raven M.S., Inameti E.E., Murray B.G., Wan Y.M., Physica C **178**, 275, (1991)
- 5 Nelson D.R., Phys Rev Lett **60** (1988) 1973.

8.10 Captions

Figure 8.1 : A typical resistance/inductance versus temperature curve of a YBCO thin film. L_{100} is taken as the inductance at 100 K.

Figure 8.2 : A typical inductance temperature curve around the critical temperature region. This film is a slightly oxygen deficient form of YBCO. T_c is taken as the peak of the inductance curve.

Figure 8.3 : The normalised inductance vs normalised temperature curve of a YBCO thin film deposited on MgO(100), obtained using equation 8.10, $L_c=16.73$ nH, $L_0=29.67$ pH.

Figure 8.4 : The normalised inductance vs normalised temperature curve of a YBCO thin film deposited on SrTiO₃(100), obtained using equation 8.10, $L_c=11.63$ nH, $L_0=128$ pH.

Figure 8.5 : The normalised inductance vs normalised temperature curve of a YBCO thin film deposited on SrTiO₃(110), obtained using equation 8.10, $L_c=8.35$ nH, $L_0=18.47$ pH.

Figure 8.6 : Anomalous inductance behaviour occurred in a YBCO thin film deposited on MgO(100). Note that the temperature as been normalised using equation 8.11. The inductance is given by 8.9.

Figure 8.7 : The anomalous region of fig 8.6 is expanded. Notice that the resistance is also anomalous in its behaviour.

Figure 8.8 : The anomalous behaviour is also visible in thin films deposited on SrTiO₃(110). This film has a T_c=85K, the anomaly occurs at around 56 K.

Figure 8.9 : The resistance-inductance of a very thin film deposited on SrTiO₃(110). Notice the anomalous behaviour between 40-60 Kelvin.

Figure 8.10 : The anomalous region of fig 8.9 as been expanded. The resonance behaviour is clearly visible.

Figure 8.11 : Fig 8.10 is modelled using equations 8.13 and 8.14. The results are very similar to the theory.

Figure 8.12 : The resistance-temperature curves of a series of YBCO strips deposited on MgO(100). The widest strip is slightly better than the rest of the strips. This may be due to a slight change in film structure, namely a slight non uniformity in the film. The film dimensions were

Figure 8.13 : The inductance-temperature curves of a series of YBCO strips deposited on MgO(100). The tiniest strip was destroyed during the etching process.

Figure 8.14 : The inductance-temperature curves of a series of YBCO strips deposited on SrTiO₃(100). The film widths are 140, 230, 370, 660 and 1000 μm.

Figure 8.15 : $(\text{Resistance})^{-1}$ and $(\text{inductance})^{-1}$ as a function of film width. The measurements were taken at 100K.

Figure 8.16 : $(\text{Resistance})^{-1}$ and $(\text{inductance})^{-1}$ as a function of film width. The measurements were taken at 79 K

Figure 8.17 : A typical critical current versus temperature curve of a c-axis orientated YBCO thin film deposited on MgO(100). The YBCO thin film was oxygen deficient resulting in a low T_c .

Figure 8.18 : The critical current behaviour was found to be in good agreement with the Ambegaokar Baratoff theory. This implies that the film may in fact be made from many Josephson Junctions.

Figure 8.19 : Equivalent model for a thin film of YBCO. The main feature is the flux flow in series with the Kinetic Inductance due to the superelectrons.

Figure 8.20 : The inductive behaviour of a thin film is investigated using an applied magnetic field. The behaviour is found to be in qualitative agreement with equation 8.29.

Figure 8.21 : The theoretical temperature dependence of the resistance and inductance produced using equations 8.20 and 8.21.

Figure 8.22 : The theoretical temperature dependence of the superconducting and

intermediate regions of a YBCO thin film.

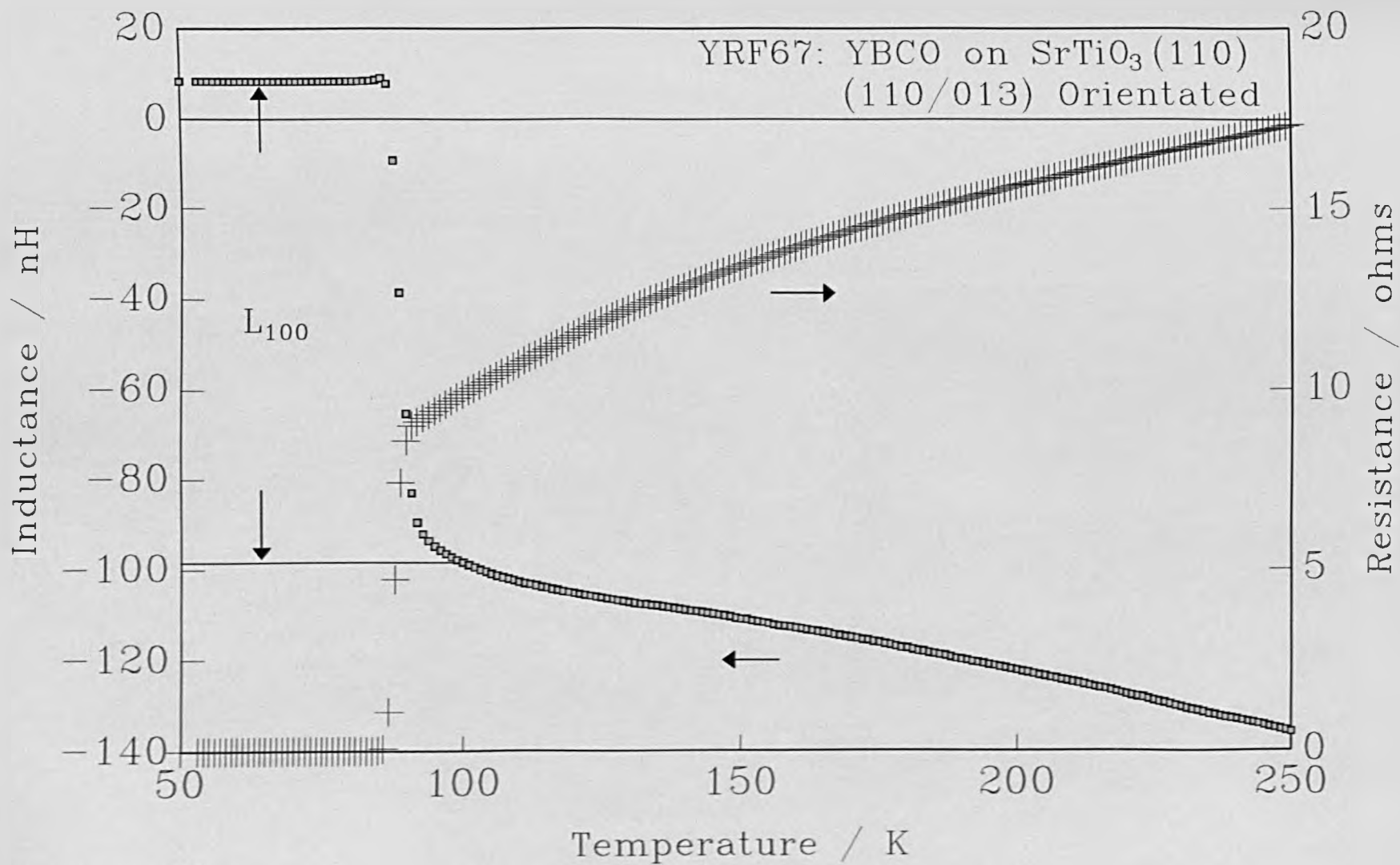


Figure 8.1

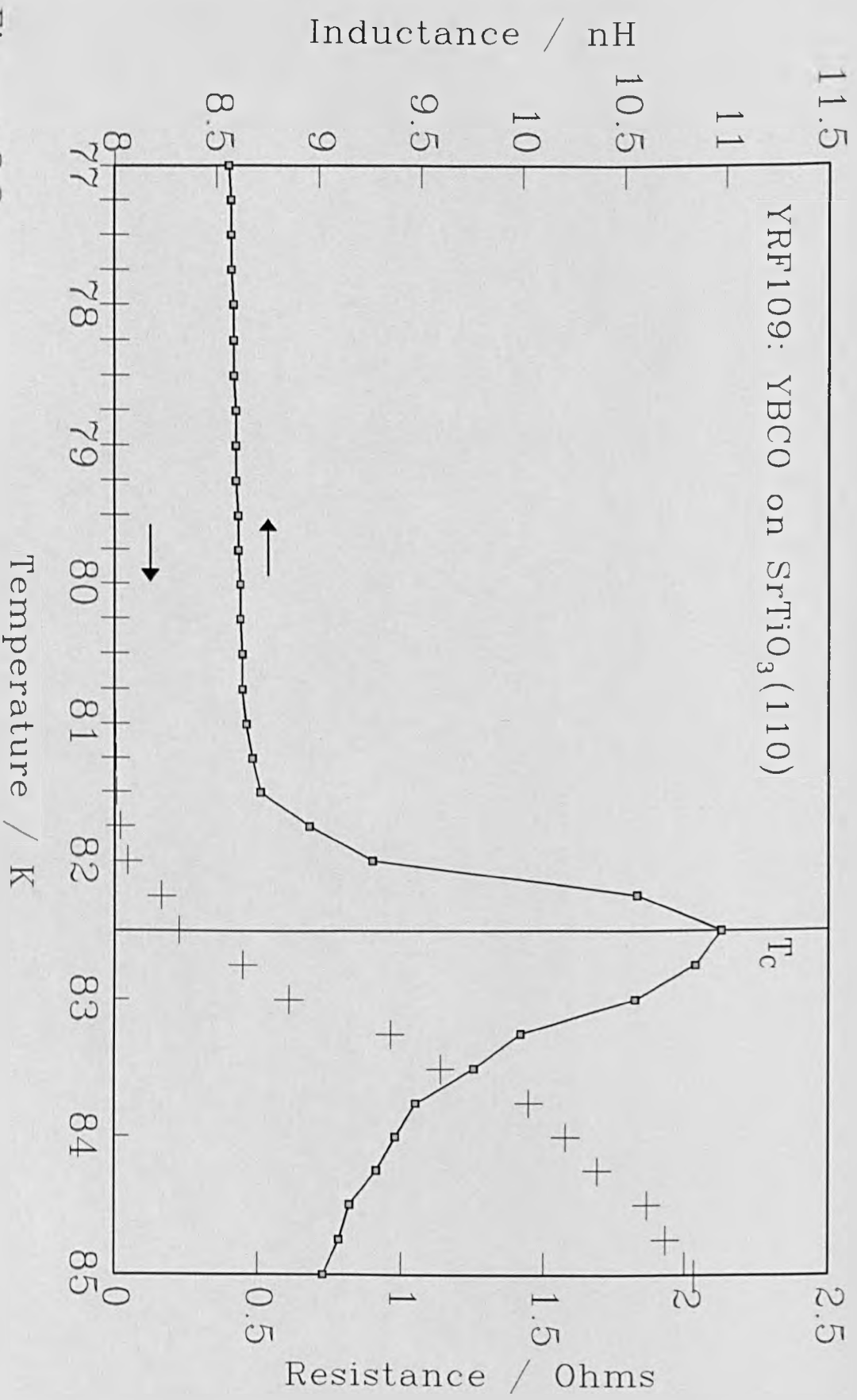


Figure 8.2

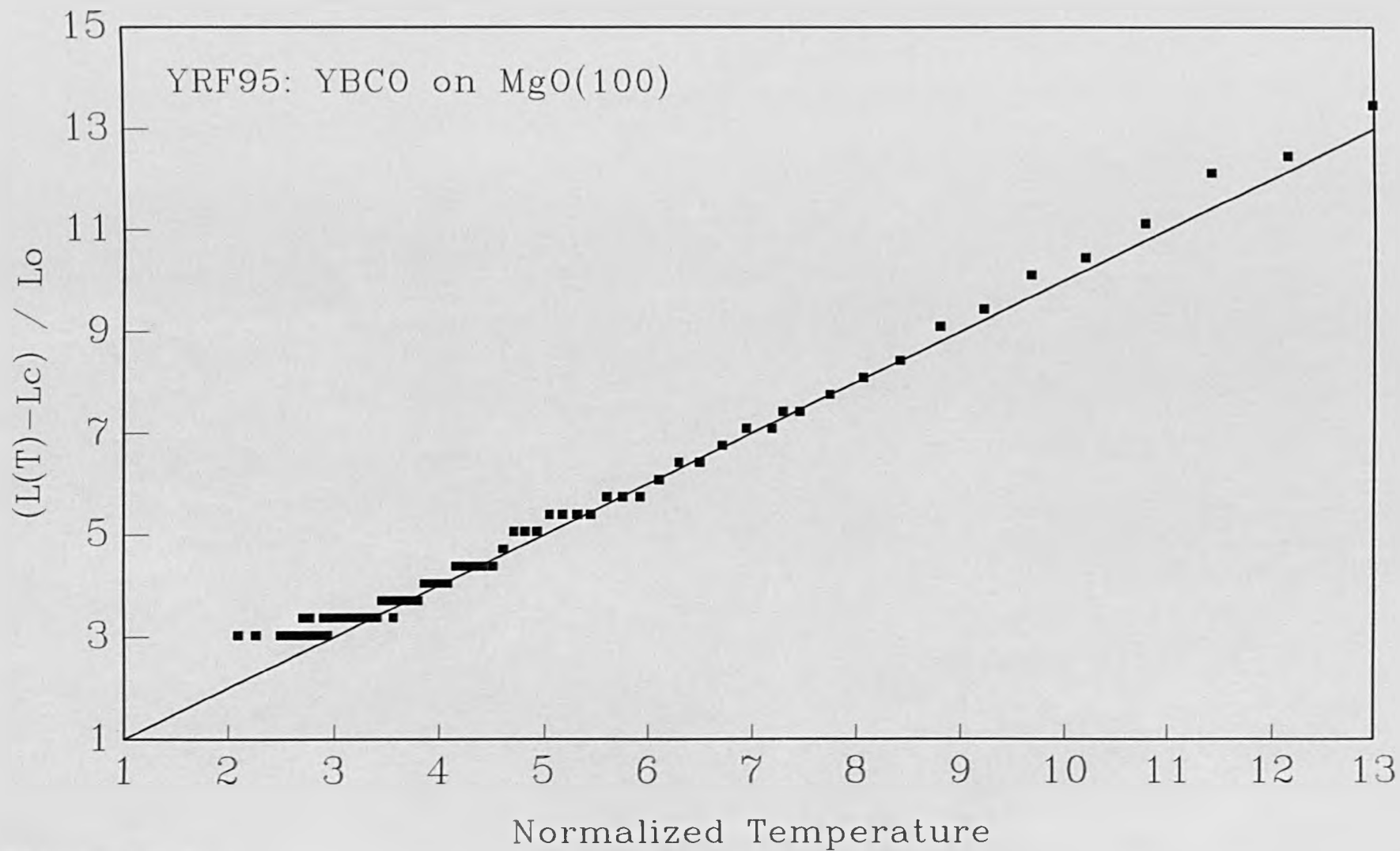


Figure 8.3

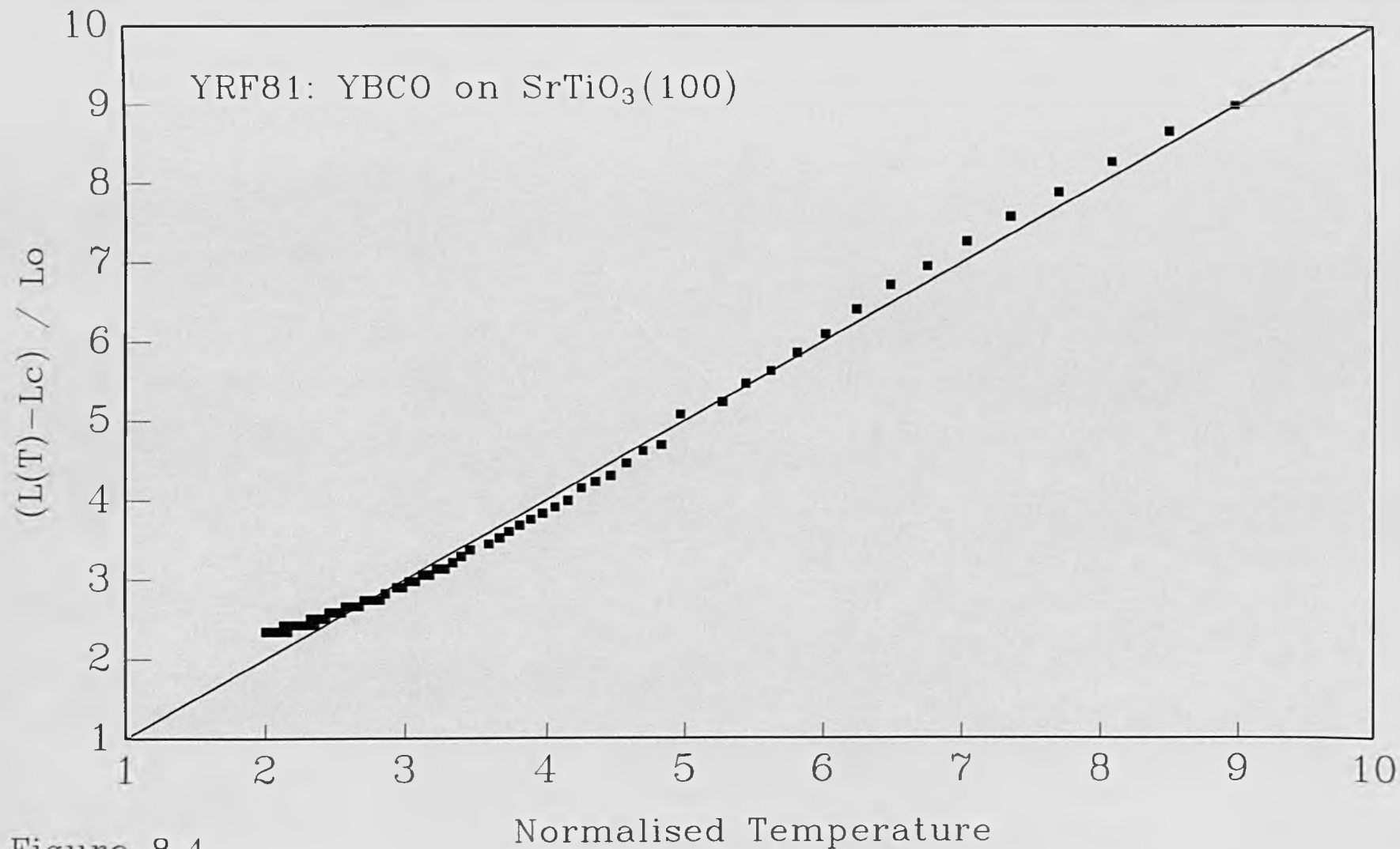


Figure 8.4

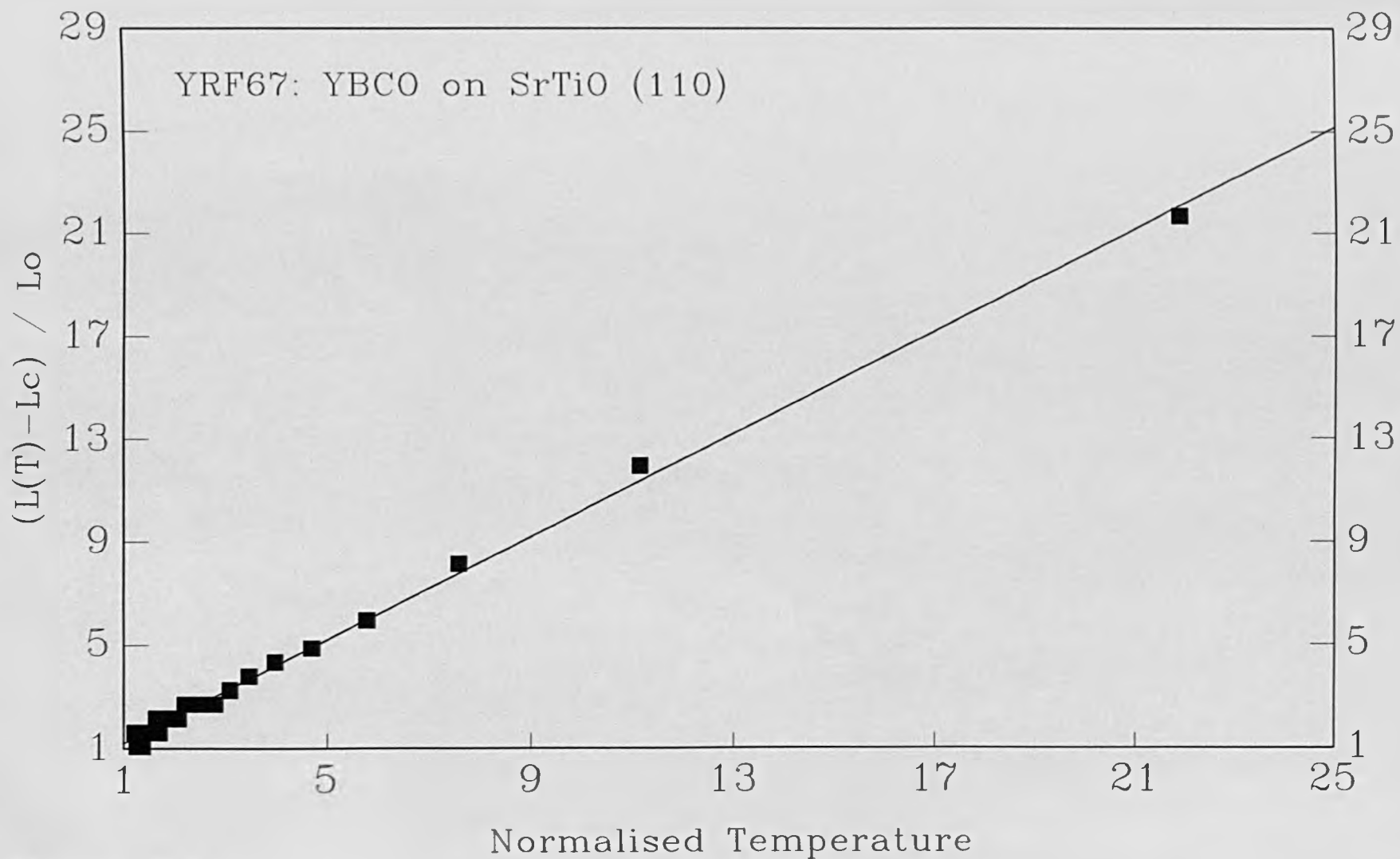


Figure 8.5

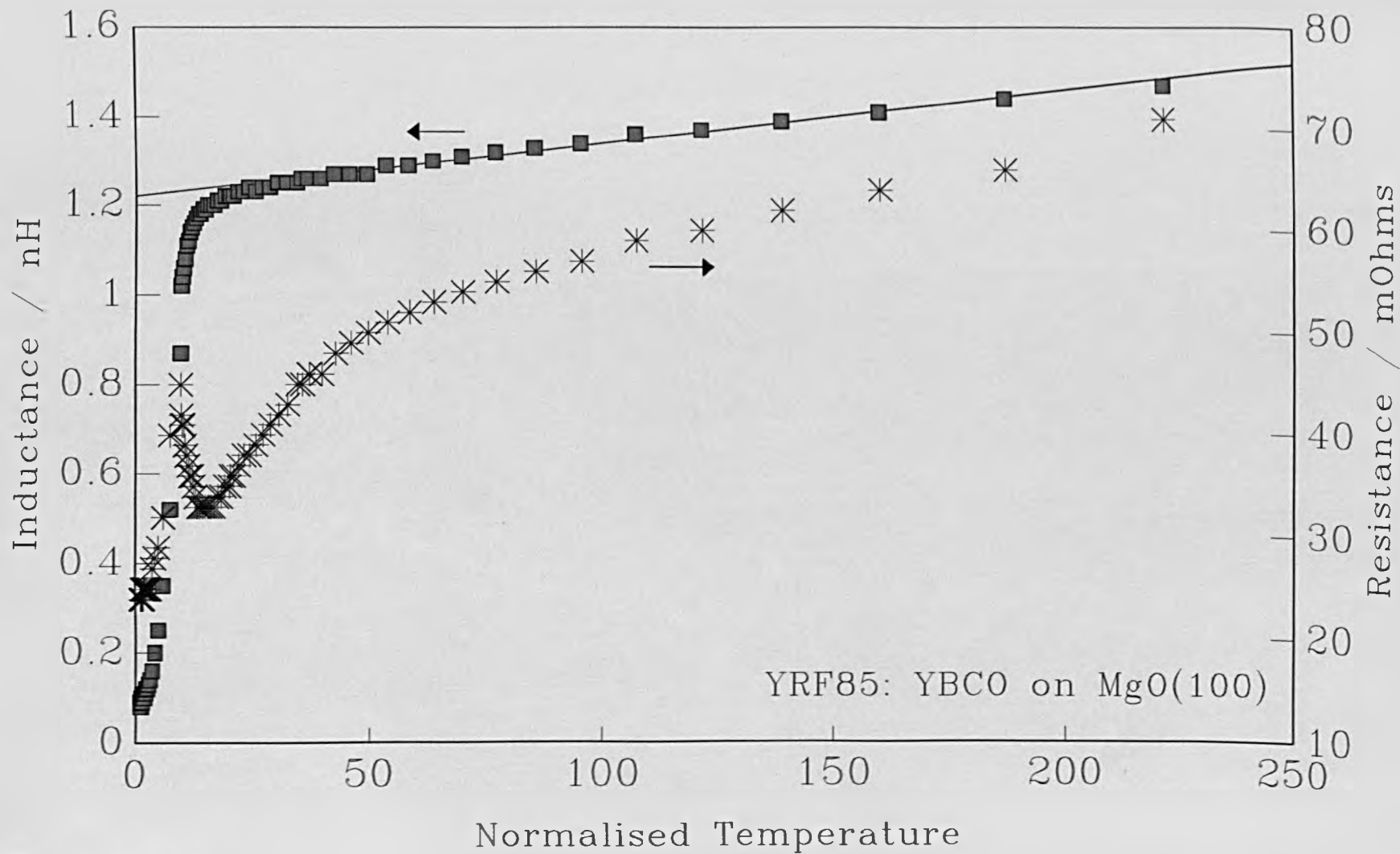


Figure 8.6

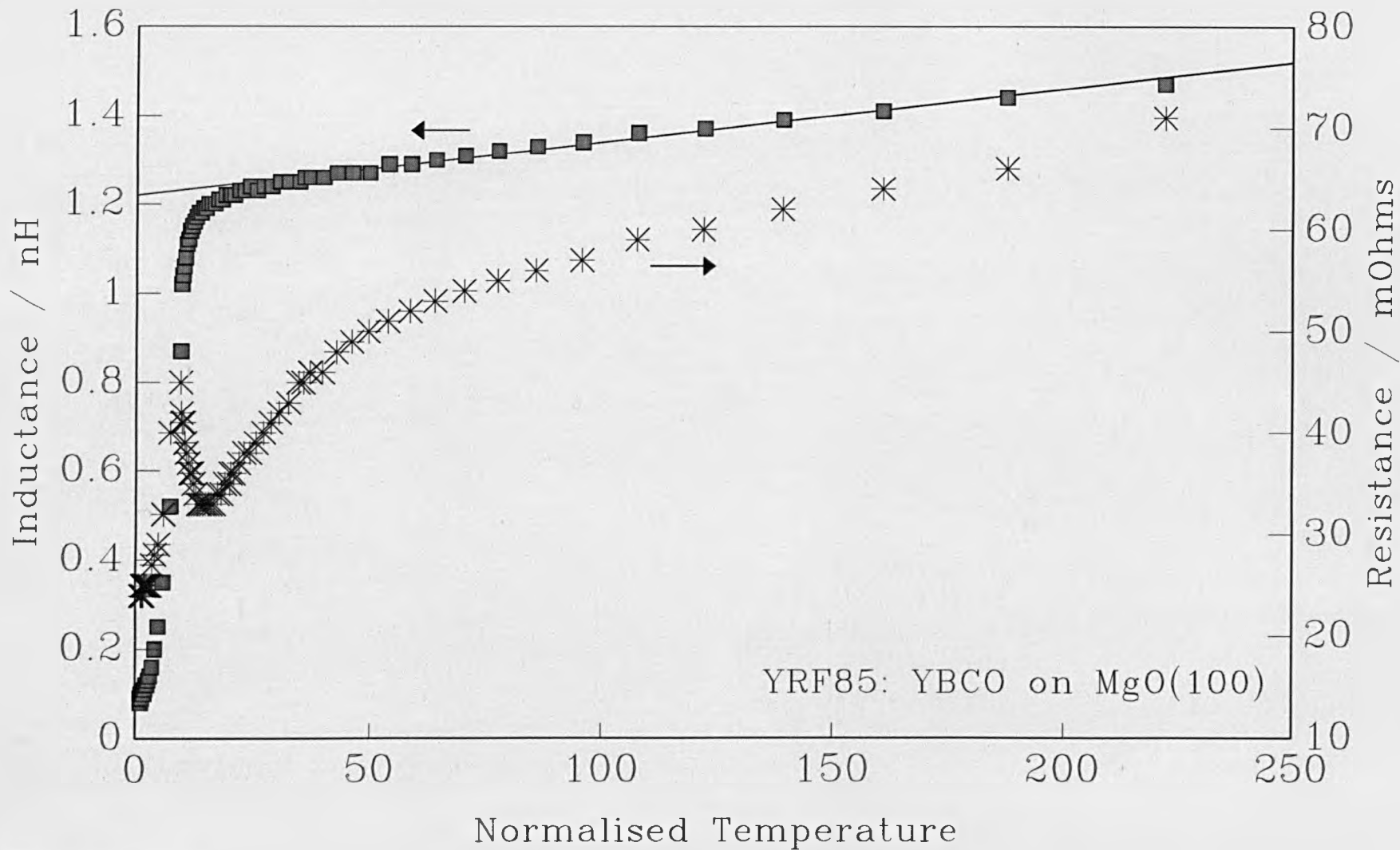


Figure 8.6

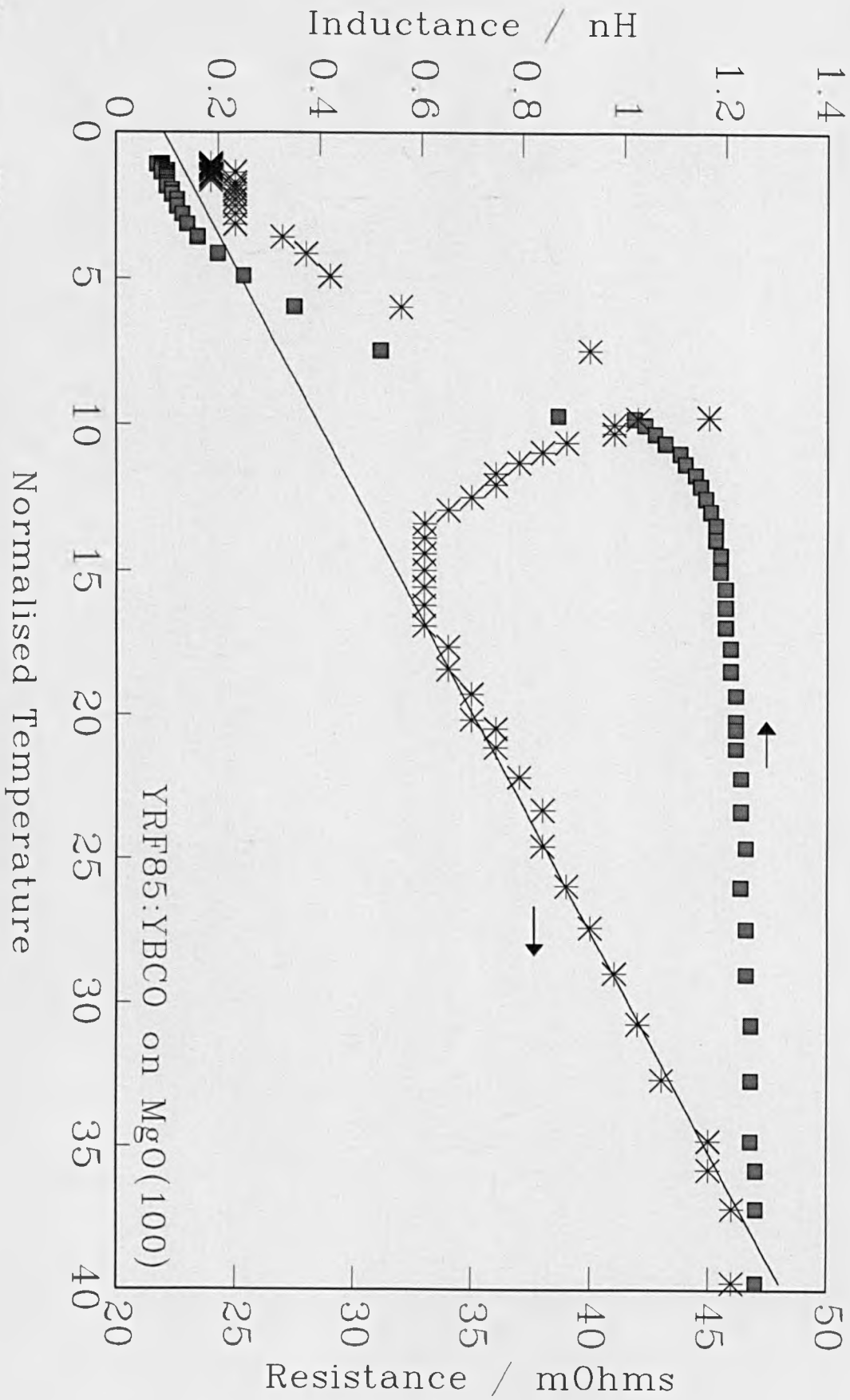


Figure 8.7

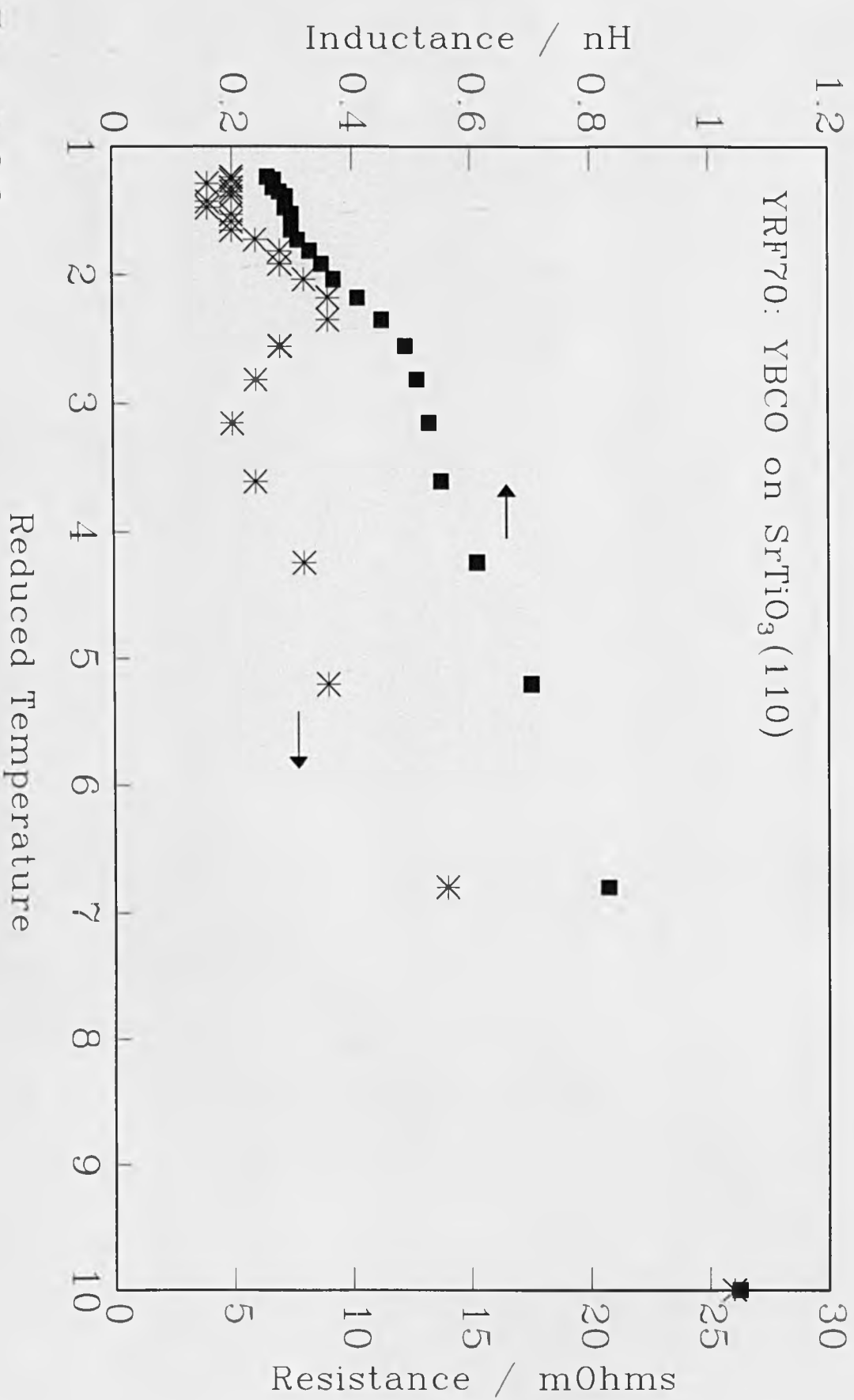


Figure 8.8

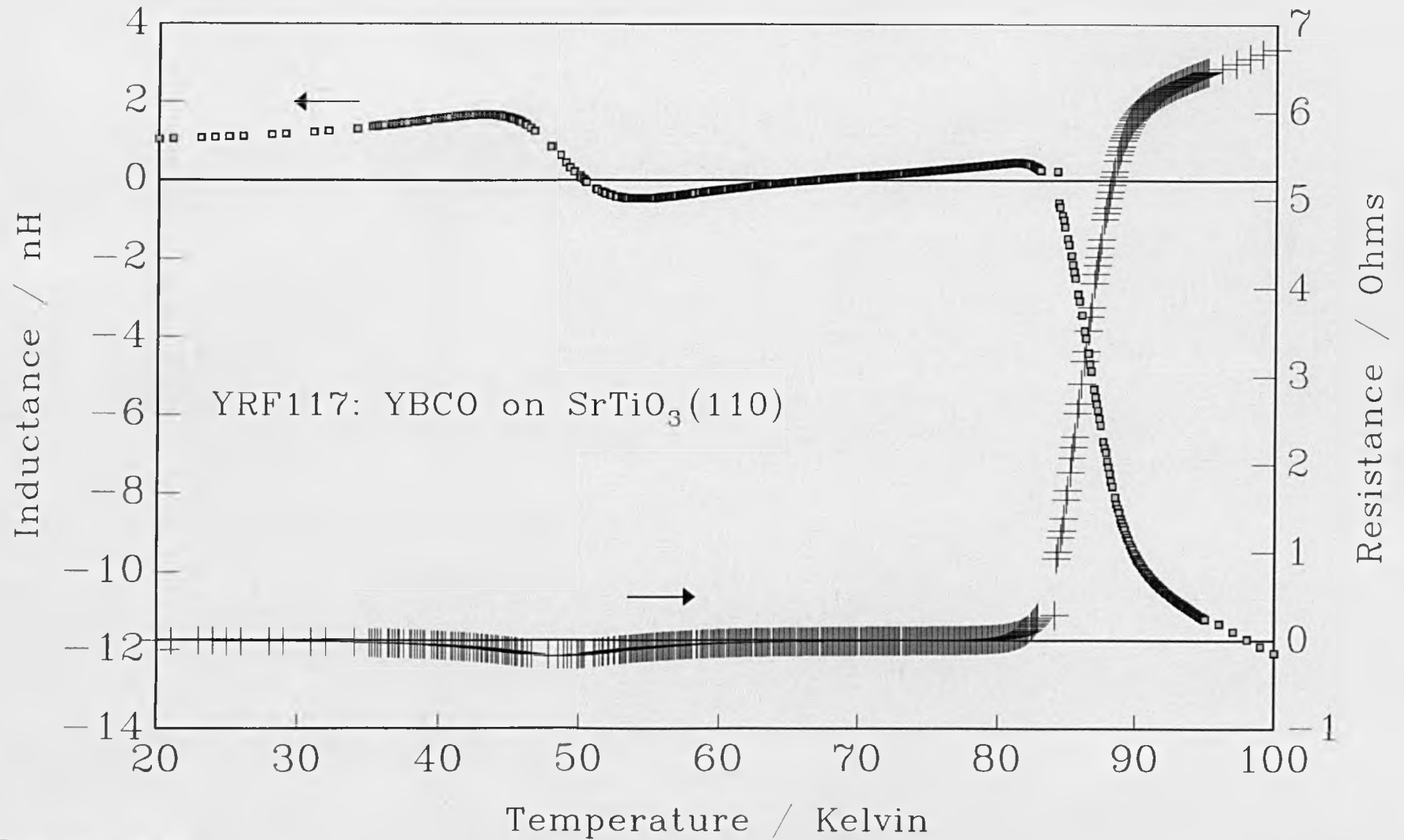


Figure 8.9

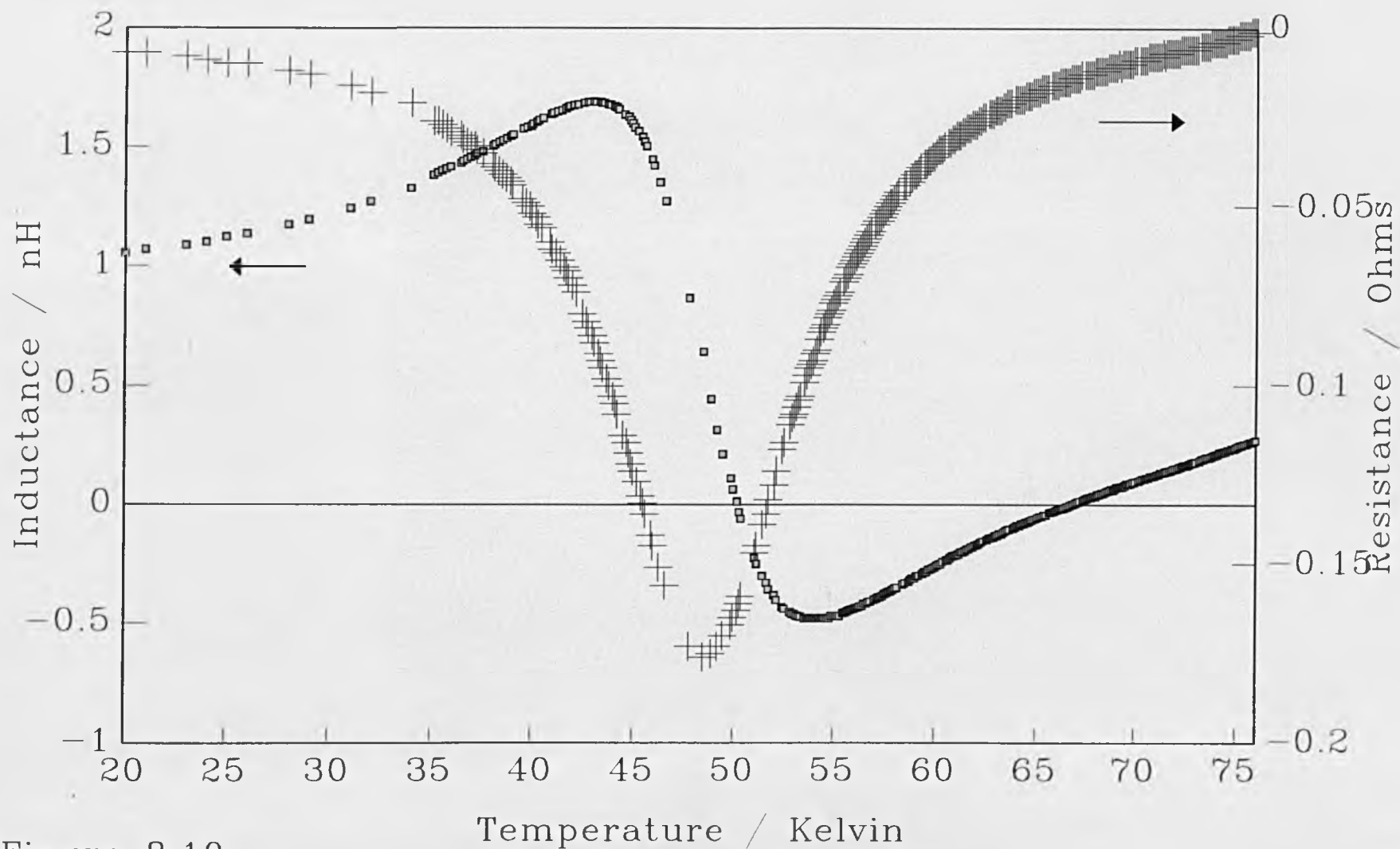


Figure 8.10

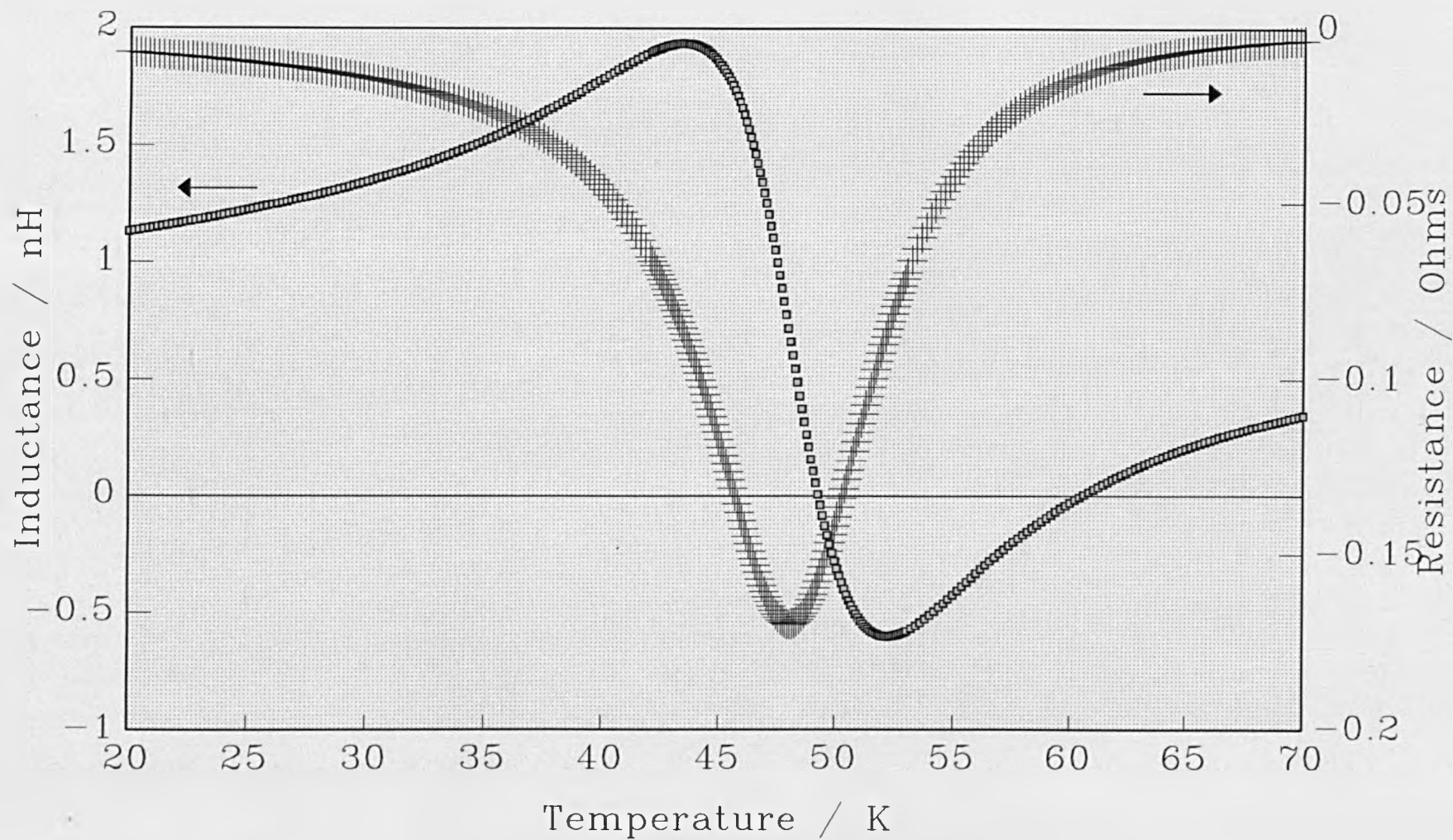


Figure 8.11

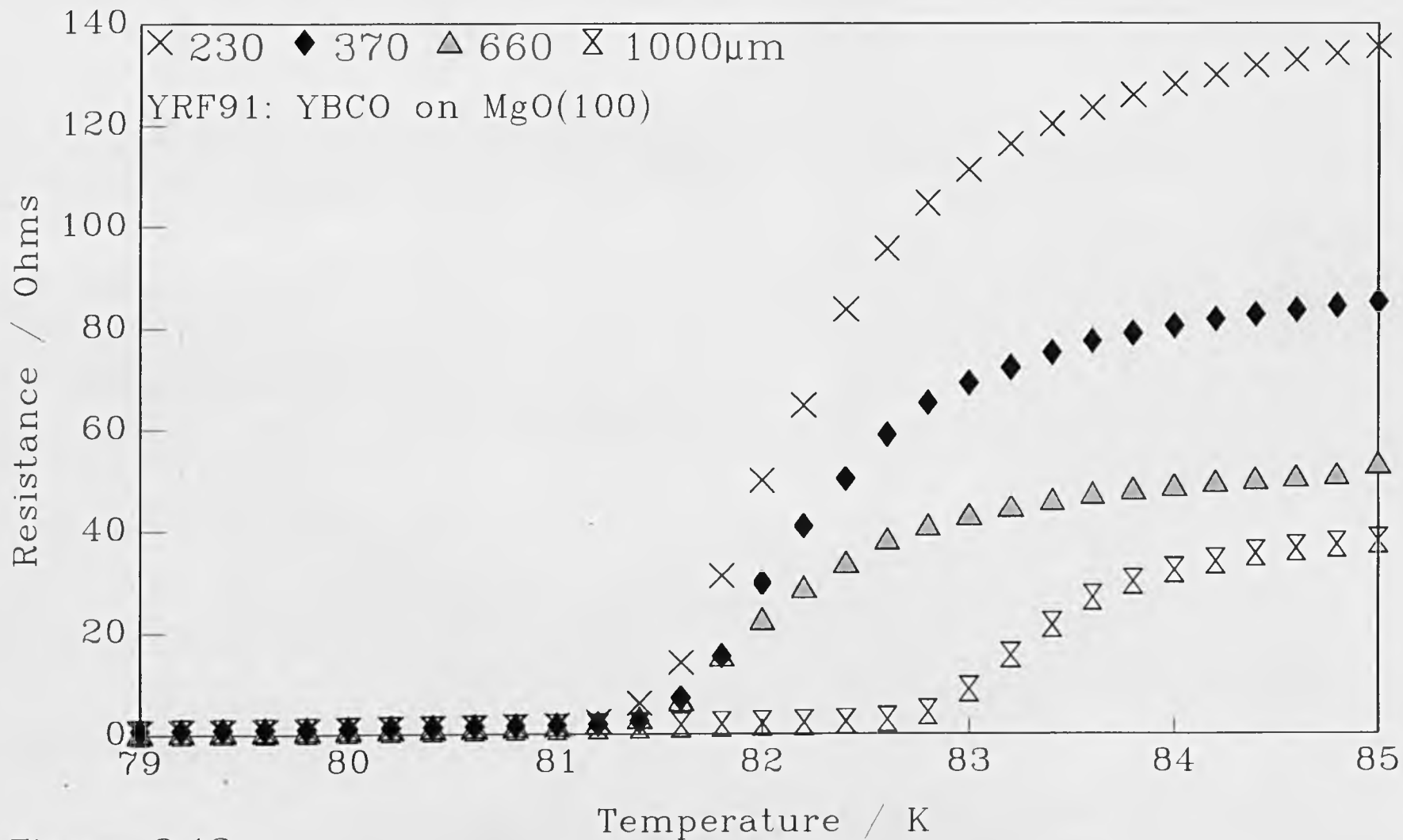


Figure 8.12

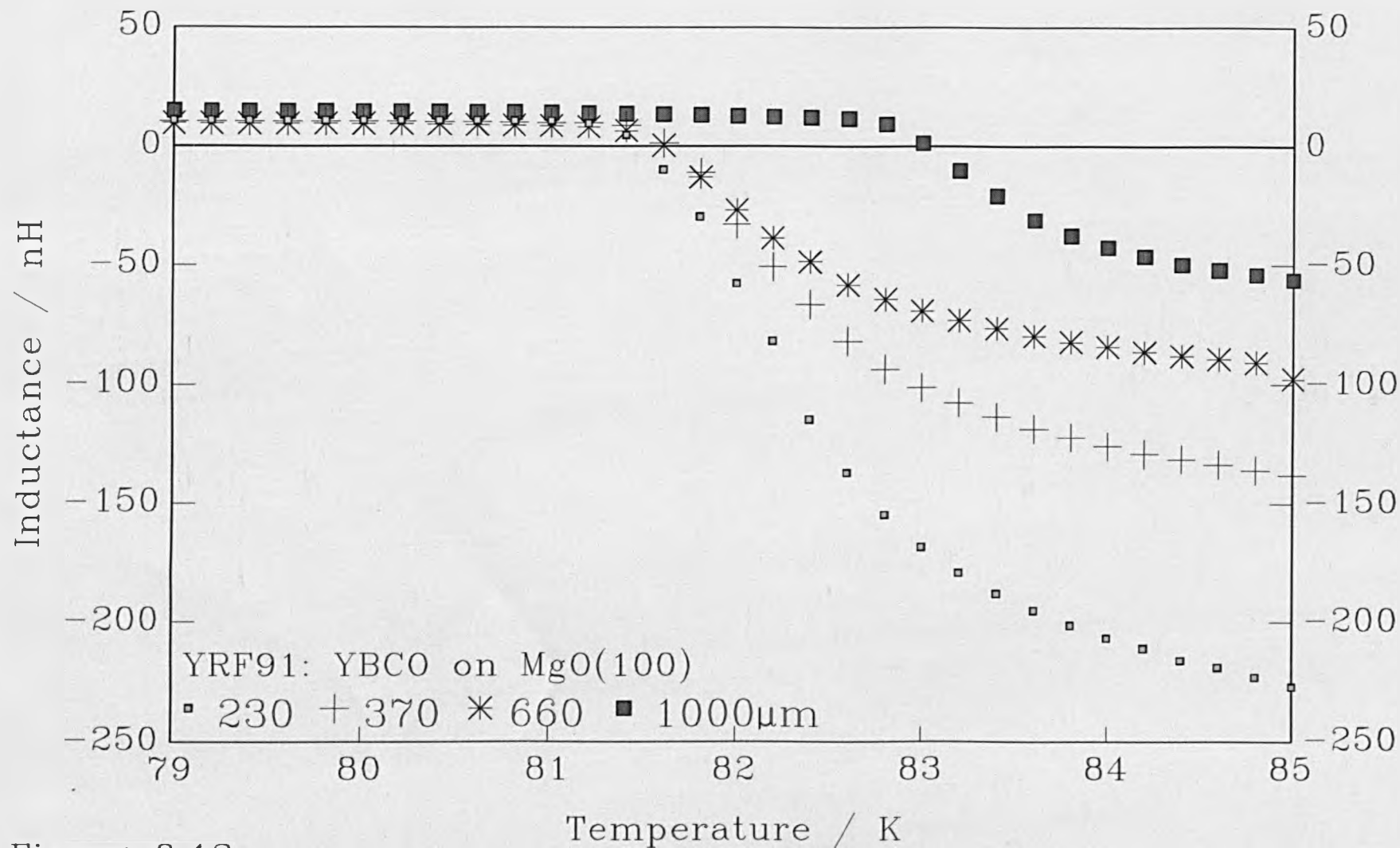


Figure 8.13

YRF109:YBCO on SrTiO₃(110)

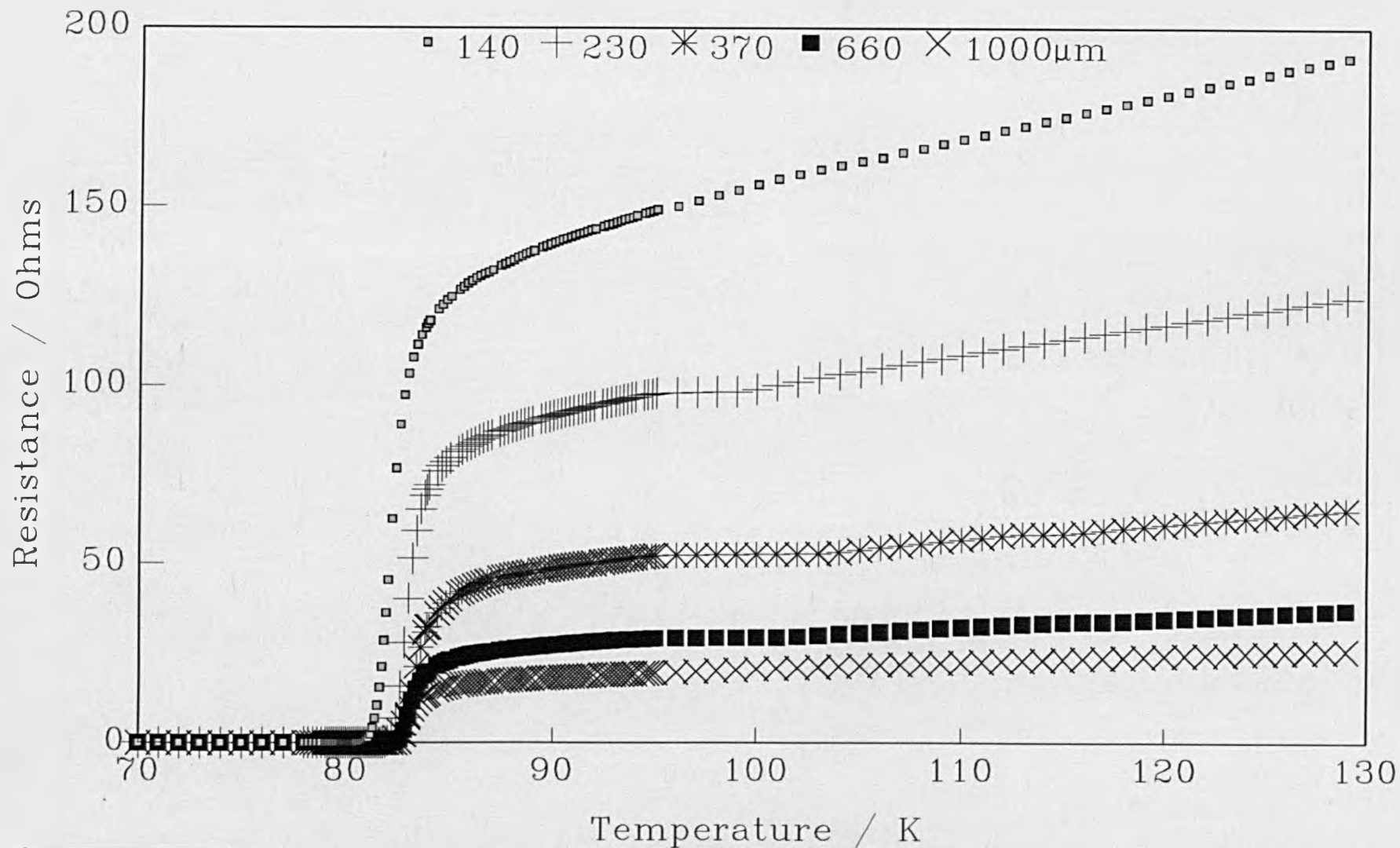


Figure 8.14

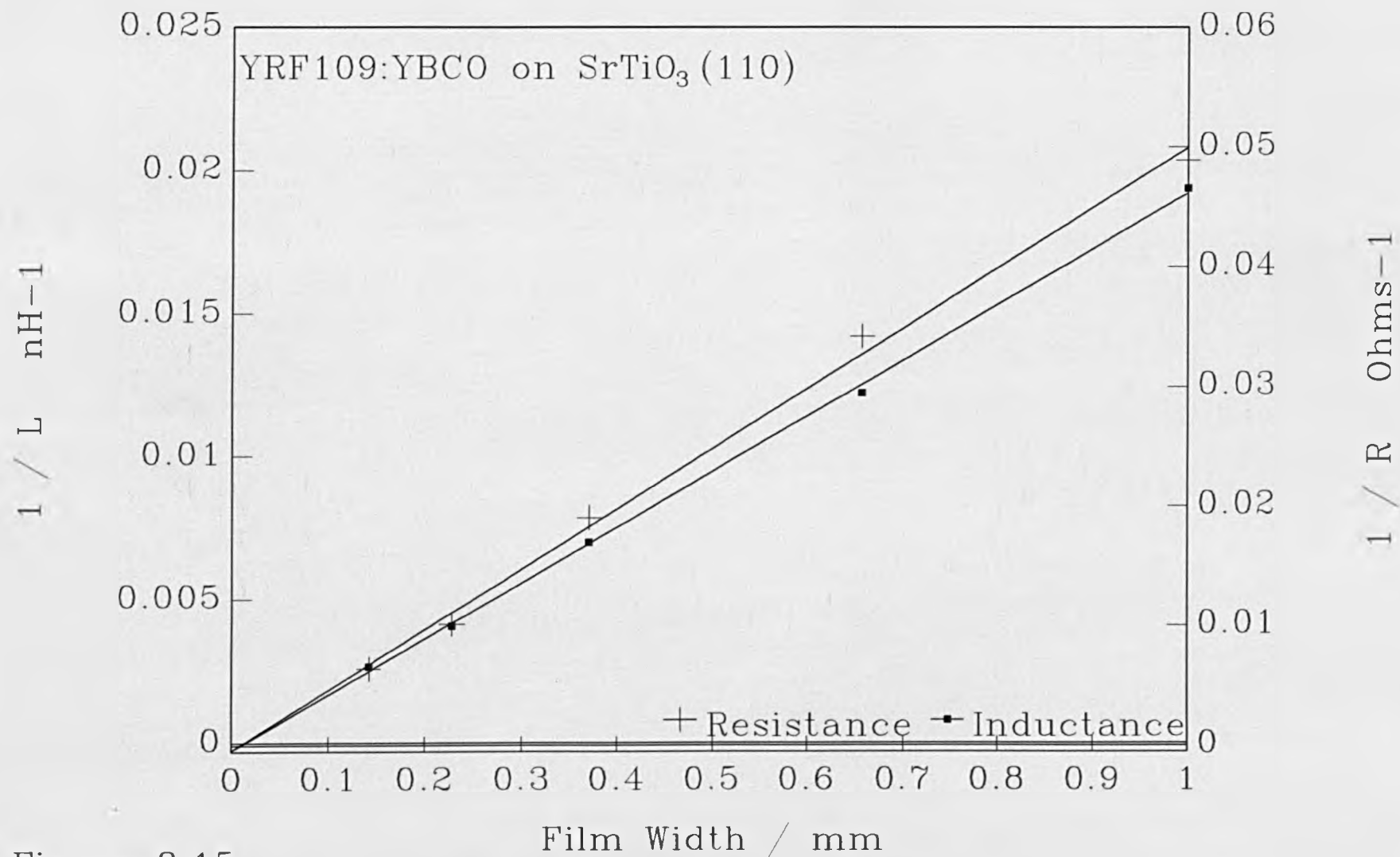


Figure 8.15

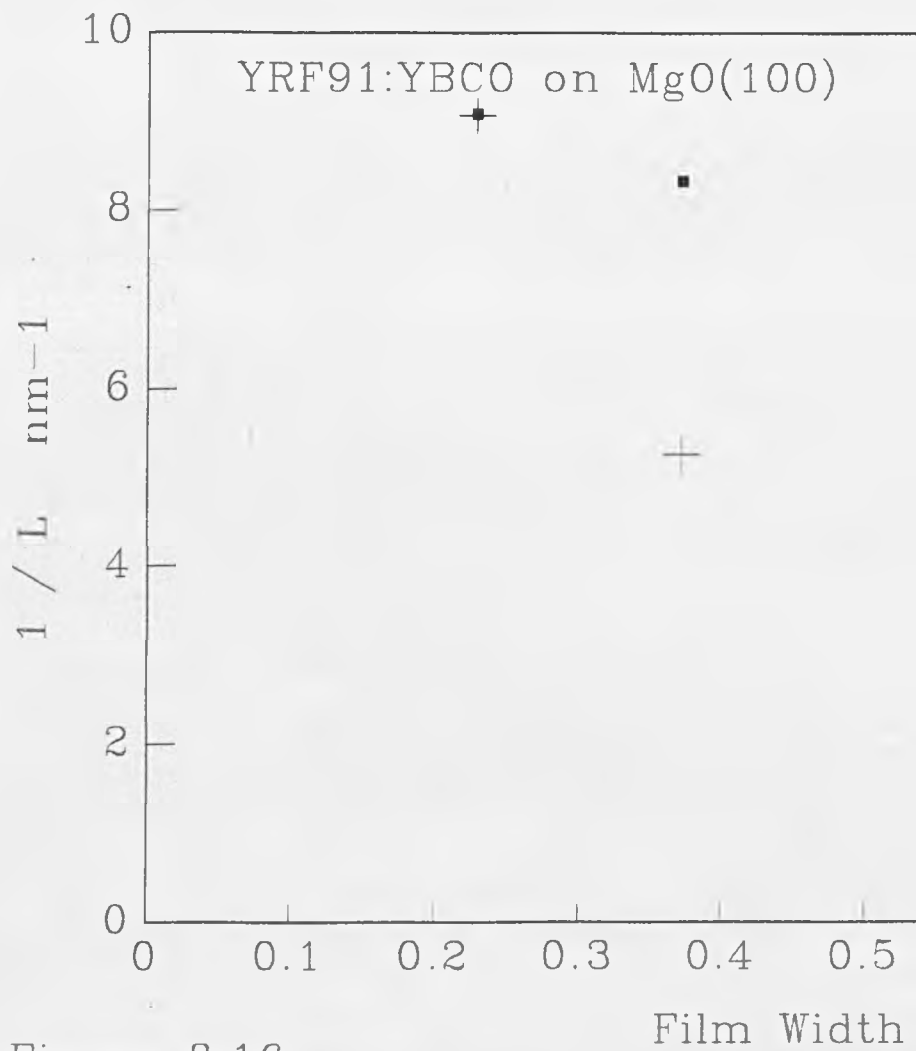
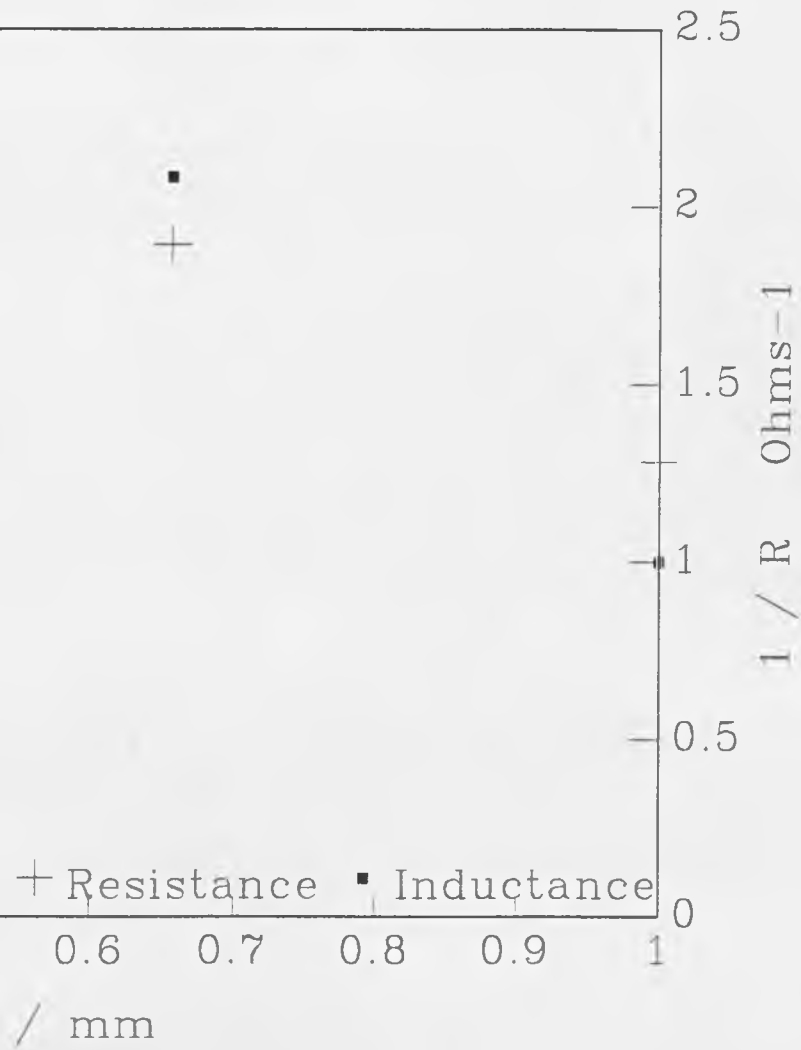


Figure 8.16



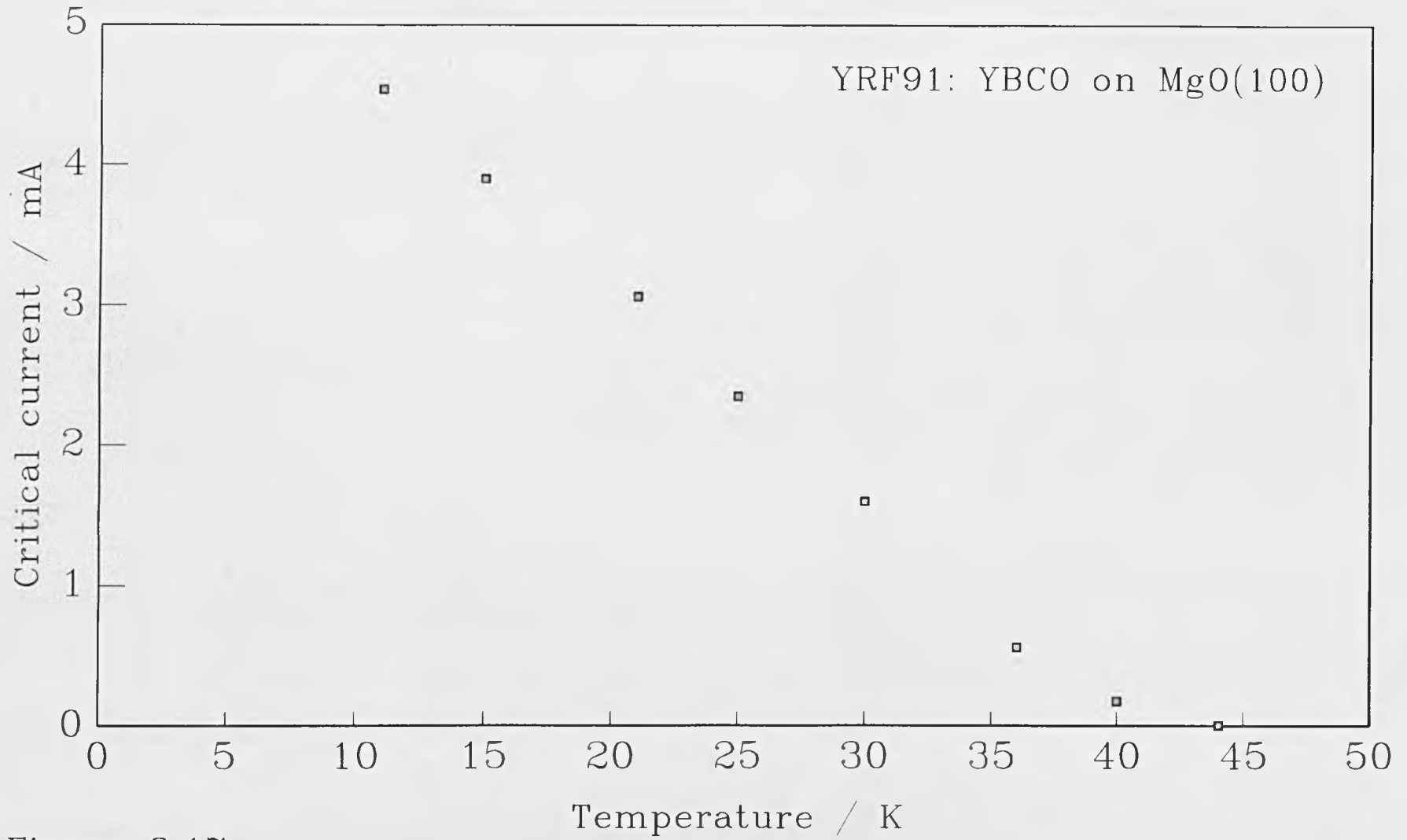


Figure 8.17

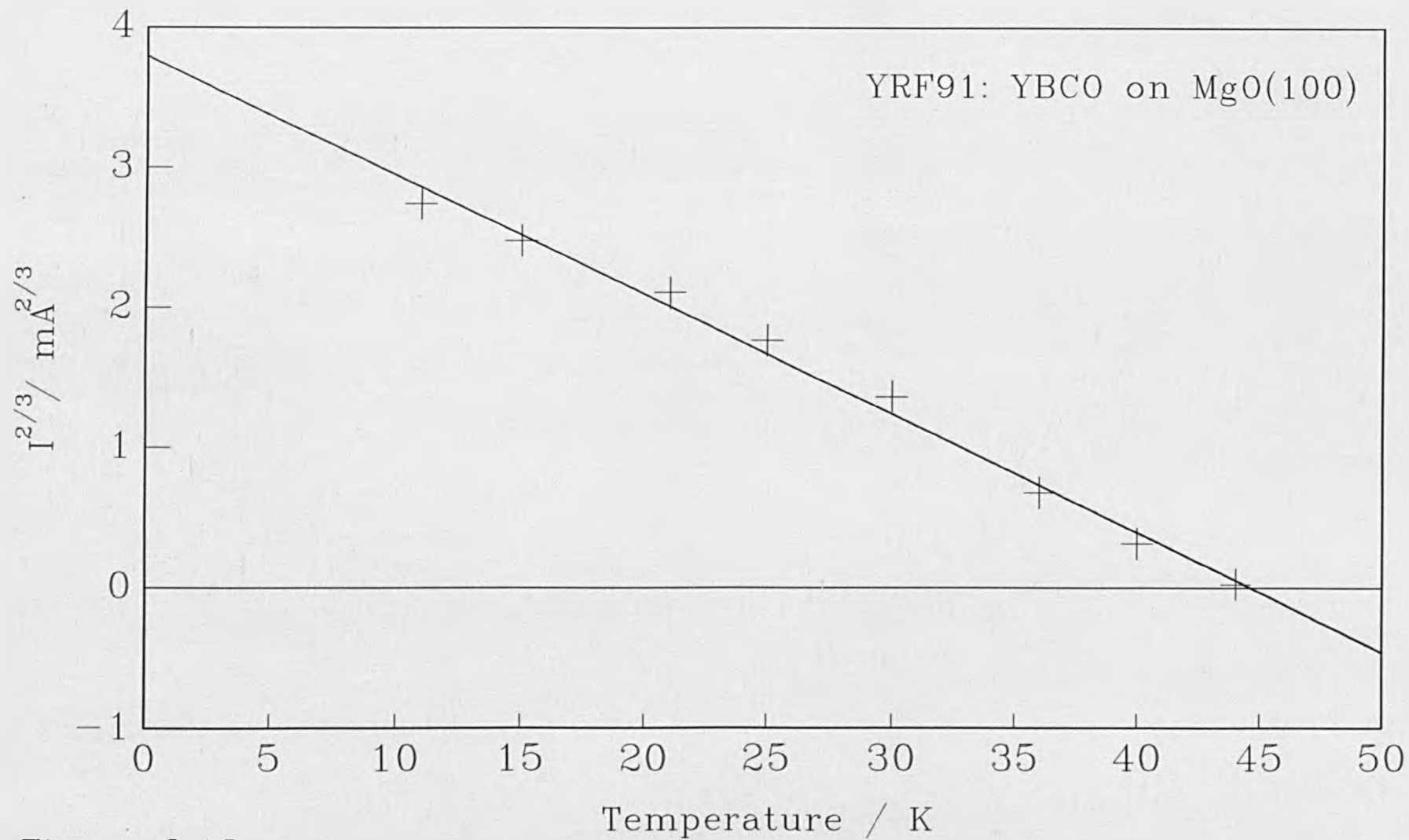


Figure 8.18

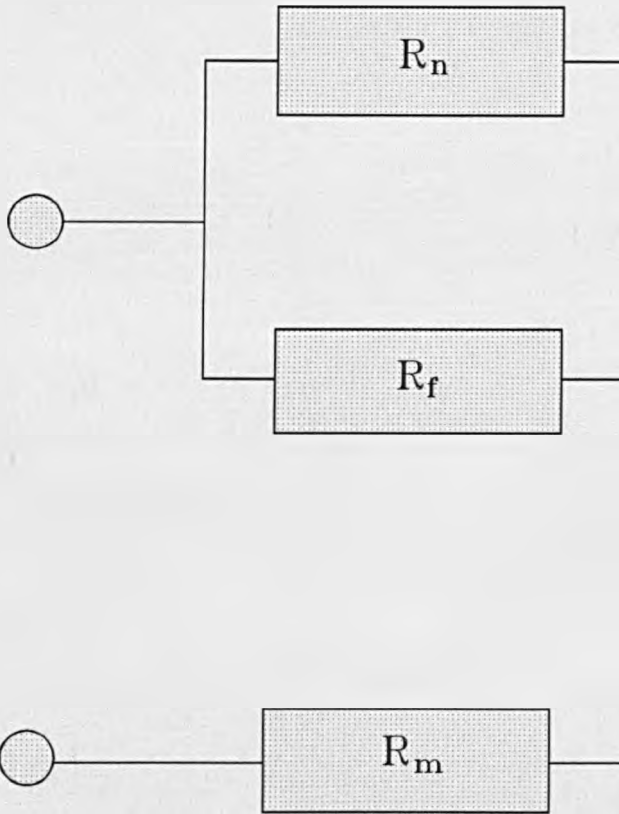
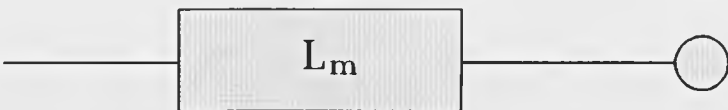
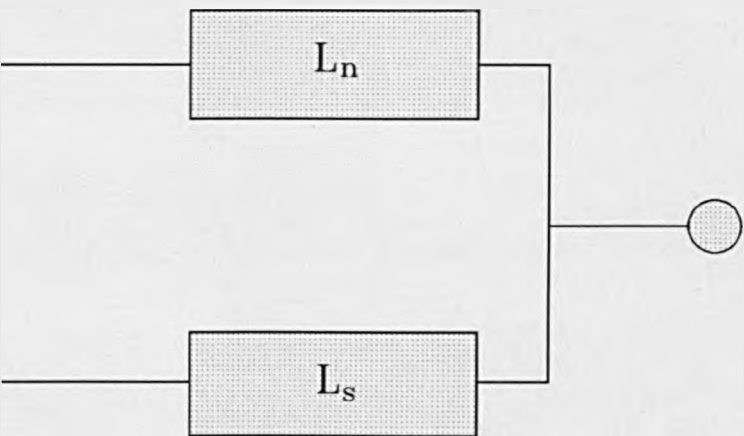


Figure 8.19



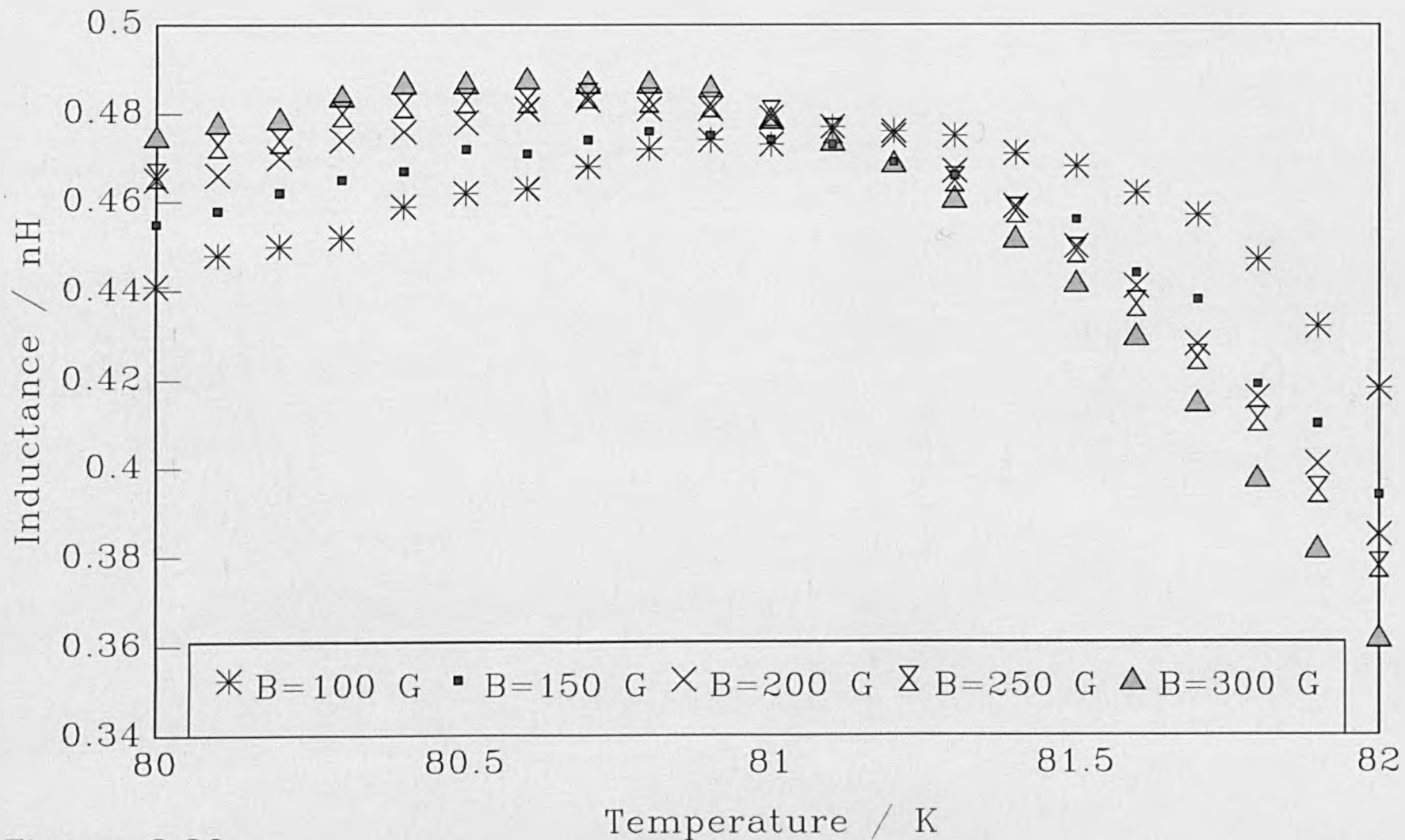


Figure 8.20

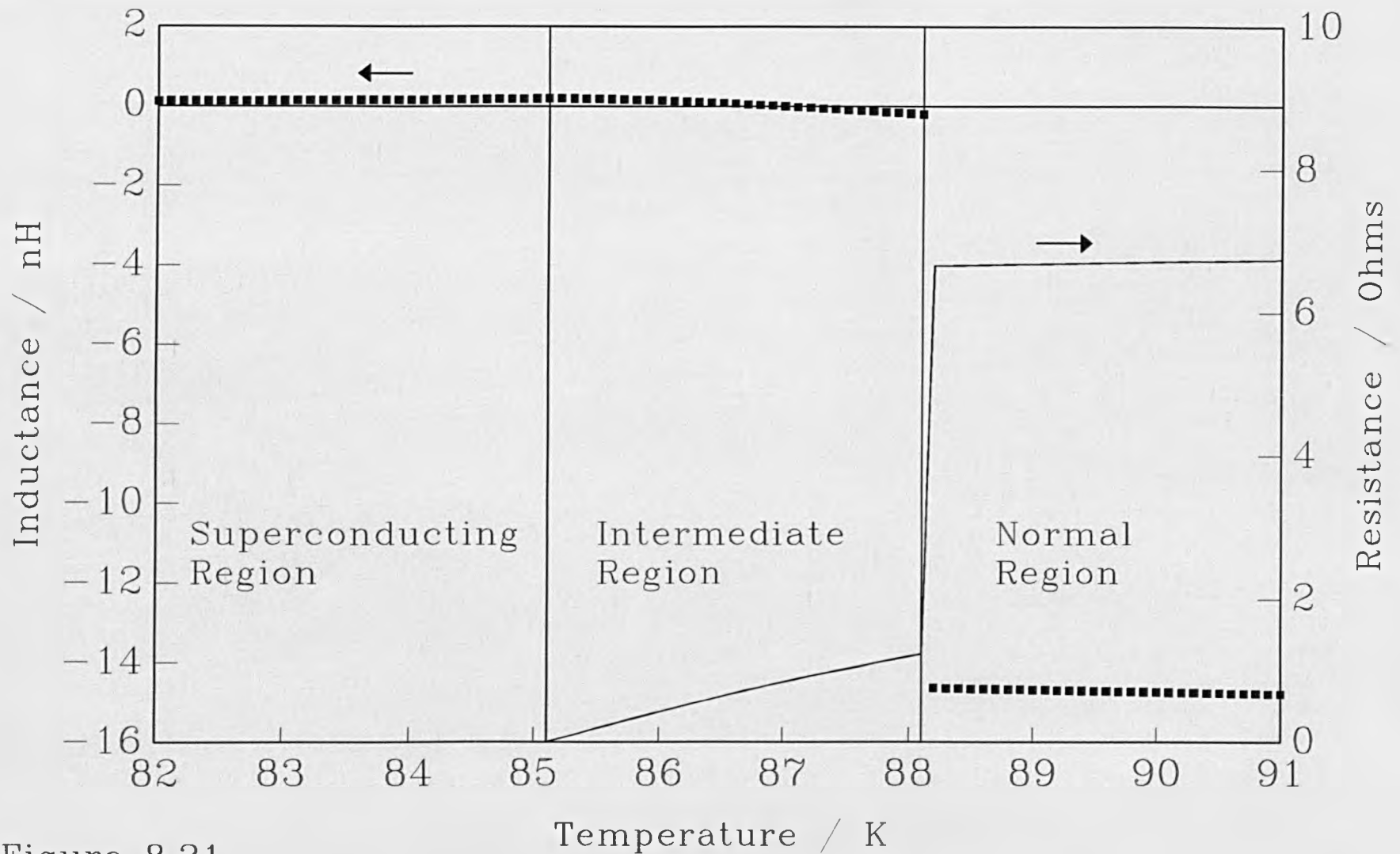


Figure 8.21

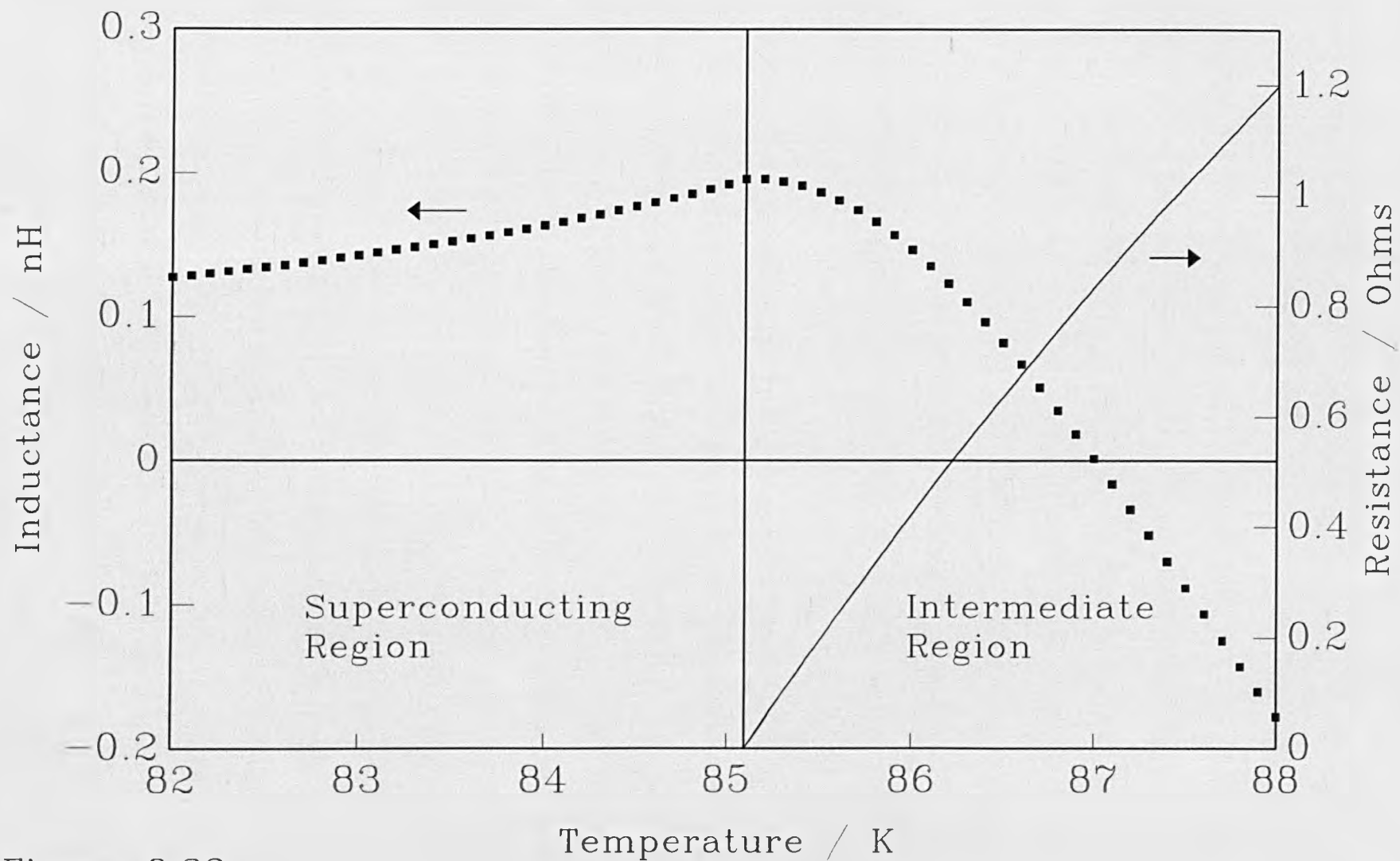


Figure 8.22

CHAPTER 9: SUMMARY AND FUTURE WORK

An R.F. sputtering technique has been used to deposit thin films of YBCO. The technique involving a deposition off axis at temperatures between 700-750 °C, followed by a low temperature post anneal in pure oxygen. The method was found to be reproducible and enabled thin films to be deposited onto SrTiO₃(110), SrTiO₃(100) and MgO(100). The films deposited on SrTiO₃(110) were found to be the best having T_{CO}'s in excess of 87 Kelvin. The conditions used here enhance ridge growth on SrTiO₃(110) over spiral growth. The films deposited on SrTiO₃(100) were generally of a poorer quality than those on SrTiO₃(110). The films were however superior to the films deposited on MgO(100). The films deposited on MgO(100) were consistently 4-7 Kelvin lower than the films deposited on SrTiO₃(100). Further investigation into deposition on MgO(100) is required.

Analysis using X-ray diffraction revealed that the orientation of the YBCO was dependent on the substrate material, substrate orientation as well as growth conditions. Films deposited on SrTiO₃(110) were found to be either (110), (013) or a mixture of (013/110) orientations. There was also some evidence of a and c-axis orientated regions deposited on the SrTiO₃(110) substrates. This is interesting since it implies that both ridge and spiral growth may have occurred, alternatively it may be that the a and c-axis orientations can result from ridge growth. The films deposited on SrTiO₃(100) were (a00), (00c) or a mixture of the two. The films deposited on SrTiO₃(100) gave evidence of a mixture of a and c-axis orientations. The a-axis phase seemed the more dominant from the X-ray diffraction results, although the electrical measurements seemed to imply that the current transport took place in the a-b plane, namely metallic as opposed to semiconductive behaviour. The X-ray diffraction patterns were used to calculate the a- and c-axis lattice parameters and these were found to be in close agreement with bulk YBCO. The orientation was also dependent on growth conditions. The films deposited on MgO(100) were all c-axis orientated. It was possible to determine the c-axis lattice

values of the films deposited on MgO(100) they ranged from 11.71-11.85Å. This change in the c-axis lattice values resulted in a change in the critical temperature of the films ranging from 73 - 49 Kelvin respectively. It appears that the larger the c-axis lattice value the lower the critical temperature of the YBCO thin film.

Transport measurements revealed that the films deposited on MgO(100) had the lowest resistivities, ranging from 0.177 to 0.271 mΩcm at 100 K. The films deposited on SrTiO₃(100) had slightly larger resistivities and this is due to the a-axis orientated YBCO that was deposited. The films deposited on SrTiO₃(110) were found to have the largest resistivities, ranging from 0.627 to 1.567 mΩcm at 100 Kelvin. The degree of (013) or (110) orientation present in the thin film influences the magnitude of the resistivity. This is of course due to the anisotropic nature of YBCO.

The resistive behaviour was investigated using Anderson's RVB theory. Although the theory is used to investigate D.C. resistive properties, here it was used to determine the low radio frequency resistive properties of the YBCO thin films. The c-axis orientated thin films gave results which were in good agreement with results from d.c. experiments performed on single crystals. Using Lawrence Doniach 2D-3D theory of paraconductivity the R.F. paraconductivity was determined. Once again this theory was generally used for D.C. experiments. It was possible to determine the coherence length and sheet thickness of the YBCO thin films. For a c-axis orientated thin film the coherence length for T=0K was 4 Å and the sheet thickness was calculated to be 11 Å, almost equal to the c-axis lattice constant. The LD theory was also used to interpret certain anomalous transitions first observed by Dubson⁽¹⁾. Results obtained from the thin films revealed that some films were 2 D to within a few degrees of T_c. These films were investigated using the Kosterlitz Thouless and Berezinskii theories for 2 dimensional superconductors. The results were found to be in good agreement with theory for films deposited on MgO(100), SrTiO₃(110) and SrTiO₃(100). The results indicate that the non universal constant b in the KTB theory may be anisotropic, having values ranging from 2.4 for c-

axis films to 6.6 for films with (013/110) orientation.

The R.F. contact experiments were also used to investigate the reactive nature of the YBCO thin films. The reactance was anisotropic and was more sensitive to changes in film orientation than the resistivity. Films deposited on MgO(100), namely c-axis orientated thin films had almost zero reactance whereas films deposited on SrTiO₃(110) had a significant measurable reactance. It is possible to conclude that the inter sheet space acts as a capacitor.

Using the reactive results it was possible to calculate the penetration depth. The values of the penetration depth varied from 2.24 to 10.58 μm . The values of penetration depth were larger than the London Penetration depth reported elsewhere^(2,3,4). Theory by Ambegaokar and Baratoff predicts that for films with granular properties, namely a film similar to a 2 dimensional array of Josephson junctions the penetration depth measured can be significantly larger than initially expected. The argument for Ambegaokar and Baratoff's theory is further strengthened by the critical current experiments, namely the $I^{2/3}$ vs temperature dependency, that as been observed in some thin films.

The inductive properties of the thin films were also found to be anomalous in certain cases. The anomaly appeared as a sharp deviation in the inductance from the temperature dependence predicted by London. Theory predicts that an anomaly of the type described can occur in 2 dimensional superconductors upon reaching the Kosterlitz Thouless Berezinskii temperature. Examination of the resistive properties reveal however that the anomaly causes a temporary decrease in resistance, see figure 8.15. This is not the resistive behaviour predicted by KT and B. Another explanation for the anomaly is that the observed effect is the film changing from 2 D to 3 D. If this is the case then the resistance behaviour observed can be interpreted as follows. Firstly the vortex/anti-vortex pairs dissociate and move freely throughout the conduction sheets dissipating energy. On reaching the cross over temperature the vortices are forced to align one on top of the other in stacks. If the stack is pinned in any of the sheets then the entire flux bundle will

no longer be able to move. Thus vortices that were initially free to move can once again become pinned at a lattice point. Since the vortices are pinned they cannot dissipate energy hence the temporary reduction in resistance as the temperature increases. Once the temperature rises above a certain point the entire flux bundle will be able to move and the resistance will increase as expected and as observed. This explanation does not explain measurements taken from a very thin film in which both the reactance and resistance underwent a resonance at 48 Kelvin. Examination revealed that the resonance temperature was frequency dependent although a comprehensive study of the behaviour as yet to be performed. The behaviour observed was easily modelled using equations originating from dielectric theory. It is not thought that it is a dielectric effect however because the film is in a superconducting state. The behaviour is particularly interesting since an anomaly as been reported within the same temperature region by Karim⁽⁵⁾. The experiments carried out using microwaves clearly show absorption between 39 and 52 Kelvin. Karim does put forward the idea that this may be due to flux melting, this would not explain the negative resistance observed. It would be interesting to examine the I-V characteristics of these films in the 2D-3D regions described above.

A film in the 3 dimensional temperature region was investigated using an applied magnetic field. The results were in agreement with traditional flux flow theory, namely that the temperature and B-field dependency were as expected for a 3D superconductor. The reactance behaviour was also examined within a magnetic field and was found to be in agreement qualitatively with theory.

Some thin films were etched into strips of different dimensions using a photolithographic technique. The etchant was ferric III nitrate which proved to be a very successful etchant. The strips were of different widths and were used to investigate the inductance and resistance in greater detail. The results demonstrated that the inductance and resistance properties in the normal region were as expected. The resistance temperature graphs revealed that 60 % of the film was unaltered by the etching i.e. 3

strips having the same critical temperature. The remaining two strips were of slightly poorer quality having a T_c 1 Kelvin lower. The behaviour expected in the superconducting region was not observed. The problem with the contact resistance and inductance made it impossible to determine the required results accurately.

The thin strips were also used to investigate the current carrying capabilities of certain YBCO thin films. The results revealed that for some films deposited on MgO(100) did have an I^{23} vs temperature dependency, as predicted by the Ambegaokar Baratoff theory. Films deposited on SrTiO₃(110) had the largest critical currents. At 77 Kelvin the YBCO thin films had critical currents in excess of 3×10^5 A/cm².

9.2 Future Work

The continued examination of the RF contact technique, since it shows some interesting results that are yet to be resolved entirely satisfactorily. No other research, giving results similar to those achieved by this method have been reported. More recent experiments for measuring penetration depth have used more conventional experiments, muon resonance, induction coils etc. It would be worth while attempting to carry out more traditional experiments to determine the penetration depth. These results could then be compared with those obtained from the RF contact experiments. The double coil experiments are normally conducted in the kHz region. The equipment necessary to produce a signal is available. The most pressing task would actually be fitting the coils into the cryostat. If it was not possible to carry out traditional penetration depth experiments within the department, it would be advantageous to the understanding of the RF contact technique to obtain films with known penetration depths and coherence lengths from elsewhere.

A re-examination of the theory used in this thesis could be conducted. particularly the approximations employed, see equations 8.2 and 8.3. It has been assumed in this thesis, that the skin depth is considerably larger than the penetration depth. This is true if we are indeed measuring the London penetration depth of say $0.14 \mu\text{m}$. If however the penetration depth is considerably larger, then the approximations may not be strictly valid particularly around T_c . It is interesting to note that if the penetration depth is considerably larger than the skin depth, then a quick analysis appears to point to the theory giving a similar result to equation 8.6, namely the London penetration depth but this time multiplied by a larger number than μ_0 . If this is the correct then penetration depth measured by this technique may be the Josephson penetration depth, which is likely to be considerably larger than the London penetration depth in these films. This would be resolved by the re-examination mentioned above.

A closer examination of the transition temperature region would be very useful.

particularly if results could be obtained every 0.01 or 0.02 K. It would be necessary to extend the existing programs which presently take readings every 0.1 K. Furthermore a method of delaying the heating of the substrate would have to be developed. Presently, when the compressor is disengaged the substrate begins to heat up. The rate of warming is too quick to obtain accurate readings of 0.01 K. This could prove considerably difficult to achieve. The actual reprogramming for recording the data would not be particularly difficult, although it could prove time consuming, since it would be necessary to store large amount of data. The results would allow the user to investigate the transition region in excellent detail. Detailed examination of the 2D/3D crossover point, and investigation of flux flow phenomena would then be possible. This would in turn allow a far closer examination of some of the theories mentioned in this thesis. Furthermore with the use of software such as Harvard Graphics 3, which can process 1000 points, it would be possible to investigate a 10-20 K region of the transition in far superior detail.

There was some problems with film uniformity, particularly if a good thermal contact was not maintained throughout deposition. This as been largely reduced with the introduction of the silver paint adhesive. An investigation into different forms of high temperature adhesive would of interest. It would be important to obtain an adhesive that does not contaminate the system. The quality of uniformity could be tested with a simple mask, similar to that described in section 8.6.1. The strips however could be made equal, for example, 10 strips, each 0.75 mm wide, 8 mm long. The production of the mask would be a relatively easy job since the technology as already be tested and found to be adequate. The etching of the film could be carried out using the method already described in this thesis. It would not be necessary to test every film, testing every tenth film initially would probably be sufficient. The film deposited using a new adhesive should be tested. This would give a clear indication of the quality of the thin films, and therefore the quality of the adhesive.

For the RF sputtering experiments, a further series of experiments to improve the oxygen content of the films is necessary. Many of the films reviewed in this thesis were probably oxygen deficient. Experiments should include a series of post anneal treatments, for example, altering the substrate temperature during post anneal, the oxygen content and pressure etc.

It would then be interesting to perform a series of experiments specifically aimed at improving the thin films deposited on MgO and SrTiO₃(100) or other, low permittivity, substrates. The majority of the depositions reported here were performed to obtain the best film possible on SrTiO₃. there was some evidence that films could be deposited on MgO using significantly different deposition parameters, this may result in a different form of deposition. A starting point would be a lower pressure, namely 200 mTorr, with a 1:1 ratio of Ar:O₂, a substrate temperature of 700⁰ C, and a 1 hour post anneal in pure oxygen at 400⁰ C. Superconducting films can be deposited on MgO using these conditions, where as films deposited on SrTiO₃(110) can not. It would be interesting to perform experiments at several temperatures from 700 - 800⁰ C to determine the effect this temperature shift has on the orientation. The majority of the films deposited on MgO(100) and investigated in this thesis were c-axis orientated perpendicular to the substrate. It may be possible to produce a-axis by deposition at different temperatures.

For the electrical experiments, there are again several lines of investigation open. For films deposited on MgO (100) which are known to be C-axis, it would be interesting to investigate the anisotropy in the a-b directions. This could be achieved by evaporating 16 dots, in the form of 4 x 4 onto the film. It would then be possible to measure the resistivity horizontally, vertically and diagonally on the film. It would be necessary to make the dots reasonably large to avoid the problem of making good contacts. A mask already exists to perform this task, although the dots were too small, it was not possible therefore to obtain quality Ohmic contacts. If a-axis films could be

deposited on MgO(100) using the sputtering technique it would interesting to repeat the electrical experiments described above to determine the effect of the orientation change. This has been investigated a little in this thesis for films deposited on SrTiO₃(100),

Each of these experiments described above do not apply strictly to YBCO and the substrates used throughout this thesis. The experiments can be used for any substrate and any high temperature superconducting material that can, or is to, be sputtered and tested using electrical means.

9.3 References

- 1 Dubson M.A., Herbert S.T., Calabrese J.J., Harris D.C., Patton B.R., Garland J.C., Phys Rev Lett 60 (1988) 1061
- 2 Harshman D.R., Aepli G., Ansaldo E.J., Batlogg B., Brewer J.H., Carolan J.F., Cava R.J., Celio M., Chaklader A.C.D., Hardy W.N., Kreitzman S.R., Luke G.M., Noakes D.R., Senba M., Phys Rev B 36 (1987) 2386
- 3 Fiory A.T., Hebard A.F., Mankiewich P.M., Howard R.E., Appl Phys Lett 52 (1988) 2165
- 4 Flueckiger P., Gavilano J.L., Leemann C., Martinoli P., Dam B., Stollman G.M., Srivastava P.K., Debely P., Hintermann H.E., Physica C 162-164 (1989) 1563
- 5 Karim R., How H., Seed R., Widom A., Vittoria C., Balestrino G., Paroli P., Solid State Comms. 71 (1989) 983

APPENDIX

Program: RLFREQ

```
10 REM      RLFREQ
20 DEF SEG=0
30 DRIVER1=PEEK(&H4F0)+256*PEEK(&H4F1)
40 DRIVER2=PEEK(&H4F4)+256*PEEK(&H4F5)
50 DEF SEG=DRIVER1: REM SELECT CARD #1
60 INIT=3: ABORTIO=6: DEVCLEAR=9: LOCAL=12
70 LOCALLOCKOUT=15: REMOTE=18: IRESUME=21: TRIGGER=24
80 OUTPUT=27: ENTER=30: STATUS=33: SETTERMINATOR=36
90 SETTIMEOUT=39: SERIALPOLL=42: SRQCHECK=45: ERRCHECK=48
100 SETEOI=51: SETTERM=54: PARALLELPOLL=57: SRVREQ=60
110 NCINIT=63: BLOCKOUT=66: BLOCKIN=69: BYTESWAP=72
120 TRANSFER=75: TALK=78: UNTALK=81: LISTEN=84
130 UNLISTEN=87: ATTN=90: MTA=93: MLA=96
140 DIM NM$(1000)
150 DIM TF$(1000)
160 PRINT"Input start frequency (MHz)";
170 INPUT TF
180 PRINT"Input stop frequency (MHz)";
190 INPUT PF
200 PRINT"Input step frequency (kHz)";
210 INPUT SF
220 TF=TF*1000:PF=PF*1000
230 TF$=STR$(TF):PF$=STR$(PF):SF$=STR$(SF)
240 FR$=TF$
250 CALL INIT
260 LCR=19
270 FR$="FR"+FR$+"EN"
280 TF$="TF"+TF$+"EN"
290 PF$="PF"+PF$+"EN"
300 SF$="SF"+SF$+"EN"
310 CALL OUTPUT(FR$,LCR)
320 CALL OUTPUT(TF$,LCR)
330 CALL OUTPUT(PF$,LCR)
340 CALL OUTPUT(SF$,LCR)
350 DATA "A3","B3","V1","C1","F0","W1","W2"
360 FOR I=1 TO 7
370 READ CMD$
```

```
380 CALL OUTPUT(CMD$,LCR)
390 NEXT I
400 FO$=SPACE$(31)
410 TS=TF/1000
420 I=0
430 CALL ENTER(FO$,LCR)
440 F1$=MID$(FO$,1,1)
450 IF F1$="N" THEN 460 ELSE 430
460 CLS
470 PRINT FO$,I
480 A$=INKEY$
490 IF A$=CHR$(32) THEN 560
500 PRINT:PRINT"Press <space> to interupt"
510 NM$(I)=FO$: TF$(I)=STR$(TS)
520 I=I+1
530 TS=TS+(SF/1000)
540 TS=CINT(TS*100):TS=TS/100
550 IF TS<=PF/1000 THEN 430
560 CMD$="W3": CALL OUTPUT(CMD$,LCR)
570 CLS: INPUT"Save data Y/N";S$
580 IF S$="N" THEN 720
590 A1$="Frequency":A2$="Inductance";A3$="Resistance"
600 INPUT"Filename";NA$
610 NA$="C:\BRYAN\RLFT\TEMP\"+NA$+".HG1"
620 OPEN"O",#1,NA$
630 PRINT#1,A1$;" ",A2$;" ",A3$
640 FOR J=0 TO I
650 NM1$=MID4(NM$(J),5,11)
660 NM2$=MID$(NM$(J),21,11)
670 TF$(J)=MID$(TF$(J),1,6)
680 PRINT #1,TF$(J);" ",NM1$;" ",NM2$
690 PRINT TF$(J),NM1$,NM2$
700 NEXT J
710 CLOSE#1
720 END
```

Program: RLTEMP

```
5 REM      RLTEMP
10 DEF SEG=0
20 DRIVER1=PEEK(&H4F0)+256*PEEK(&H4F1)
30 DRIVER2=PEEK(&H4F4)+256*PEEK(&H4F5)
40 DEF SEG=DRIVER1: REM SELECT CARD #1
50 INIT=3: ABORTIO=6: DEVCLEAR=9: LOCAL=12
60 LOCALLOCKOUT=15: REMOTE=18: IRESUME=21: TRIGGER=24
70 OUTPUT=27: ENTER=30: STATUS=33: SETTERMINATOR=36
80 SETTIMEOUT=39: SERIALPOLL=42: SRQCHECK=45: ERRCHECK=48
90 SETEOI=51: SETTERM=54: PARALLEL POLL=57: SRVREQ=60
100 NCINIT=63: BLOCKOUT=66: BLOCKIN=69: BYTESWAP=72
110 TRANSFER=75: TALK=78: UNTALK=81: LISTEN=84
120 UNLISTEN=87: ATTN=90: MTA=93: MLA=96
130 TF=0
140 DIM NM$(2500),TF$(2500)
150 DIM VCHART(25)
160 DIM TCHART(25)
170DATA0.09032,0.12536,0.18696,0.31180,0.42238,0.56707,0.68580,0.76717,0.8354
1,0.89082,0.94455,0.98574,1.02044,1.05277,1.08105,1.09477,1.10465,1.11202,1.1151
7,1.11896,1.12463,1.13598,1.21555,1.24928,1.36687
180DATA475,460,435,385,340,280,230,195,165,140,115,95,77.4,60,44,36,31,28,27,26
,25,24,20,18,12
190 RESTORE 170
200 FOR LOOP=1 TO 25
210 READ VCHART(LOOP)
220 NEXT
230 FOR LOOP=1 TO 25
240 READ TCHART(LOOP)
250 NEXT
260 KEITH=27
270 CALL INIT
280 CMD$="FOX": CALL OUTPUT(CMD$,KEITH)
290 CMD$="COX": CALL OUTPUT(CMD$,KEITH)
300 CMD$="ROX": CALL OUTPUT(CMD$,KEITH)
310 LCR=19
320 PRINT"Input test frequency (MHz)";
330 INPUT FR
340 FR=FR*1000: FR$=STR$(FR)
350 FR1$="FR"+"FR$+"EN"
```

```

360 CALL OUTPUT(FR1$,LCR)
370 DATA "A3","B3","V1","C1","F0"
380 FOR I=1 TO 5
390 READ CMD$
400 CALL OUPUT(CMD$,LCR)
410 NEXT
420 ST1=320: I=0
430 F$=SPACE$(31)
440 F1$=SPACE$(31)
450 CALL ENTER(F1$,LCR)
460 CALL ENTER(F$,LCR)
470 A$=INKEY$:IF A$=CHR$(32) THEN GOSUB 1040
480 GOSUB 760
490 IF T=ST1 THEN 450
500 ST1=T
510 I=I+1
520 CLS
530 PRINT T,ST1,I,F1$
540 PRINT:PRINT"Press <space> to interupt"
550 NM$(I)=F1$: TF$(I)=STR$(T)
560 IF T>10 THEN 450
570 CALL UNTALK
580 CLS:INPUT"Save Data Y/N ";S$
590 IF S$="N" THEN 1030
600 INPUT"Filename"; NA$
640 LET FR$="Frequency="+FR$
650 OPEN"O",#1,NA$
660 A1$="Temperature":A2$="Inductance":A3$="Resistance"
670 PRINT#1,FR$
680 PRINT#1,A1$;" ",A2$;" ",A3$
690 FOR ZX=0 TO I
700 NM1$=MID$(NM$(ZX),5,11)
710 NM2$=MID$(NM$(ZX),21,11)
720 PRINT#1,TF$(ZX);" ",NM1$;" ",NM2$
730 NEXT ZX
740 CLOSE#1
750 GOTO 1030
760 V$=SPACE$(30)
770 CALL ENTER(V$,KEITH)
780 V=VAL(MID$(V$,5,12)
790 BP=0

```

```
800 BP=BP+1
810 V1=VCHART(BP)
820 IF V1>=V THEN 830 ELSE 800
830 V2=VCHART(BP-1)
840 T1=TCHART(BP)
850 T2=TCHART(BP-1)
860 T=(((V-V1)/(V2-V1))*(T2-T1))+T1
870 IF T<10 THEN 910
880 IF T-INT(T)<.5 THEN T=INT(T)
890 IF T-INT(T)>=.5 THEN T=INT(T)+1
900 RETURN
910 IF T<95 THEN 880
920 IF T>INT(T)+.95 THEN T=INT(T)+1
930 IF T>INT(T)+.85 AND T<INT(T)+.95 THEN T=INT(T)+.9
940 IF T>INT(T)+.75 AND T<INT(T)+.85 THEN T=INT(T)+.8
950 IF T>INT(T)+.65 AND T<INT(T)+.75 THEN T=INT(T)+.7
960 IF T>INT(T)+.55 AND T<INT(T)+.65 THEN T=INT(T)+.6
970 IF T>INT(T)+.45 AND T<INT(T)+.55 THEN T=INT(T)+.5
980 IF T>INT(T)+.35 AND T<INT(T)+.45 THEN T=INT(T)+.4
990 IF T>INT(T)+.25 AND T<INT(T)+.35 THEN T=INT(T)+.3
1000 IF T>INT(T)+.15 AND T<INT(T)+.25 THEN T=INT(T)+.2
1010 IF T>INT(T)+.05 AND T<INT(T)+.15 THEN T=INT(T)+.1
1015 IF T>INT(T)+0 AND T<INT(T)+.05 THEN T=INT(T)+0
1020 RETURN
1030 END
1040 PRINT"Paused"
1050 PRINT"press 'A' to continue"
1060 PRINT" 'B' to interupt"
1070 LET B$=INKEY$
1080 IF B$=CHR$(65) THEN RETURN
1090 IF B$=CHR$(66) THEN 570
1100 GOTO 1070
```

Program: DCTEMP

```
5 REM      DCTEMP
10 DEF SEG=0
20 DRIVER1=PEEK(&H4F0)+256*PEEK(&H4F1)
30 DRIVER2=PEEK(&H4F4)+256*PEEK(&H4F5)
40 DEF SEG=DRIVER1: REM SELECT CARD #1
50 INIT=3: ABORTIO=6: DEVCLEAR=9: LOCAL=12
60 LOCALLOCKOUT=15: REMOTE=18: IRESUME=21: TRIGGER=24
70 OUTPUT=27: ENTER=30: STATUS=33: SETTERMINATOR=36
80 SETTIMEOUT=39: SERIALPOLL=42: SRQCHECK=45: ERRCHECK=48
90 SETEOI=51: SETTERM=54: PARALLEL POLL=57: SRVREQ=60
100 NCINIT=63: BLOCKOUT=66: BLOCKIN=69: BYTESWAP=72
110 TRANSFER=75: TALK=78: UNTALK=81: LISTEN=84
120 UNLISTEN=87: ATTN=90: MTA=93: MLA=96
130 TF=0
140 DIM NM$(2500),TF$(2500)
150 DIM VCHART(25)
160 DIM TCHART(25)
170DATA0.09032,0.12536,0.18696,0.31180,0.42238,0.56707,0.68580,0.76717,0.8354
1,0.89082,0.94455,0.98574,1.02044,1.05277,1.08105,1.09477,1.10465,1.11202,1.1151
7,1.11896,1.12463,1.13598,1.21555,1.24928,1.36687
180DATA475,460,435,385,340,280,230,195,165,140,115,95,77.4,60,44,36,31,28,27,26
,25,24,20,18,12
190 RESTORE 170
200 FOR LOOP=1 TO 25
210 READ VCHART(LOOP)
220 NEXT
230 FOR LOOP=1 TO 25
240 READ TCHART(LOOP)
250 NEXT
251 INPUT"Input current ";CURRENT
260 KEITH=27
270 CALL INIT
280 CMD$="FOX": CALL OUTPUT(CMD$,KEITH)
290 CMD$="COX": CALL OUTPUT(CMD$,KEITH)
300 CMD$="ROX": CALL OUTPUT(CMD$,KEITH)
310 KE12=7
320 CALL INIT
330 CMD$="FOX": CALL OUTPUT(CMD$,KE12)
340 CMD$="ROX": CALL OUTPUT(CMD$,KE12)
```

```

350 CMD$="P20X": CALL OUTPUT(CMD$,KE12)
360 ST1=320: I=0
370 F$=SPACES$(31)
380 F1$=SPACES$(31)
390 CALL ENTER(F1$,KE12)
400 CALL ENTER(F$,KE12)
410 A$=INKEY$:IF A$=CHR$(32) THEN GOSUB 960
420 GOSUB 680
430 IF T=ST1 THEN 390
440 ST1=T
450 I=I+1
460 CLS
470 PRINT T,ST1,I,F1$
480 PRINT:PRINT"Press <space> to interupt"
490 NM$(I)=F1$: TF$(I)=STR$(T)
500 IF T>10 THEN 390
510 CALL UNTALK
520 CLS:INPUT"Save Data Y/N ";S$
530 IF S$="N" THEN 950
540 INPUT"Filename"; NA$
550 NA$="C:\BRYAN\RLFT\BMDATA\"+NA$+".HP1"
570 OPEN"O",#1,NA$
610 FOR ZX=0 TO I
620 NM1$=MID$(NM$(ZX),5,11)
630 NM2$=MID$(NM$(ZX),21,11)
640 PRINT#1,TF$(ZX);" ",NM1$;" ",NM2$
650 NEXT ZX
660 CLOSE#1
670 GOTO 950
680 V$=SPACES$(30)
690 CALL ENTER(V$,KEITH)
700 V=VAL(MID$(V$,5,12)
710 BP=0
720 BP=BP+1
730 V1=VCHART(BP)
740 IF V1>=V THEN 750 ELSE 720
750 V2=VCHART(BP-1)
760 T1=TCHART(BP)
770 T2=TCHART(BP-1)
780 T=(((V-V1)/(V2-V1))*(T2-T1))+T1
790 IF T<10 THEN 830

```

```
800 IF T-INT(T)<.5 THEN T=INT(T)
810 IF T-INT(T)>=.5 THEN T=INT(T)+1
820 RETURN
830 IF T<95 THEN 800
840 IF T>INT(T)+.95 THEN T=INT(T)+1
850 IF T>INT(T)+.85 AND T<INT(T)+.95 THEN T=INT(T)+.9
860 IF T>INT(T)+.75 AND T<INT(T)+.85 THEN T=INT(T)+.8
870 IF T>INT(T)+.65 AND T<INT(T)+.75 THEN T=INT(T)+.7
880 IF T>INT(T)+.55 AND T<INT(T)+.65 THEN T=INT(T)+.6
890 IF T>INT(T)+.45 AND T<INT(T)+.55 THEN T=INT(T)+.5
900 IF T>INT(T)+.35 AND T<INT(T)+.45 THEN T=INT(T)+.4
910 IF T>INT(T)+.25 AND T<INT(T)+.35 THEN T=INT(T)+.3
920 IF T>INT(T)+.15 AND T<INT(T)+.25 THEN T=INT(T)+.2
930 IF T>INT(T)+.05 AND T<INT(T)+.15 THEN T=INT(T)+.1
935 IF T>INT(T)+0 AND T<INT(T)+.05 THEN T=INT(T)+0
940 RETURN
950 END
960 PRINT"Paused"
970 PRINT"press 'A' to continue"
980 PRINT"      'B' to interupt"
990 LET B$=INKEY$
1000 IF B$=CHR$(65) THEN RETURN
1010 IF B$=CHR$(66) THEN 510
1020 GOTO 990
```

